A novel platform for the synthesis of inorganic Janus nanoparticles with tailored cell interactions

Eine neuartige Plattform für die Synthese anorganischer Janus-Nanopartikel mit maßgeschneiderten Zellinteraktionen

Vom Fachbereich Produktionstechnik

der

UNIVERSITÄT BREMEN

Zur Erlangung des Grades

Doktor der Ingenieurwissenschaften (Dr.-Ing)

genehmigte

Dissertation

Von

M.Sc.

Reshma Sampat Kadam

Gutachter und Gutachterin:

Prof.Dr.- Ing. Kurosch Rezwan

Prof.Dr. Rita Gross-Hardt

Tag der mündlichen Prüfung: 30.03.2022

Dedicated to my family…

Acknowledgements

A doctorate being such an important milestone in every academic career, I would like to begin by expressing my heartfelt gratitude to Prof. Dr.-Ing. Kurosch Rezwan for giving me a chance to work at the Centre of Advanced Ceramics, University of Bremen. I would like to thank him for all the support and supervision provided during the course of my work here. I would further like to thank PD Dr. rer. nat. Michael Maas for advising me during the tenure of my work for my thesis, for all the guidance with experimental work, encouragement and all the wise words during my work. I would also like to thank my second reviewer, Prof.Dr. Rita Gross-Hardt, for taking the time and the effort in reading and being a part of this dissertation.

I would like to further thank Dr.rer.nat. Mario Waespy for his help and supervision during the finishing year of my thesis and the final publication. Your expertise and discussions with the experiments really benefitted the work. I would also like to express my gratitude to Dr. rer. nat. Annette Peter (AG Stick, University of Bremen) for help with the CLSM, Ute Helmboldt-Caesar (AG Stick, University of Bremen) for help with the microtome and Petra Witte (AG Petrologie der Ozeankrüste) for making all the SEM sessions fun. I would also like to thank Tina Kühn, Cristian Nuortilla, Christian Ellenberg, Jürgen Horvath and Gabriela Berger for all the help in the lab, SEM sessions, technical support and help with daily needs.

I would also like to thank my students Marina Zilli and Cristiano Enke that have contributed to the work by choosing to complete their internship projects, that have been there at odd times when called for and for all the dedicated efforts during their stays in Germany. A special thanks is dedicated to Jaee Ghawali for being part of the journey, for all the sincere experimental work help even when things did not run smoothly.

This journey would not have been complete without thanking all the colleagues who have been a part of my time at the Advanced Ceramics group. I would like to thank Victor Lauth and Tobias Bollhorst, who I began this journey with, for all the help in the lab and for all the discussions we had. The great discussions we have had during our group meeting sessions with Marieke Hoog-Antink, Jessica Mainardi and Joeri Smits helped in sparking interesting ideas and fun times. Special thanks to Joeri Smits, who has been the funniest office mate and for sharing some wonderful memorable conversations.

Table of contents

Summary

In this thesis, we describe the preparation of Janus particles with face-separated compartments. These are anisotropic spherical colloidal particles of the inorganic origin. These compartmentalized particles have unique properties, such as different chemistries designed to specifically target bio applications. Biofunctionalized Janus particles with tailored surface chemistry in general have been gathering interest. The dual nature of the surface chemistry of Janus particles can be exploited to immobilize drugs, cell surface targets, and/or other functional molecules on both sides of the particle surface.

There have been several reports and studies based on the preparation of Janus materials including several shapes and materials along with their widespread applications since a few years. The use of micro-sized particles with unique "Janus" character has been widely exploited over the years. However, there are certain limitations pertaining to the use of micro-sized particles when bio applications are concerned. In addition, there is a limited amount of research performed with nano-sized particles exhibiting the "Janus" character and their bio applications. In this thesis, we adapted the current state of the art to synthesize nano-sized Janus particles in bulk-quantities and used these particles to demonstrate bio applications including dual protein functionalization, agglomerate-free bacterial separation from mixtures and attachment to the cell surfaces of eukaryotic cells with minimal uptake.

First, we established a model system for the scalable preparation of nanoscale Janus particles with dual protein functionalization with the proteins ferritin and streptavidin. We used 80 nm silica NPs (SiNPs) modified with azidosilane to prepare Pickering emulsions with molten wax as the droplet phase. The azide-functionalized SiNPs on the Pickering emulsion droplets were further subjected to face-selective silanization with biotin-polyethylene glycol (PEG) ethoxy silane. Afterwards, we grafted ferritin on the azide-functionalized side via a click-reaction and the biotin groups were conjugated with streptavidin which was labeled with ultra-small gold NPs. In order to elucidate the advantages and limits of our approach, we performed a detailed characterization of the particles at every process step. The results showed that this method represented a

scalable platform for the versatile preparation of protein- nanoscale Janus NPs that can potentially be used with a wide variety of proteins.

We further took advantage of the established method where protein-protein functionalization at the nanoscale was demonstrated, to prepare Janus SiNPs for bio application on a prokaryote-based system. We presented a scalable method for designing magnetic Janus NPs which are capable of performing bacterial capture while preventing agglomeration between bacterial cells. To this end, we prepared silica-coated magnetite (Fe_3O_4) Janus NPs functionalized with a bacteria-specific antibody on one side and PEG chains on the other, using the established wax-in-water emulsion strategy. These magnetic Janus NPs specifically interacted with one type of bacteria from a mixture of bacteria via specific antigen-antibody interactions. Contrary to bacterial capture with isotropically functionalized particles, the bacterial suspensions remained free from cell-NP-cell agglomerates owing to the passivation coating with PEG chains attached to the half of the magnetic NPs pointing away from the bacterial surface after capture. Selective magnetic capture of *Escherichia coli (E.coli)* cells was achieved from a mixture with *Staphylococcus simulans (S.simulans)* without compromising bacterial viability and with an efficiency over 80%. This approach is a promising method for rapid and agglomeration-free separation of live bacteria for identification, enrichment and cell counting of bacteria from biological samples.

Furthermore, after the successful preparation of Janus NPs for the selective capture of bacteria, we prepared Janus NPs that are designed for the attachment to eukaryotic cell surface molecules with minimal cell uptake. To this end, we synthesized rhodamine-doped SiNPs functionalized with 1,2-Distearoyl-sn-glycero-3-phosphoethanolamine (DSPE) on one hemisphere of the NP surface and high-molecular-weight long-chain PEG on the other one using the wax-Pickering emulsion technique. NP localization was studied with mouse fibroblasts *in vitro*. In these studies, the Janus NPs were attached to the cell surface and, in contrast to isotropic control particles, only negligible uptake into the cells was observed, even after 24 h of incubation. The study revealed that the prolonged attachment of the Janus NPs is most likely the result of an incomplete macropinocytosis process, and it seems to be independent from caveolae- and receptor-mediated endocytosis. Consequently, by design, these Janus NPs have the potential to firmly anchor onto cell surfaces for extended periods of time which might be utilized in various

biotechnological and biomedical applications like cell surface tagging, magnetic manipulation of the cell membrane or non-invasive drug and gene delivery.

Zusammenfassung

In dieser Arbeit beschreiben wir die Herstellung von Janus-Partikeln, bei denen es sich um anisotrope kugelförmige kolloidale Partikel anorganischen Ursprungs handelt, mit flächengetrennten Unterteilungen. Diese unterteilten Partikel weisen einzigartige Eigenschaften auf, wie z. B. verschiedene chemische Funktionalitäten, die speziell auf Bioanwendungen abzielen. Biofunktionalisierte Janus-Partikel mit maßgeschneiderter Oberflächenchemie im Allgemeinen stoßen auf großes Interesse. Die duale Natur der Oberflächenchemie von Janus-Partikeln kann genutzt werden, um Arzneimittel, Bindestellen für Zelloberflächen und/oder andere funktionelle Moleküle auf beiden Seiten der Partikeloberfläche zu immobilisieren. Seit einigen Jahren gibt es zunehmend Studien, die auf der Herstellung von Janus-Materialien basieren, einschließlich verschiedener Formen und Materialien sowie ihrer weit verbreiteten Anwendung. Die Verwendung von Partikeln in Mikrogröße mit einzigartigem „Janus" -Charakter wurde im Laufe der Jahre in großem Umfang genutzt. Es gibt jedoch bestimmte Einschränkungen hinsichtlich der Verwendung von Partikeln in Mikrogröße, wenn es um Bioanwendungen geht. Darüber hinaus wurden nur begrenzte Forschungsarbeiten mit Partikeln in Nanogröße durchgeführt, die den „Janus" -Charakter und ihre Bioanwendungen aufweisen. In dieser Arbeit haben wir den aktuellen Stand der Technik weiterentwickelt, um Janus-Partikel in Nanogröße in großen Mengen zu synthetisieren und diese Partikel weiter zu verwenden, um Bioanwendungen zu demonstrieren, einschließlich dualer Proteinfunktionalisierung, agglomeratfreier bakterieller Trennung aus Bakteriengemischen und Anlagerung an den Zelloberflächen von eukaryotischen Zellen mit minimaler Aufnahme. Zunächst haben wir ein Modellsystem für die skalierbare Herstellung nanoskaliger Janus-Partikel mit doppelter Proteinfunktionalisierung mit den Proteinen Ferritin und Streptavidin etabliert. Wir verwendeten mit Azidosilan modifizierte 80 nm Silica NPs (SiNPs), um Pickering-Emulsionen mit geschmolzenem Wachs als Tröpfchenphase herzustellen. Die Azid-funktionalisierten SiNPs auf den Pickering-Emulsionströpfchen wurden ferner einer seitenselektiven Silanisierung mit Biotin-Polyethylenglykol (PEG) -Ethoxysilan unterzogen. Danach immobilisierten wir Ferritin mittels Klickreaktion auf die Azid-funktionalisierte Seite und die Biotingruppen wurden mit Streptavidin konjugiert, das mit ultrakleinen Gold-NPs markiert war. Um die Vorteile und Limitationen unseres Ansatzes

aufzuklären, haben wir bei jedem Prozessschritt eine detaillierte Charakterisierung der Partikel durchgeführt. Die Ergebnisse zeigten, dass diese Methode eine skalierbare Plattform für die vielseitige Herstellung von Janus-NPs im Protein-Nanobereich darstellt, die prinzipiell mit einer Vielzahl von Proteinen verwendet werden können. Wir nutzten ferner die etablierte Methode, mit der die Protein-Protein-Funktionalisierung im Nanobereich demonstriert wurde, um Janus-SiNPs für eine bestimmte Bioanwendung auf einem Prokaryoten-basierten System herzustellen. Wir haben eine skalierbare Methode für die Herstellung magnetischer Janus-NPs vorgestellt, die in der Lage sind, an Bakterien zu binden und gleichzeitig eine Agglomeration zwischen Bakterienzellen zu verhindern. Zu diesem Zweck haben wir Silica-beschichtete Magnetit-Janus-NPs hergestellt, die mit einem bakterienspezifischen Antikörper auf der einen Seite und PEG-Ketten auf der anderen Seite funktionalisiert sind, wobei die etablierte Wachs-in-Wasser-Emulsionsstrategie verwendet wurde. Diese magnetischen Janus-NPs interagierten spezifisch mit einer Art von Bakterien aus einer Mischung von Bakterien über spezifische Antigen-Antikörper-Wechselwirkungen. Im Gegensatz zum Einfangen von Bakterien mit isotrop funktionalisierten Partikeln blieben die Bakteriensuspensionen frei von Zell-NP-Zell-Agglomeraten. Dies ist in der Passivierungsbeschichtung mit PEG-Ketten begründet, die an einer Hälfte der magnetischen NPs angebracht waren und welche von der Bakterienoberfläche wegzeigen. Das selektive magnetische Einfangen von *Escherichia coli (E. coli)*-Zellen wurde aus einer Mischung mit *Staphylococcus simulans (S. simulans)* erreicht, ohne die Lebensfähigkeit der Bakterien zu beeinträchtigen, und mit einer Effizienz von über 80%. Dieser Ansatz ist eine vielversprechende Methode zur schnellen und agglomerationsfreien Trennung lebender Bakterien zur Identifizierung, Anreicherung und Zellzählung von Bakterien aus biologischen Proben. Darüber hinaus haben wir nach der erfolgreichen Herstellung von Janus-NPs für das selektive Einfangen von Bakterien Janus-NPs hergestellt, die für die Anlagerung an eukaryotische Zelloberflächenmoleküle mit minimaler Zellaufnahme ausgelegt sind. Zu diesem Zweck synthetisierten wir Rhodamin-dotierte SiNPs, die mit 1,2-Distearoyl-sn-glycero-3-phosphoethanolamin (DSPE) auf einer Hemisphäre der NP-Oberfläche funktionalisiert waren, und langkettiges PEG auf der anderen mittels der Wachs-Pickering-Emulsionstechnik. Die NP-Lokalisierung wurde mit NIH 3T3-Mausfibroblasten *in vitro* untersucht. In diesen Studien wurden die Janus-NPs an die Zelloberfläche gebunden und im Gegensatz zu isotropen

Kontrollpartikeln wurde selbst nach 24-stündiger Inkubation nur eine vernachlässigbare Aufnahme in die Zellen beobachtet. Die Studie ergab, dass die verlängerte Anlagerung der Janus-NPs höchstwahrscheinlich das Ergebnis eines unvollständigen Makropinozytoseprozesses ist und unabhängig von der Caveolae- und Rezeptor-vermittelten Endozytose zu sein scheint. Konstruktionsbedingt haben diese Janus-NPs folglich das Potenzial sich über längere Zeiträume fest auf Zelloberflächen zu verankern, was in verschiedenen biotechnologischen und biomedizinischen Anwendungen wie der Markierung von Zelloberflächen, der magnetischen Manipulation der Zellmembran oder der nicht-invasiven Arzneimittel- und Genabgabe eingesetzt werden kann.

Glossary

APTES	(3-Aminopropyl) triethoxysilane
Ab	antibody
AB/AM	antibiotic-antimycotic solution
Au	gold
Az	azide
azidosilane	3-azidopropyltriethoxysilane
B	Magnetic flux density
BSA	bovine serum albumin
BSE	backscattered electrons
$C\equiv C$	acetylene group
CD	cluster of differentiation
COOH	carboxylic acid group
CTAB	cetyl trimethyl ammonium bromide
CFU(s)	colony forming unit(s)
CuAAC	copper(I)-catalyzed azide-alkyne cycloaddition
Cy3	cyanine dye derivative
D	dimensional
D_H	hydrodynamic diameter
DBCO-Cy3	dibenzylcyclooctyne-Cy3
DDAB	didodecydimethylammonium bromide
DDSA	dodecyl succinic anhydride
DLS	dynamic light scattering
DMEM	Dulbecco's Vogt modified Eagle's minimum essential medium
DMP-30	2,4,6-(Tris dimethyl)-phenol
DNA	deoxyribonucleic acid
DSPE	1,2-Distearoyl-sn-glycero-3-phosphoethanolamine
E'	storage modulus (elastic modulus)
E*	complex surface elasticity
E''	loss modulus (or viscous modulus)

E.coli	*Escherichia coli*
EDC	1-Ethyl-3-(3-dimethylaminopropyl) carbodiimide • HCl
EDTA	ethylenediaminetetraacetic acid
EPON™812	epoxy resin
FCS	fetal calf serum
h	hour(s)
H	magnetic force
IGEPAL®CO-520	polyoxyethylene nonylphenylether
K_d	dissociation constant
magnetite	Fe_3O_4 (iron oxide)
magnetite@SiO_2	silica coated magnetite
mPEG	methoxy poly(ethylene glycol)
MTT	3-(4,5-dimethylthiazol-2-yl)-2,5-diphenyltetrazolium bromide
NAD^+	nicotinamide adenine dinucleotide
NADH	nicotinamide adenine dinucleotide (hydrogen)
NH_2	amine group
NIH 3T3	3-day transfer inoculum of 3×10^5 of NIH mouse embryo cells
nm	nanometer
NHS	*N*-hydroxysuccinimide
NMA	nadic methyl nhydride
NPs	nanoparticle(s)
o/w	oil-in-water
OD	optical density
PAA	poly (acrylic acid)
PBS	phosphate buffered saline
PCR	polymerase chain reaction
Pd	palladium
PDI	poly dispersity index
PEG	poly (ethylene glycol)
PI	propidium iodide
PMS	phenazine methyl sulphate
PS	polystyrene

RBITC	rhodamine b isothiocyanate mixed isomers
RH	relative humidity
rpm	rotation per minute
r_H	hydrodynamic radius
RS	reductase system
RT	room temperature
SDS	sodium dodecyl sulphate
SE	secondary electrons
SEM	Scanning Electron Microscopy
S.simulans	*Staphylococcus simulans*
SiO_2	silica
SH	thiol group
SiNPs	silica NPs
SSA	Specific Surface Area
θ_{ow}	contact angle at oil-water interface
TEM	Transmission Electron Microscopy
TEOS	tetraethyl orthosilicate
w/o	water-in-oil
WST-1	water-soluble tetrazolium salt
ZP (ζ)	zeta potential

Nomenclature of Janus particles

For describing the stepwise surface functionalization introduced on the Janus particles, we use the forward slash (/) to denote the segregated sides on a single particle surface and further functionalizations introduced on the respective sides are denoted by using a hyphen (-). For the "Janus azidosilane – ferritin / biotin-PEG silane – streptavidin ", silica particles that have been functionalized on one side with azidosilane followed by ferritin and on the other side with the biotin-PEG silane followed by streptavidin. In case of the "PEG/azide-biotin-streptavidin-antibody(Ab) magnetite@SiO_2" particles, is a silica-coated magnetite particle that has been functionalized on one side with PEG and on the other side with azide, followed by biotin, followed by streptavidin-conjugated antibody. The

"PEG/DSPE" describes a RBITC doped silica particle that has been functionalized on one side with PEG and on the other side with DSPE (the PEG linker between DSPE and the particle surface as well as the 3-aminopropyltriethoxysilane (APTES)-functionalization to attach this PEG linker have been omitted for brevity).

Chapter 1

General Introduction

1. Introduction

1.1 General introduction

The design of different materials with unique properties, structures and functions for different applications has been an interesting field of research. Since several years, macro- to nano-sized materials exhibiting a multitude of functions have gained importance in medical, chemical, electronic and technological applications. Nanomaterials are especially attractive since they exhibit large surface areas when compared to macroscopic materials.

Tunability of properties, functions, shapes, materials make it possible to synthesize nanomaterials of choice. Such nanomaterials are an attractive platform for fulfilling innovative applications. Among a wide choice of materials chosen to synthesize nanomaterials, silica NPs have been widely used over the years. The ease of adjustment of the structural properties of silica makes it possible to immobilize proteins such as antibodies, dyes, lipids and other biomolecules. The alteration of surface properties to introduce new functionalizations using silanization as well as dye- and drug-loading properties are some of the commonly used applications among silica NPs.

Different combinations of materials can be used alongside silica to create engineered materials at the nanoscale along with a different array of functions to fit the needs of specific applications. With the continued development of the nanotechnology-based research, we have come a long way in discovering innovative nanoscale materials. They further have the potential to be applied in real-life scenarios including pharmaceutical formulations, catalysis, and biotechnological processes to name a few.

Anisotropy in materials can be defined as the variation in physical, chemical, or mechanical properties, when observed along different planes of the material. The use of anisotropic colloidal particles has been vastly exploited in the past years. In nanomaterials, the patchy, multicompartment and Janus types of anisotropies are shown in Figure 1-1. Put forth by Du et al., the geometries imparting anisotropy can be chosen

such that either the bulk properties vary, or the surface chemistry can be altered for multifunctionality [1]. Control over the fine tuning of materials to create anisotropies is one of the challenges when preparing anisotropic nanostructures. Shape and property-based anisotropy along with regiospecific surface chemistry anisotropy can also be the grounds for building interesting nanomaterials [1–5].

One such type of anisotropy, namely "Janus" has gained popularity since the past 30 years and has attracted the interest of the colloidal research community. "Janus" is the term derived from the Greek god Janus who has two oppositely directed faces. Uniqueness of the term Janus for modification of materials with opposite features, similar to the Greek god, makes the idea extremely interesting to deploy. Janus materials, therefore, present asymmetric features on face-separated sides making them multifunctional tools for several applications.
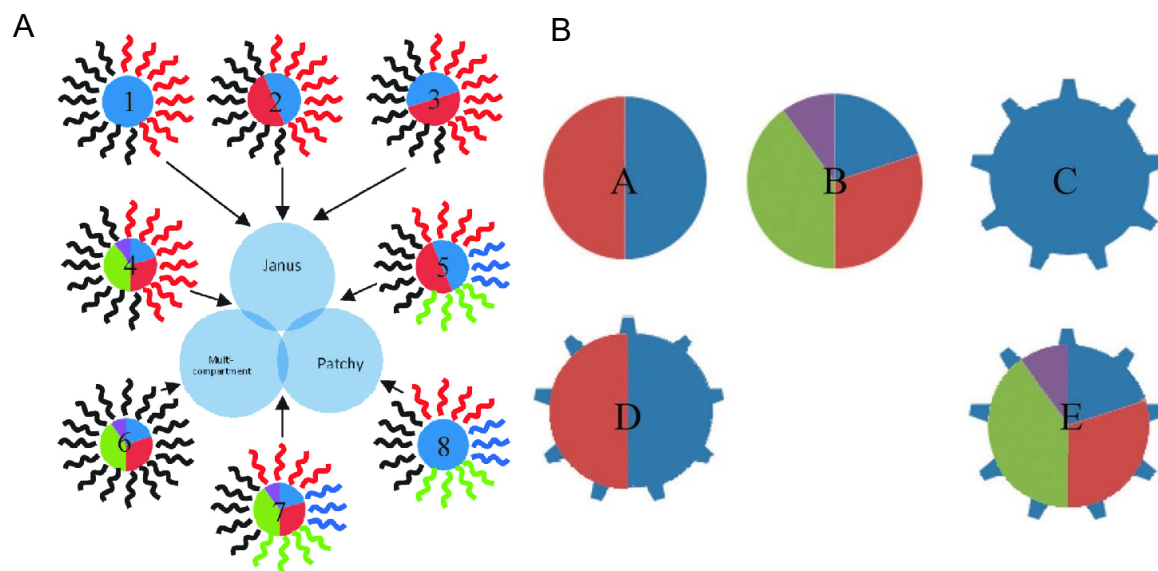
Figure 1-1: Different types of anisotropy: A) (1-3) Janus micelles; (4) Janus multicompartment micelles; (5) patchy Janus micelles; (6) multi-compartment micelles; (7) patchy multi-compartment micelles; (8) patchy micelles. B) Different types of anisotropic particles (A) Janus (B) multicompartment (C) patchy particles (D) patchy Janus particles (E) multicompartment patchy particles. Adapted from [1] with permission from the Royal Society of Chemistry.

In the area of nanotechnology, Janus NPs are nano-sized particles with optical, magnetic, oppositely charged, etc. on the opposite sides of the particle. The presentation of the properties can vary along the different faces of the particle, making the presence of

incompatible properties on a single NP surface possible. Based on the application of the Janus particles, properties for the functionalization on the NP surface can be customized. Various fabrication techniques have been used for the synthesis of the Janus particles.

Theoretically, the general idea of preparation of Janus particles is to mask one-half of the particle and to coat the other half with the property of interest. The process of introducing two separate faces on particles has been realized by methods such as spray coating, metal vapor deposition, polymer-based phase separation and/or microfluidic systems based on biphasic polymer chemistry, all summarized in recent reviews [2,6,7]. Many of these strategies rely on the deposition of particles on planar substrates which inherently allow production of only very limited quantities of particles [8]. While some techniques used to synthesize polymer-based Janus particles are able to yield successfully synthesized particles in large quantities, these methods were reported to work with very specific polymers like block-copolymers, and the resulting soft NPs often lack the flexible surface chemistry of inorganic NPs [9,10].

Another method for Janus particle synthesis is the sputtering method, where particles are attached to a substrate as a monolayer followed by metal deposition on the exposed surface to create half-metal coated Janus colloids [11–13]. This method is commonly used to fabricate micro-sized Janus particles. For hard particles, the Pickering wax emulsion technique introduced by Granick is a particularly promising method in terms of scalability and yield [14–20]. The Pickering emulsion technique is used for masking one of the sides of the spherical particle surface using solid wax and is known to be a scalable method for the preparation of gram quantities of particles and is noted to produce Janus particles even at the nanoscale.

Biofunctional Janus particles are an emerging tool in cell targeting [21,22], imaging [8,23], manipulation of cell immune response [24], and are particularly promising for tailoring cell membrane interactions due to their inherent amphiphilicity [25–28]. For use in applications at the nano-bio interface, Janus NPs need to be functionalized with biological ligands, such as proteins. Homogenous chemical surface functionalization of NPs has been widely reported in the last years with numerous possible industrial and biotechnological applications [9,14,29,30], while combining multiple surface features have recently gained

importance to enable functions such as dual targeting or the combination of properties for both targeting and diagnostics in theranostic nanomedicine [24,31–33].

While the preparation of biofunctionalized Janus particles at the microscale has seen considerable research interest in the last years [14,31,34,35], fewer reports exist on nanoscale Janus particles [6]. Like the particles themselves, this challenge presents two separate faces: first, the initial realization of the Janus aspect by generating two separate sides; second, the utilization of orthogonal methods that allow highly selective functionalization's of the respective hemispheres..

1.2 Aim of the thesis

Several research groups over the years have put forth synthesis techniques for preparation of Janus particles and their applications. However, most of the research groups have demonstrated the successful preparation methods and applications using micron-sized particles. The challenge here lies in producing Janus particles at the nanoscale and at the same time controlling the balance of Janus anisotropy. Additionally, the developed methods of synthesis produce extremely low yields, making these approaches unsuitable for biomedical and technical applications, where the demand of significantly smaller sized particles (less than <1µm) and good quantities exists. Fewer reports exist on the preparation and use of bulk quantities of nanoscale Janus particles for bio applications.

To investigate Janus nanoparticles in a biological setting, we had to choose, adapt and develop the respective synthesis methods. The wax Pickering emulsion technique has been reported to yield Janus particles in large gram quantities and therefore it was used throughout this thesis.

To achieve this goal, we focused on the preparation of Janus particles using the introduction of Janus character via bio functionalization. Here, we formulated design strategies to graft two different functional groups on the same NP surface, which is a challenge on its own. We took advantage of the introduced functional groups to further functionalize two different proteins on the particle surface and therefore establish anisotropy using biofunctionalization. We took a step further using the established

protocol with dual biofunctionalized NPs, to design Janus particles that selectively separate a single bacterial species from a two-bacteria mixture. The functional groups introduced on inorganic SiNPs with a magnetic core, were specifically chosen to fulfil the purpose of prevention of agglomeration at the same time as selective separation of the bacterial species. And finally, we introduced a synthesis protocol for Janus NPs with capabilities to attach to eukaryotic cell surfaces over an extended period of time without undergoing endocytosis for up to 6 hours. The nanosized inorganic Janus particles were doped with a dye and remained attached to the surface of fibroblasts, the model cell type used in this thesis to evaluate the persistent attachment of the NPs. The design strategy of the particles in this thesis was primarily aimed at tailoring surface properties of inorganic silica particles at the nanoscale and fulfilling the bio application that we envisioned.

1.3 Thesis overview

This thesis is divided into 6 chapters. The introduction of the thesis gives an overview of the unique features of the Janus particles and their versatile applications in different fields. This chapter also introduces the aim of the thesis including the motivation behind the research performed. Chapter 2 summarizes the up-to date literature on the Janus particle research, an overview of the multitude of synthesis techniques used for the preparation of the Janus particles, the interesting properties functionalized on the particle surfaces and subsequently their potential bio applications. This chapter gives an insight into the wide-spread popularity of Janus particles within the nanotechnology research community and the advantages of using such particles as biomaterials. Chapter 3 describes in detail all the methods used in the thesis, including the original synthesis technique for Janus particles that was adapted and further developed in this thesis as well as the methods used to confirm the successes of the proposed potential bio applications. As starting material, silica particles either commercially purchased or synthesized have been used and modified according to the required functionalizations and applications. One of the proposed bio applications in this thesis concerning the Janus particles is the functionalization of two proteins on the particle surfaces at the nanoscale. The results have been summarized the Chapter 4 which gives an overview of the synthesis technique and the detailed characterization of the prepared particles. Chapter 5 includes the results

and the discussion concerning the experiments performed using Janus NPs for the selective removal of one bacterial type. The as-prepared Janus particles were applied to achieve a selective agglomerate-free separation of the bacterial species from a two-bacteria mixture. Finally, Janus particles were prepared as potential agents for attachment to the surfaces of eukaryotic cells for prolonged periods of time. The preparation of such Janus NPs as well the results obtained after application of these particles on mouse fibroblasts, has been summarized in Chapter 6.

Chapter 2

State of the art

Parts of this chapter have been adapted from the following publications with permissions from Wiley, the American Chemical Society (ACS) and the Royal Society of Chemistry:

*Kadam.R, Zilli.M, Maas.M and Rezwan.K. „Nanoscale Janus particles with dual protein functionalization" Particle and Particle systems characterization, **2018**, 35, 1700332.*

*Kadam.R, Maas.M and Rezwan.K. „Selective, agglomerate-free separation of bacteria using biofunctionalized, magnetic Janus nanoparticles" ACS Applied Bio Materials, **2019**, 8, 3528-3531.*

*Kadam.R, Ghawali.J, Waespy.M, Maas.M and Rezwan.K. „Janus nanoparticles designed for extended cell surface attachment" RSC Nanoscale, **2020**, 12, 18938-18949.*

2. State of the art

2.1 Introduction to NPs

NPs are ultrasmall entities in the size range from 1 nanometer (nm) to 100 nm (1 nm = 10^{-9} m). According to the International Organization of Standardization in 2008, an entity can be termed "nano" if all three dimensions of the object according to the Cartesian system are below 100 nm. However, a revised definition was then provided in 2011, wherein nanosized objects can be classified, if any one of the Cartesian dimension is under 100 nm [36,37]. According to that definition, objects possessing the characteristic dimensions ranging from 1 nm - 100 nm can be termed as "nano" [38]. Colloidal particles are solid particles of the inorganic, metal, glass, or polymer origin that are suspended in liquid [39]. Properties such as particle size, shape, surface charge, crystallinity, material are some of the deciding factors when a colloidal dispersion is studied. All the factors can be fine-tuned, thus making it possible to prepare colloidal dispersions from a variety of materials with interesting properties. Such colloidal dispersions consisting of particles of various sizes and shapes are used for applications in the areas of material sciences, food, cosmetics, electronics, medicine among several other applications [40,41].

NPs are attractive compared to their large-scale counterparts. Specially, when compared to larger micro-sized particles, they project a higher surface area-to-volume ratio [42,43]. Keeping in mind that the rate of a chemical reaction is directly proportional to the available surface area of the reacting material [44], NPs used in such reactions are favored compared to micro-sized particles.

NPs have been used for applications such as biological sensing, recognition, delivery of drugs and for bioimaging purposes. In the field of pharmaceuticals, the first nanotechnology-based pharmaceutical was approved in the 1990s [38,45]. Uses of nanomedicine-based research has been aimed at producing nanomaterials and nano instruments as biosensors, in the field of molecular genetics, proteomics and making use of NPs for the rapid diagnosis of diseases for therapy [46]. Other popular uses of nanomedicine include drug delivery, theranostics, tissue engineering and magnetofunction [47]. Small hollow nanosized vesicles called liposomes decorated on

their surfaces using ligands such as proteins, peptides, and carbohydrates are loaded with active substances and are now being increasingly used to attack pathogens, viruses and tumors without affecting the neighboring tissue. Liposomes are also gaining importance as attractive nanomedicines due to features such as biocompatibility, small size, freedom to load active substances of choice, biodegradability, low toxicity to name a few [48,49]. Other examples of nanomedicine such as micelles and some specific polymers are also popular and can be used for the transport of active substances [47].

Since several decades, advanced research is being made wherein NPs are applied to combat cancer. Pedziwiatr-Werbicka et al., reviewed the research including the use of unique NPs for tackling cancer and describing the 7use of NPs as effective nanomedical tools for anticancer therapy by means of anti-cancer drug encapsulation [50]. Using such loaded NPs is aimed to increase the targeted delivery of the drugs and significantly decrease the potential side-effects of the drugs in use. This targeted delivery also ensures the aimed supply of the drug to the desired organ or body part. Review articles exist that summarize the advantages of using NPs in cancer treatment [51–53]. NPs have been popular materials for drug delivery. The encapsulation of drug molecules within NPs is beneficial for their targeted as well as controlled delivery of the drug molecules. Reports have shown that drug encapsulation tends to improve their pharmacokinetics, biodistribution as well as their efficiency. NPs can be fine-tuned to project selective target specific ligands, increased half-life in *vivo*, effective payload delivery and efficient drug loading characteristics. Experiments showed that NPs are beneficial in protecting the structural and chemical properties of the encapsulated drugs in *vivo*. [54] The use of NPs as effective drug delivery agents for maximizing the therapeutic benefit of the encapsulated agents has been a popular method of choice over the years[55–57].

However, using nanomaterials for biomedical applications entail certain challenges. Designed NPs for targeted delivery need to be agglomerate-free and target specific. Since the discovery of protein corona, there have been questions regarding the effectivity of the use of nanomaterials for cancer therapy and other diseases. The protein corona has known to render particles ineffective for their targeted use. [58] Other factors such as long-term storage and the stability of nanomaterial formulations has also to be taken into account when using NP based therapy for diseases. Results obtained from *in vitro*

application of NPs lack comparable results when used on in vivo systems making them difficult to be used for clinical trials. The scalability of the intricately engineered particles is challenging and sometimes costly [59]. Along with that, exposure of NPs to biological systems can cause long-term irreversible damages to healthy cells including detrimental effects such as toxicity [60].

De et al., reviewed the use of NPs of metallic, inorganic, polymeric and metallic oxide origin for biological applications. The core material used for NP synthesis can be varied and surface properties can be tuned to engineer them according to the envisioned application [61].
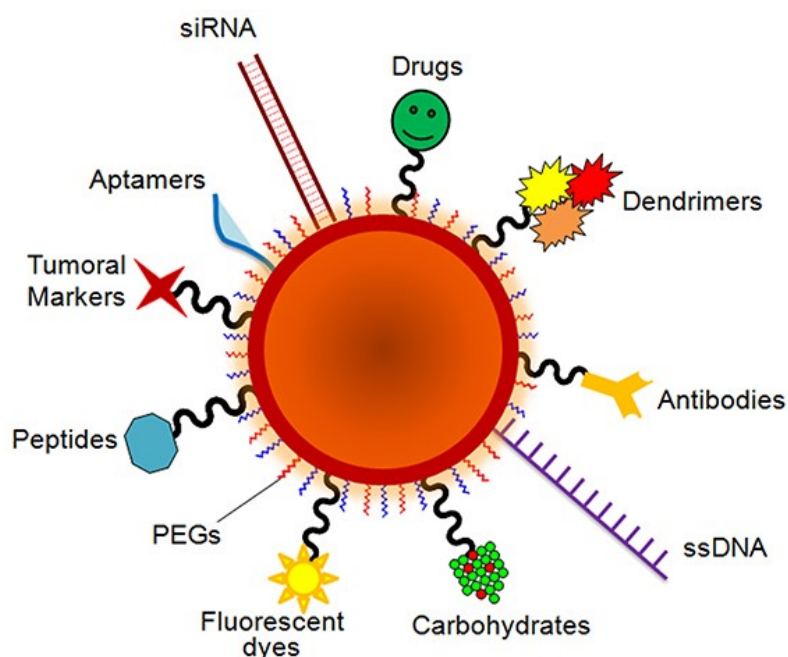
Figure 2-1: Overview of biofunctionalization possibilities on an inorganic NP surface to create a multifunctional particle. Biofunctionalizations make it possible to apply such nanocarriers in applications such as colorimetric probes (carbohydrates), drug delivery agents (drugs, aptamers), tracking and contrast probes (fluorescent dyes), increasing circulation time and decreasing immunogenicity (PEG), gene silencing (RNA, DNA). Reproduced from [57] with permission from Frontiers.

Some popular biological ligands chosen to be functionalized on particles to tune their surface properties include proteins, carbohydrates, deoxyribonucleic acid (DNA), oligonucleotides, peptides, fluorescent dyes, drugs, PEG (Figure 2-1). Such NP-biomolecule conjugates have been applied as agents for transcription- [61,62], gene regulation- [63,64], and enzyme-associated biological reactions [65,66].

2.1.1   What are Janus particles?

Discovery of materials with interesting properties both surface and physical properties has been given significant importance in the last years. The bottom-up approach of designing materials using smaller interesting building blocks has been a popular choice for nanotechnology-based research all around the globe. The idea is to use smart engineered NPs preferably with a multitude of properties as building blocks for the design of such materials.

Introduction of different and unique properties, such as optic, magnetic, electric, metallic, polymer, inorganic, organic or biomolecules on particle surfaces makes them widely applicable tools in a broad range of scenarios. A combination of more than one property on the surface of NPs makes them multifunctional and thus applicable for more than one of the desired functions. One such unique way of synthesizing and combining properties on a single material surface is the "Janus" way. This type of anisotropy has been popular in combining more than property on face-separated sides of the surface. Sometimes, the "Janus" type of anisotropy can be used to combine non-compatible properties. Colloidal particles imparting a "Janus" feature can be defined as a particle with different physical or chemical properties, with side-separated distinction. Depicted in the Greek mythology, Janus was the god of beginning and endings, with two faces each facing in the opposite direction and believed to be symbolizing both the past and the future.

Based on this concept, Nobel laureate Pierre deGennes introduced the concept of "Janus" particles in his acceptance speech in 1991 [67]. DeGennes promoted the Janus particles as tools of self-assembly that aggregate at liquid-liquid interfaces and facilitate the interparticle transport of materials through the gaps between the amphiphilic Janus particles that occur between the interfaces. Casagrande and coworkers brought to light amphiphilic "Janus beads" with both opposing hydrophobic and hydrophilic properties on the surface of individual glass beads in 1988, however the speech by deGennes on dark matter in 1991, made Janus particles a popular concept among researchers of the colloid chemistry community [68]. Breaking the symmetry of particles with uniform surface chemistries using additional features on opposite faces of the surfaces, makes Janus

particles capable of performing a combination of roles including cellular targeting [31–33,69], targeted drug delivery agents [22,69,70], biosensors[71], catalysts[72], surfactants [73,74]. (Figure 2-3)
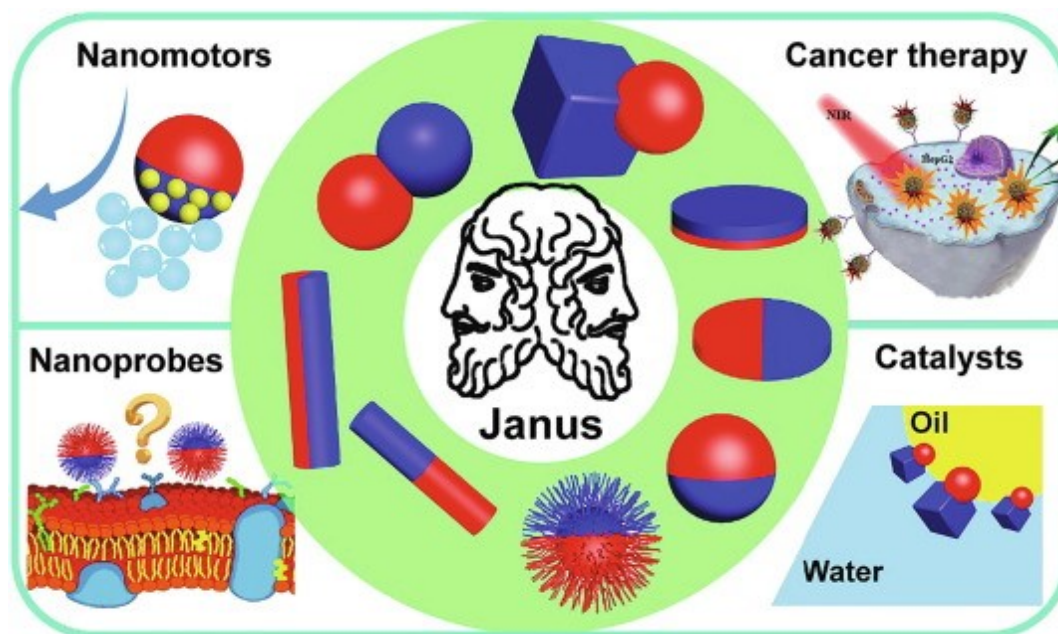
Figure 2-2: Overview of the Janus particles prepared using either separated combinations of properties on a single surface or two particle types fused together (middle), and different applications of the as-prepared Janus particles. Reproduced from [75] with permission from Elsevier.

Concerning the structural build-up of these materials, they can be classified into spherical 3-dimensional (3D), cylindrical (2D), disk-like (1D) type of anisotropy (Figure 2-3).
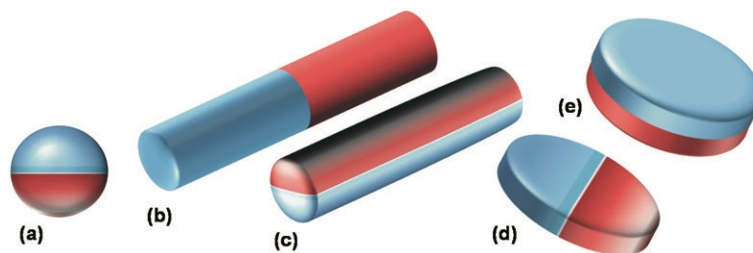
Figure 2-3: Variety of Janus materials based on structural anisotropies. (a) spherical, (b,c) rod-like- (d,e) disc-like-. Reproduced from [3] with permission from RSC.

Since the introduction of the "Janus" idea to the field of colloid chemistry about 30 years ago, the research related to different synthesis techniques, their unique features and

applications in different aspects ranging from bio-sensing techniques to their use as surfactants has gained popularity.

The properties functionalized on the surfaces of Janus particles could be different and moreover even opposing, making such particles unique and interesting materials to work with. Since the introduction of the Janus concept, different materials including micro- and nano- particles with interesting properties and their combinations along with an array of synthesis techniques and thereafter a wide variety of applications have been studied. Such anisotropic particles possessing unique properties capable of interesting applications have been directly compared to their individual traditional homogenous NP counterparts. For example, Janus NPs consisting of functionalized hydrophobic and hydrophilic surfaces within a single NP have advantages compared to homogenous hydrophilic- or hydrophobic particles. Such Janus particles can be directly compared to surfactants to stabilize water-in oil or oil-in water emulsions [70]. Such amphiphilic particles can also be used as platforms for the functionalization of both hydrophilic and hydrophobic drugs and thereafter their targeted delivery [70]. Other such examples include the introduction of optical and magnetic properties on a single particle surface making them controllable via switching optical- and magnetic- fields [76]. Particles consisting of stimuli responsive degradable polymers as separated faces of a particle or their surfaces are useful for controlled drug delivery and for their release purpose triggered by the respective stimuli [69,77–79]. The use of cellular targeting ligands and drug delivery ligands/molecules both functionalized on a single NP surface can be used for targeted drug delivery purposes [28,31,75].

Other interesting properties of Janus particles include their unique aggregation behavior compared to spherical uniformly functionalized NPs. A pH induced aggregation into chain like structures was observed by the polymer-based Janus particles synthesized by Ruhland et al., after they were subjected to pH and temperature changes [80]. This effect was observed due to the combined properties of pH- and temperature-dependency on two halves of nanoscale particles. This unique aggregation was not observed when isotropic particles were studied, thus making aggregation and self-assembly distinct and noteworthy features of such Janus particles.

2.1.2   Synthesis strategies

After the introduction of "Janus" particles by deGennes in 1991, there have been a wide variety of methods chosen to synthesize Janus particles which are multifunctional and present interesting properties with varied sizes, materials, shapes and functions. Some of the methods include lithography [81,82], templating [83,84], partial masking [17,85], microfluidic techniques [76,86] (Figure 2-4) [87]. However, all the methods used till date are based on three basic methods; masking, phase separation and self-assembly [2,88]. Although a wide range of techniques have been employed to synthesize particles from the nanoscopic scale to larger particles, the real challenge in obtaining the "Janus" distinction lies in attaining the exact precision of the Janus balance. The methods entail a fair number of challenges during the synthesis. During the synthesis of Janus particles at the nanoscale, there are a limited number of techniques that can be used to successfully synthesize particles. Along with that the methods are multi-step and successful preparation of Janus particles in bulk quantities are not always guaranteed. Therefore, it is extremely important to choose the right type of synthesis technique when undertaking Janus NP synthesis. The methods used to confirm the success of preparation using experimental methods are sparse [7]. Therefore, it is extremely important to choose the right type of synthesis technique when undertaking Janus NP synthesis. Additionally, techniques such as transmission electron microscopy (TEM) can be used to visualize and confirm the compartmentalization of the particles. For example, Janus particles with two-metallic faces can be confirmed using TEM [89–91].
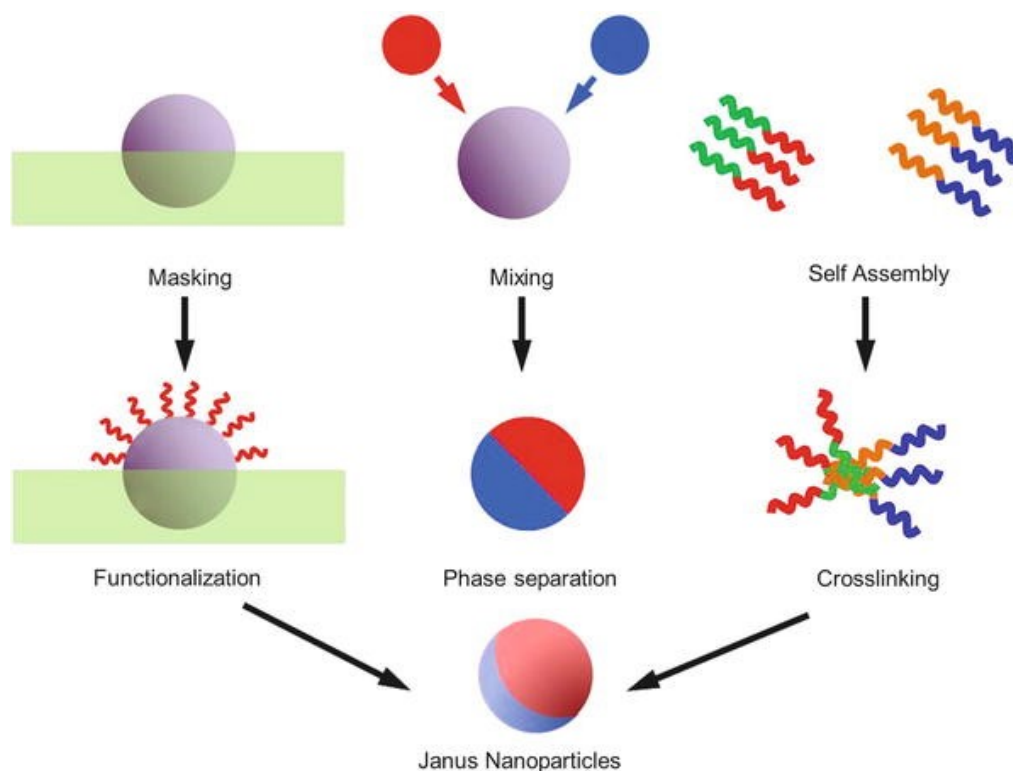
Figure 2-4: An overview of the techniques used for the synthesis of Janus nanoparticles. Reproduced from [88] with permission from Elsevier.

One of the most common strategies for synthesizing Janus NPs is the masking of the particle on one side, and modification of the other exposed surface, with the functionality of interest. The temporary masking from one end of the material is then further used to easily modify the other face of the particle via techniques such as sputtering. Another technique that follows the strategy of masking for Janus particle synthesis is the Pickering emulsion technique. The interface of immiscible liquids such as oil and water that is stabilized at the interface using solid particles is called a Pickering emulsion. [92]There are different steps involved in the modification of particles via masking. i) partial chemical or physical immobilization of particles on a surface. ii) modification using physical deposition techniques such as sputtering or chemical treatment of the exposed surface iii) release of the immobilized particles iv) chemical modification of the other face of the NPs [7].

The method of sputtering based on the strategy of masking has been used in several publications for Janus particle synthesis [12,77]. One of the pre-requisites of the sputtering technique is the need to obtain a closely packed deposited layer of the material of interest.

Wittmeier et al. prepared a closely packed monolayer of silica particles followed by sputtering of the exposed surface using gold (Au) or palladium (Pd) metal vapors (Figure 2-5) [93]. This method of preparation of silica Janus particles with half metal coated layers can be modified to adjust the thickness of the metal layers based on alterations in the sputtering time, the directionality of the coating based on the deposition of the silica particles and the angle in which sputtering is performed [77]. Sputtering has been commonly used to synthesize dual functionalized micro-sized Janus particles, following the above-mentioned steps followed by releasing the deposited particles and specifically modifying the released surface of the particle. Gold particles coated with polystyrene (PS) on one side were prepared using the sputtering method. The polymer coating was then released from the exposed particle side using plasma etching, followed by the selective deposition of (poly(4-vinyl pyridene) (P4VP). The as-prepared PS/P4VP Janus particles exhibited two polymer domains which was confirmed using water contact angle measurement. Preparation of Janus particles using the sputtering method has been frequently used to modify micro-sized particles [7]. The particles need to be spaced out on a flat surface to ensure regular deposition of the property of choice on the exposed particle half , which is challenging, and the bulk synthesis of the Janus particles more than a few milligrams is not possible using this method [7,71,94]. Further studies of the interesting properties and the applications of the Janus particles are restricted due to the miniscule quantities of the produced particles. Along with sputtering, the plasma-etching ligand grafting method is another technique used to synthesize Janus particles. This has been used for preparing micro-sized Janus particles particles and creates binding sites on NPs surfaces using surface plasma treatment. These areas are then immobilized with the desired functional group. Wang et al. used this method to obtain polymer grafted silica particles [95]. To combat the scalability issue from the sputtering technique mentioned above, the Pickering emulsion technique was used for nanoscale Janus particle synthesis [16].
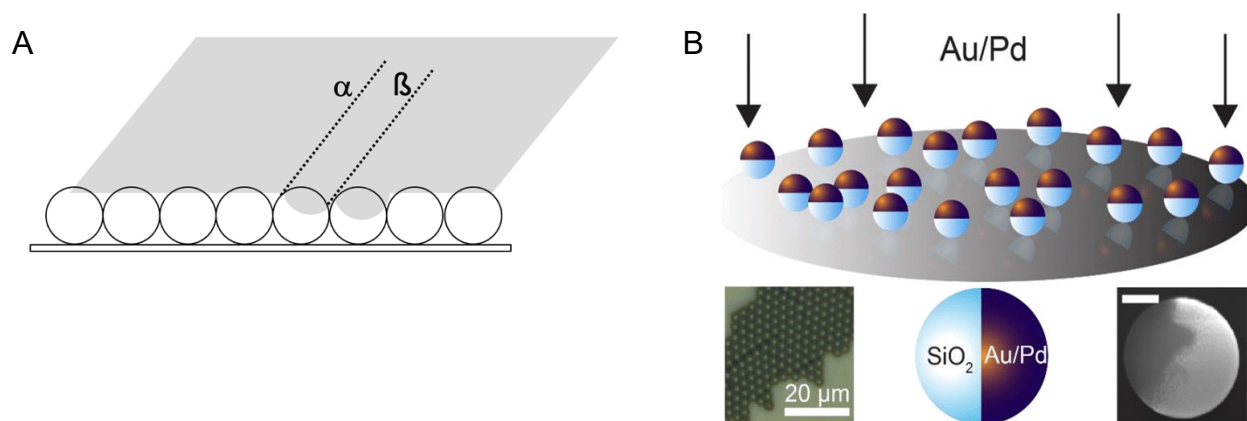
Figure 2-5: (A) Schematic representation of Janus particle synthesis using the sputtering method. Particles on a glass slide are sputtered using metal vapors. Evaporating or sputtering metal onto a monolayer of particles coated onto, e.g., a glass slide. The amount of metal deposition (coated patch on the three particles in the center) to impart the Janus character is determined by the masking to a neighboring particle (dotted line β) and the angle of self-shadowing (dotted line α). (B) Janus particles with silica and Au/Pd halves prepared using the sputter method.(A) Redrawn from [71], (B) adapted from [93] with permission from ACS.

2.1.3   The Pickering emulsion technique – advantages and disadvantages

Compared to a classic emulsion, the Pickering emulsion typically uses solid particles that stabilize the oil-water interface without the requirement of surfactants. Solid particles stabilize the two liquid system and prevent the coalescence of the droplets. The type of emulsion depends on the hydrophobicity or hydrophilicity of the used particles. Other factors such as shape and size of the NPs also play a significant role in the stabilization of these droplets [92]. The method of Pickering emulsion is used for the synthesis of Janus particle synthesis.

Since the method of Janus particle synthesis by partial masking of the particle surface using 2-D immobilization on a flat surface has been frequently used for the synthesis of micro-sized particles and cannot be used to produce larger quantities of particles, an alternative solution of producing oil-in water Pickering emulsions using colloidal particles was proposed by Hong et al. [16].

The problem of active rotation of particles at the interface of liquid/liquid emulsions [96] can be avoided by freezing the particles at the interface followed by modification of the

exposed surface (Figure 2-6). The method introduced by Hong et al., from the research group of S. Granick includes the preparation of oil-water emulsions using molten wax as the oil phase [16]. A diagrammatic representation of the method of preparation is shown in Figure 2-7.
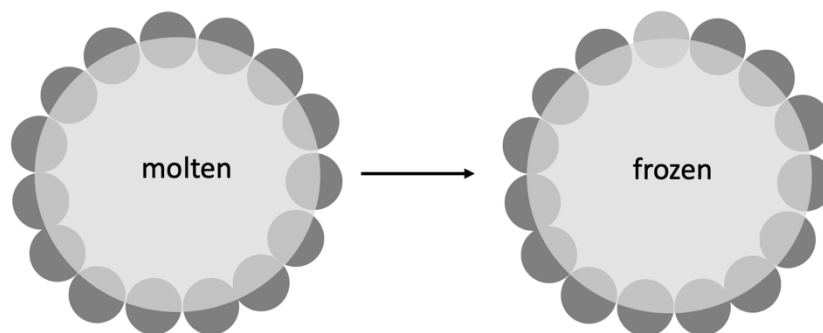
Figure 2-6: Schematic representation of Janus particle synthesis using an emulsion of molten wax and water. These wax Pickering emulsion droplets are stabilized on the surface by inorganic silica particles and further subjected to lower temperatures causing the molten wax to transform into "frozen" droplets, thus resulting in the locking of the particles at the interface. The freezing of the oil phase allowed the manipulation of the exposed surfaces (lighter upper half highlighted in the "frozen" wax droplet- right). Redrawn from [71].

After cooling down the temperature of the molten wax and water emulsion, solid wax droplets were formed with particles locked at the interface and remained partially surface-protected by the wax. A chemical modification was then introduced to the exposed side via the water phase followed by dissolution of the wax to release the Janus particles using cyclohexane. The dissolved wax was then removed. Micron-sized Janus particles with dual properties were prepared in gram-quantities (Figure 2-8). Bipolar Janus particles with cationic and anionic halves using the wax emulsion technique as well as hydrophobic and hydrophilic halves were prepared by Hong et al. [16]. Several groups have thereafter followed the inexpensive, however effective bulk synthesis concept for Janus particle preparation introduced by Granick et al. and presented different modifications on the particles. The advantages of the wax Pickering emulsion technique as highlighted by Hong et al., include the stability of the wax droplets and the retention of the particles at the interface of wax and water phase. This further enables the easy chemical modification of the particles that are not protected by the solid wax droplets. The wax Pickering emulsion technique was also termed effective in preparing stable wax emulsions with smaller nanosized particles and thereafter also for the synthesis of Janus particles [16]. Ever

since, Janus NPs were synthesized using this method with a wide array of functionalities [17,18,89–91,97–101]. Being a rather cost-effective technique using wax wherein good yield of successfully prepared particles is assured, makes this technique popular among researchers synthesizing Janus particles. [102]
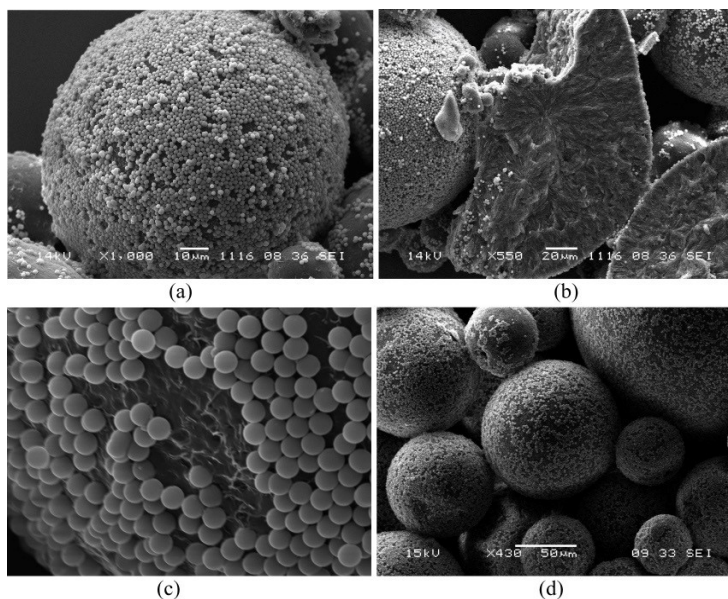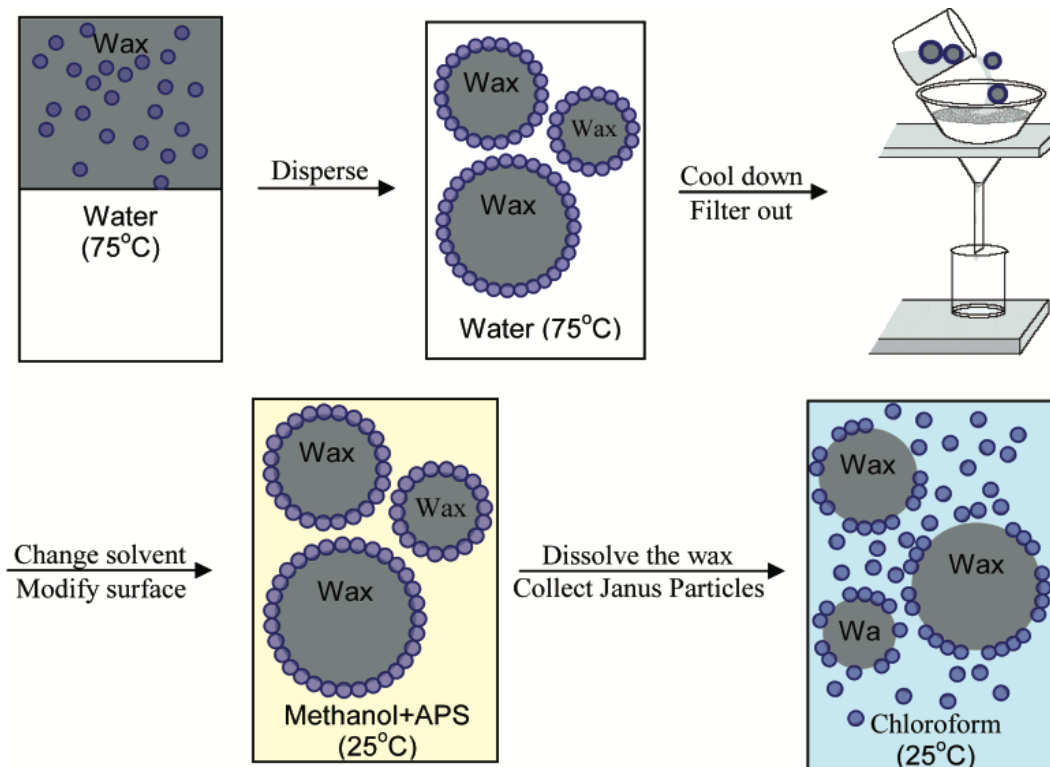
Figure 2-7: Schematic representation of Janus particle synthesis using the molten wax in water liquid-liquid emulsion demonstrated by Granick et al. Wax Pickering emulsion droplets stabilized on the surface using 1.5 μm silica particles. a) scanning electron microscopy (SEM) image of a single micron-sized wax droplet post filtration b) cross section view of the wax droplet c) close-up view showing particles on the outer surface of the solid wax d) large quantities of solid wax droplets decorated with silica particles. Adapted from [16] with permission from ACS.

As demonstrated by Jiang et al., amphiphilic particles were prepared using the wax Pickering emulsion technique, as well [97]. After the preparation of the wax droplets, the solid spheres were then subjected to chemical modification to introduce the Janus character. The adsorption of the particles on the surface of the wax needs to be studied before and after chemical modification. Any losses encountered need to be noted, which is most popularly studied using SEM analyses [16,17,97]. As shown in Figure 2-8, the morphology of the emulsion droplets before and after chemical modification to observe the particle adsorbed on the wax droplets was studied using SEM. It is important to note the presence of the particles after chemical modification to ensure the success of the chemical modification and thereafter the Janus alteration [97].
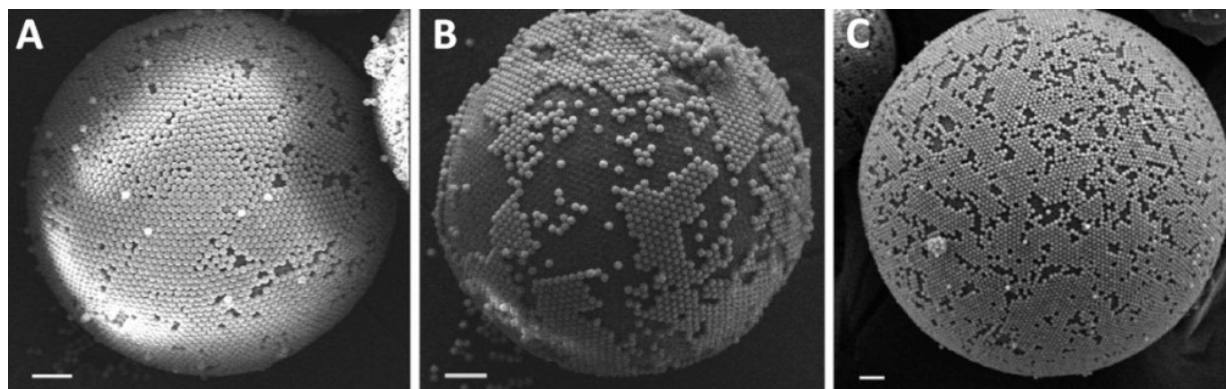
Figure 2-8: SEM images of the wax Pickering emulsion technique used for the synthesis of amphiphilic Janus particles. The outward projecting side of the particles were modified chemically before being released from the wax surface. The morphology of the droplets was analyzed using SEM; A) before chemical treatment B) after chemical modification to render the particles on the solid wax droplets hydrophobic via solvent based modification. C). hydrophobic wax droplets decorated with particles post-chemical modification. Reproduced from [97] with permission from ACS.

In order to successfully functionalize silica particles deposited on the surface of the wax droplets, without causing any potential particle loss, wax droplets were exposed to silane vapors in dry nitrogen or argon gas. The adhesion of the particles to the wax surfaces was observed to be better in case of the solvent-free Janus particle chemical modification compared to the otherwise solution-based modification [97]. The Pickering emulsion technique has been used not only in the case of inorganic Janus particles but also in case of soft particles [74,88,95,98,103]. For example, Berger et al., prepared micrometer-sized

Janus particles with stimuli responsive polymers using the wax Pickering emulsion technique[103].
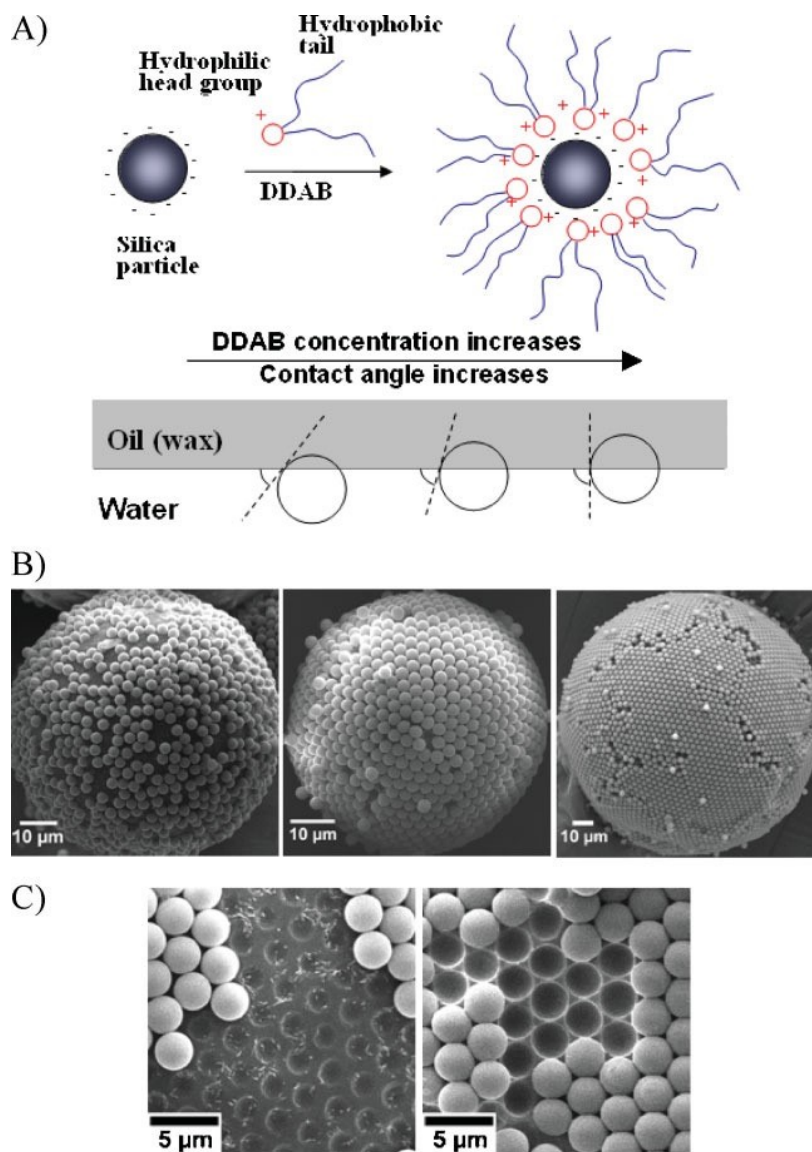
Figure 2-9: Particles at the oil-water interface stabilized using the surfactant didodecydimethylammonium bromide (DDAB). A). By increasing concentration of the DDAB causes silica particles to penetrate deeper into the wax. B). SEM images of the wax droplets synthesized using silica particles combined with increasing concentrations of DDAB (left to right- 0, 20, 60 mg L^{-1} respectively) C). The holes created in the wax surface after particles were washed off, were used to study the contact angle in the presence of 20 (left) and 60 mg L^{-1} (right) of DDAB. Reproduced from [104] with permission from ACS.

The work required to move a dual functionalized hydrophilic-hydrophobic Janus particle present at the oil-water interface into the oil phase normalized to the work required for the

transfer into the water phase was termed as the "Janus" balance for particles by Jiang et al. The balance of the chemical modification on the Janus particles prepared using the wax Pickering emulsion strategy was noted to be dependent on the three-phase contact angle of the particles at the wax-water interface and the geometry imparted on the particles [105]. The three-phase contact angle is the equilibrium contact angle formed at the solid-liquid-gas interface [106]. To understand and study the Janus balance achieved after chemical modification of the particles, it is important to study the three-phase contact angle. This was done by Jiang et al., wherein, the holes created by the particles, after they were removed from the solid wax droplet surfaces, were studied and the contact angle was determined. Those voids can also be used to study the variation of different parameters during the emulsification process, for example variation of surfactant concentration (Figure 2-9).

Addition of a surfactant that is oppositely charged compared to particle surfaces can be used to alter the three-phase contact angle [107]. As shown in Figure 2-10, if the contact angle (θ_{ow}) of the particles at the oil-water interface is <90°, a larger portion of particle remains in the aqueous phase compared to the oil phase. In case of hydrophobic particles with θ_{ow}>90°, larger portion of the particle remains in the oil phase. When surfactants are added into such an emulsion system, the otherwise planar oil-water interface, would be curved aiding emulsion formation [107]. Based on the θ_{ow}, the larger portion of the particles remains on the outside of the curved interface, which determines the type of emulsion. In case of the hydrophilic particles (θ_{ow}<90°) and hydrophobic particles (θ_{ow}>90°), oil in water (o/w) and water in oil (w/o) emulsions were formed respectively [104,107]. Studies have showed that altering the concentration of the surfactants during the emulsification process has an impact on the packing of the particles on the emulsion droplets. Electrostatic repulsion of the particle surface charge is screened due to the addition of the oppositely charged surfactant which leads to close packing of the hydrophobized particles. Variations in surfactant concentrations and thereby alterations in the contact angle have also caused better adsorption of otherwise hydrophilic particles at the interface [17,99,104,108]. As shown in Figure 2-9, variation in the DDAB surfactant concentration caused better embedding of the particles in wax. Surfactants that are oppositely charged compared to the particles have been used to successfully prepare wax Pickering emulsions, however, such effects were not observed when similar charged- or

neutral surfactants were used. This effect was caused due to no significant contact angle alterations observed while using such surfactants. This can be attributed to low surfactant-particle adsorption when neutral and same charge surfactants were used. Accordingly, oppositely charged surfactants can be used to prepare nanoscale particle stabilized wax-water emulsions and thereafter also for their Janus modification [17,89–91,95,99,104].
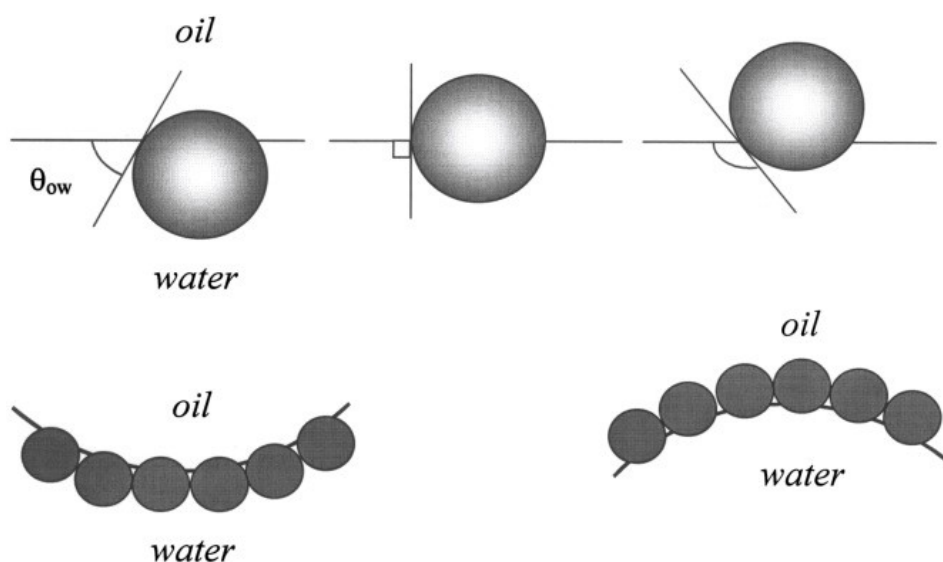
Figure 2-10: Diagrammatic representation of the contact angle (θ_{ow}) measurement of a spherical particle at a plane oil-water interface θ_{ow} <90°(left), exactly 90° and >90°(lower) particles, based on the θ_{ow}, at a curved oil-water interface. The θ_{ow} determines whether o/w- or w/o emulsions are formed. Reproduced from [107] with permission from Elsevier.

In this thesis, the method of Janus particle preparation using the wax Pickering emulsion technique and was chosen due to the following advantages:

1) This method is scalable, and up to gram quantities of Janus particles can be obtained using the wax Pickering emulsion technique.
2) Despite being a multi-step modification method, this method is cheap and is found to be an effective method of synthesis.
3) By varying the amounts of surfactants used during the synthesis, the contact angle of the particles at the wax-water interface can be varied and therefore the Janus balance can also be altered.

4) a multitude of chemistries according to the function of choice can be immobilized on particle surfaces providing a basis to obtain versatile multifunctional Janus particles. Initially, the method was proposed for the preparation of amphiphilic particles [16] and has now been extended to the preparation of Janus particles at the nanoscale and with a combination of functions ranging from effective surfactants, catalysts to cell labelling and drug delivery.

Along with the advantages, certain disadvantages of the wax Pickering emulsion technique for Janus particle preparation method should also be noted:

1) There is less control over the Janus balance.

2) This is a multi-step method, which is also time- extensive.

3) The wax Pickering emulsion technique is not particularly costly however, it depends on the intended functionalization for the introduction of the Janus character.

2.1.4   Tailoring surface functionalization

In the field of chemistry, surface functionalization can be defined as the introduction of new chemistries, functionalities, properties or features on a material surface. Tailoring surface properties of materials can be used for increasing biocompatibility, adding functionalities as well as increasing stability of materials. Materials such as NPs are versatile materials used to introduce additional functionality using tailored surface functionalization [109–113]. Tuning surface properties of SiNPs using functionalization can further be used for the conjugation of biomolecules such as proteins [89,114,115], other fluorescent molecules [22,116,117], peptides [118–120], antibodies [90,91,121,122] as well as for the attachment to bacteria [90,123–126] and viruses [127,128]. Tailoring surface properties has been a popular method of choice to create multifunctional NPs. NPs have been commonly conjugated with functional groups such as amine (NH_2) [91,112,129–131], carboxylic acid group (COOH)[129,132,133], thiol (SH)[134,135], azide(Az) [89,136,137] to name a few. Positively charged NPs prepared using amine group functionalization can be used to further conjugate negatively charged carboxylic acid groups present on other molecules or particles via non-covalent electrostatic interactions. Similarly, negatively charged particles can be also be used to attach positively charged particles.

NPs have been frequently used for the functionalization with biomolecules such as proteins[34,89,114,132,138]. Several different types of forces of interaction such as van der Waals, electrostatic and ionic play an important role during the bioconjugation of NPs with proteins and other biomolecules and can be functionalized onto NPs using charge modification and electric potential alteration. Alteration of the pH of an incubation solution according to the protein's isoelectric point to tune the net overall charge of the protein is a technique popularly used to attach proteins onto NPs. The interactions of such biomolecules with material surfaces cannot be understood completely, however, certain factors such as surface chemistries of the material and density and type of the functional groups are some of the key deciding factors that influence the success of functionalization [112,133]. When protein interactions with materials and surfaces are studied, emphasis has been given to the understanding of different forces that come into play. Material surface chemistry as well as the protein orientation need to be considered when biomolecule conjugation onto NPs is done. Microparticles and NPs are commonly used materials of choice for the functionalization of different proteins. Protein functionalized particles have further been used for applications in the field of medicine as drug delivery agents, sensors, pharmaceuticals and in bioreactor systems to name a few [22,55,115,138].

2.1.4.1   Functionalization strategies for nanoparticles

In this thesis NPs were functionalized with azide, biotin, amine and carboxylic acid groups according to the choice of the Janus features and the bio applications envisioned. A general introduction into the chemical reaction for the introduction of the chemical functionalization is presented in the forthcoming subsection, the detailed procedure of each functionalization is introduced in chapter 3 and the results of their characterization are shown in chapters 4, 5, and 6.

There are different strategies to couple biomolecules onto NPs. The choice of chemical functionalization is dependent on the application intended and the chemical makeup of the NP surface. There have been many publications describing different functionalization strategies. Non-covalent coupling including electrostatic binding, physical adsorption, hydrophobic coupling, biotin-avidin as well as covalent coupling including carbodiimide

reaction, click chemistry, maleimide coupling reactions are up-to-date known methods to introduce biofunctionalization on particles.

Physio adsorption of organic groups on the surface of SiNPs would eventually lead to desorption of the functionalized groups in ionic liquid environments. One of the commonly used approaches to avoid any unstable functionalization is using silanization. Silanization is popularly used for immobilizing functional groups on SiNPs. Silanization is the method of surface functionalization using alkoxysilane molecules with organofunctional groups [112,129,139–142]. Due to a displacement reaction between the hydroxy groups on particles and alkoxy groups on the silane to form a covalent bond -Si-O-Si-, surface modification of SiNPs is possible (Figure 2-11).
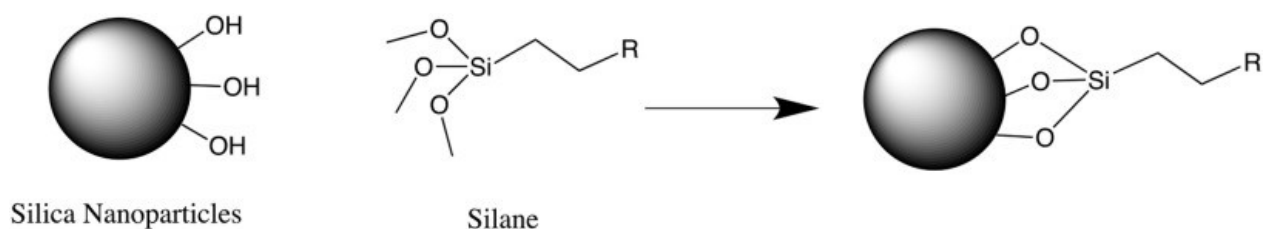
Figure 2-11: General scheme of surface modification of SiNPs using silanization. Silica NPs are subjected to silanization using a silane containing the functional group "R". Hydroxy groups on the surface of the particle react with the alkoxysilane groups on the silane yielding surface modified silica particles with the functional group "R". Reproduced from [143] with permission from Elsevier.

This method has been commonly used to introduce specific functionalization on materials and popularly on SiNPs in the past years. In this thesis we have designed experiments to introduce different functionalization on the specific halves of the particles to impart the Janus character. Based on this approach, we purchased silanes with the respective functional groups of choice. We also used already established methods to introduce functionalization and adapted it according to the application intended. We grafted our particles with azide, biotin, polyethylene glycol (PEG) and amine to further immobilize other biomolecules such as proteins and antibodies.

2.1.4.1.1   Azide

Azide functionalization has been commonly used for conjugation with other molecules with either acetylene ($C\equiv C$) or thiol (SH) groups via copper-mediated or copper-free click chemistry technique respectively [144]. The term click chemistry introduced by Sharpless

et al. in 2001 is a one pot chemical reaction between azide and alkyne groups performed at room temperature (RT) and in aqueous solutions [144]. Click chemistry is commonly used for bioconjugation between the two reactive groups. The azide-alkyne click chemistry reaction used in this thesis requires the presence of copper as a catalyst for the success of the reaction and is commonly termed as Copper(I)-catalyzed azide-alkyne cycloaddition (CuAAC). A schematic representation of the reaction is shown below (Figure 2-12).
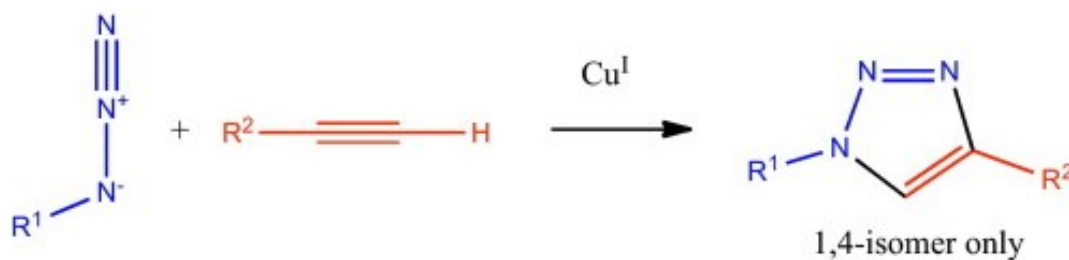
Figure 2-12: Copper catalyzed reaction between azide and acetylene groups termed as CuAAC. The final product is a 1-2-3 triazole compound and is commonly used for the coupling of NPs and biomolecules. Reproduced from [145] with permission from Elsevier.

This chemical reaction is highly specific and is often used in reactions involving drug discoveries, proteomics and bioconjugation reactions. The triazole biproduct formed using the click reaction can further react with other biomolecules and cell targets via hydrogen bonding and dipole-dipole interactions. Thus, the CuAAC plays a significant role in functionalization reactions and further for drug delivery based discoveries [146].

2.1.4.1.2   Biotin

Another type of functionalization is the NP surface modification using biotin [57,72,147]. Biotin is a vitamin present in several living systems and playing an important role in the day-to-day functioning of the regulatory processes. Biotin itself is a small molecule and is well known for its affinity to streptavidin. This affinity reaction can be used for specific conjugation to other proteins such as antibodies, thus making it an excellent component of detection assays often used in biochemistry. In nature, the biotin-streptavidin non-covalent reactions are widespread, highly specific and observed to occur in several biological reactions. Biotin attached to a molecule also called as a biotin tag is often used in combination with biotin-binding proteins in applications such as affinity purification of

the molecule, co-immunoprecipitation, pull-down assays, enzyme-linked immunosorbent assay (ELISA). Since the reaction between biotin and the biotin-binding proteins is extremely specific, biotin functionalization is considered advantageous in several experiments. There are several commercially available biotin-labelling assays, biotinylated proteins and biotin-silanes [57,109,148]. Aslan et al., studied the induced aggregation of biotin functionalized gold NPs in the presence of streptavidin with potential application in the development of colorimetric assays for DNA hybridization detection, immunoassays assays and understanding the controlled assembly of NPs [147]. Keeping in mind the advantages of the biotin-functionalization strategy, we used biotin-silanes in this thesis to functionalize the different SiNPs. The biotin-silane modified NPs were further attached with streptavidin-labelled proteins to get protein functionalized NPs.

Chemical functionalization of ligands on the surface of pre-synthesized particles have been often used for applications including targeted drug delivery and cell tagging. Modification of NPs with the ligand of choice using chemical coupling reaction are often known to be expensive however ensures the success of functionalization. Using silanes coupled with the required functional groups and following established methods of silanization can yield particles modified with the ligand of choice. One such commonly used ligand for tumor targeting, targeted drug delivery functions and theranostic agents in cancer therapy is biotin [72,112,148,149]. Biotinylation of NPs can also be achieved using commercially available constructs with the choice of functional groups and biomolecules of interest. An antibody combined with spacers such as long chain PEG also with functional groups such as primary amine is one such example. Biotinylated gold NPs were prepared using carboxyl group functionalized particles in the presence of (+)-biotinyl-3,6,9-trioxaunddecanediamine and the functionalization was confirmed using aggregation caused due to interaction with streptavidin (Figure 2-13) [147].
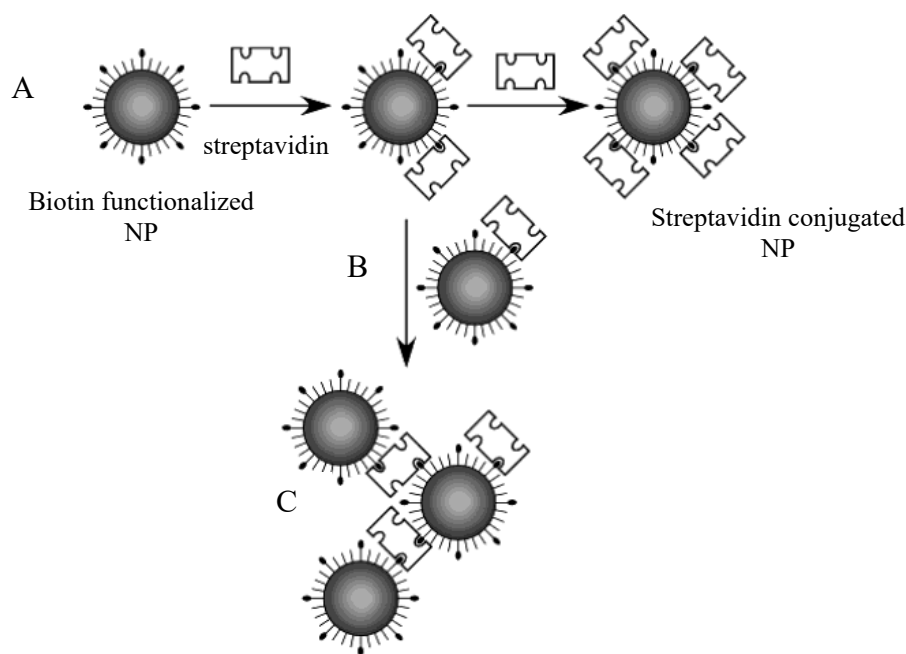
Figure 2-13: Schematic representation of the biotin functionalized NPs interacting with streptavidin. (A) Due to the specific interactions between biotin and streptavidin, biotin functionalized NPs incubated in the presence of streptavidin yield NPs decorated with streptavidin (B). The coverage of the streptavidin on the NP surface can either be monolayer (B) or can bind with other biotin functionalized particles further leading to aggregation (C). Reproduced from [147] with permission from ACS.

The streptavidin-biotin reaction is of high specificity and has a dissociation constant (K_d) around 10^{-14} [150]. Another protein, avidin, is also known to show affinity to free biotin molecules. Both biotin-avidin and biotin-streptavidin reactions are well known in biochemistry. Biotinylated NPs can also be biofunctionalized with avidin conjugated proteins, for example, to prepare protein functionalized NPs. Biosensors prepared using biotin have made the detection of molecules much easier due to the specific biotin-avidin interaction [72,147]. The isoelectric point of avidin is 10 [150]. Even though biotin-avidin reactions are known to be specific, the pH of the solution and the high isoelectric point of the glycoprotein avidin may cause unspecific interactions between the components of the reaction mixture. Hence another related molecule, streptavidin has also been a popular choice when studying biotinylation of a NP. Streptavidin produced from *Streptomyces avidnii*, unlike avidin, is not a glycoprotein and has an isoelectric point of 5-6. Therefore, the problem of unspecific interactions in the case of streptavidin are sparse. Additionally, the structure of avidin as well as streptavidin have 4 binding sites for biotin [150].

In this thesis, biotinylated SiNPs were incubated in the presence of streptavidin functionalized proteins and antibodies for the purpose of biofunctionalization of NPs.

2.1.4.1.3   PEG

In applications including drug delivery and targeted cell therapy, it is necessary for the particles to circumvent macrophage-based uptake, increase circulation time and to have a longer plasma half-life. To fulfill all such functions, particles are often functionalized with long polymer chains of poly- (ethylene glycol). Along with the above-mentioned advantages, PEG functionalization has been known to prevent the binding of other proteins present in the circulation system termed the "protein corona" formed around particles designed for *in vitro* and *in vivo* applications by creating an inert hydrophilic layer around NPs [57,58,129,138,151]. Steric hindrance provided by PEG functionalization is known to prevent binding of other biomolecules in the circulation system. Functionalization of PEG on NPs requires choosing the density of PEG groups which also contributes to the colloidal stability of the particles [149,152].

Difference in the uptake of the particles by macrophages *in vitro* was observed based on the length of the PEG chains functionalized on magnetic NPs. Macrophages were incapable of taking up particles with PEG, with molecular weights higher than 3000 Da, functionalized particles [153] and this in turn also increased the half-life of the particles around macrophages [112,153–155].

In some cases, PEG functionalization is carried out using commercially synthesized silanes containing varying molecular weight polymer chains and sometimes as spacer molecules combined with biomolecule moieties as well as a functional group such as amine, thiol etc. Advantages such as increased circulation time of the functionalized particles and prolonged half-lives were recorded irrespective of whether the PEG groups occurred on the particles as end groups or as spacers [90,112,155–157]. Certain disadvantages were also recorded. Due to the opposition created by long PEG chains functionalized on NPs, the targeted delivery of therapeutics was affected [158], however, this can be averted by using stimuli based PEG detachment from the functionalized NPs.

2.1.4.1.4   EDC-NHS coupling

For physisorption of biomolecules onto NPs based on electrostatic interactions, negatively- or positively charged molecules can be attached to amine- or carboxylic acid-functionalized NPs. However, carboxylic acid groups in biomolecules can be covalently cross-linked to primary amine groups functionalized on NPs using the carbodiimide chemical linking using the compounds 1-Ethyl-3-(3-dimethylaminopropyl) carbodiimide hydrochloric acid (EDC) and sulfo-N-hydroxy succinimide (NHS) (see Figure 2-14).
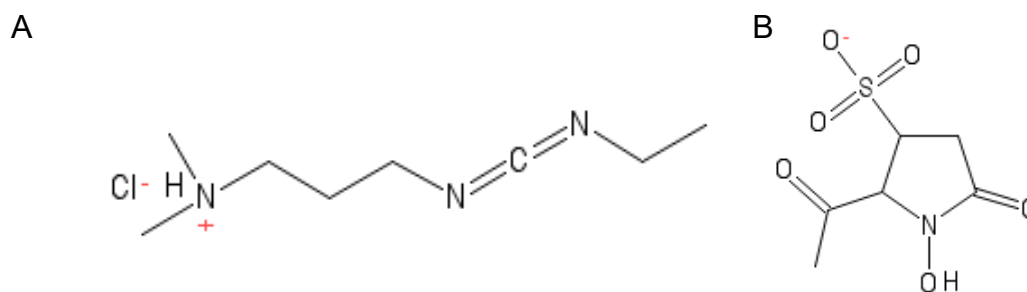
Figure 2-14: EDC (A) and sulfo-NHS (B) used for the covalent carbodiimide coupling reaction of amine groups and carboxylic acid groups.

Functionalization of amine (-NH$_2$) groups is done to impart a net positive charge on the particle surface. Based on the ionic interactions between charged components in the solutions, NPs can be coupled with either other oppositely charged NPs [5,7,159–161] or biomolecules such as proteins [162–164]. NPs functionalized with the transferrin via ionic interactions were used to study their interaction with the blood-brain barrier and tumor cells as potential cancer treatment agents [165].

With intended applications such as self-assembly and aggregation, NPs assembled using the simple ionic coupling strategy can further be used to form macrostructures [5,7,159–161]. The success of the coupling reaction using amine functionalization is dependent on factors such as the available amine groups on the particles, available oppositely charged functional groups, and the overall net charge of the reaction solution. In case of the protein coupling onto NPs via amine functionalization, it is important to note the isoelectric point of the protein and the pH of the solution. The isoelectric point is the pH at which the net charge of the protein is zero [138]. Ionic interactions occur not only between the NPs and

the biomolecules, but also between other components of the reaction system. Hence there are possibilities of some non-specific interactions as well. The adsorption of the proteins onto particle surfaces may also affect the structural properties of the protein. Such structural alterations might in turn disturb the overall functioning of the protein and its biological activity when applications such as cell targeting, and other such functions are considered. Formation of protein coronas are predominantly observed when NPs are present in systemic circulation such as body fluids [58,112,129,133,136]. Hence careful studies of the structure and the required orientation of the biomolecule needs to be done before adopting the ionic coupling method of functionalization. (Figure 2-15)
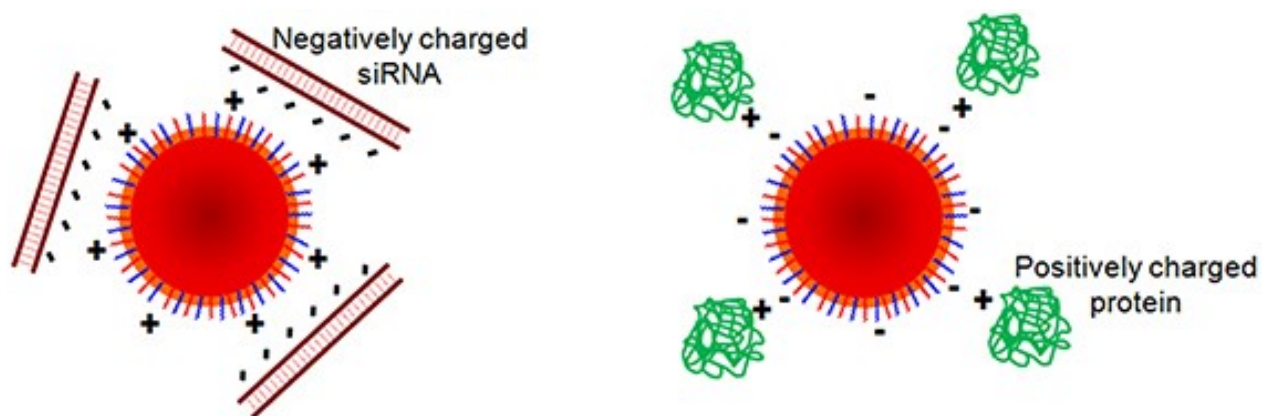
Figure 2-15: Using ionic interactions to immobilize biomolecules onto charged particles. (left) positively charged NP surface coupled with negatively charged small interfering ribonucleic acid (siRNA). (right) negatively charged particles coupled with positively charged proteins. Reproduced from [57] with permission from Frontiers.

The surface functionalization of the NPs with amine groups can be further used to immobilize other biomolecules [91,115,154,166].

EDC is a small molecule that is used to combine functional groups such as primary amines with carboxyl groups and the amine reactive ester formed during the reaction is further stabilized by the presence of sulfo-NHS. Amine groups from proteins, peptides etc. and carboxyl groups have been frequently used to create biofunctionalization on materials. The method is advantageous because reactions can take place in aqueous solutions, the by-products formed can easily be separated from the reaction mixtures by using dialysis or gel filtration [167] and this method is widely applicable for imparting biofunctionalization

using biomolecules such as enzymes, peptides, antibodies on a wide range of materials. Nevertheless, there are certain disadvantages to the EDC/NHS carbodiimide coupling reaction. The reaction occurs fast under suitable experimental conditions to yield an intermediate amine-reactive-sulfo NHS ester, that is crucial for the reaction and can immediately undergo hydrolysis. Along with that, the amount of EDC is calculated such that excess of the compound present in the solution can be avoided. An excess of EDC might affect the stability of the NPs, in turn causing aggregation. The ratio of EDC and NHS also needs to be adjusted for the successful biofunctionalization of NPs using this coupling method [151,154,166,168–174]. An overview of the EDC/NHS coupling reaction commonly used by researchers is shown in figure 2-12 [57].
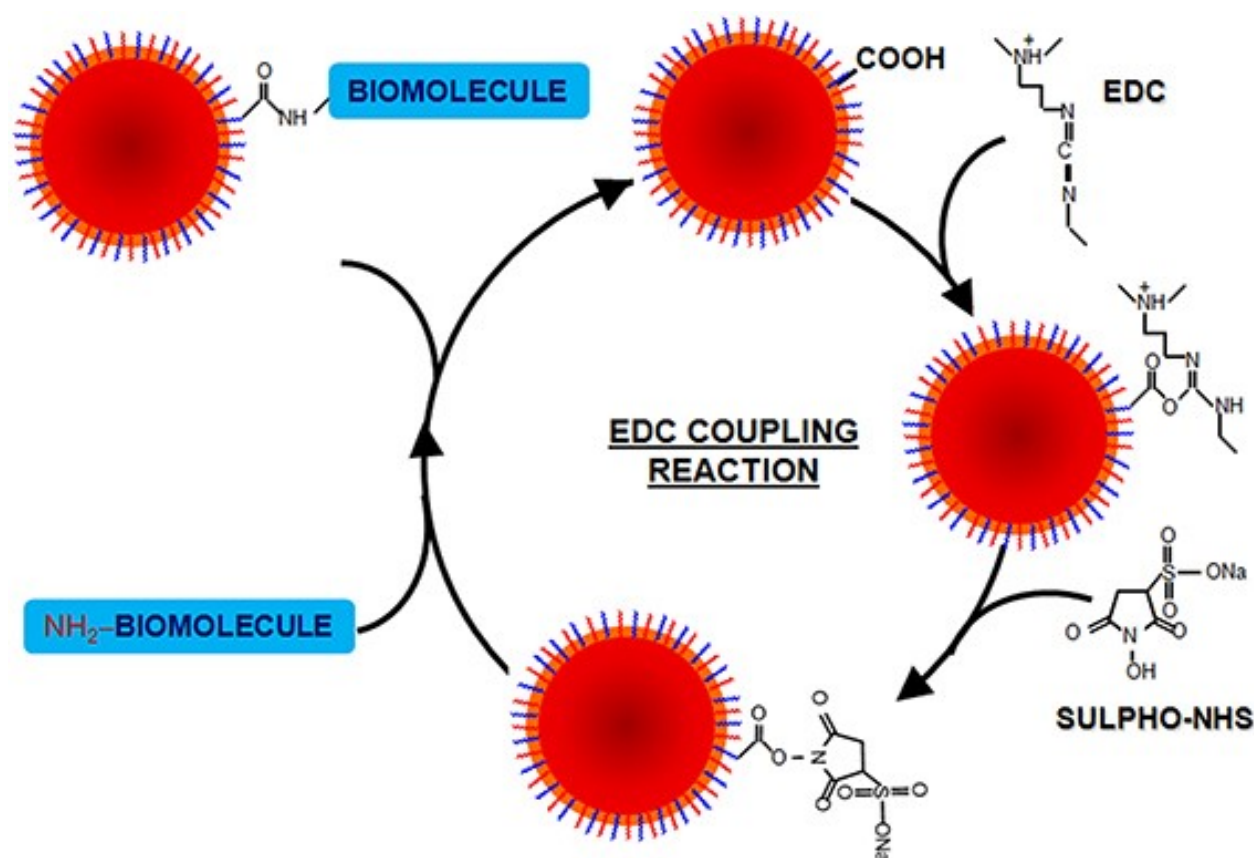
Figure 2-12: Functionalization of a biomolecule with free primary amine groups onto a carboxyl group functionalized NP using the EDC-NHS coupling reaction. EDC in the reaction mixture combines with the carboxyl groups to yield amine-reactive sulfo-NHS. Reproduced from [57] with permission from Frontiers.

2.1.5 Special properties and applications of Janus particles

A combination of the functionalization mentioned above can be used to impart multifunctionality. Multifunctional particles such as the Janus particles have been widely applied due to their face separated opposing properties such as hydrophilicity-hydrophobicity, positive-negatively charged, metallic-non-metallic etc. One striking feature of Janus NPs is the ability of the particles to undergo self-assembly. Lattuada et al, prepared particles that were functionalized with on one side with a pH responsive polymer poly(acrylic acid) (PAA) and the other half with either positively charged polydimethylamino ethylmethylacrylate, a negatively charged pH responsive polymer or temperature responsive poly N-isopropyl acrylamide. These particles were further subjected to temperature changes which caused the particles to undergo random

clustering. Clustering was observed on particles that were functionalized on all the polymer combinations charged polymer combinations, which further affected the particle stability. The combination of uncharged and positively charged particles resulted in the formation of finite clusters whereas uncharged and negatively charged particles caused an increased particle stability when subjected to solutions with varying pH values [175,176].

One of the initial ideas for confirming the preparation of Janus particles was imparting incompatible properties on the NP surface. Rendering the particles amphiphilic by combining hydrophilic and hydrophobic features on the particle surface thus depicting the success of the "Janus" feature was performed by Granick et al., and further followed by several other researchers [16]. Surface active properties of bimetallic Janus particles consisting of gold and iron oxide halves prepared by Glaser et al., were directly compared to isotropic metallic iron or gold particles by measuring the interfacial tension at the water/n-hexane interface. The gold/iron Janus particles tended to be more surface active than the isotropic iron and the gold metallic particles. The bimetallic particles were touted to be excellent Pickering emulsion stabilizers [27]. Another example of the Janus characteristic imparted on silica particles was by functionalizing one side with alkyl silane. The unfunctionalized half of the particle consisting of silanol groups helped render the particle "Janus". Such particles were prepared by several researchers using varied alkyl groups and used as examples of amphiphilic particles to analyze their orientation at an oil-water interface. In the case of Takahora et al., spherical assemblies of such amphiphilic particles were used to encapsulate other water-immiscible agents. Silica particles were rendered partially hydrophobic by the functionalization of the surfactant cetyltrimethylammonium bromide (CTAB) on the particle surface and the particles assembled at the dichloromethane/water interface [17]. The exceptional behavior of assembly at the interface was the result of the face-separated properties of Janus particles, otherwise lacking in the isotropic ones. Janus particles were prepared using two incompatible polymer solutions PS and PAA halves. When the two polymer solutions were mixed, the Janus particles were observed at the interface It was observed that the particles accumulate at the interface of the polymer solutions and stayed there even when high temperature and shear conditions were applied [177]. When particles functionalized with hydrophobic and hydrophilic properties were exposed to an atomic force microscope

tip to study their asymmetric surface properties, a strong adhesion was observed due to the confirmation changes by the particles towards the tip [178]. Janus particles have been observed to exhibit interesting properties with tailorable functions and high applicability.

In this thesis, we prepared Janus particles in gram quantities for three different applications such as functionalization of proteins on two halves of the particles, for performing selective agglomerate-free separation of prokaryotes such as bacteria from a mixture of bacteria and for extended cell attachment on the surface of eukaryotic cells such as fibroblasts.

2.1.5.1   Functionalization with proteins

Materials have been rendered bio functional by the immobilization of biomolecules such as proteins on their surfaces for creating a unique biomaterial type or for imparting an additional functionality. Different protein types such as membrane, globular and fibrous can be used for immobilization on inorganic materials to impart interesting features. The combination of protein types on the surfaces of inorganic materials can be used to impart structural and functional variations on such materials. Hence Janus particles with multiple protein types can be used to create multifunctional particles. The properties imparted by the proteins combined with a variety of metallic, metallic oxide, inorganic or conductive properties of the materials makes such biofunctionalization an attractive method for generating multifunctional materials [1,7,19,35]. One such protein type, ferritin, which is a cage protein with iron storage capacity has been functionalized on particles to impart biohybrid features. Ferritin also exhibits interesting structural features such as reversible self-assembly and disassembly [179]. Due to the presence of an iron core, ferritin can also be observed using the TEM. Particles functionalized with ferritin can therefore be visualized to confirm the success of functionalization [89]. Functionalizing Janus particles with two different proteins would allow the combination of otherwise incompatible proteins on a single NP surface and would thus enable applications in targeting, signaling or a similar combination of functions. Face-selective functionalization usually starts with equipping the surface with specific functional groups [180] or by creating a single patch of a different material on the NP surface [28,31,181]. The functional groups can thereafter be used to attach (bio)molecules onto the respective sides. Here, azide-alkyne copper

catalyzed click chemistry or the thiol-maleimide chemical reaction are mostly used for protein functionalization [136] on Janus particles due to their superior specificity compared to the otherwise regularly used carbodiimide-based coupling methods. High specificity is especially critical for protein-functionalization at the nanoscale due to the general stickiness of particles and proteins at this size range [182]. Moreover, care needs to be taken to avoid or to mitigate the formation of a non-covalently bound protein corona which can rapidly form on NPs in the presence of biological media [58].
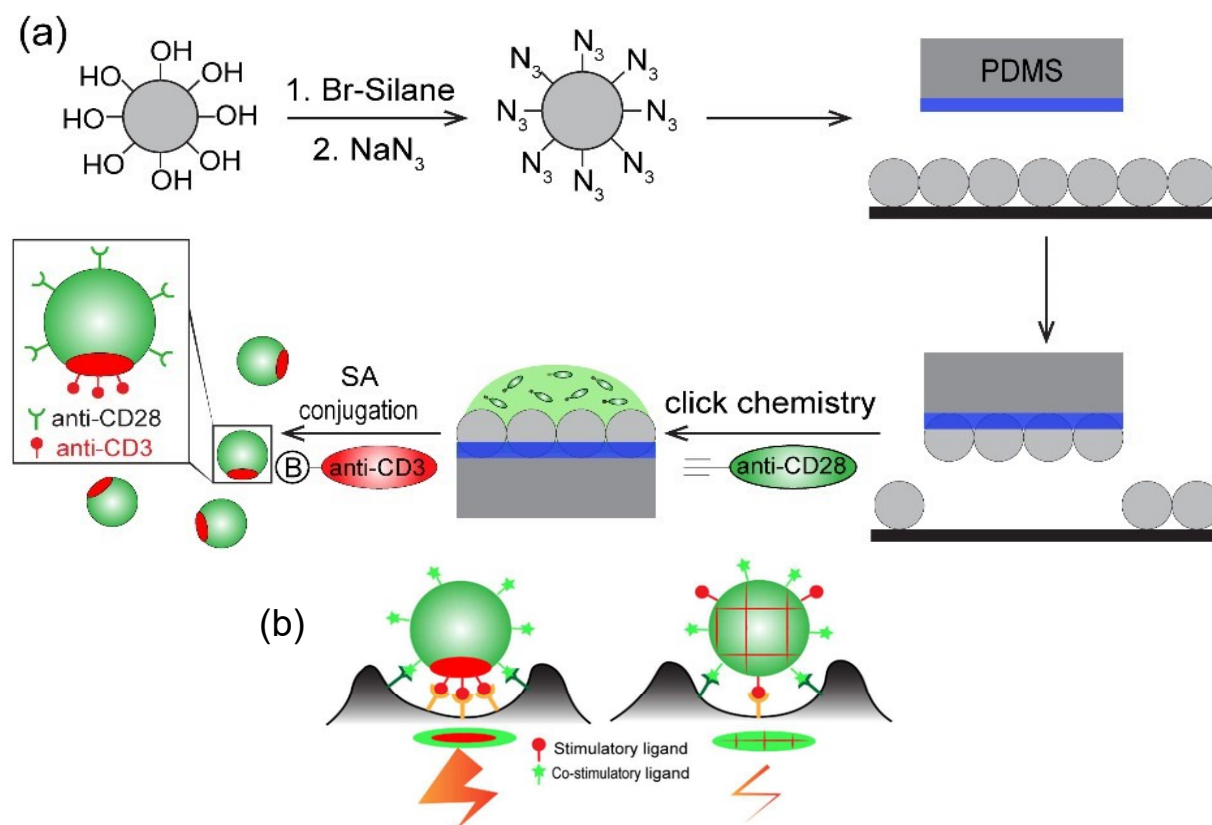
Figure 2-13: Schematic representation of the procedure of 500 nm silica Janus particles. (a) The method of synthesis is by using masking and the conjugation of antibodies CD3 and CD25 using azide-alkyne click chemistry and biotin-streptavidin method. The particles were masked using the PDMS stamping method followed by release of the masked particles using sonication. (b) These micro-sized Janus particles were prepared to activate T-cells and in turn manipulate immune responses. Reproduced from [24] with permission from RSC.

As of yet, only few reports exist on dual biofunctionalization of Janus particles, most of them utilizing particles at the micrometer to sub-micrometer scale. At the lower end of the

size spectrum, Lee et al. prepared 500 nm silica Janus particles using a microcontact printing procedure with azide functionalized SiNPs followed by side-specific antibody attachment via amine-carboxy carbodiimide chemistry. The covalently attached antibodies were thereafter shown to selectively target cluster of differentiation(CD)3 and CD25 receptors on T-cells (figure 2-13) [24].

Tang et al. prepared bifunctional 2.0-4.5 μm silica and PS Janus particles using a metal deposition technique followed by the orthogonal approaches of carbodiimide chemistry and biotin-streptavidin binding for protein functionalization at the respective faces [34]. Similarly, Bradley et al. presented 850 nm Janus particles with multiple clickable PS and poly(propargyl acrylate) sides using thiol-yne click chemistry for conjugation. Here, the initial face separation was realized via the seed emulsion technique [183]. Honeggar and coworkers prepared 1 μm PS and silica particles which were partially coated with gold using a metal evaporation technique to introduce the Janus character [114]. An even smaller number of reports exist that describe the preparation of inorganic Janus particles with dual biofunctionalization at the nanoscale [15,20,180]. Sánchez et al. used the wax Pickering emulsion technique to prepare 100 nm silica particles with single gold patches and then attached horseradish peroxidase on the silica face and biotin on the gold face [20]. Villalonga et al. presented a similar preparation technique using mesoporous silica particles with a gold face for the controlled release of the dye tris(2,2-bipyridyl) ruthenium(II) chloride [15]. Zhang et al. described a preparation technique using PS instead of wax, and prepared 150 nm silica Janus particles with conjugated proteins using click chemistry [180]. López et al. again used the wax-emulsion technique to prepare mesoporous silica Janus NPs (d = 160 nm) with folic acid and triphenylphosphate using carbodiimide chemistry for dual targeting of tumor cells and mitochondria [32]. Since detection of proteins with TEM can be difficult, in the paper by López et al., the Janus aspect was verified by adsorbing ultra-small gold NPs to the aminated hemisphere before biofunctionalization. Similarly, the other mentioned papers mostly describe successful preparation of nanoscale Janus particles as proof-of-principle for specific applications [13–16,24,32,74,75].

2.1.5.2 Janus particle application on prokaryotes and prokaryote-based systems

With increasing resistance against antibiotics, bacterial contamination and infection are both long-standing and pressing issues in healthcare, nutritional industries and environmental engineering. Although new ways for eliminating pathogens have been developed in the last years, for example based on metal NPs [186] or carbon nanomaterials,[187–189] the precise detection and efficient elimination of pathogenic bacteria remain significant challenges [116,124,190,191]. An especially promising approach for clinical diagnosis as well as environmental monitoring of pathogens is based on superparamagnetic iron oxide NPs, which have become a staple in biomedicine in the last decades for cell labeling, separation and tracking [192–195]. Magnetic NPs can be employed to capture and magnetically separate live bacteria from sewage water, biological fluids and similar systems for further analysis or elimination [121,122,130,196–199]. However, bare magnetic NPs show low bacterial capture efficiency without further functionalization, especially due to their poor colloidal stability in biological media [190]. Consequently, the development of magnetic-NP-based systems with highly improved bacterial capture, separation and elimination efficiency is desired. To this end, various surface functionalizations of magnetic particles have been reported in recent publications, e.g. bacteria-specific antibodies[190,200,201], amino acids [194,202], aminated silanes[115,203,204], drugs[115], surfactants[205] or synthetic ligands[206] which have improved capture efficiency to some extent.
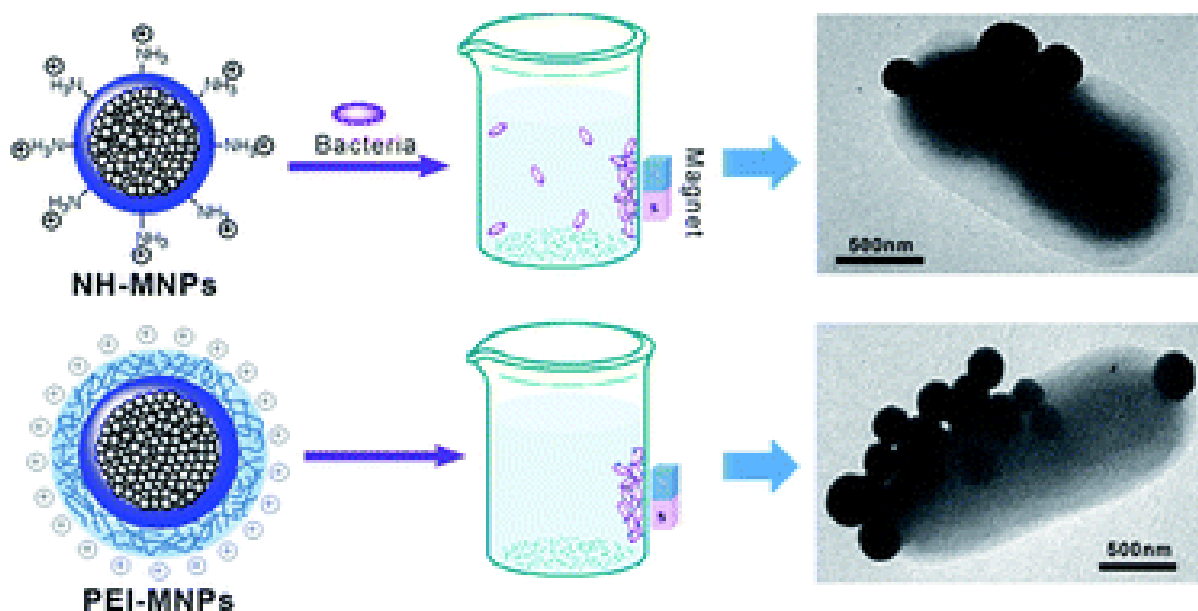
Figure 2-14: Schematic representation of positively charged magnetite@SiO_2 NPs used for bacterial separation. Amino- and polyethyleneimine- functionalized particles were used to selectively capture the negatively charged bacteria via electrostatic interactions. Reproduced from [126] with permission from Wiley.

Because the surfaces of bacteria are mostly negatively charged at physiological pH, efficient bacterial capture has been demonstrated with various positively charged NPs that efficiently bind to bacteria surfaces. In this respect, Fang et al. showed that the larger the number of amine groups on magnetic NPs surfaces, the higher is the capture efficiency of the *Escherichia coli* (*E. coli*) cells (figure 2-14) [126]. Zhang et al. demonstrated the synthesis of polyallylamine functionalized cationic magnetic NPs to isolate negatively charged bacteria and to identify which species actively took part in phenol degradation [196]. Bhaisare et al. used positively charged magnetic NPs functionalized with an imidazole derivate to capture bacteria from blood [123]. As a more specific alternative to positively charged particles, several groups described the synthesis of antibody-functionalized magnetic polymer nanospheres for rapid capture and enrichment of one bacterial type [190,200,201].

However, since positively charged particles unspecifically bind to negatively charged bacterial surfaces, NP-bacteria complexes can result in agglomerated biomasses and rapid flocculation due to electrostatic heteroagglomeration. Similarly, particles that are

isotropically functionalized with bacteria-specific antibodies cause agglomeration by forming bacteria-particle-bacteria bridges. Agglomeration and flocculation can strongly hamper isolation and analysis of bacterial species [115,126,191,203,204,206,207]. Particularily, agglomeration can lead to incorrect bacterial cell counts [191,208–211]. Furthermore, agglomerates of one bacteria type might potentially engulf other types of bacteria or other dispersed components of the bacteria suspensions.

Hence, for sensitive detection of bacteria along with realization of exact bacterial counts, Janus particles can be used. Such Janus particles could be designed for bacteria-specific capture on one side and for preventing binding on the other side. In this respect, functionalization with PEG is a common strategy to suppress particle binding to cell surfaces and most biomolecules [58,112,212,213].

Janus particles that are equipped with a combination of bio functional properties on a single NP surface are gaining interest over the past several years [6,88,89,204,214,215]. In the context of bacterial capture, Vilela et al. used magnesium Janus particles coated with magnetite and silver halves, which provide magnetic and bactericidal properties respectively. These so-called microbots are effective tools for rapid water disinfection [216]. Chang et al. reported the rapid detection of food-borne bacteria by using Janus nanorods consisting of a single magnetite NP attached to a mesoporous silica particle that was loaded with an antibacterial agent. While the reported anisotropic systems at this point seem to provide no clear functional benefit over magnetite particles fully embedded in a spherical structure or other isotropic designs, in these works, the authors clearly demonstrate the potential of sophisticated multifunctional nanostructures for such applications [116,124].

2.1.5.3 Janus particle application on eukaryotes and eukaryote-based systems

Based on the powerful properties of NPs in biomedical applications, it is highly desirable to attach NPs to the plasma membrane of living cells. However, NPs that adhere to the surface of eukaryotic cells, as a general rule, are rapidly incorporated via various endocytosis pathways, depending on physical and chemical parameters of the particles including size, shape, charge and surface chemistry [94–96]. This process, which usually

leads to NPs being engulfed in endosomes and transported into the cytosol, makes it extremely difficult to retain NPs at the cell surface for relevant periods of time.

NP uptake into cells can be mostly avoided by coating the particles with a passivation layer, which is commonly comprised of PEG [155,220]. This so-called stealth coating prevents interactions with serum proteins and cell surface receptors while also reducing non-specific physico-chemical interactions between particles and cell surface molecules. On the other hand, NPs can be modified with a wide variety of surface functionalizations [9] to tailor the particles for specific interactions including antigen-antibody binding, receptor-mediated recognition or anchoring of lipids into the plasma membrane [217]. This results in two opposing functionalization strategies: minimization of NP-cell interactions altogether via stealth coating or utilizing specific interactions that quickly result in endocytosis. The fundamental approach of the present work is to use Janus NPs to incorporate both functionalization strategies on opposing hemispheres of the same NP to create particles that firmly adhere to cell surfaces without being promptly endocytosed [155,221].

Janus particles have gained popularity since their introduction by de Gennes in 1991 [67] and have since been used in various applications like bioimaging [6], drug delivery systems(figure 2-15) [21,69,214,222,223], magnetotherapy [224] or bacterial extraction[90,124]. Janus particle preparation can be achieved by several methods including masking at interfaces [225], templating using emulsions [99] and self-assembly, [226]. While most methods result in a relatively small number of produced Janus particles, Janus particle preparation using the wax Pickering emulsion method is a scalable method which easily yields gram quantities of approximately half-coated particles. In this approach, one hemisphere of the particles is masked at the surface of solidified wax emulsion droplets and hence the exposed particle hemisphere can be modified with a separate functionality [14,16,89].
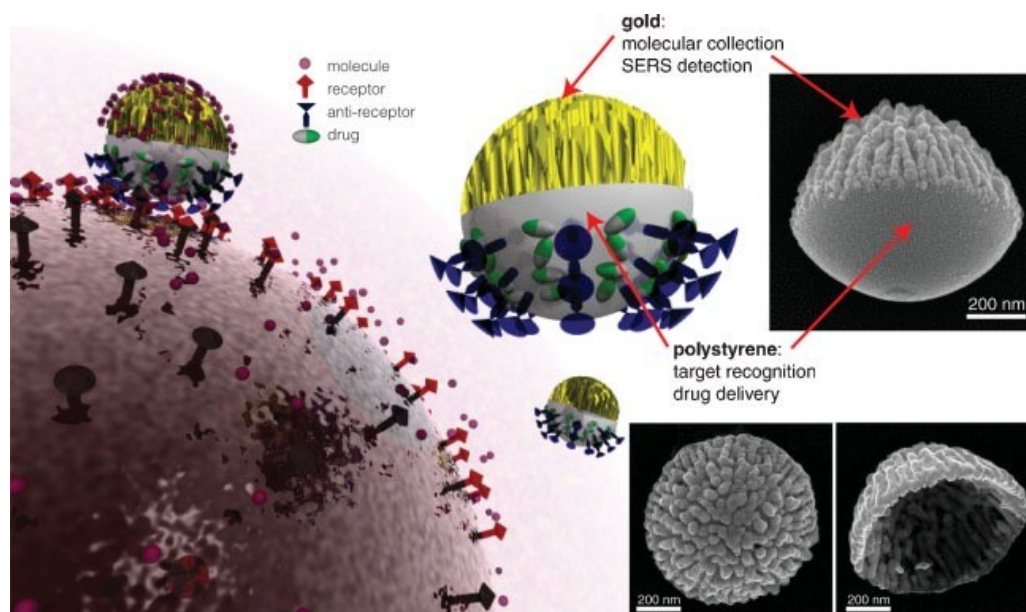
Figure 2-15: Nanocorals prepared using gold capping on one half of the particle as well as anti-receptor antibody as well as drugs for targeted drug delivery. These multifunctional entities are useful in functions such as targeting and sensing along with drug delivery. (left) diagrammatic representation wherein gold (yellow) and PS (grey) halves of the particles were synthesized followed by ligand and drug functionalization on the PS half. (right) SEM images of the gold and PS Janus particles. Reproduced from [21] with permission from Wiley.

In a seminal paper from 2013 [221] and its follow-up from 2015 [227], Gao and Yu explored the endocytosis and fate of micron-sized Janus particles which were coated with anti-CD3 antibodies and a passivation layer of bovine serum albumin (BSA) on respective sides. In this first detailed study on the uptake of Janus particles, the authors were able to show a two-step endocytosis pathway in which the antibody-coated side was progressively engulfed via receptor-mediated endocytosis. Afterwards the BSA-coated side was covered with a further extension of the cell membrane in an actin-mediated process. Full endocytosis of these Janus microparticles by Jurkat T cells was reported to take 1-5 min, which was significantly longer than endocytosis of isotropic particles (figure 2-16).
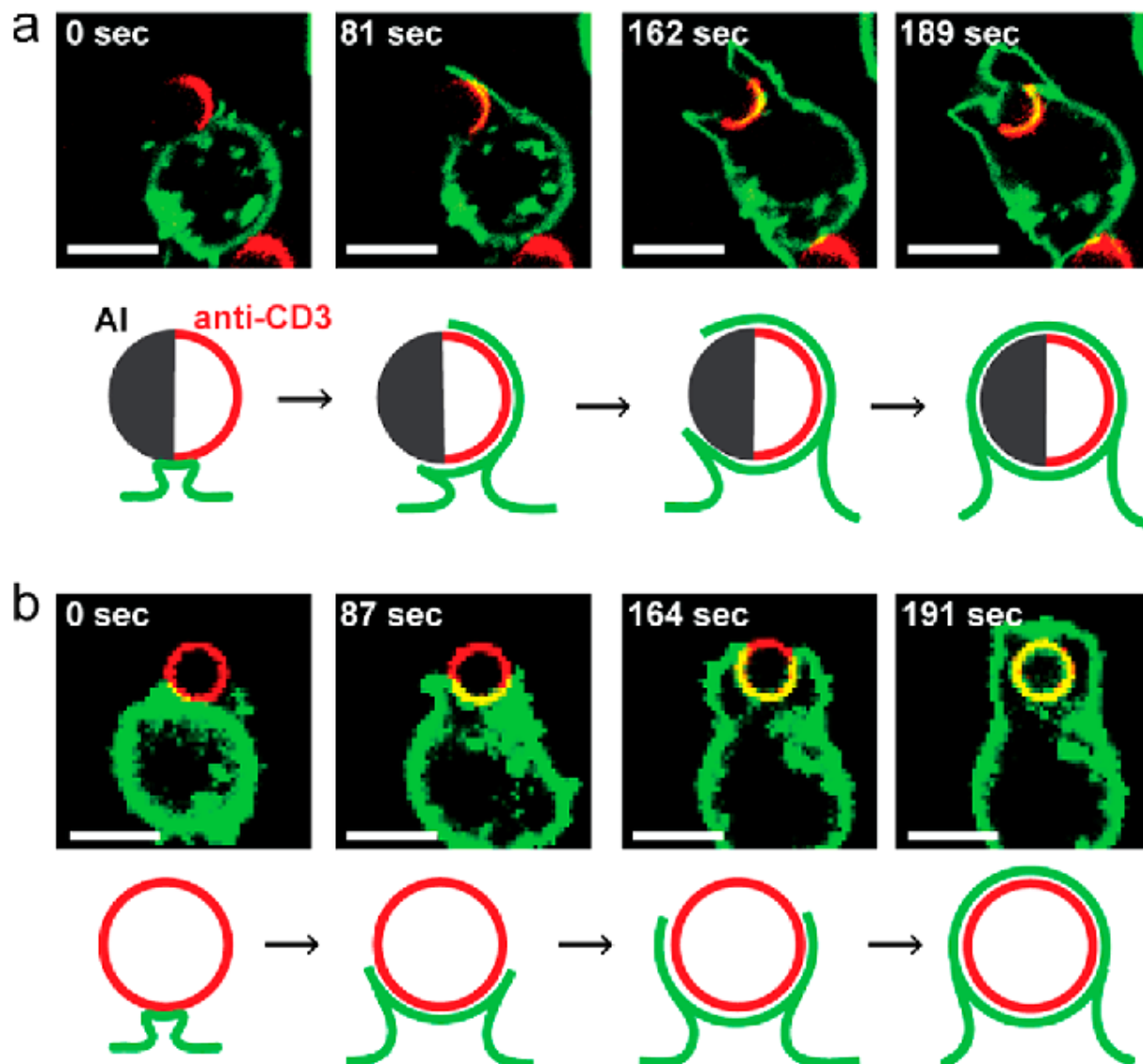
Figure 2-16: anti-CD3 antibody functionalized on one half of a particle surface and the other half coated with aluminum (Al) metal. After particles reach the target cell, endocytosis begins with membrane protrusion. Time elapse images are made to understand the uptake of the a) janus particles b) isotropic silica particle by macrophages. Reproduced from [221] with permission from ACS.

In a similar approach, Sanchez et al. studied the effect of PEG functionalization on one hemisphere of Janus microparticles on their uptake by macrophages. The passivation with PEG instead of BSA resulted in strongly reduced internalization of about 25 % of the incubated particles measured after 30 min. With anti-CD3 antibodies on the binding hemisphere, they report that also about 25 % of the particles remain bound to the cell surface after an incubation time of 30 min [155]. Note that the reported experimental

studies have been carried out with micron-sized particles whose anisotropic features are easily visualized with fluorescence microscopy. Compared to microparticles, NPs interact significantly different with biological systems due to their much higher surface area to volume ratio and dimensions that are much closer to proteins which might lead to drastically different uptake behavior [182]. Additionally, a fairly large body of computational studies about Janus particle interactions with phospholipid membranes provide theoretical background to some aspects of these observations which are summarized in a recent review [228].

Chapter 3

Experimental section

Parts of this chapter have been adapted from the following publications with permission from Wiley, ACS and RSC:

*Kadam.R, Zilli.M, Maas.M and Rezwan.K. „Nanoscale Janus particles with dual protein functionalization" Particle and Particle systems characterization, **2018**, 35, 1700332*

*Kadam.R, Maas.M and Rezwan.K. „Selective, agglomerate-free separation of bacteria using biofunctionalized, magnetic Janus NPs, ACS Applied Bio Materials, **2019**, 8, 3528-3531.*

*Kadam.R, Ghawali.J, Waespy.M, Maas.M and Rezwan.K., „Janus NPs for extended cell surface attachment" RSC Nanoscale, **2020**, 12, 18938-18949*

3. Experimental section

3.1 Synthesis of inorganic silica Janus NPs

3.1.1   Wax Pickering emulsion method

The preparation and application of Janus particles presenting surface asymmetry entails issues like preparation of bulk quantities of particles at the nanoscale and the ability to control and fine tune the Janus balance. Isotropic particles are easily modifiable to attain surface properties of interest, however, imparting surface "Janus" anisotropy at a nanoscale in bulk quantities has been a challenge. Preparation of Janus microparticles and to some extent at a nanoscale has been successfully done using different methods of preparations. Effective synthesis techniques for Janus particle preparation should be able to regioselectively modify surface properties of particles at the nanoscale and provide high success rates of preparation along with good yields. To fulfill such requirements, several techniques have been adapted and modified over several years using three major phenomena, phase separation [229], self-assembly [230] and masking [3].

Following the principle of masking, the Pickering emulsion technique was used to prepare Janus particles. Pickering emulsions are formed when two immiscible liquids are mixed together and are stabilized at the interface using solid particles. First proposed by Ramsden and further recognized and utilized by S.U. Pickering in 1907, Pickering emulsions are created when oil and water are mixed with each other to form an o/w emulsion and solid particles are used to stabilize these droplets. These droplets do not coalesce because the particles impart stability [92]. The wettability of the particles by either of the phases, determines whether the particles have the ability to stabilize such emulsions. Other factors such as shape and size of the particles also affect the stability of Pickering emulsions. In this thesis, nanoscale inorganic particles such as silica were used to create stable Pickering emulsion droplets, where molten wax as the oil-phase and the water phase such as aqueous liquids were used. In order to realize adsorption of the highly hydrophilic particles such as the silica particles used in this thesis were coated with oppositely charged surfactants. In case of the negatively charged silica particles, positively charged surfactant CTAB, (Sigma Aldrich, Germany, product number 855820)

was used to increase their hydrophobicity. In case of the positively charged particles, which were silica particles functionalized with amine groups, sodium dodecyl sulphate (SDS, Sigma Aldrich, Germany, product number 436143) was used [17]. A stable emulsion is established because of the particles deposit themselves at the interface of the two liquids and stay at the interface. The molten wax then solidfies after the emulsion is cooled. This protocol for Janus particles synthesis was used in this thesis and published in one of our publications [89], which was adapted from the approach by Granick et al.[16]. Compared to the original protocol, the surfactant concentration was roughly proportional to the increased surface area after functionalization exhibited by the nanoscale particles [89]. A paraffin wax-in water emulsion was prepared in batches of 50 ml adapting the protocol described by the Granick group who first introduced it [16]. 140 mg of the functionalized particles were homogenously dispersed in water. 2 mg CTAB was added to this mixture to partially hydrophobize the NPs by physio adsorption. 1 g of wax (melting point 75°C to 90°C, Merck Millipore, Germany, product number 8002-74-2) is then added to this dispersion. This entire setup was heated to a temperature of 80˚C to melt the wax, and an emulsion was prepared using an ultra Turrax homogenizer at 9500 rotations per minute (rpm) for 90 s. This setup was allowed to cool down for the solidification of the wax. The solidified wax droplets were then washed three times with water using vacuum filtration to remove excess of CTAB and unbound NPs. Analysis of the solid wax emulsions after the washing steps and the upcoming functionalization steps was done using the SEM.

3.1.3   Janus particle synthesis

To introduce different functionalities on the particle surfaces, we grafted functional groups on two halves of the particle using the wax Pickering emulsion technique. In this thesis, we used functional groups such azide and biotin groups (Chapter 4), azide and polyethylene glycol (PEG) (Chapter 5), amine and PEG groups (Chapter 6). Surface functionalization can be achieved using surface chemistry modification post particle synthesis. Silanization is commonly used to create surface functionalized inorganic particles [231]. The specific surface area (SSA) of the particles was measured using the BET method (section 3.2.5) and accordingly the amount of silane used for the

functionalization was adjusted. Modification of the surface properties using functionalization was done to introduce additional functionalities and attach other bio functional moieties or to increase colloidal stability [57,111].

Chapter 4 includes the use of two commercially purchased SiNPs of two different sizes (80 nm and 150 nm) functionalized with azide groups and biotin groups. The method was adapted from the functionalization protocol described by Lo Giudice et al. [136]. To prepare the fully azide functionalized particles, silica particles were first dispersed in an organic solvent such as absolute ethanol (9 mL) using sonication at a concentration of 8.7 mg/mL. 0.5 mL of ethanol containing 21 μL of azidosilane (ABCR GmbH, Germany, product number AB268770) were added dropwise to the NP solution at RT over a period of 60 min followed by heating for another 60 min at 90°C. The azide-functionalized NPs were then dried and used as required. The azide group quantification was performed using the protocol described in [136] using dibenzylcyclooctyne-cyanine dye derivative (DBCO-Cy3, Biomol GmbH, Germany, product number 920). The particles were washed three times using MilliQ water to remove unspecifically bound dye by repeated centrifugation at 12,000 rpm for 20 min and redispersion using ultrasonic bath. The fluorescence of the bound- and unbound-Cy3 was determined by excitation at 553 nm and emission at 563 nm using the spectrometer plate reader (Chameleon™ V, Finland). To prepare fully functionalized biotin functionalized particles, 5 ml of 10 mg/ml particles were dispersed in ethanol and then incubated with 40 µl of ethoxy-PEG-biotin silane 3400 (biotin-PEG-silane, Laysan Bio *Inc*, USA, product number 145-40) for 8 h under stirring at RT. The particles were washed using ethanol and water by performing centrifugation and redispersion steps. The particles were air dried before use. Biotin group quantification was done using Fluoreporter biotin quantification kit (Invitrogen, Germany, product number F30751). Following the product specification sheet, biotin end groups on the particles were determined. The kit consists of ligands that attach to biotin groups on the NPs which in turn quenches the fluorescent dye „Biotective™ green reagent", also present in the kit. The fluorescence signal is directly proportional to the amount of biotin functionalized on the particle surfaces. The number of biotin groups on test samples are calculated based on a calibration curve prepared using known concentrations of biotin. The fluorescence of the dye was determined by excitation at 495 nm and emission at 519 nm using the

spectrometer plate reader. For the preparation of Janus azidosilane/biotin-PEG-silane silica particles, 10 mg of the aforementioned Pickering emulsion droplets decorated with azide SiNPs were further dispersed in 9 ml absolute ethanol. 1 ml of 8 mg/ml biotin-PEG silane solution in ethanol was slowly added to this mixture under nitrogen bubbling conditions at RT for 2 h. This amount corresponds to approximately 9 times a monolayer of silane molecules related to the total SiNP surface area. The functionalized Pickering emulsion droplets were then washed thrice with ethanol to remove any silane residues.

Cyclohexane (Sigma Aldrich, product number 227048) was added to these wax droplets overnight at ambient temperature to dissolve the wax. The particles were extracted using 10 mM 2-(N-morpholino)ethanesulfonic acid buffer (MES buffer, Sigma Aldrich, Germany, product number 011M8418). The prepared NPs were immediately used for protein conjugation purposes.

The particles were centrifuged at 3000 rpm for 3 min to remove excess of the agglomerated SiNP. Three repeated centrifugation and redispersion cycles in MES buffer were used to wash the particles. The final supernatant was used as the final particle suspension for the protein conjugation purposes. The particle concentration used in every protein conjugation step was 10 mg/ml of MES buffer. The protein conjugation steps were performed in a two-step method. Ferritin, which is attached via copper mediated click chemistry to the azide side, was functionalized with an acetylene group using the protocol described in [136]. The particles were dispersed in 2 ml of 10 mM MES buffer, and then incubated with 10 µl of streptavidin-gold for 2 h at 4° C to enable protein bioconjugation with biotin. As stated by the manufacturer, each 10 nm gold NP is decorated with 20 streptavidin molecules. SiNP conjugated with ferritin and streptavidin-gold were further washed with 10 mM MES buffer thrice using centrifugation and redispersion steps as done previously. Finally, the particles were dispersed in 2 ml of fresh 10 mM MES buffer. A schematic representation of the Janus particle synthesis is shown in figure 3-1.
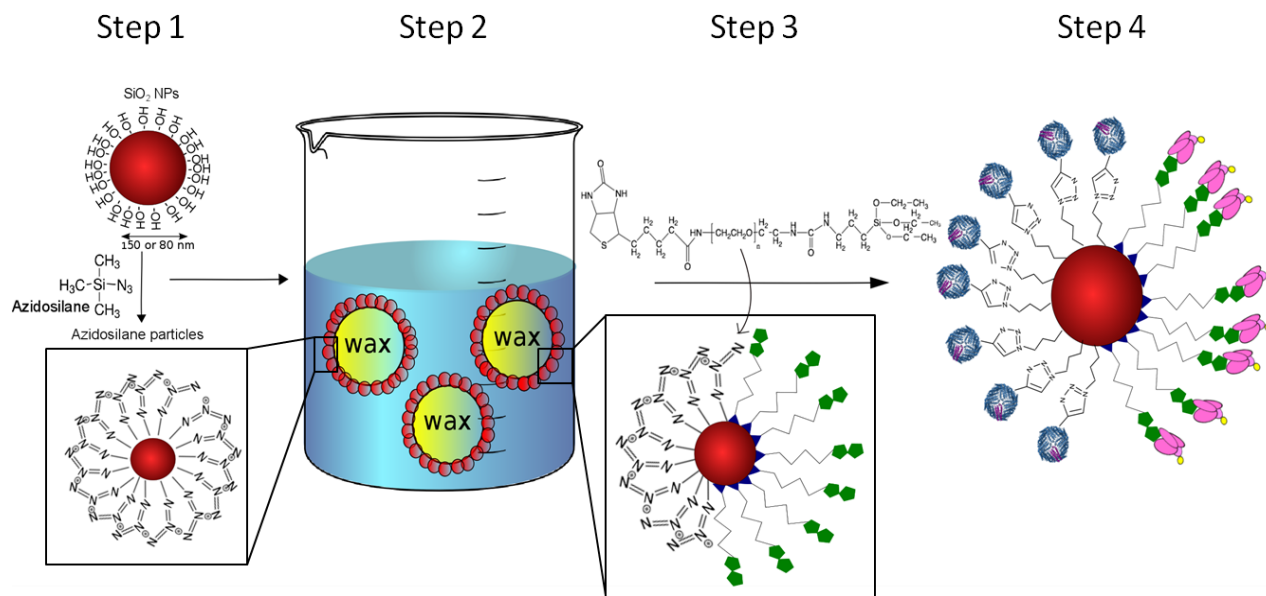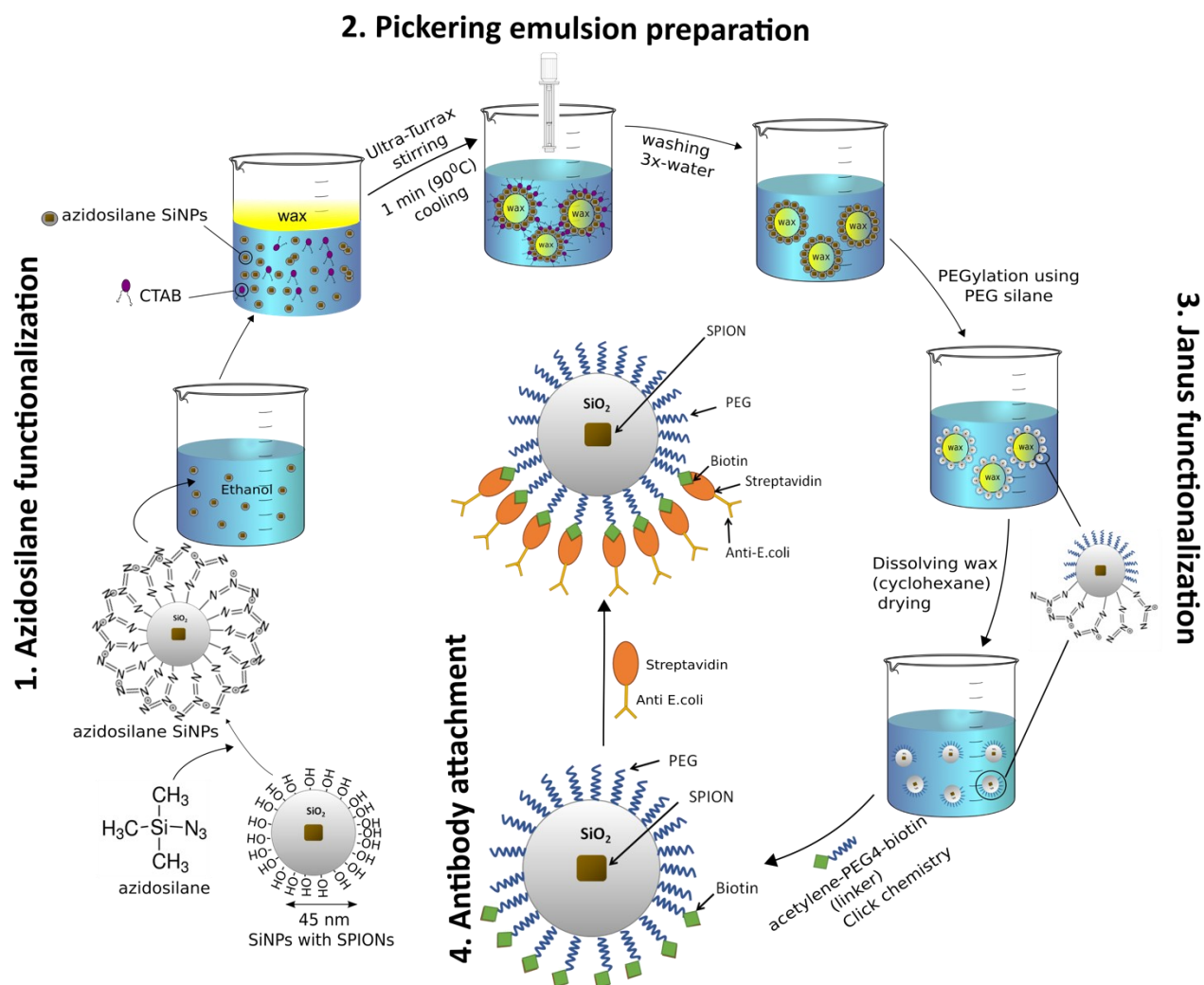
Figure 3-1: Schematic representation of the synthesis route of nanoscale Janus particles with dual protein functionalization. Step 1: Unfunctionalized SiNPs were coated with azidosilane. Step 2: Formation of a wax-in-water Pickering emulsion stabilized by the azidosilane-functionalized particles and the surfactant CTAB. Step 3: The emulsion droplets are functionalized with biotin-PEG silane (green) and the wax was further dissolved to yield a Janus NP dispersion in MES buffer. Step 4: Janus particles with azide and biotin end groups are functionalized with the proteins ferritin (blue) and gold-conjugated streptavidin (pink), respectively. Reproduced from [89] with permission from Wiley.

Chapter 5 includes the use of magnetite@SiO_2 NPs functionalized with azide and PEG groups. The protocol used for the functionalization of azide and PEG groups on magnetite@SiO_2 NPs is similar to the method used previously for azide and biotin functionalization with slight changes in the amount of silane used, which was calculated according to the available SSA of the NPs. Other parameters such as incubation time and temperature of functionalization remained unaltered. PEG functionalization on NPs has been widely studied to improve targeting efficiencies of NPs by reducing protein corona formation [58,111]. Polymer chains arising from PEGylation on NPs precludes them from interacting with other NPs and components of biological systems, particularly surface-active proteins. This renders such NPs less vulnerable to agglomeration and strongly reduces their interactions with cell surfaces. To prepare PEG functionalized particles, 2 [methoxypoly (ethyleneoxy)propyl] trimethoxy-silane (PEG silane, 90%, 6-9 PE units, molecular weight 459-591 g/mol, Gelest *Inc.*, Germany, product number SIM6492.7) was used. Confirmation of the successful functionalization of PEG on the NPs was performed

by adsorption of Lysozyme (from chicken egg white, Sigma Aldrich, Germany, product number L6876) and albumin from bovine serum fluorescein isothiocyanate conjugate (FITC BSA, ThermoFischer Scientific, USA, product number A23015), which was assessed by measuring the zeta-potential and residual protein concentrations, respectively. 10 mg ml^{-1} of PEG functionalized NPs were dispersed in 1 ml of 1 mM phosphate buffered saline (PBS, Sigma Aldrich, USA, product number P4417) and incubated with 2 mg ml^{-1} of FITC-BSA for 1 h. This mixture was then washed thrice with PBS to remove unbound FITC-BSA. The residual and adsorbed FITC-BSA concentrations were then quantified using a fluorescence plate reader. By measuring of fluorescence signal at λ_{ex}: 495 nm, λ_{em}:525 nm of known increasing concentrations of FITC-BSA (1 nmol to 20 nmol FITC/ml of PBS), a calibration curve was prepared which was used to calculate unknown concentrations of FITC-BSA from the samples. Additionally, functionalization of PEG functionalization was confirmed by lysozyme adsorption. Lysozyme exhibits an isoelectric point of 11 [232] and therefore is positively charged in PBS at pH 6.2. Consequently, it adsorbs on negatively charged magnetite@SiO$_2$ due to electrostatic interactions, which would be evidenced by the change in surface charge of the NPs. The zeta potential (ZP) of the particles was measured before and after lysozyme adsorption using the DLS (Zeta Sizer Nano ZSP, Malvern instruments, USA) device.

To prepare azide/PEG magnetite@SiO$_2$ Janus NPs, the 10 mg of the as-prepared particle-coated wax droplets were functionalized using 20 μl PEG silane following our established protocol. The concentration of the PEG-silane was twice the theoretically calculated monolayer coverage on the particle surfaces to ensure successful functionalization. After dissolving the solid wax droplets using cyclohexane with repeated sonication steps, the azide/PEG magnetite@SiO$_2$ NPs were extracted with water. Using the azide-acetylene copper mediated click chemistry reaction,[136] the linker acetylene-PEG$_4$-Biotin (Jena Bioscience, Germany, product number CLK-TA105) was attached to the azide-functionalized side of the Janus particles. This linker is required for the attachment of streptavidin-conjugated anti-*E. coli* antibody. The PEG backbone in this case is used as a spacer to improve accessibility and flexibility of the conjugated antibodies. The linker attachment was performed in ethanol following the protocol from reference [89]. After 16 h, the Janus NPs were collected via magnetic separation and washed with ethanol. To synthesize antibody-conjugated Janus NPs, anti-*E. coli* antibody (Abcam, United

Kingdom, product number ab137967) was first conjugated with streptavidin using the Lynx Rapid Streptavidin Antibody Conjugation Kit (BioRad, USA, product number LNK161STR). 10 μL of streptavidin anti-*E. coli* antibody (1 mg/ml) were incubated with 10 mg of azide-biotin/PEG magnetite@SiO_2 NPs in PBS for 2 h at 4°C to allow for binding between the streptavidin conjugated antibody and the biotin groups on the Janus NPs. Fully antibody functionalized NPs (non-Janus) were used as the positive control in our experiments. Success of this functionalization step was assessed by conjugating the surface grafted biotin groups with gold-labeled streptavidin (O.D 10, Cytodiagnostics, Canada, product number AC-10-04-15) instead of the streptavidin-conjugated antibody for visualizing with TEM. Schematic representation of the synthesis procedure has been shown in figure 3-2.
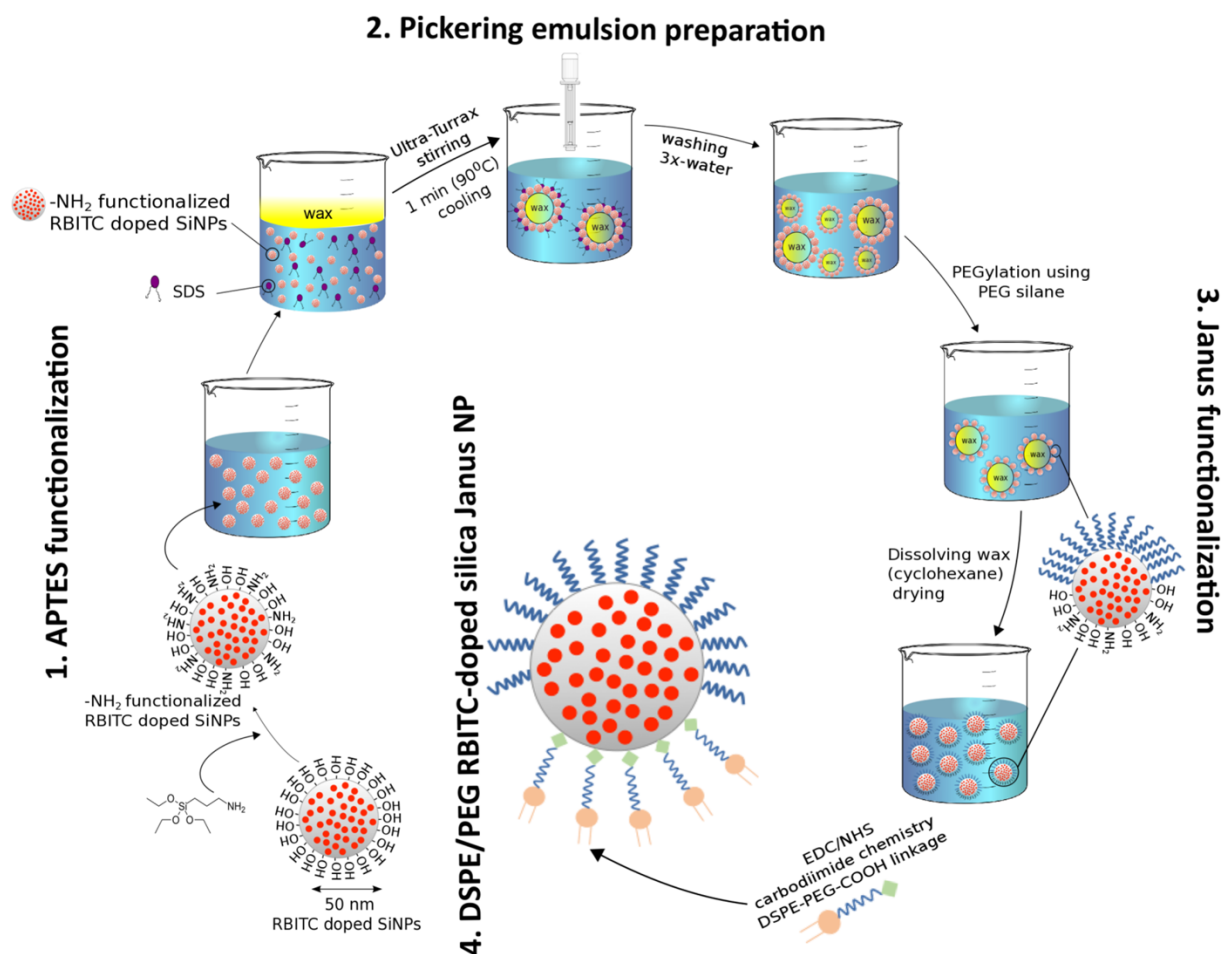
Figure 3-2: Schematic representation of the synthetic route of the preparation of magnetite@SiO$_2$ PEG/azide-biotin-streptavidin-Ab functionalized Janus NPs. Step 1: azidosilane functionalization of magnetite@SiO$_2$ prepared using magnetite and tetraethyl orthosilicate (TEOS). Step 2: Preparation of wax Pickering emulsion droplets using azide-functionalized magnetite@SiO$_2$ in the presence of CTAB. Step 3: PEGylation of the wax droplets was performed using PEG-silane to attach a second functionality on the exposed surfaces of the NP. The linker acetylene-PEG$_4$-biotin was attached using azide-acetylene click chemistry. Step 4: anti-*E. coli* antibody labeled with streptavidin was then used to produce magnetite@SiO$_2$ PEG/azide-biotin-streptavidin-Ab NPs. Reproduced from [90] with permission from ACS.

Functionalization of amine groups on SiNPs is commonly done to impart a positive surface charge to a negatively charged particles. One of the popular methods of functionalization of amine groups on silica particles is, by using a silane with amine end groups. Chapter 6 includes the design of PEG/DSPE functionalized RBITC doped SiO$_2$ NPs for extended cell surface attachment. Grafting of amine and PEG groups onto RBITC doped SiO$_2$ NPs is

done using APTES (Sigma Aldrich, USA, product number 440140) and mPEG (methoxy poly(ethylene glycol)) silane (molecular weight 5000 g/mol, Laysan Bio. *Inc*, USA, product number MPEG-SIL-5000) respectively. 10 mg/ml of RBITC doped SiO_2 NPs were suspended in 20 ml toluene using a sonication bath for 10 min and subjected to heating at 70°C. 21 µl APTES was added dropwise to the solution and stirred for 6 h. After functionalization, NPs were washed twice with both ethanol and water sequentially. The NPs were air-dried and stored at RT. The density of the grafted amine groups on NH_2-functionalized RBITC doped SiO_2 was then quantified spectrophotometrically using the reagent ninhydrin by adapting the procedure described by Soto-Cantu et al.[131]. The NPs were dispersed in absolute alcohol at a concentration of 10 mg/ml using ultrasonication for 10 min. 200 µl of 0.35 % (w/v) solution of ninhydrin (Sigma Aldrich, USA, product no. 151173) in ethanol was added to the particle solution followed by sonication for 5 min. This sonicated ninhydrin-NP mixture was incubated in a heating bath at 65 ºC for 5 min, which was further left to cool for 5 min. The Eppendorf tubes were centrifuged to remove any unreacted ninhydrin molecules at 13,000 rpm for 20 min. The absorbance of 1 ml of the supernatant was then measured using a spectrometer (MultiscanGo, Thermo Scientific, Finland, product number 5111930) at 588 nm. The amount of unbound ninhydrin was used to calculate the amount of bound ninhydrin, from which the amount of NH_2 groups/nm^2 of the surface area of the NPs was deduced. Increasing concentrations of a standard solution of hexylamine (0.12 mM to 0.87 mM) was used to prepare a calibration curve. Functionalization of PEG using mPEG silane for RBITC doped SiO_2 particles and their characterization was similar to the method described for magnetite@SiO_2 NPs. For the preparation of azide/PEG RBITC doped SiO_2 Janus NPs, the wax-embedded azide particles were functionalized first with PEG on the exposed hemispheres. To this end, 10 mg of wax droplets were incubated with 20 mg of mPEG silane using the protocol mentioned previously. For the PEG-functionalization step, twice the calculated monolayer concentration of the silane was used in the functionalization protocol. The NPs were then extracted by dissolving the wax spheres in cyclohexane. The as-prepared NH_2/PEG functionalized Janus NPs were air-dried and stored in the dark. Following the protocol of carbodiimide based coupling described by the manufacturer,[72,233] 0.5 ml of 10 mg/ml NH_2/PEG functionalized Janus NPs were incubated with 0.5 ml of 10 mg/ml of DSPE-PEG(2000)-carboxylic acid (DSPE-PEG-

COOH, Avanti Polar Lipids, *Inc,* USA, product number 880135) in 4 % (v/v) ethanol-water to obtain lipid-functionalized Janus NPs. To this mixture, EDC (Sigma Aldrich, USA, product number E6383) and NHS (Sigma Aldrich, USA, product number 130672) were added at a molar ratio of 5:1, also prepared in 4 % (v/v) ethanol(> 98%, Sigma Aldrich, USA, lot number SZBB1570 V)-water and thoroughly vortexed for 1 min. The reaction mixture was incubated at 4 °C under constant shaking. After 16 h, the obtained DSPE/PEG RBITC-doped SiO_2 Janus NPs were washed several times, dried and stored in the dark. With the same approach, further NPs were prepared with and without Janus functionalization for control experiments: isotropic unfunctionalized particles, fully APTES-coated particles, fully PEG-coated particles, fully DSPE-coated particles and anisotropic APTES/PEG Janus NPs. Isotropic unfunctionalized particles were utilized as prepared. The preparation of the fully APTES-coated silica particles is mentioned above. For the preparation of fully PEG-coated particles, 5 ml of 10 mg/ml RBITC-doped SiO_2 NPs in ethanol was incubated with 40 μl of mPEG silane incubated for 8 h under stirring at RT [112]. The silanized particles were washed several times using absolute ethanol and double deionized water (conductivity< 0.4 μS cm^{-1} purified using SynergyUltra Water System, Millipore Corp., USA) using alternative centrifugation and redispersion cycles. In case of the fully DSPE-coated particles, 5 ml of 10 mg/ml fully APTES-coated particles in ethanol were incubated with 40 μl of DSPE-PEG-COOH using the EDC-NHS coupling procedure as mentioned previously. An overview of the synthesis procedure of DSPE/PEG RBITC-doped silica Janus NPs is shown figure 3-3.

Figure 3-3: Schematic representation of the synthesis route of DSPE/PEG functionalized RBITC-doped SiO$_2$ Janus NPs. Step 1: NH$_2$-functionalization using silanization with APTES on RBITC-doped SiO$_2$ NPs. Step 2: Wax Pickering emulsions are prepared with the NH$_2$-functionalized NPs. Step 3: The solidified wax droplets are functionalized with PEG-silane. Step 4: DSPE-PEG-COOH is conjugated to the non-PEGylated half of the NPs based on EDC-NHS carbodiimide linkage. Reproduced from [91] with permission from RSC.

All particle types were prepared and characterized in triplicates and the amount of azide-, biotin-, PEG-, and amine- functional groups/nm^2 were expressed along with their respective standard deviations.

3.2 Characterization techniques for biofunctionalized Janus nanoparticles

3.2.1 Dynamic light scattering: Particle size measurement and zeta potential analysis

Dynamic light scattering is a method used to characterize the hydrodynamic size of colloidal particles in aqueous solutions [234,235]. Based on this data, it is also possible to obtain information regarding the colloidal stability of dispersed particles.

In particle dispersions, there is constant movement of the particles through the liquid medium. Small particles such as NPs dispersed in liquids undergo Brownian motion due to collisions with diffusing liquid molecules occurring throughout the sample. Smaller particles tend to move at a higher speed. The translational diffusion coefficient (D_T) can be used to deduce the motion of the particles in the solution which can be calculated using the Stokes-Einstein equation (equation 3.1). Thereafter particle sizes can also be obtained.

$$D_T = \frac{k_b \mathrm{T}}{6\pi\eta(T)r_H} = \frac{k_b \mathrm{T}}{3\pi\eta(T)D_H} \qquad (3.1)$$

where, r_H and D_H is the hydrodynamic radius and diameter, k_b is the Boltzmann's constant, T is the temperature, $\eta(T)$ is the temperature dependent viscosity,

The dynamic light scattering technique measures the hydrodynamic diameter of the particle. When particles are dispersed in solution, a thin electric dipole is formed on the surface of the particle due to the adsorption of oppositely charged ions. The hydrodynamic size is the hypothetical sphere that is assumed to diffuse, migrate and scatter light similar to the actual particle itself [236]. The values obtained by D_h measurements are higher due to the adsorbed cloud of electrons on the particle surface measured using the DLS when compared to other techniques such as electron microscopy.

Factors such as the ionic strength and temperature of the solution have an impact on the D_H values obtained. In this thesis, the NP dispersions were subjected to sonication before size measurements, which led to slight heating of the particle solutions. Temperature in

turn also influences the viscosity, which is another determining factor for size analysis. To avoid the influence of temperature on the size measurements, the samples were cooled to RT.

Particles that have large diameters as well as particle agglomerates scatter light more than the particles with smaller diameters [237].

When nanoscale particle dispersions are prepared in cell culture media substituted with protein containing solutions such as fetal calf serum (FCS, Invitrogen, Germany, product number 010M3395), the proteins adsorb to their surface and form a protein corona around the particles. This in turn directly affects the D_H measurement causing increased diameters values [58,112,129].

Polydispersity index (PDI) values can also be obtained using the DLS. The PDI shows the broadness of the particle size distributions dispersed in the solution. Monodispersed samples will show a narrow width of size distribution peak and whereas polydisperse dispersions will mostly give information about larger particles, since they significantly scatter more light. PDI values range between 0.1(10%) to 0.2(20%). In the presence of monomodal (single size particle distribution) particles throughout the sample, a value of 0.1 is obtained and indicates monodispersed particles.

The basic setup of the DLS is depicted in the figure shown below (Figure 3-4). The light from a monochromatic laser is projected via an attenuator onto the sample placed in cuvette positioned in a sample holder. The attenuator tunes the intensity of the laser beam incident onto the sample. As described above, the light is scattered from the moving particles in the dispersions. This motion leads to fluctuations in the intensity of the scattered light over time (figure 3.4-bottom left). Theses fluctuations are analyzed by an autocorrelator which provides the correlation coefficient as a function of the correlation time (Figure 3.4- bottom right). In the simplest case of a perfectly monodisperse dispersion, this graph describes an exponential decay and the diffusion coefficient of the NP is its decay coefficient in the exponent. More complex mathematical approaches are required for polydisperse systems, as described in the Mie theory.[238]
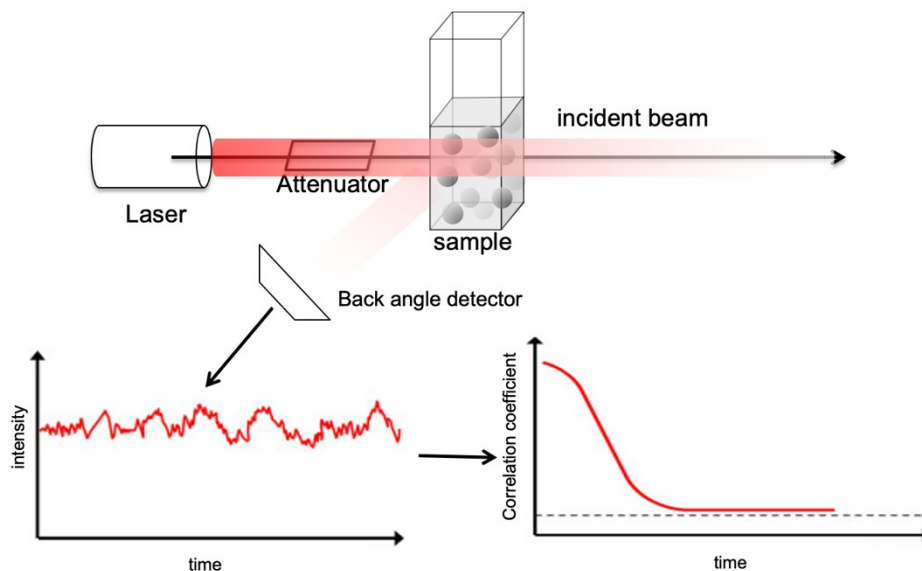
Figure 3-4: View of the setup of the DLS device. It consists of a laser that further passes through an attenuator before passing through a sample consisting of a colloidal dispersion of particles. Size of the particles, speed of migration through the sample, ion concentration in the solution, the laser is reflected through the sample, which is captured using the back angle detector (173 degree).Time dependent intensity-based graph is plotted by the device based on the continuous motion of the particles through the solution. This curve is further correlated to create a correlation curve also plotted against time which may be evaluated using algorithms to provide a size distribution.

When a particle is dispersed in liquid, an opposite charge develops on the particle surface due to the adhesion of oppositely charged ions in the solution. The strongly bound ions on the particle outer surface make up the Stern layer. The stern layer is followed by a layer of loosely bound charges, which consist of both same and oppositely charged ions. These two layers are together called the electric double layer. It forms due to the surface charge of particles. The electric double layer is also called the diffuse layer, since the ions in this layer are mobile. The net charge on the particle is dependent upon the ions and the charge distribution throughout the stern- and the diffuse layer. The zeta potential (ZP, ζ) is the electrostatic potential measured at the slipping (shear) plane close to the point at which the Stern layer ends and the diffuse layer begins in the bulk dispersion medium (see figure 3-5). The surface charge measured by DLS is also dependent on the adsorption and desorption of the ions on the particles, thus altering the stern layer and therefore the mobile diffuse layer [234,235,239].

The ZP can be obtained using the method of electrophoretic light scattering. On application of an oscillating electric field based on its surface charge, the particle is set into motion towards the cathode or the anode. The particles are again scattering incident laser light and the particle velocity can be obtained by analyzing the frequency shift of the scattered light due to the Doppler effect. The speed of the particle motion toward to the respective electrodes is influenced by the dielectric constant of the medium, the surface charge of the particles, and the strength of the electric field applied shown by the Smoluchowski equation [240].

$$\upsilon_E = 4\pi\varepsilon_0 \frac{D\zeta}{6\pi\eta}(1 + \kappa a)$$
(3.2)

where υ_E is the electrophoretic mobility, ε_0 is the permittivity of free space, D is the dielectric constant of the solution relative to the dielectric constant of vacuum, η is the viscosity of the solution, κ is the Debye-Hückel parameter, a is the diameter of the particle. Accordingly, the ZP is calculated from the electrophoretic mobility of the particles.

SiNPs are populated with hydroxyl groups on their surface and undergo protonation and deprotonation in aqueous media. In this thesis, the NPs were functionalized with functional groups such as azide, biotin, amine, long chain polymers such as PEG, lipids and proteins. Biofunctionalization of silica particles were mostly done in aqueous buffer solutions with known ionic strengths and pH values. These conditions were chosen to avoid alterations in structural and functional properties of the functionalized biomolecules. The surface charge of the particles was analyzed before and after all surface modifications [89,111,112,129,234,235,239,241,242].
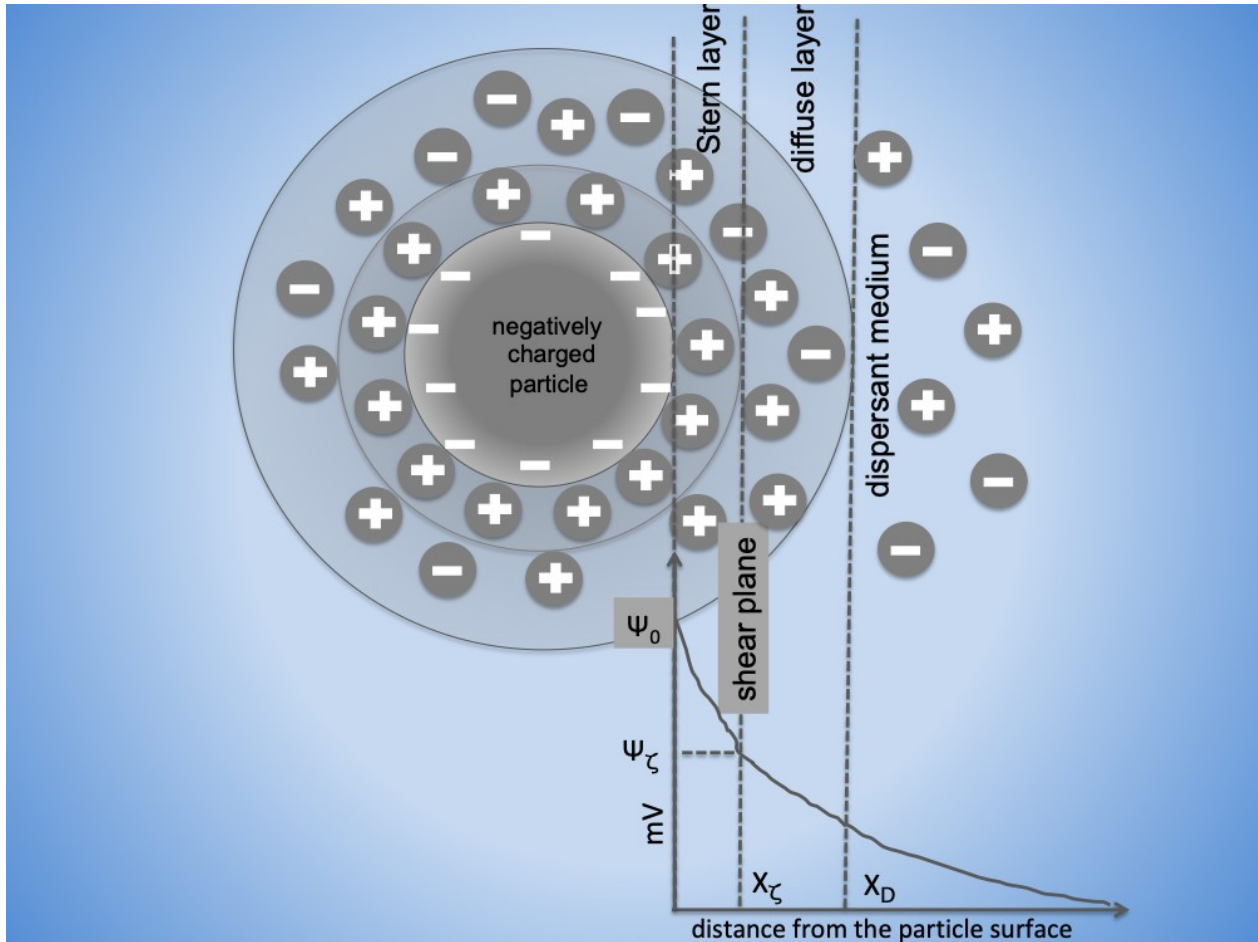
Figure 3-5: Electric double layer surrounding a negatively charged particle suspended in a dispersant medium. The layer immediately surrounding the particle surface is the Stern layer consisting of oppositely charged ions. The diffuse electric double layer consists of both positive and negative ions. The interface between the Stern and the diffuse layer is the shear plane and the point where the zeta potential (Ψ_ζ) measurement is made at. Ψ_0 is the surface potential of the particle and X_ζ is the distance from the surface to the shear plane. X_d is the Debye-Hückel length, which is defined as the length from the surface of the particle to the end of the diffuse layer after which the charge between the diffuse layer and the dispersant medium is not distinguishable.

3.2.2   Scanning electron microscopy

Scanning electron microscopy is a method commonly used to study external morphological properties such as texture, surface roughness as well as surface elemental compositions. This type of microscopy uses a beam of high energy electrons in a vacuum enclosed environment using a heated filament. Imaging using this method helps

characterize surfaces due to this electron-surface interaction creating a 2D image which helps understand the surface properties better. The incident beam of electrons is decelerated on the solid surface of the sample. One of the type of electrons are the secondary electrons (SE), which are knocked out of the sample itself and which are predominantly used for generating an SEM image. The electrons from the beam can also be reflected back, which as their name suggests, are called the backscattered electrons (BSE). The SE help in obtaining the topographical illustration of the sample and the BSE indicate multiple contrast levels based on differences in the composition of the materials. Each type of electron is received by a specific type of detector and are used to create an SEM image.

Good image quality is ensured by avoiding the accumulation of the electrons on the sample surfaces by using conductive specimen holders as well as rendering the samples conductive. By using conductive metal coatings such as gold or carbon, the electron scattering is ensured and hence accumulation of electrons is prevented [243,244]. However such coatings might limit the observation of the particles using SEM and therefore metal coating on samples was avoided. Silicon wafers glued onto a carbon tape placed on a metal holder were used to observe all the samples.

Electron microscopy imaging using SEM is known to provide accurate information at scales of 1-2 nm [243]. In this thesis, electron microscopy using SEM was performed using the device, Supra 40 (Carl Zeiss, Germany) operated at a voltage of 1 kV. Different NP decorated wax Pickering emulsion droplets and Janus particle attachment on bacteria were studied using SEM.

For observation of the NP decorated wax Pickering emulsion droplets, the washed vacuum dried wax droplets decorated with NPs before and after surface functionalization were left to dry overnight at RT. The dried wax droplets were deposited onto the silica wafers (3×3 mm). Electron microscopy images of overview and close-up view of the wax droplets were prepared to ensure the presence of particles on the surfaces of the wax structures. Confirmation of the selective attachment of NPs onto surfaces of the bacteria such as *E.coli* and *S.simulans* as a part of the experiments described in chapter 5, was also achieved using SEM [116,126,245]. The bacterial suspension with the attached NPs

was deposited onto silica wafers placed in a 6-well plate. To ensure that the negatively charged bacteria attach to the silica wafers, we first functionalized the silica wafers with APTES. Due to electrostatic interactions between the negatively charged bacteria and the positively charged wafers, we ensured that the bacteria would not be washed away by the upcoming steps of fixation, washing and dehydration. These steps were important due to the potential interference of the electrons inside the cells, due to the inherent water that they contain. These silica wafers were first fixed using 2.5% glutaraldehyde and further dehydrated using increasing concentrations of alcohol. 25, 40, 60,80, 95 and 100% absolute alcohol diluted using PBS was used as a part of the dehydration protocol [188]. The silica wafers were dried at RT before analysis.

3.2.3   Transmission electron microscopy

Transmission electron microscopy, similar to SEM, makes use of electrons from an electron beam which are transmitted through the sample. TEM consists of an electron gun producing the electron beam and the condenser system, which helps focus the beam onto the sample. The projection of a highly magnified image is dependent on the image producing system consisting of a fluorescent screen and a digital camera. The electron generated image must be converted to a visible image. The monochromatic visible image produced by the TEM makes viewing of the minute details possible. The electrons from the electron gun interact with the atoms in the sample before penetrating the sample. Variation in the atomic number throughout the sample contributes to the differences in the contrast obtained in the image of the sample. Based on the theory of mass-thickness contrast, the regions of the sample with higher atomic number would scatter more electrons and therefore create a darker region of an image whereas areas of the sample with lower atomic number make up the brighter parts of the image [246,247].

In this thesis, TEM analysis of NPs before and after Janus modification was done by creating a dispersion of the NP sample in aqueous solutions at a concentration of 0.1 g/L using ultrasonication. 4 µL of this solution was pipetted onto Formvar light carbon coated copper grids (Plano GmbH, Germany) and allowed to dry overnight. The carbon layer provides extra stability and added protection from the high intensity electron beam. TEM microscopy was performed using Zeiss EM900 (Zeiss, Germany, product number

SN8246) at a voltage of 80 kV. Images were acquired using a charge-coupled device camera attached to the software ImageSP.

Biological samples such as NIH3T3 fibroblasts with Janus particles were also analyzed using the TEM following the procedure described by Apte et al.[248]. NIH 3T3 cells incubated for 1 h, 6 h and 24 h in the absence or presence of NPs, respectively, were washed twice with 1 mM PBS (Sigma Aldrich, product number SLBF5741 V) followed by trypsin-EDTA treatment to detach cells. Cells were centrifuged at 6,000 rpm for 3 min and further treated for 1 h with 2.5% formaldehyde in 0.1 M Na-cacodylate at RT. After that, cells were washed with PBS and stained using 1 mM osmium tetroxide solution in PBS for 1 h at RT, resulting in a black cell pellet. This cell pellet was further washed twice with PBS, embedded in 2% agar in water and solidified at 4°C. Small 1 mm wide blocks were cut into squares and dehydrated with increasing concentrations of ethanol such as 30% (twice for 5 min each), 50% (twice for 5 min each), 70% (3 times for 10 min), 90% (3 times for 10 min), and 100% (twice for 15 min). Epoxy resin (Epon™812, Sigma Aldrich, Germany, product number 45345) embedding was performed on the dehydrated agar blocks containing the fixed cell pellet. To perform epoxy resin embedding of the cell pellet, 5 ml of the resin mixture was prepared using 5 ml the resin mixture containing 3 volumes of Epon A (6.2 ml of glycidether and 10 ml of Dodeceyl Succinic Anhydride (DDSA hardener)) and 7 volumes of Epon B (5 ml of glycidether and 13.35 ml of Nadic Methyl Anhydride (NMA) hardener). Finally, 4 drops of 2,4,6-(Tris dimethyl)-phenol (DMP-30) was added to the above prepared mixture and mixed thoroughly. The dehydrated agar blocks containing the fixed and stained cell pellet were then incubated with the resin solution mixed with 100% ethanol (1:1) for 30 min each twice. The blocks were then treated with a 1:2 mixture of 100% ethanol and resin solution twice for 90 min each. The cell pellets were then immersed in the resin solution containing the DMP-30 and carefully poured into molds followed by incubation at 60°C overnight. When analyzing biological samples such as the NIH3T3 fibroblasts in this thesis, it was important that the sample thickness is below 100 nm. This helps in the easy penetration of the electrons from the TEM through the samples. Sectioning of the cells embedded in epoxy resin was performed using the ultramicrotome (Ultracut R, Leica, Germany) [248]. The ultrathin cuts obtained were collected on mesh copper grids, allowed to dry overnight and then analyzed using the TEM set at a voltage of 80 kV. The localization of the Janus NPs in fibroblasts was

also studied using fluorescence microscopy. Since, the Janus particles used to perform cell surface attachment studies were fluorescently labelled, an additional method such as the TEM would give further information on the localization of the NPs.

3.2.4   Pendant drop tensiometry

Pendant drop tensiometry is a method commonly used to determine the surface tension of liquids using the curvature of a suspended drop [249]. It is a technique used to study wetting phenomena of particles, to gain in-depth understanding of emulsions and other interesting phenomena with colloidal particles and surface-active molecules [25,26,250]. Compared to particles with uniform wettability, Janus particles project interesting behavior when studied at interfaces [25–27,107,251].

The volume of the liquid drop containing the sample suspended from the tip of a needle is oscillated over a period of time. Dilational interfacial rheology is the method used to study stability of emulsions using time-based expansion and contraction of an emulsion droplet. The oscillating pendant drop was photographed and the obtained drop images were further used to determine the interfacial tension (figure 3-6).

The obtained droplet profiles were fitted by an algorithm that uses the Young-Laplace equation to obtain interfacial tension values as a function of time. These interfacial tension values can be used to understand the adsorption-desorption kinetics of surface-active molecules at interfaces. Analysis of the interfacial tension using the pendant drop tensiometry is advantageous since precise measurements can be done using small sample volumes. The tip of the needle generates a drop using the heavier phase (usually the liquid) within a lighter phase (in the work of this thesis, air).
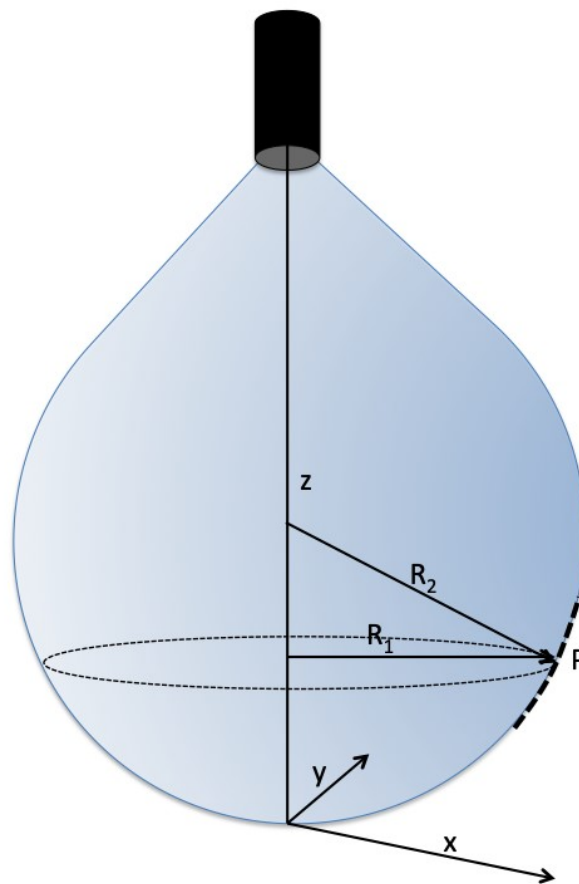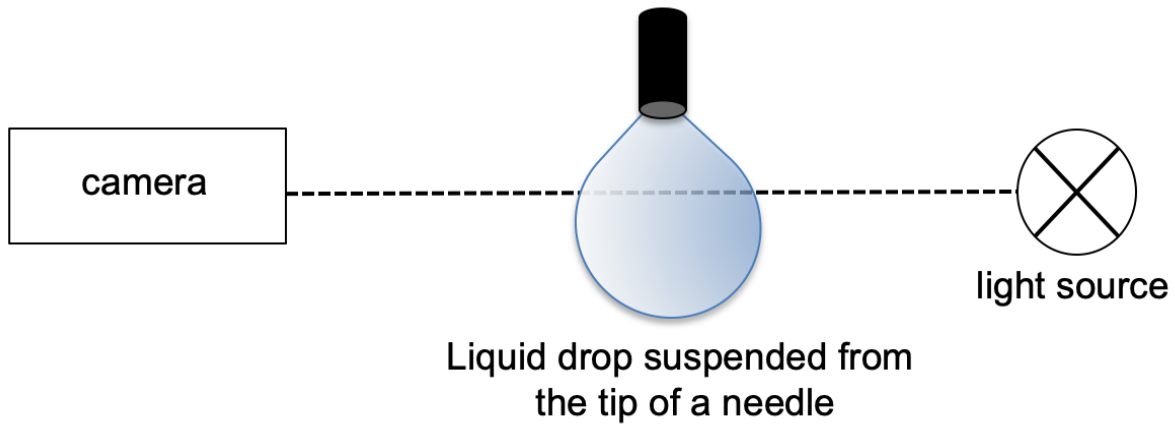
Figure 3-6: (above) Schematic representation of the general setup of a drop which is illuminated by a light source on one side and the camera to record images of the drop at defined time points on the other. (below) The Young-Laplace equation fitted on the pendant drop. The drop is suspended from the tip of the needle, which is oscillated, and images recorded are used to fit on the Young Laplace equation to further calculate interfacial surface tension. For calculating the principle radii of the curvature, R_1 and R_2 are shown, and P is the principle point, which is the last point of the drop. The drop shape is used to analyze and define the radii.

In this thesis Janus NPs with face separated protein halves were prepared (Chapter 4). The changes in the interfacial tension (γ) properties of the dispersion of Janus particles at a buffer-air interface was measured using pendant drop tensiometry (DataPhysics, Germany, product number OCA25) over a period of 2.5 h. In order to study the viscoelastic properties of the protein-protein functionalized Janus NPs, movies of the oscillating drop formed at the tip of a small steel capillary were recorded and the changes in the interfacial tension (IFT) over time were used to calculate values of storage modulus (or elastic modulus) E', which is the real part of the complex surface elasticity E* and loss modulus (or viscous modulus) E'', which is the imaginary part of E*. An 8 μl drop of 10 mg/ml NP dispersions in 10 mM MES buffer was created at the tip of the capillary (size Ø of 0.5mm) and oscillated at an amplitude dA/A of 1% and a frequency of 1 Hz over a period of 2.5 h.

3.2.5   Gas adsorption for specific surface area measurement

The theory of surface area measurement was first proposed by Brunauer, Emmett and Teller (BET), which involves the use of physical adsorption of gas molecules onto solid materials as well as powders. The method is simple and straightforward and uses non-reactive gases such as nitrogen and argon to calculate parameters such as pore sizes and SSA. Famously termed as BET theory based on the initials of the scientists who discovered it, the amount of gas adsorbed can be corresponded to the specific external and internal area of the material. For SSA measurements, the amount of gas adsorbed onto surfaces of materials was measured at the boiling point of liquid nitrogen (-196°C). [252,253] The condensation of liquid nitrogen occurs onto the surface of the sample because at the boiling temperature, liquid nitrogen is below its critical temperature. Assuming the amount of gas adsorbed onto the sample surface is a monolayer, the amount of adsorbed gas is correlated to the amount of surface area available. Physical adsorption occurs due to the relatively weak van der Waals forces between the gases and the surface of the materials. This method has been frequently used to measure the SSAs of nano powders and has also been used in this thesis to calculate the SSA of SiNPs

either commercially purchased (chapter 4) or synthesized (chapter 5 and 6). BET theory is expressed using the formula 3.7.

$$\frac{P}{n_a(P_0-P)}S_{total} = \frac{1}{n_m C} + \frac{(C-1)}{n_m C} \times P/P_0 \qquad (3.7)$$

where n_a is the quantity of adsorbed gas in volume units, P is the equilibrium pressure and P_0 is the saturation pressure of the gases at adsorption, S_{total} is the total surface area, N_m is the monolayer gas quantity, C is the BET constant, and P/P_0 is the relative pressure. SSA measurements using BET follows steps such as degassing, evacuation, volume, evacuation, adsorption and finally desorption.

Commercially obtained nano powders used for the experiments described in chapter 4, were dried for 24 h at 70°C prior to SSA determination. Aqueous solutions containing magnetite@SiO_2 NPs and RBITC doped SiO_2 NPs prepared and used for the experiments described in chapters 5 and 6 respectively were concentrated using centrifuged followed by drying at 70°C. All the dried nano powders were then subjected to a degassing step. BET measurements aimed to determine the gas adsorption isotherms and usually involve the degassing step as the initial step. Degassing is important so that any vapors or previously adsorbed gasses can be removed from the sample surfaces to obtain accurate and precise adsorption isotherms during BET measurement. In this thesis, nitrogen gas was flushed through the sample at an elevated temperature taking care of any temperature dependent alterations to the sample under analysis. The sample was then cooled and the before and after weight of the sample was noted down to compare any mass losses incurred during degassing. Evacuation of the sample and reference tube was performed using vacuum flushing. A dead volume measurement was performed using inert gas such as helium followed by noting the amount of the adsorbate on the sample and further corrected with the sample value. The amount of helium adsorbed on the sample should also be equally adsorbed onto the reference tube. The dead volume was then evacuated. During the adsorption phase, a Dewar vessel containing liquid nitrogen (77.4 K) was raised up to a certain point so that the sample and reference tube were immersed. A specific volume of adsorbant gas was allowed to enter into the sample which caused the pressure inside the tube to fall. This occured until the adsorbate such as the

atoms and molecules on the surface of the sample and the adsorptive, which is the adsorbant gas inserted into the sample, were in equilibrium. The volume of adsorptive gas on the sample at the equilibrium pressure, is the difference of the volume of gas admitted into the sample and the volume of gas remaining in the gas phase of the sample [252–254]. For the experiments performed in the thesis, no desorption step was performed.

The NPs used in this thesis were functionalized with functional groups such as azide, biotin, PEG, amine. The modification of the surface properties using silanization onto silica particles was performed according to the SSA values. As the first step of modification, silica particles were modified based on the SSA values obtained from the BET measurements for the introduction of the first functionality. This step was followed by the preparation of the wax Pickering emulsion droplets as mentioned above (see section 3.1.2 and 3.1.3). This was followed by an approximation based on the measured SSA of the unmodified particles for the introduction of the "Janus" character i.e., second functionality via the wax Pickering emulsion droplets. After the introduction of the functionalizations, the "Janus" character was expressed based on the number of functional groups characterized using the above-mentioned assays (see section 3.1.2). Specific assays were used to express „number of functional groups/nm^2" and thereafter gave an insight into the Janus character of the prepared particles. In order to achieve the Janus feature, understanding and calculating the theoretical SSA available for functionalization has been used throughout the thesis to design the Janus particles. In addition, the amount of surfactants used to prepare wax Pickering emulsion droplets using functionalized particles was also calculated according to the SSA of the NPs.

3.2.6   Vibrating Sample Magnetometry

Based on Faradays law of induction, if there are changes in the magnetic field an electric current will be produced. The current produced in this way can be measured and helps understand the magnetic field. The vibrating sample magnetometry (VSM) works on the same principle and is a technique used to measure magnetic properties of materials. When a sample placed in the VSM is subjected to a uniform magnetic field, magnetization of the sample will occur. Since the sample is magnetic, a magnetic dipole moment is created around the sample due to the constant magnetic field. Due to the vibration and

up- down movement of the sample in the magnetometer placed between the electromagnet pole, changes in the magnetic dipole moment are noted as a function of time as well as their magnetic hysteresis loop to give a detailed insight into the magnetic properties of the material. A magnetic hysteresis loop is expressed as a correlation between the magnetic flux density (B) and the magnetization field strength (H) of a magnetic material. This loop is often termed as the B-H loop. The magnetic hysteresis loop gives additional information of the magnetism projected by magnetic materials such as iron wherein the changes in the magnetization intensity are measured in relation to the magnetization field [255,256].

In this thesis, magnetite particles were prepared using the technique by Ding et al.[257] and were further coated with silica (Chapter 5). The results concerning the characterization of magnetic properties of magnetite and magnetite@SiO_2 NPs has been described in detail in chapter 5. The magnetism of the dried samples of magnetite and magnetite@ SiO_2 NP powders was analyzed using VSM (EZ9, Microsense, USA). Any changes in magnetic properties after coating of magnetic NPs with SiO_2 was recorded after the VSM analysis. Selective separation of bacterial cells using magnetite@SiO_2 Janus NPs was based on the magnetic properties of the as-prepared particles analyzed using the VSM method.

3.3 Characterization of prokaryotes after Janus particle application

3.3.1 Selective recognition of *E. coli*

In this thesis, bacterial concentrations were measured for the experiments including selective agglomerate-free separation of one bacterial species from a mixture of bacteria. The pure cultures of *E. coli* K12 (DSMZ-1077) and *S. simulans* (DMSZ 20324) were purchased from "Deutsche Sammlung Mikroorganismen und Zell Kulturen" (Germany) and were grown overnight in Luria broth medium and Tryptic soy broth respectively at 37°C for 24 h at 150 rpm continuous shaking. Concentrations of *E. coli* and *S. simulans* individually and in combination were adjusted by measuring the optical density (OD) at 595 nm (OD$_{595}$) to obtain a total concentration of 10^7 cells/ml in PBS (pH 6.2) according to McFarland standards [191].

3.3.2   Fluorescence microscopy

Fluorescence microscopy is an important technique used in several biomedical and biotechnological applications. Fluorescence microscopy offers several advantages compared to traditional optical microscopy. Fluorescence microscopy is specific and highly sensitive for visualizing different parts of materials or biological specimens based on the fluorophores used. When specimens do not exhibit autofluorescence, fluorophores are used to stain specific parts of the cell. Fluorophores are molecules capable of absorbing the light of a specific wavelength and then emitting light of a different wavelength. Such fluorophores which are fluorescent markers can be used to selectively stain different compartments of the cells. Fluorophores conjugated to an antibody which attaches to antigens in specific parts of the cells, makes the visualization of sub-compartments of the cells possible [258–260].

The fluorescence microscope along with the excitation and emission lamps, also consists of specific filters that collect specific wavelength of light, thus making visualization of different fluorophores and mapping of specific areas of the cells possible. Fluorescence microscopy visualization of the sample itself such as tissue sections, cells in well plates, ceramic materials doped with fluorophores, depends on the physical properties of the sample itself [260]. Attributes such as thickness, amount of fluorophore tagged, and the absorption characteristics of the sample are important parameters to note in order to obtain good quality images. Other parameters such as exposure time, brightness, contrast and light intensity are important factors to fine tune the images obtained from the imaging software. Care needs to be taken when adjusting exposure times or contrasts so that no manipulation of the imaging signal occurs and in turn does not lead to loss of information and alteration of the results [258,259]. For example, when performing localization studies of NPs in eukaryotic cells, increasing exposure times could also be mistaken for background signals or noise being interpreted as NPs [112,259]. When performing toxicity studies using the fluorescence microscopy based live-dead staining, increasing or decreasing exposure times or sharply increasing contrasts, could mask signals which would otherwise be interpreted as dead or alive cells. When increasing exposure times, the sample is exposed to specific wavelengths of light for longer times which might also result in photobleaching. Photobleaching of the fluorophore causes the chemical structure

of the fluorescent molecule to be permanently altered due to longer exposures. This can render the sample unable to fluoresce anymore following such an irradiation. Therefore, care needs to be taken when visualizing the samples and thereafter interpreting results obtained using fluorescence microscopy [258–260].

## 3.3.3   Optical density measurement

Measurement of bacterial cell concentration in a liquid solution can be done using the spectrometry-based technique such as McFarland turbidity standards. Alternatively, colony forming unit (CFU)/ml values can be obtained using the plate count method (see section 3.3.4.1). When bacterial suspensions observed in visible light appear to be "milky", cells are present in the sample. The McFarland turbidity standards are based on a similar visual tool of cell number estimation wherein sample cell concentration can be calculated using standards containing specific concentrations of bacterial cells [261]. Another technique based on the principle of light scattering is the spectrophotometry-based turbidity measurement technique. Turbidity in samples is measured using the spectrophotometer using visible light. The wavelength of this measurement is fixed at 595 nm. OD measurements are based on the Beer-Lambert law and are an easy way to monitor continuous growth of bacterial cells along with cell count estimation [262]. Based on the concentrations of cells present in the light path, light scattering is observed since most bacteria are known to scatter light [263]. Alongside the scattering regime, the remaining outgoing light intensity passing through the solution is read by the detector. The light intensity captured by the detector is used to obtain OD values. This value is then used to interpret the number of cells using the McFarland standards (see figure 3-7) [261,262,264].

The ability of the designed Janus particles to extract bacteria was tested by dispersing 100 µg of Janus NPs in 1 ml *E. coli* suspension in the absence or presence of *S. simulans* in PBS buffer (Chapter 5). The negative controls included the exposure of NPs to *S. simulans* without *E. coli* to confirm the specificity of the conjugated antibody. After 1 h of incubation, an external magnetic field was applied by placing a large neodymium magnet (50.8×50.8×25.4 mm, 10.5-12.0 kOe) under each bacteria-containing well to collect the Janus NPs and the OD_{595} of the supernatant as well as the pellet was measured using a

spectrophotometer-based plate reader (Chameleon V, Hidex, Germany). Based on this data, the bacterial capture efficiency was calculated based on the equation 3.8.

$$\text{Capture efficiency}(\%) = \frac{\text{Initial [bacteria]OD}_{595} - \text{magnetically seperated [bacteria]OD}_{595}}{\text{Initial [bacteria]OD}_{595}} \times 100 \quad (3.8)$$

Bacterial suspensions without NPs were analyzed as growth control.
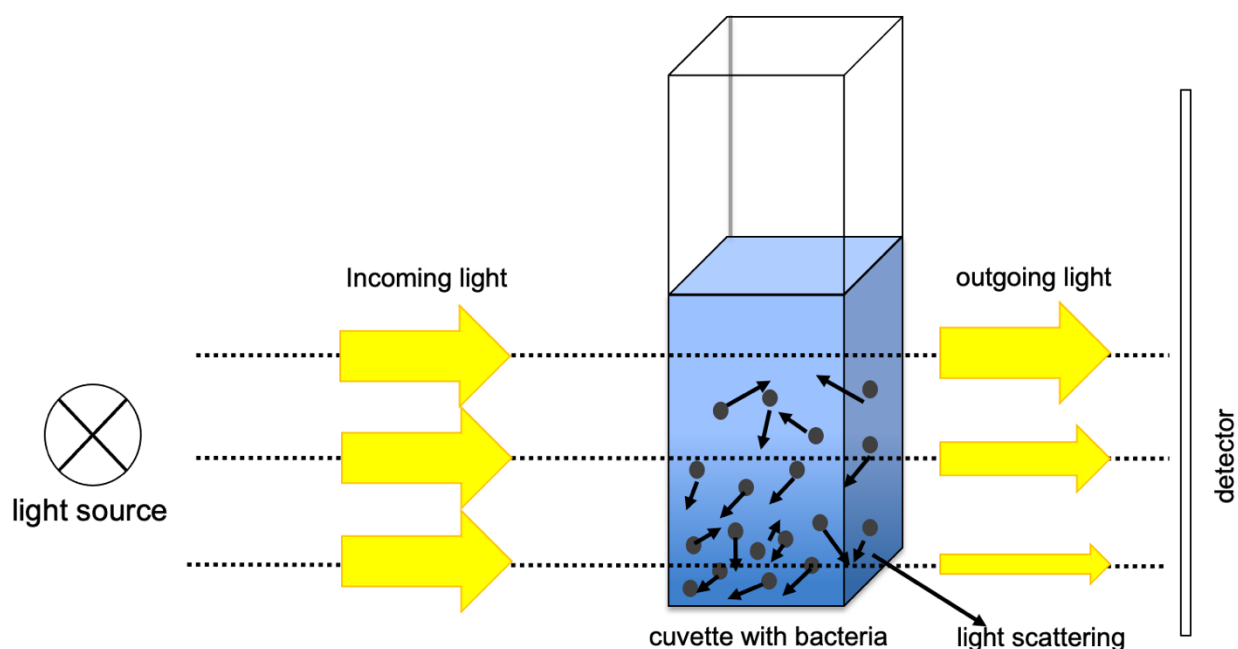
Figure 3-7: OD measurement using spectrophotometry. Sample is placed in a cuvette is irradiated with light (595 nm). Depending on the concentration of the cells present in the sample, higher the concentration of the cells, more light scatter is observed and less outgoing light is sensed by the detector. The Beer-Lambert law is used by the spectrophotometer to obtain OD values thereafter an estimation of the number of microbial cells.

3.3.4   Bacterial viability

Growth and division of bacteria is a crucial factor in the lifespan of these organisms and has been commonly used to measure cell viability. Commonly used methods for determining bacterial cell viability include methods assessing cell division, active metabolism [265] and membrane integrity [191,266,267]. The ability of bacterial cells to divide and multiply in nutrient medium thus forming visible colonies on agar plates can be

used to understand principles such as anabolic activity of the cells as well as toxic effects of a test material [191,268,269]. Bacterial membrane integrity is another assessment that can be used to determine cell viability. Using a mixture of two nucleic acid dyes such as green, fluorescent dye SYTO 9 that stains all bacterial cells and red fluorescent Propidium iodide (PI) that enters and stains only membrane damaged cells, makes the method of live dead staining easier to qualitatively determine bacterial cell viability. Hence as a measure of cytotoxicity in bacterial cells after being exposed to NPs, bacterial viability was tested using methods such as CFU counting, adenosine triphosphate (ATP) quantification and live-dead staining in this thesis.

3.3.4.1 Colony forming unit quantification

When individual bacterial cells are plated onto agar in petri dishes, the cells grow and develop into colonies. Each colony developed from a single bacterial cell is termed as a CFU. Viable cells would in turn form CFUs, making the method of colony counting an important measurement tool in studying toxicity effects of particles when exposed to bacteria. This method of viability analysis is an important method when new nanomaterials are designed for biological applications [269,270].

The cells were plated onto nutrient media with agar in petri dishes after serial dilutions since overcrowded plates would make manual counting extremely difficult. If bacteria cells plated onto agar would form larger number of colonies, the problem of underestimation would arise since plates would be packed with colonies making it difficult to distinguish and count. There is also the possibility of achieving smaller colonies than normal, due to limited substrate availability and confinement of space [271]. Hence dilutions of the bacterial samples were made for the toxicity studies of the NPs on bacteria. Compared to other methods of toxicity analysis such as microarray based probing and quantitative polymerase chain reaction (PCR), measuring CFUs to understand cytotoxicity is a straightforward and reliable method. Compared to PCR and microarray based methods, CFU counting involves lesser pipetting errors and is cost friendly since no extra reagent addition is required [272].

In our experiments, we measured CFUs formed after known concentrations of *E. coli* in the presence/absence of *S. simulans* were incubated with the NPs under experimental

conditions further described in chapter 5 were plated onto agar. These plates were incubated at 37°C and the colonies formed were counted manually after 24 h. Under conventional conditions, an optimal count is colonies between 30 and 300 obtained on an agar plate of 8 cm in diameter [273]. It is necessary to accordingly adjust the concentration of the bacterial solutions by performing optimization experiments using serial dilutions of the cells. The number of colonies obtained after pipetting a serially diluted sample to achieve countable colonies is further multiplied by the dilution factor to obtain the number of colonies in the original sample. The formula for calculation of CFU/ml (equation 3.9) is as follows:

$$c = \frac{n}{S \times d}$$ (3.9)

where, c is the concentration CFU/ml, n is the number of colonies counted, S is the volume of the sample used, and d is the dilution factor.

CFU/ml was used to address cytotoxicity of the NPs tested on the bacterial cells, *E.coli* and *S.simulans*.

3.3.4.2   Adenosine Triphosphate quantification

Quantification of adenosine triphosphate (ATP) amounts is a useful parameter in estimating the number of live and viable cells in the system. Alive cells contain ATP that are produced when the cells metabolize sugar, fats and other such biomolecules thus generating copious amounts of ATP [274]. When cells are exposed to particles, they might face cytotoxicity and loss of membrane integrity which in turn leads to the loss of cytosolic ATP production [269,270]. The ATPases in the cells utilize the ATP present as a part of their energy generation process [274]. The luciferase-based BacTiter-Glo™ Luminescent Cell Viability Assay (Promega GmbH, Germany, product number G8231) was used to measure the amounts of ATP-activated bioluminescence of luciferin and further correlate that to the number of viable cells present after particle exposure. The kit consists of a single reagent (BacTiter Glo) is directly added to the medium containing the bacterial cells and luminescence was recorded using the plate reader (Chameleon V, Hidex, Germany). Bioluminescence of luciferin, which is activated by ATP present in viable bacterial cells was measured using this assay.

3.3.4.3   Membrane integrity assessment

Membrane integrity was assessed using the live/dead assay (Live/Dead®, BacLight™, Life technologies, Germany, product number L7007). For the live/dead assay, a mixture of the cell staining dyes PI and SYTO 9 was added to the bacteria suspension after exposure to NPs according to the manufacturer instructions. Equal parts of the stock solutions of both the dyes were mixed thoroughly and 10 µl aliquots of were prepared. 3 µl of this dye mixture was added to the wells containing 1 ml of the cell culture media with bacteria. The dye mixture was carefully pipetted up and down followed by incubation in the dark for 15 minutes. The bacterial suspension stained using the Live/Dead assay was then analyzed using fluorescence microscopy (Axiovert Imager M1, Zeiss, Germany) at an excitation wavelength 485 nm and an emission wavelength of 530 nm (green) and 630 nm (red).

3.4 Characterization of eukaryotes after Janus particle application

3.4.1   Confocal laser scanning microscopy

CLSM is a visualization technique used very often to analyze biological samples where a high intensity and highly penetrating laser beam is used to 3-D reconstruct the cells or other biological materials. In this technique, the laser scans the sample on several focal points and different depths. It further combines the images taken at these points to create a 3-D image. CLSM follows the basic principles of optical microscopy, however, it differs in the type of principle light source used. CLSM uses a laser beam whereas traditional optical microscopy technique uses visible light for imaging. An overview of the general setup of the CLSM is depicted in the figure 3-8 below. The detectors present on the emission end of the CLSM act as a photomultiplier that functions to convert the received photons into electric signals [275,276].

In this thesis, evaluation of potential NP attachment and cellular uptake in fibroblasts was done using CLSM. After exposure of the cells to the NPs for the respective time points, the NP dispersions were removed, and cells were washed thrice with pre-warmed PBS to

remove any loosely or unspecifically bound (for example as a result of sedimentation) and non-internalized NPs. The cells were then fixed with 4 % paraformaldehyde (PFA, Sigma Aldrich, Germany, product number 53260) for 15 min at RT and then permeabilized using 0.5% Triton X-100 (Sigma Aldrich, Germany, product number MKBL5839V) for 3 min at RT. Similar to the staining protocol used to perform fluorescence microscopy, NIH3T3 fibroblasts were incubated with RBITC dye doped SiNPs for specific time points on glass coverslips and further stained using 4',6-diamidino-2-phenylindole (DAPI, $0.5\mu g\ ml^{-1}$, Sigma Aldrich, Germany, product number 1242642) and Alexa fluor 488 phalloidin (AF488, 2U/ml, Sigma Aldrich, Germany, product number 1151587) as nuclei and cytoplasm- specific dyes.
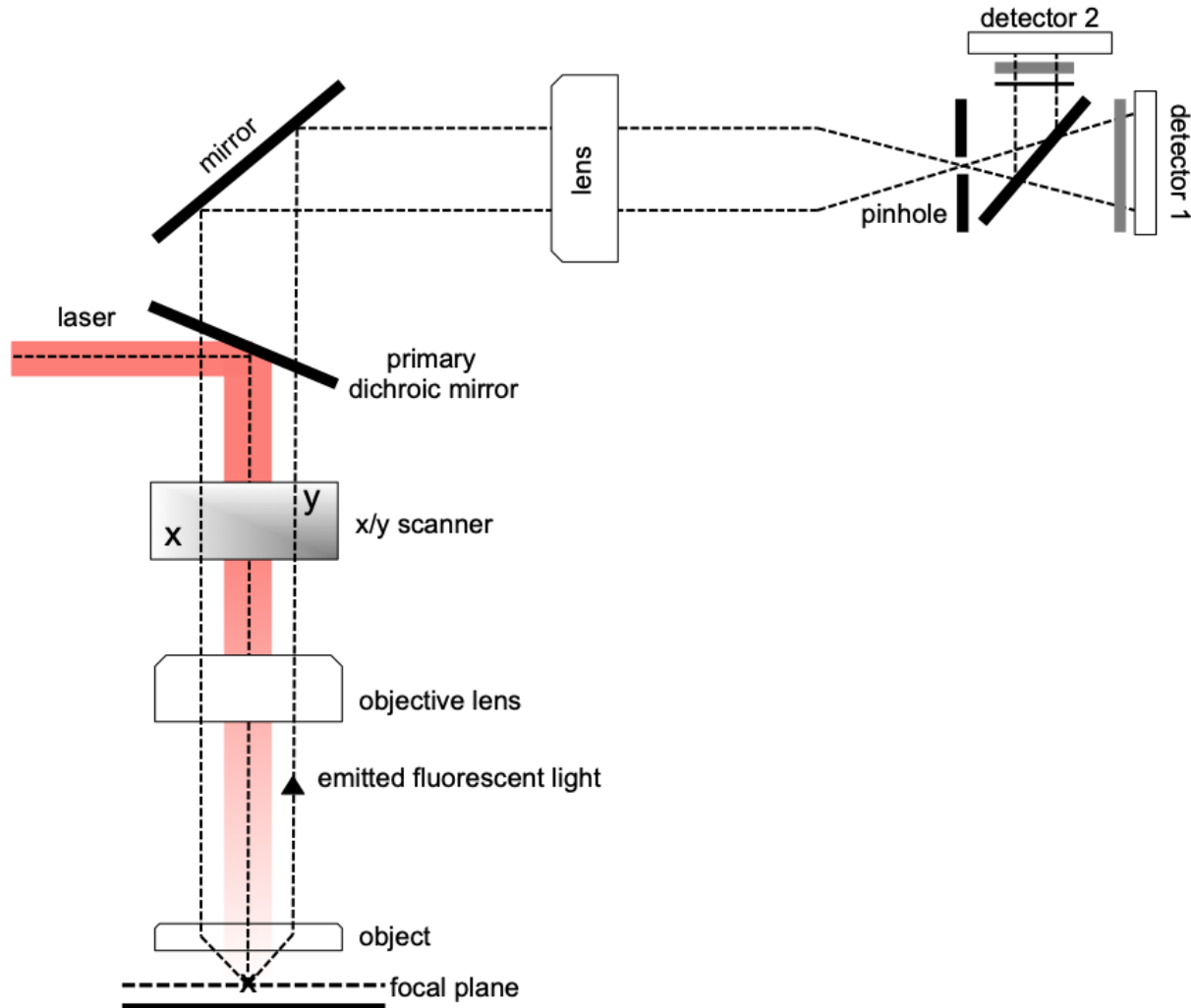
Figure 3-8: Diagrammatic setup of the CLSM. Light from a laser passes through a primary dichroic mirror, which also acts as a beam splitter. The beam then passes through the x and y scanners where it is set to raster scan. The laser light is further directed to raster scan the sample via the objective lens. Samples, either labelled using fluorophores or exhibiting autofluorescence, emit the fluorescent light towards the mirror and then the pinhole. The pinhole is further projected through a secondary dichroic mirror that separates the specific wavelength of this emission onto detectors. These detectors convert the photons eventually into pictures. Adapted from [276].

Images were acquired using the CLSM (Zeiss LSM 880, Zeiss, Germany) with a Plan-Apochromat 63/1.4 DIC M27 lens. The following settings were used for measurement: DAPI: track 2 Ch1 emission filter 410-494 nm laser 405 nm (exposure time 20 ms). Actin AF488 phalloidin: track 1 ChS1 emission filter 490-544 nm, laser 488 nm (exposure time 40 ms). RBITC NPs: track 2 Ch2 emission filter 566-685 nm laser 561 nm (exposure time

50 ms). The pinhole setting for all the measurements was 50 µm for the 3 channels mentioned above.

3.4.2   Microtome slicing

The electrons sourced from the TEM are unable to penetrate through biological samples that are more than 150 nm thick. Hence for precise examination of biological samples using the electron microscope, ultra-thin sections between thickness of 30-60 nm should be prepared. The ultramicrotome is a device used for making ultra-thin sections of the cells used for viewing using the TEM [277]. Biological samples were first embedded into an epoxy resin as described in the section 3.2.3 followed by sectioning using the microtome. The samples were trimmed into 1 mm×1 mm front block face which are either square or trapezoidal to maximize the presence of the sample at the front using a razor blade. Trimming was continued to obtain initial cuts using the glass knife attached to the microtome (Ultracut R, Leica, Germany), where semi-thin sections of the sample were cut (0.5 µm to 2 µm). The semi-thin sections were first hydrolyzed in water followed by an incubation in toluidine blue staining solution (0.01 vol% in water) for 3 min. These cuts were then washed several times with water before observing them under the light microscope. This step was used to confirm the presence of the sample in the cuts prepared. Finally, ultra-thin sectioning was made using the diamond knife with a trough containing water, where the cuts float after being sliced from the sample block. The cuts were collected using copper grids which were used to lift the cuts from under the water surface. The grids containing the slices were left to dry overnight before being observed under the TEM at a voltage of 80 kV [248,278,279].

3.4.3   Inhibition of endocytosis

Endocytosis is the process of uptake of nutrients, biomolecules and fluids into the cells. Through the process of endocytosis, engulfment of matter occurs by creating an invagination of the plasma membrane around the material followed by vesicle formation. This vesicle is pinched off. This vesicle travels within the cell before releasing the cargo to the targeted compartments or are sent towards the process of degradation as

lysosomes. There are different types of endocytosis pathways occurring at the cell surfaces for the transport of NPs namely, clathrin-, caveolae- and macropinocytosis-mediated [217,219].

Clathrin-mediated endocytosis is the most commonly observed endocytosis pathway in cells. The protein clathrin binds onto the pits to form a clathrin coated vesicle. Receptor mediated endocytosis occurs using this endocytosis pathway. NPs that attach to receptors on the cell surface trigger clathrin-mediated endocytosis, which are further taken up during vesicle formation. The endosomes containing NPs are further transported for degradation by fusion into lysosomes that contain hydrolytic enzymes. These degradation processes inside the lysosomes makes the process of using NPs targeting molecules challenging for biomedical applications. Additionally, it is also important to elucidate the endocytosis pathway used by the cells to ingest the NPs into the cells. To understand this process, it is necessary to use commercially available endocytosis inhibitors to inhibit such pathways and gain knowledge of the cellular processes for NP entry [217].

In this thesis, two different commercial endocytosis inhibitors were used to identify the potential uptake pathways that are triggered by our synthetic NPs. NIH 3T3 cells were incubated in the presence of hypertonic medium containing highly concentrated sucrose (0.45 M, Sigma Aldrich, Sigma Aldrich, Germany, lot number 1076511000), nystatin (10 µM, Sigma Aldrich, lot number 020M13491) or wortmannin (300 nM, Sigma Aldrich, Germany, lot number 023M4072) in combination with the NPs for 1 h, 6 h or 24 h, respectively. To prevent effective endocytosis, cells were incubated at 4°C for 1 h, 6 h and 24 h in the absence or presence of NPs. Following incubation, cells were fluorescently stained and imaged as described in 3.4.1. As control, cells were analyzed in the absence of endocytosis inhibitors at all the respective time points.

3.4.4   Membrane integrity measurement

Cellular toxicity assessment is vital factor to be taken into consideration while performing invitro studies using NPs. Such colloidal systems interact with cells and alter the normal cellular processes and one of them being affecting cellular viability. Toxicity studies are

important to derive conclusions of the effects of the particles on cells and to rule out possibilities of effects occurring due to cellular toxicity such as membrane damages. Effects of such particles on viability of the cells can be assessed using several tools that measure cell membrane integrity. Effects such as reduced metabolic activity, the presence of cytosolic enzyme LDH in the extracellular fluid, membrane impermeable dyes, such as trypan blue or PI that enter cells further staining intracellular components due to compromised cell membrane integrity are indicators of cellular toxicity [269]. Many live-cell and dead-cell protease markers have also been designed that stain live and dead cells based on membrane integrity [268]. Two such methods have been used in this thesis to measure NP induced cell toxicity including LDH quantification and reduction of metabolic activity using the water-soluble tetrazolium salt (WST-1) assay.

3.4.4.1   Lactate dehydrogenase quantification

As a part of the cell viability analysis, membrane integrity of the cells was measured. An intact membrane indicates a healthy cell. Damages to this membrane would result in the displacement of some of the cellular constituents. One such constituent is the cytosolic enzyme lactate dehydrogenase (LDH). The presence of LDH in the extracellular environment is one of the first indicators of damage to the cellular membrane and reduced cell viability. The leakage of LDH was assessed by quantification of LDH in the extracellular liquid as well as the cellular LDH to determine the totality of LDH present in the cell. Comparisons were made to an ideal setup, where the natural conditions were maintained, and no foreign materials were exposed to the cells. the LDH quantification and in turn cell toxicity is dependent on the type of cells used, concentration of the particles and the time of exposure of the particles [280,281].

LDH quantification proceeds by catalyzing the enzymatic conversion of lactate to pyruvate coupled with the reduction of nicotinamide adenine dinucleotide (NAD^+) to NADH. Diaphorase, a part of the quantification kit, further uses NADH to reduce the tetrazolium salt (INT) to formazan. The red colored formazan can be quantified colorimetrically at 490 nm. LDH amounts can be proportionally correlated to the amount of formazan quantified

using this assay. The chemical reaction of this assay has been depicted in the figure below (figure 3-9).
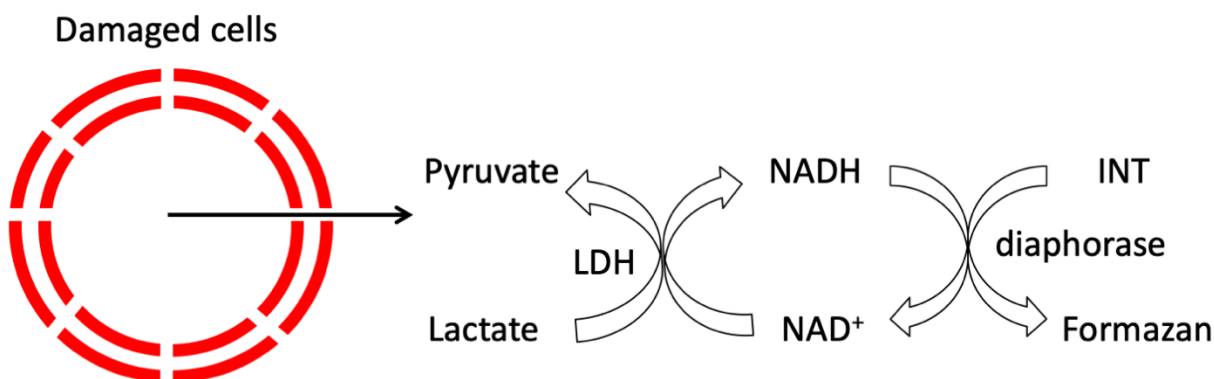
Figure 3-9: Cell viability measurement using the LDH assay. Membrane integrity measurements using quantification of LDH enzyme secreted due to holes created in the membrane as an effect of cytotoxicity. Final product, Formazan, was quantified colorimetrically at 490 nm. The figure has been adapted from the data sheet provided by the manufacturer (Thermo Fisher Scientific GmbH, Germany).

In this thesis, intra- and extracellular quantities of LDH were quantified in the absence and presence of the NP dispersions using the Pierce assay (Thermo Scientific, Germany, lot number OL17881450). For the quantification of extracellular LDH released by damaged cells due to the loss of membrane integrity, the media was collected after incubation of the cells with the NPs and centrifuged at 10,000 g for 3 min to remove any dispersed NPs. The quantification of released LDH was performed following supplier instructions using 50 µL of cell culture medium. To obtain the intracellular LDH concentration, cells were detached from cell culture plates by trypsin-EDTA treatment and centrifuged at 600 x g for 10 min to harvest the cells. Afterwards, cell lysis was performed using lysis solution (1 % v/v Triton X-100 in 0.9% w/v NaCl in water). The suspension was mixed by pipetting several times to obtain a clear solution and 50 µl of the cell lysate was used for the LDH assay. After incubation for 30 min in the dark, the absorbance of the samples after addition of 50 µl of the assay solution was analyzed at 490 nm along with a reference measurement at 680 nm using the Multiscan GO spectrophotometer. Cells incubated in DMEM+FCS (10%) and AB/AM (1%) were used as minimum LDH activity control (100% cell viability) and cells incubated with 2 % v/v Triton X-100 in 1 mM PBS buffer were used as maximum

LDH activity control (0% cell viability). The amount of LDH was normalized to the total LDH concentration (extracellular LDH + intracellular LDH).

3.4.4.2 WST-1 assay

Similar to LDH quantification, the WST-1 assay is based on the colorimetric method for quantification of cell growth, proliferation and cell toxicity. The assay kit used in this method includes the water-soluble tetrazolium (4-[3-(4-Iodophenyl)-2-(4-nitro-phenyl)-2H-5-tetrazolio]-1,3-benzene sulfonate (WST-1), which in turn converted into formazan, a colored soluble product. This product is quantified using a spectrometer at 440 nm with a background measurement at 600 nm. Cell toxicity studies are performed using salts such as 3-(4,5-dimethylthiazol-2-yl)-2,5-diphenyltetrazolium bromide (MTT) and WST-1. NADH occurring inside the cells acts as an electron acceptor for the reduction of the MTT salt, an indicator of metabolically active cells. The second generation tetrazolium salt WST-1 [269], unlike MTT, is a negatively charged salt, which makes it membrane impermeable [282]. Hence the reaction predominantly proceeds at the surface of the cells. Being unable to penetrate the cells, this salt also requires an intermediate electron acceptor for the reduction reaction that can transfer the electrons from the cytoplasm to the cell surface to form the colored formazan product. NADH is oxidized to NAD^+ yielding the electrons that are accepted by phenazine methyl sulphate (PMS), also a part of the reaction solution. The reduced PMS product leaves the cells to further convert the WST-1 to formazan. This reaction is catalyzed by the mitochondrial succinate-tetrazolium reductase system, which is associated with the enzyme mitochondrial dehydrogenase. This enzyme is present in metabolically active cells. Increasing amounts of formazan correspond to the increase in cell proliferation where active cells have actively increasing amounts of dehydrogenase enzyme. The reaction using the WST-1 for quantification of cell viability has been shown in figure 3-10.
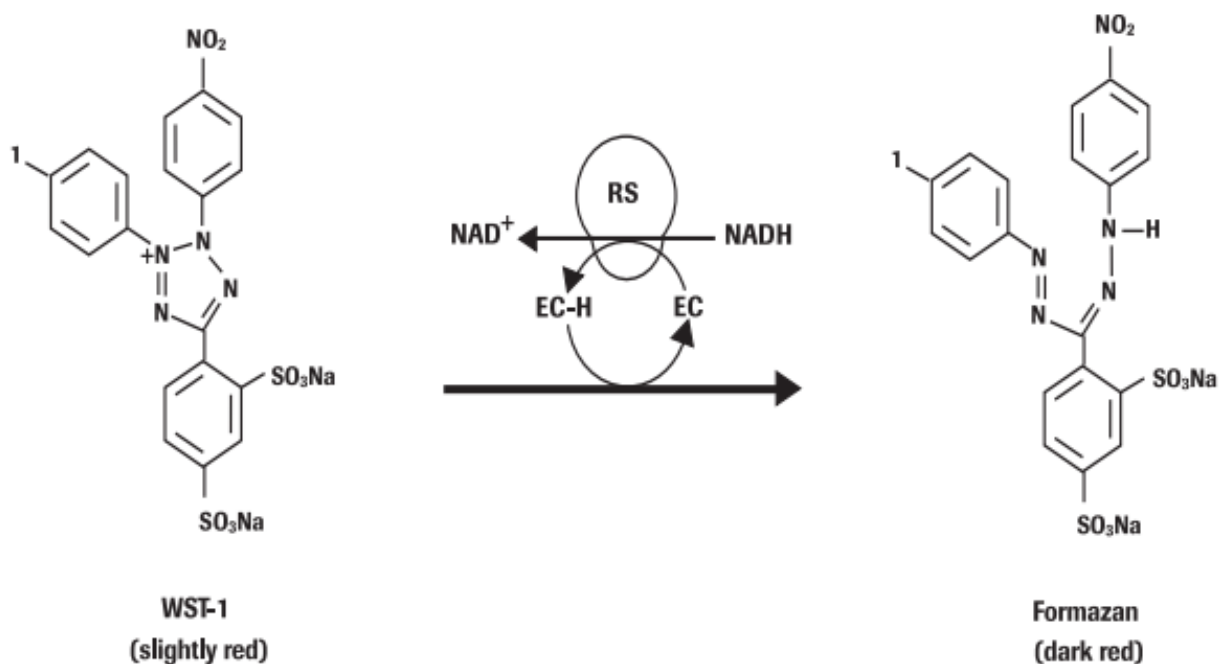
Figure 3-10: Conversion of WST-1 salt to formazan. WST-1 is slightly red in color and the final product, formazan which is dark red in color, is photometrically quantified at 440 nm. EC is the electron coupling agent such as PMS and the reaction in the cytoplasm is catalyzed by the mitochondrial succinate-tetrazolium-reductase system (RS). Figure has been adapted from the datasheet provided by the kit manufacturer (Merck Millipore, Germany).

In order to determine whether the synthesized NPs and/or the endocytosis inhibitors affected cell viability, a colorimetric WST-1 cell proliferation assay was performed as described in refs [129,283]. In brief, 100 µl of WST-1 (Roche Diagnostics GmbH, Germany, product number 14310100) cell proliferation reagent was added to the cell culture wells and incubated for 1 h at 37 °C, 10% CO_2 and 95% RH. The medium containing the WST-1 proliferation reagent was then collected from the wells and centrifuged at 10,000 g for 5 min to remove the NPs. The cells attached to the bottom of the cell culture plates were trypsinized using trypsin-EDTA solution and centrifuged at 1000 g to collect the cells. Formazan, which is a product of the enzymatic conversion of tetrazolium within living cells, was quantified by measuring adsorption at 450 nm using the Multiscan GO spectrophotometer (Thermo Scientific, Finland). DMEM+FCS (10%) + AB/AM (1%) which has not been in contact with cells was incubated with the WST-1 reagent and used as a background signal control.

Chapter 4

Nanoscale Janus particles with dual protein functionalization

4. Nanoscale Janus particles with dual protein functionalization

In this thesis, we designed a general approach for the preparation of nanoscale (below 100 nm) Janus particles with dual protein functionalization to establish a platform for the synthesis of such particles with a wide variety of proteins. Specifically, we chose proteins that could be easily visualized in TEM in order to straightforwardly elucidate success and limitations of our approach. To this end, we synthesized biofunctionalized Janus particles by combining and extending several well-known techniques. We used 80 nm SiNPs modified with 3-azidopropyltriethoxysilane (azidosilane) surface to prepare Pickering emulsions using molten wax as the droplet phase. The presence of the azide groups on the SiNPs enables the subsequent use of click chemistry. The azide functionalized SiNPs on the Pickering emulsion droplets were further subjected to face-selective silanization with biotin- PEG ethoxy silane. Afterwards, we grafted ferritin on the azide-functionalized side via a click reaction and the biotin groups were conjugated with streptavidin, which was labeled with ultra-small gold NPs. Ferritin, which contains an iron oxide core, and gold-labeled streptavidin were primarily selected for their visibility in transmission electron microscopy and can in principle be substituted by many other proteins via click chemistry on one side and by using biotin-conjugated proteins to bind to streptavidin on the other side. To prove the existence of Janus particles in a quantifiable way, we performed a full colloidal characterization of the particles including quantification of the surface groups, dynamic light scattering (DLS) and TEM. Since DLS does not provide information on the distribution of proteins on the particle surface and the statistics of TEM analysis are generally poor, we also characterized the collective behavior of the Janus NPs in dispersion by investigating the viscoelastic properties of thin films of particles adsorbed at the air/water interface. All measurements were repeated for 150 nm silica particles to confirm the general applicability of the method.

4.1 Results and Discussion

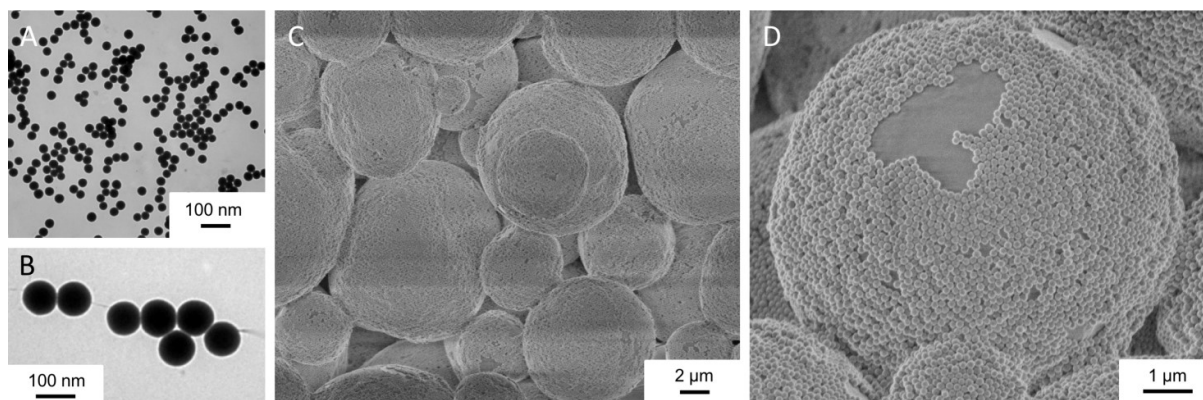## 4.1.1 Preparation of azidosilane-functionalized particles

For the preparation of Janus NPs with protein immobilization on face-separated halves of the particle surface, commercially purchased SiNPs (FiberOptic Center, USA, product number SIOP010-01-100G) of the size 80 nm and 150 nm were used. The first step of our preparation strategy is the functionalization of SiNPs with an azidosilane using an established sol-gel coating method.[136] BET measurements to calculate the SSA of 80 nm and 150 nm SiNPs was observed to be 2.83×10^{16} nm^2/mg and 1.509×10^{16} nm^2/mg particles.

The particle size before functionalization is 80 nm ± 20 nm with fairly low polydispersity (PDI = 0.15). After functionalization, the size of the particles is 90 nm ± 10 nm, and some agglomerates can be observed (PDI = 0.26). The success of surface functionalization can be mainly assessed via a change in ZP of the NP surface; here, the presence of azide groups on the surface of SiNPs (R-N=N$^+$=N$^-$) should neutralize the surface potential. Immobilization of azide groups on 80 nm SiNPs yielded a net negative charge of -25 ± 2 mV, which is moderately less negative compared to the non-functionalized particles (-37 ± 3 mV). The moderate change in ZP indicates that most of the SiNP surface is still covered by OH$^-$ groups, which is also indicated by the quantitative analysis of surface groups (Figure 4-4 and 4-5). Figure 4-1 A and B show representative TEM micrographs of the azide-SiNPs. See Table 4-1 for an overview of the prepared particles and their sizes, polydispersity and ZPs. An overview of the Janus particle synthesis is shown in chapter 3 (figure 3-1).

4.1.2 Preparation of wax-water Pickering emulsions

In the next step, the azide-functionalized particles were adsorbed at the surfaces of emulsion droplets of molten wax at 80°C using the method first described by Granick et al. [16] Adsorption proceeds via the well-known Ramsden-Pickering effect [92] that leads

to a decrease in surface free energy upon adsorption of particles at the liquid-liquid droplet interface, but only if the particles are able to be wetted by both liquid phases.
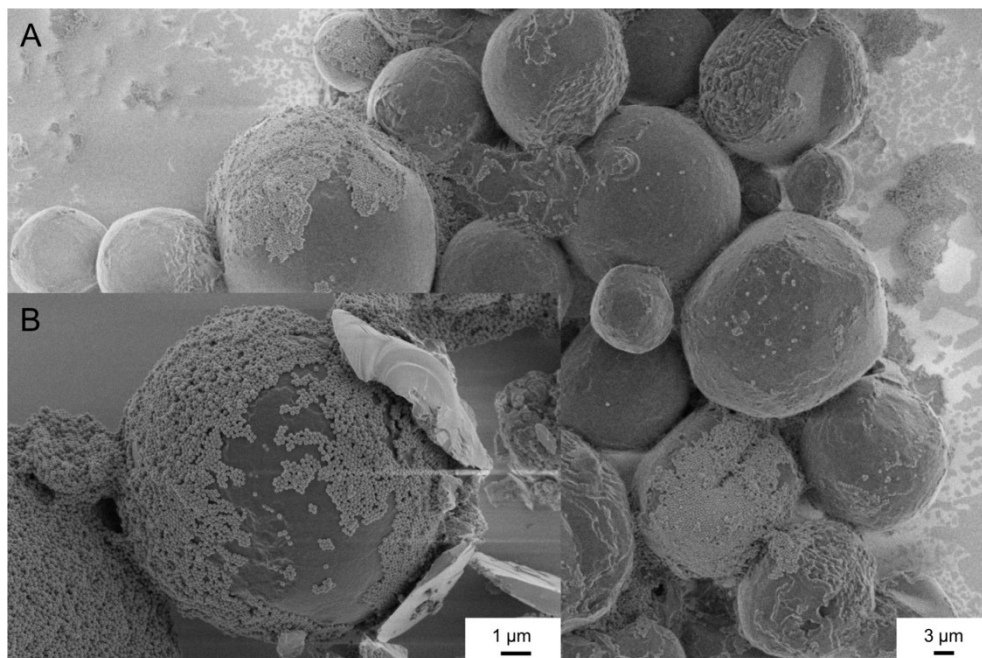

Figure 4-1: A and B. TEM micrographs of the prepared azidosilane-functionalized NPs. C. SEM micrograph of wax-water Pickering emulsion stabilized by azide particles and the surfactant CTAB. D. Close-up view of a wax core stabilized with monolayer of azidosilane-functionalized particles.

In order to realize adsorption of the highly hydrophilic silica particles, they were coated with the positively charged surfactant CTAB to increase their hydrophobicity.[16,17] Due to the high surface area of the nanoscale particles, the surfactant concentration in the silica/wax/water dispersion had to be significantly increased compared to the original protocol, directly proportional to the actual surface area of the particles. After cooling of the emulsion to RT, and with that solidifying of the Pickering emulsion droplets, the NP-covered wax microparticles have been analyzed via SEM (Figure 4-1 C and D).

The wax microspheres showed sizes between 10 to 60 μm with an irregular monolayer of azide-SiNPs on the surface that was able to withstand the filtration and washing steps that were necessary to remove excess surfactant. Since this method easily allows the production of these microparticles in gram quantities, it is a scalable approach for the production of Janus particles.

By firmly adsorbing at the wax droplet surfaces, the NPs are partially masked against functionalization from the wax phase which allowed the modification of the water-facing surface using biotin-PEG silane, again via a simple sol-gel coating procedure in ethanol at ambient temperature. Here, an excess of the biotin-PEG silane ensured that an

adequate amount of biotin groups covered the exposed azide functionalized particle surface.

Figure 4-2: A. SEM micrograph of wax-in-water Pickering emulsion droplets stabilized by azide particles and the surfactant CTAB after functionalization with biotin-PEG silane. B. Close-up view of a wax-core coated with azidosilane-functionalized particles.

Since this ethanol-based method might cause harm to the wax microparticles, we again investigated the morphology of the wax spheres using SEM after the modification of the spheres with biotin-PEG silane (Figure 4-2).

After sol-gel coating, the wax spheres tend to shed some SiNPs from their surface, however, a majority of the particles remained, ensuring the success of the functionalization of the water-exposed SiNP face with biotin end groups. The partial dissolving of wax in some areas during the reaction and, subsequently, several washing steps to wash off any residual silane molecules, might be the reason for the loss of the SiNPs from the wax droplet surfaces.
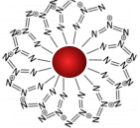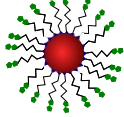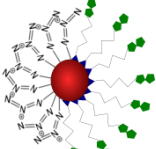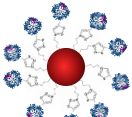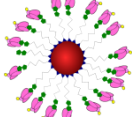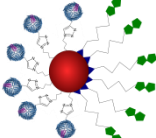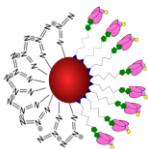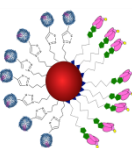
We already optimized this coating method for maintaining the integrity of the NP-covered wax microspheres. Experiments with methanol, toluene, longer reaction times and slightly elevated reaction temperatures proved unsuccessful (data not shown). Wax microspheres
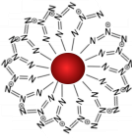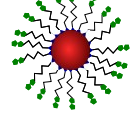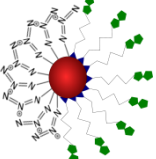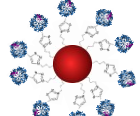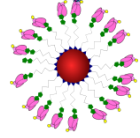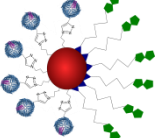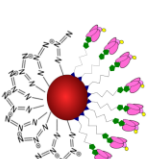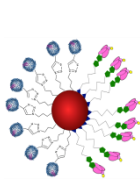
prepared with other organic solvents such as methanol, toluene did not sustain the experimental conditions and hence after SEM analysis yielded either deformed or melted wax spheres with no NPs on their surfaces respectively. Varied temperature and elevated temperature conditions also contributed to the deterioration of the microsphere shape.

After side-selective functionalization of the SiNPs with biotin-PEG silane, cyclohexane was used to dissolve the wax cores and hence to release the SiNPs with azide and biotin end groups on their respective sides. After wax removal, these Janus SiNPs were observed to be less negatively charged (-11.3 ± 2 mV) compared to the homogeneously azidosilane-functionalized SiNPs. This trend was also confirmed with fully (non-Janus) biotin-functionalized 80 nm particles (-4.4 ± 0.5 mV). Due to their low zeta-potential, the Janus particles were only slightly agglomerated (92 ± 15 nm, PDI 0.22) which was also observed in case of the 150 nm Janus NPs (Table 4-2).

Table 4-1: Size and ZP analysis of the 80 nm SiNPs after the applied functionalization steps. Functionalization of the respective hemispheres is marked by a dash.

NP surface functionalization	NP type	Zeta potential (mV)	Size average (d.nm)	PDI
Unfunctionalized		-37.3 ± 3	80 ± 20	0.15
Azidosilane (control)		-25.2 ± 2	90 ± 10	0.26
Biotin-PEG silane (control)		-4.4 ± 0.5	160 ± 6	0.14
Janus azidosilane / biotin-PEG silane		-11.3 ± 2	92 ± 15	0.22
Azidosilane – ferritin (control)		-27.3 ± 5	165 ± 25	0.33
Biotin-PEG silane – streptavidin (control)		+18.1 ± 6	80 ± 25	0.25
Janus azidosilane – ferritin / biotin-PEG silane		-17.1 ± 5.5	145 ± 68	0.15
Janus azidosilane / biotin-PEG silane – streptavidin		+7.6 ± 2.3	96 ± 50	0.18
Janus azidosilane – ferritin / biotin-PEG silane – streptavidin		+18.3 ± 6	156 ± 20	0.21

Table 4-2: Size and ZP analysis of the 150 nm SiNPs after the various functionalization steps. Functionalization of the respective hemispheres is marked by a dash.

NP surface functionalization	NP type	Zeta potential (mV)	Size average (d.nm)	PDI
Unfunctionalized		-33.2 ± 3	150 ± 20	0.21
Azidosilane (control)		-23. 5 ± 6	152 ± 52	0.40
Biotin-PEG silane (control)		-21.6 ± 7	160 ± 46	0.32
Janus azidosilane / biotin-PEG silane		-6.7 ± 2.4	155 ± 7	0.21
Azidosilane – ferritin (control)		+15.5 ± 7	310 ± 7	0.23
Biotin-PEG silane – streptavidin (control)		-7.8 ± 6.1	160 ± 20	0.19
Janus azidosilane – ferritin / biotin-PEG silane		-11.4 ± 8.6	300 ± 48	0.16
Janus azidosilane / biotin-PEG silane – streptavidin		+10.4 ± 4.7	165 ± 21	0.15
Janus azidosilane – ferritin / biotin-PEG silane – streptavidin		+29.7± 4	310 ± 50	0.25

The number of biotin and azide surface groups were quantified using the Fluoreporter® biotin quantification kit and the fluorescence of DBCO-Cy3, respectively. We attained a much higher number of biotin groups on the SiNPs compared to the number of azide groups (Figure 4-3 and 4-4). An analysis of the azide groups using the DBCO-Cy3 fluorometric analysis yielded only 8.03 ± 2.3 groups per fully azide-coated 80 nm SiNP (Figure 4-4). An average of 63.6 ± 7.3 azide groups were found on each fully azide-coated 150 nm SiNP (Figure 4-4). Comparatively, 80 nm and 150 nm Janus particles with an azide-coated hemisphere presented only 6.02 ± 4.5 and 21.2 ± 0.3 azide groups per SiNP, respectively. This difference between the 80 and 150 nm particles correlates directly to the surface area ratio based on the two particle diameters of 3.5. The surprisingly low number of azide groups still provides sufficient moieties for the subsequent click reaction as described below and are also reflected in the minor change in ZP as discussed above, as well as in the patchy binding with ferritin as shown below. Using the Fluoreporter® Biotin quantification kit, an average of 6430 ± 44 biotin groups on fully biotin-functionalized 80 nm SiNPs and of 2009 ± 12 groups per 80 nm Janus SiNP were found (Figure 4-3).
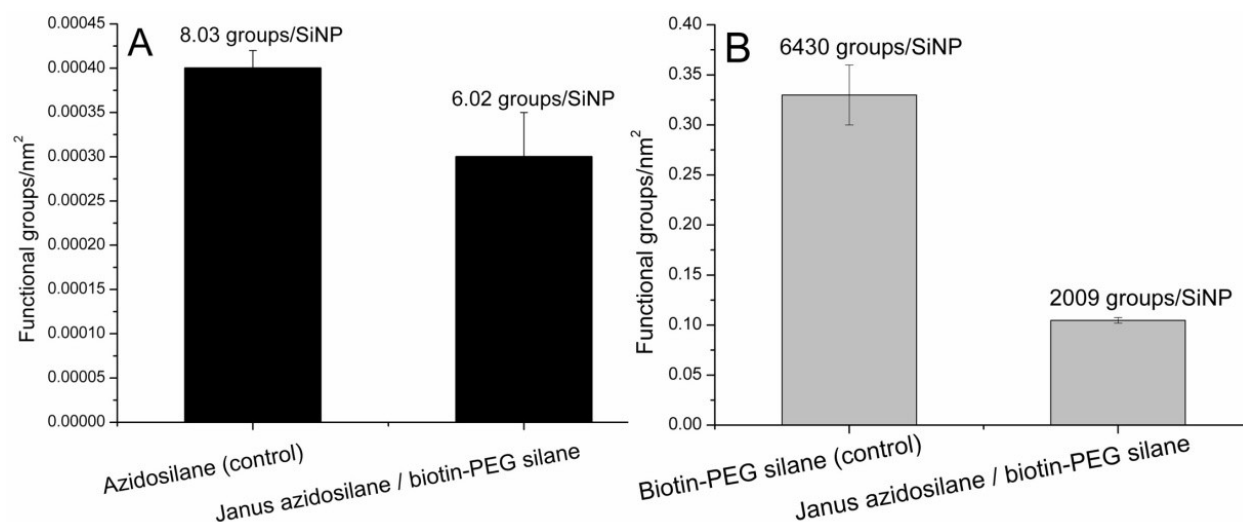
Figure 4-3: Number of biotin and azide functional groups per square nanometer on the surface of 80 nm NPs. The number of available and azide and biotin groups on the SiNPs were determined using the fluorescence of DBCO-Cy3 and the Fluoreporter® Biotin quantification kit, respectively. The numbers on the dark black and shaded bars represent the number of biotin (A) and azide groups (B) per SiNP. The fully coated SiNPs (first bar), were compared to the half-functionalized Janus azidosilane-biotin PEG silane NPs (second bar).

A similar evaluation of the 150 nm fully and half biotin-functionalized Janus particles yielded 28260 ± 25 and 8478 ± 53 groups, respectively (Figure 4-4) which again closely represents the surface area ratio between these two particles. The high numbers of biotin moieties on the silica surface represent roughly 0.3 functional groups per surface area, which shows that the surface is densely covered with biotin groups.
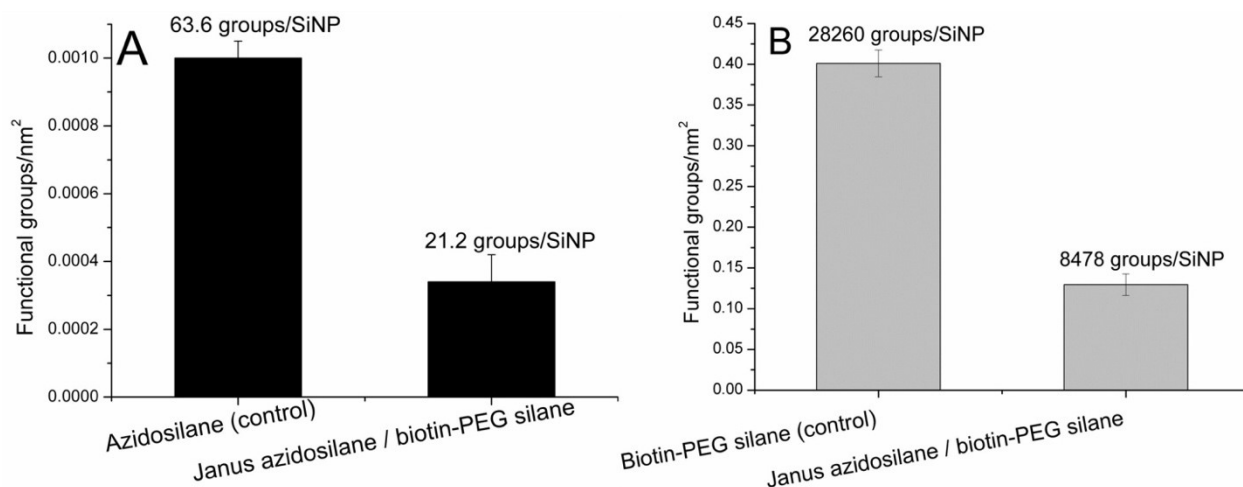
Figure 4-4: Number of biotin and azide functional groups per square nanometer on the surface of 150 nm NPs. The number of available and azide and biotin groups on the SiNPs were determined using the fluorescence of DBCO-Cy3 and the Fluoreporter® Biotin quantification kit, respectively. The numbers on the dark black and shaded bars represent the number of azide (A) and biotin groups (B) per SiNP. The fully coated SiNPs (first bar), were compared to the half-functionalized Janus azidosilane-biotin PEG silane NPs (second bar).

4.1.3   Preparation of Dual Biofunctional Janus NPs

The functionalization strategy with azide and biotin groups on the respective sides of the SiNPs enables orthogonal binding of proteins in further reaction steps. This we demonstrate with the model proteins ferritin and streptavidin. The azide groups can be utilized for the azide-acetylene cycloaddition click reaction, [284] which is able to link proteins that are modified with an acetylene group. Here, we used acetylene-modified ferritin, which, owing to its iron-containing core, can be efficiently visualized using TEM. The protein immobilization strategy, which is compatible with proteins and avoids the use of harsh chemicals, is performed in 10 mM MES buffer (pH 6.1) at RT. The isoelectric point of ferritin of 5.5 imparts a slight negative charge to the non-Janus SiNPs after

functionalization at the buffer pH of 6.1, which was confirmed by ZP measurements (-27.3 $\pm$ 5 mV) (see Table 4-1). Similarly, ferritin functionalization on the azide/biotin-PEG Janus particles restores the negative charge of the non-protein origin of the patches is most likely the low surface density of azide groups as discussed above. Non-covalent adsorption of ferritin was ruled out by control experiments in the absence of the copper catalyst for the click reaction. Uncontrolled protein adsorption onto NPs, the well-known protein corona effect, can be attributed to the clustered iron cores that can be observed on all ferritin-conjugated particles (Figure 4-5 A-C, G-I and Figure 4-6 A-C, G-I). In solution, ferritin is only slightly negatively charged (-1.62 $\pm$ 0.2 mV), which might further contribute to agglomeration between the protein molecules. functionalized SiNPs from -11.3 $\pm$ 2 mV to -17 $\pm$ 5 mV. TEM analysis shows the presence of agglomerated ferritin patches on the 80 nm control particles (full azide functionalization, Figure 4-7 A-B) as well as on the Janus particles (Figure 4-6 A-C).
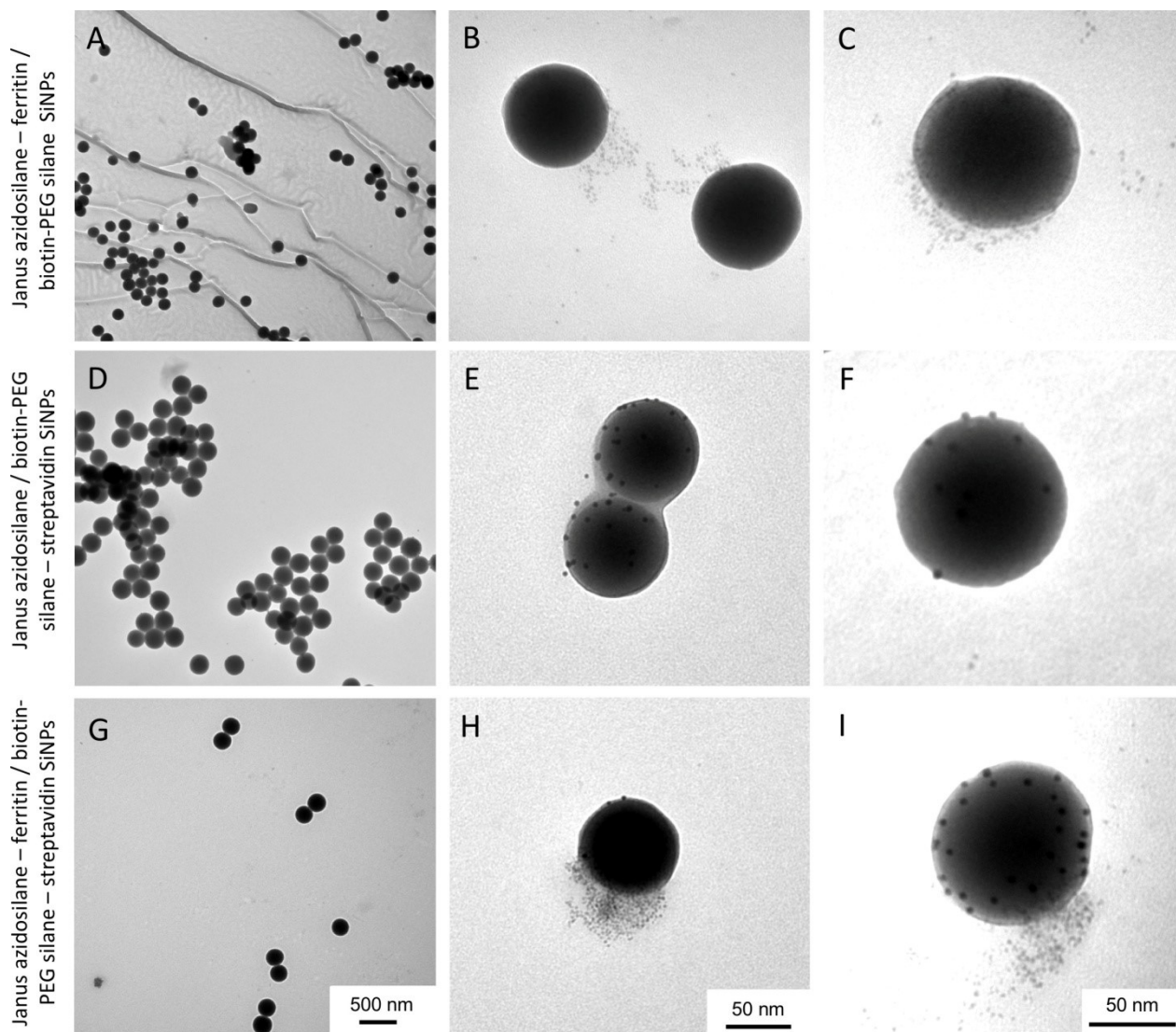
Figure 4-5: TEM micrographs of the prepared 80 nm Janus particles functionalized with azidosilane on one side and biotin-PEG silane on the other side. The rows show the different combinations of protein conjugation: (A-C) and conjugated only with ferritin, (D-F) only streptavidin (G-I) and both proteins. Column A, D, G shows overview images, while the remaining images show close-ups of individual, representative particles. The scale bars in A-C apply to each image in the respective columns.

The other hemisphere of the Janus particle was biofunctionalized with biotin-PEG silane, which was chosen to avoid unspecific interaction with proteins due to the PEG backbone and to ensure face-selective protein attachment via the highly specific biotin-streptavidin moiety. We used as-purchased streptavidin molecules that were conjugated to 10 nm gold particles to again ensure visibility in TEM and a good contrast to the iron oxide cores of ferritin.

Janus azidosilane – ferritin / biotin-PEG silane SiNPs

Janus azidosilane / biotin-PEG silane – streptavidin SiNPs

Janus azidosilane – ferritin / biotin-PEG silane – streptavidin SiNPs
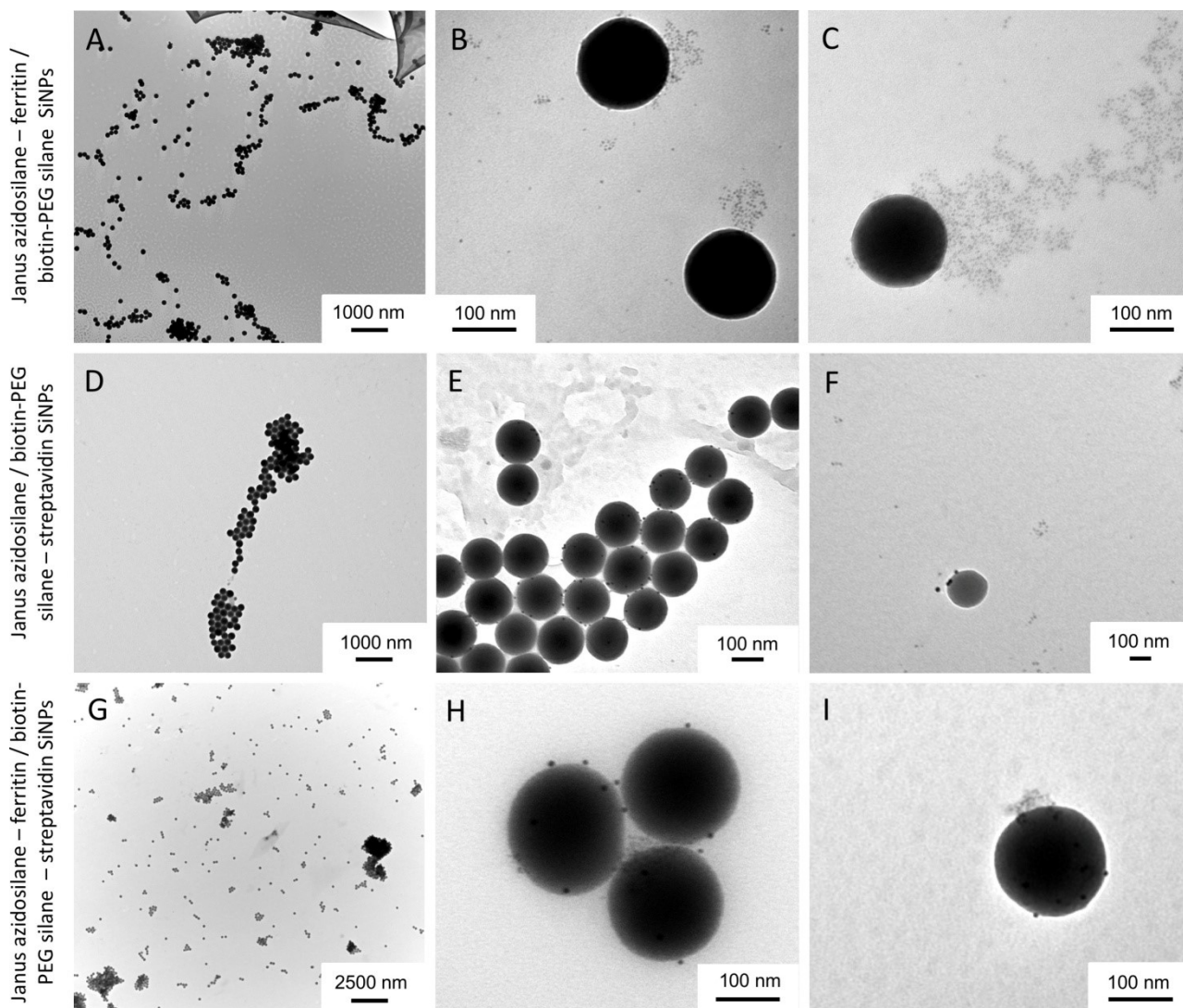
Figure 4-6: TEM micrographs of the prepared 150 nm Janus particles functionalized with azidosilane on one side and biotin-PEG silane on the other side. The rows show the different combinations of protein conjugation: (A-C) and conjugated only with ferritin, (D-F) only streptavidin (G-I) and both proteins. Column A, D, G shows overview images, while the remaining images show close-ups of individual, representative particles. The scale bars are indicated for the respective images.

Functionalization with streptavidin was performed in 10 mM MES buffer and was first tested for the non-Janus particles with full biotin-PEG coating (Figure 4-7 C,D). These fully biotin-PEG coated 80 nm particles had a positive net charge after streptavidin functionalization (+18.6 ± 6 mV, -4.4 ± 0.5 mV before coating). On the Janus particles, side-specific functionalization with streptavidin could be observed, as well (Figure 4-6, D-F). As expected for only half a coating, the ZP is lower (+7.6 ± 2.3), while size and PDI

remain stable, which indicates a stable dispersion. The 150 nm particles which were biofunctionalized in the same way as described here closely follow the same trends (see Table 4-2, Figure 4-6).
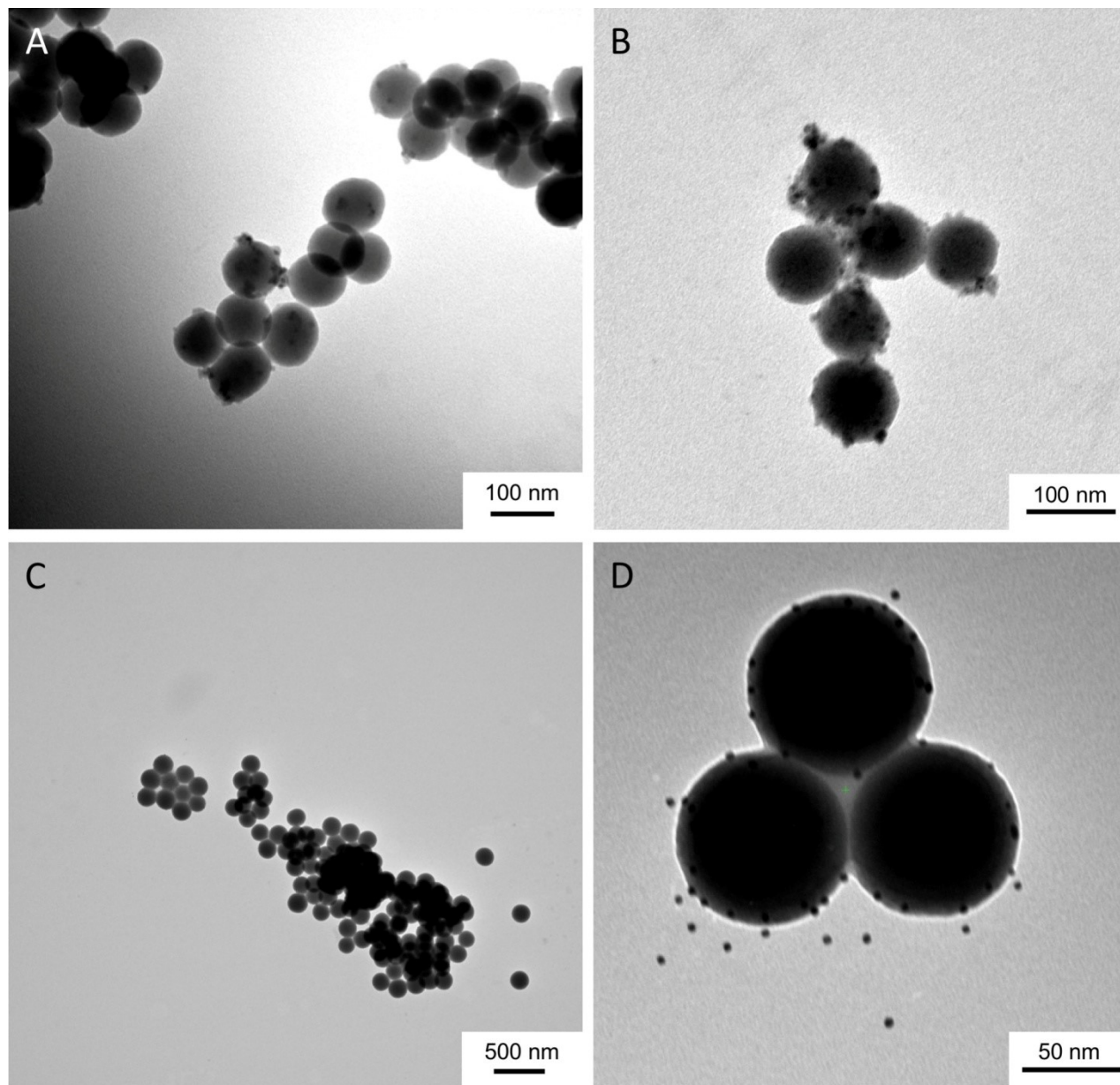
Figure 4-7: TEM micrographs of the prepared 80 nm monofunctional SiNPs (controls). A, C. Overview TEM micrographs of SiNPs monofunctionalized with azidosilane (A) or biotin PEG silane (C) respectively functionalized with azide functionality on one side and a biotin end group on the other. Size bars are indicated in the figure above. B, D. Close up of particles with respective protein functionalized on either of the silanes. These images indicate the success of the functionalization protocols for the preparation of the Janus particles.

Finally, Janus particles with dual protein faces were successfully prepared and the clear segregation of the ferritin and streptavidin sides is evident from the differences in iron and gold contrasts in the TEM micrographs (Figure 4-5 and Figure 4-6, G-I). Note, however, that the functionalization is not completely homogeneous which is most likely a result of a varying immersion of the particles in the wax surface as well as multilayer formation on some parts of the wax surface. The dual biofunctionalized particles maintain their colloidal stability with only minor changes in PDI and some dimerization. The success rate of this face-wise two-step protein functionalization was determined by counting the number of Janus particles in the TEM micrographs of the samples with dual biofunctionalization. We observed that 24 % of the 80 nm SiNPs were successfully coated with bifacially separated proteins, while 60 % were Janus particles with only one protein and only 8 % did not show any Janus aspect. The remaining particles were Janus particles with either ferritin or streptavidin coatings on one side (Table 4-3). In case of the 150 nm biofunctionalized Janus particles the success rate for dual biofunctionalization was 28 %, as summarized in Table 4-4.

Table 4-3: Success rate of protein functionalization of the 80 nm Janus particles. 50 random particles in each sample from three separate samples were examined and counted manually using TEM to assess the success of the preparation technique.

Name	Number	%
Janus azidosilane – ferritin / biotin-PEG silane – streptavidin	12 ± 6	24 ± 12
Janus azidosilane/biotin-PEG silane – streptavidin	10 ± 3	20 ± 6
Janus azidosilane – ferritin/biotin-PEG silane	20 ± 4	40 ± 8
Not biofunctionalized	8 ± 1	16 ± 2

Along with the mentioned irregularities of the wax spheres, moderate agglomeration of the particles prior to protein immobilization may influence the functionalization and hence may cause the lowering of the reported success rates. However, the observed dimerization (DLS sizes around 160 nm for 80 nm particles) is not necessarily connected to the Janus properties of the particles, as it was also observed in some of the homogeneously functionalized controls (see Table 4-1). Additionally, some complications

might arise as a result of incomplete dissolution of the wax causing particles to be trapped in residual wax, which might also prevent proper redispersion of the NPs. This aspect might necessitate further process optimization in regard to the envisioned biological applications of these Janus particles [136].

Table 4-4: Success rate of protein functionalization of the 150 nm Janus particles. 50 random particles in each sample from three separate samples were examined and counted manually using TEM to assess the success of the preparation technique.

Name	Number	%
Janus azidosilane – ferritin / biotin-PEG silane – streptavidin	14 ± 2	28 ± 4
Janus azidosilane/biotin-PEG silane – streptavidin	12 ± 3	24 ± 6
Janus azidosilane – ferritin/biotin-PEG silane	18 ± 2	36 ± 4
Not biofunctionalized	6 ± 1	12 ± 2

4.1.4   Pendant drop tensiometry

In order to characterize the collective behavior of the Janus particle dispersions, pendant drop tensiometry was used to measure the interfacial tension of the various Janus NPs over periods of several hours at the air/MES-buffer interface (Figure 4-8 A). Additionally, the interfacial dilatational rheology of the droplet interface was characterized by oscillating the droplet volume and recording the complex two-dimensional elasticity of the surface (Figure 4-8 B). The number of particles chosen for the analysis was maintained at 10 mg/ml, which is more than sufficient for populating the full droplet surface [25]. The aqueous MES buffer showed a surface tension of 69 mN/m which was not significantly changed by the presence of unfunctionalized (black) and non-biofunctionalized Janus SiNPs (green), indicating that the highly hydrophilic SiNPs themselves are not surface active [285,286]. The freely dissolved proteins ferritin and gold-conjugated streptavidin were highly surface active (Figure 4-8 A), as is well documented for various other proteins [287]. Here, ferritin seems to have slightly a slightly stronger effect when compared to streptavidin-gold. They both form highly elastic interfacial films (Figure 4-8 B) as is evidenced by the high two-dimensional storage modulus E', which again has a typical

value for proteins [287]. Based on the surface activity of the conjugated proteins, the protein-coated particles are all observed to decrease interfacial tension.
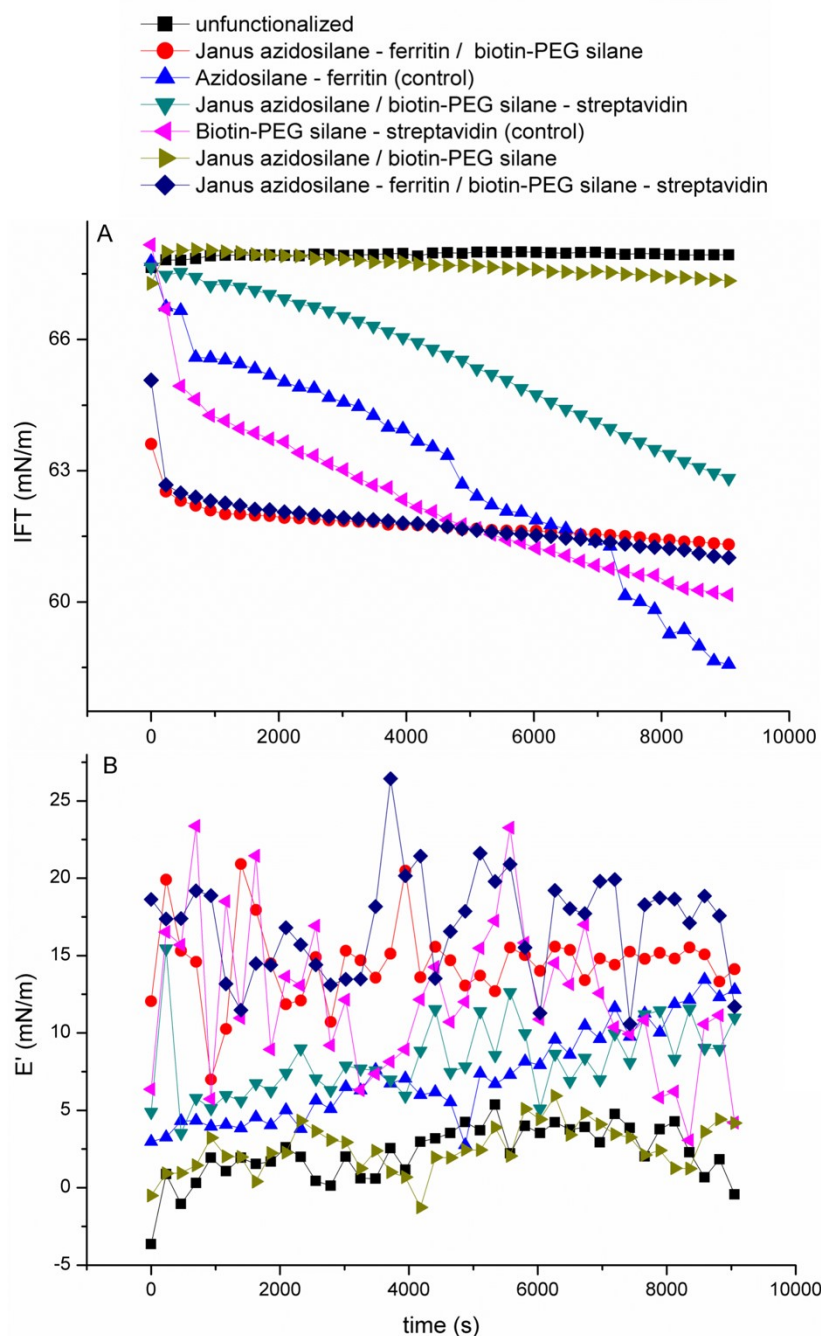
Figure 4-8: Interfacial tension and elastic storage modulus vs time using a pendant drop tensiometer for the 80 nm SiNPs. 0.1 M MES buffer was used as the drop phase. A. Average interfacial tensions recorded at the air-water interface. B. The two-dimensional storage module E' of the droplet interface at a constant frequency of 1/s and an amplitude (dA/A) of 1%.

Accordingly, the fully protein coated SiNPs (pink and bright blue) are more surface active compared to their half protein counterparts (green and red). Following the trend for the free proteins (Figure 4-9), half and fully ferritin functionalized SiNPs show a stronger effect compared to the streptavidin functionalized controls (Figure 4-8 A). This is also reflected in the two-dimensional elastic modulus (Figure 4-8 B) and viscous modulus (Figure 4-10) of the dilatational rheological measurements. The dual biofunctionalized Janus particles (dark blue) are highly surface active compared to non-functionalized SiNPs (black).
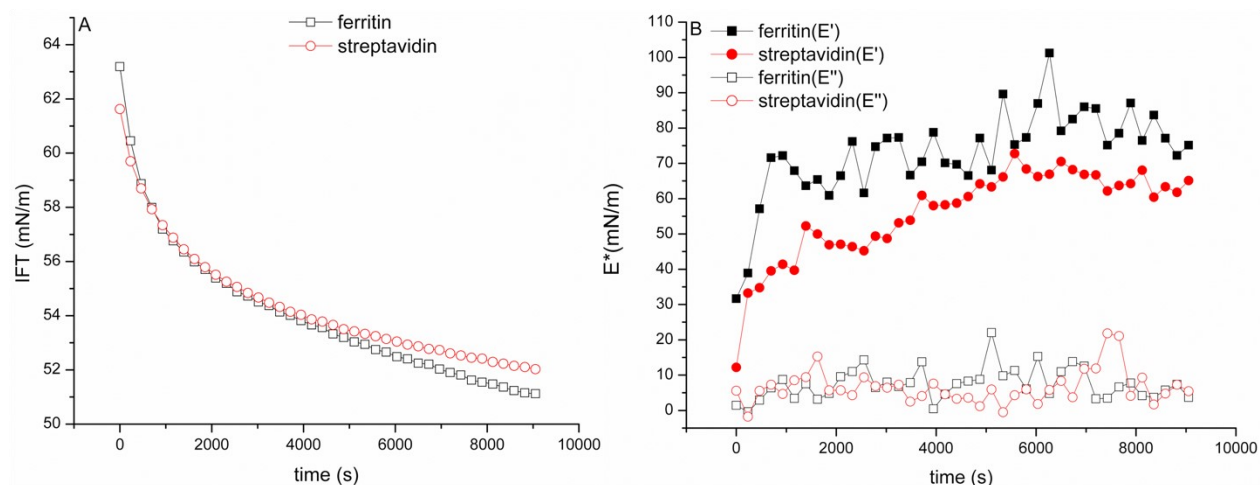
Figure 4-9: Interfacial tension, elastic (storage) modulus and viscous (loss) modulus vs time using a pendant drop tensiometer for the pure protein's ferritin and gold-conjugated streptavidin with 0.1 M MES buffer as the drop phase. A. Average interfacial tensions recorded at the air-buffer interface. B. The two-dimensional storage and viscous moduli E' and E'' of the droplet interface at a constant frequency of 1/s and amplitude dA/A of 1%.

While the interfacial tension of dual biofunctionalized Janus particles is comparable to that of the half ferritin coated SiNPs (red) (Figure 4-8 A), the surface elasticity of the dual biofunctionalized particles is the highest of all analyzed particles (Figure 4-8 B), showing that the Janus aspect influences the collective behavior of the particles at the air/water interface.

115
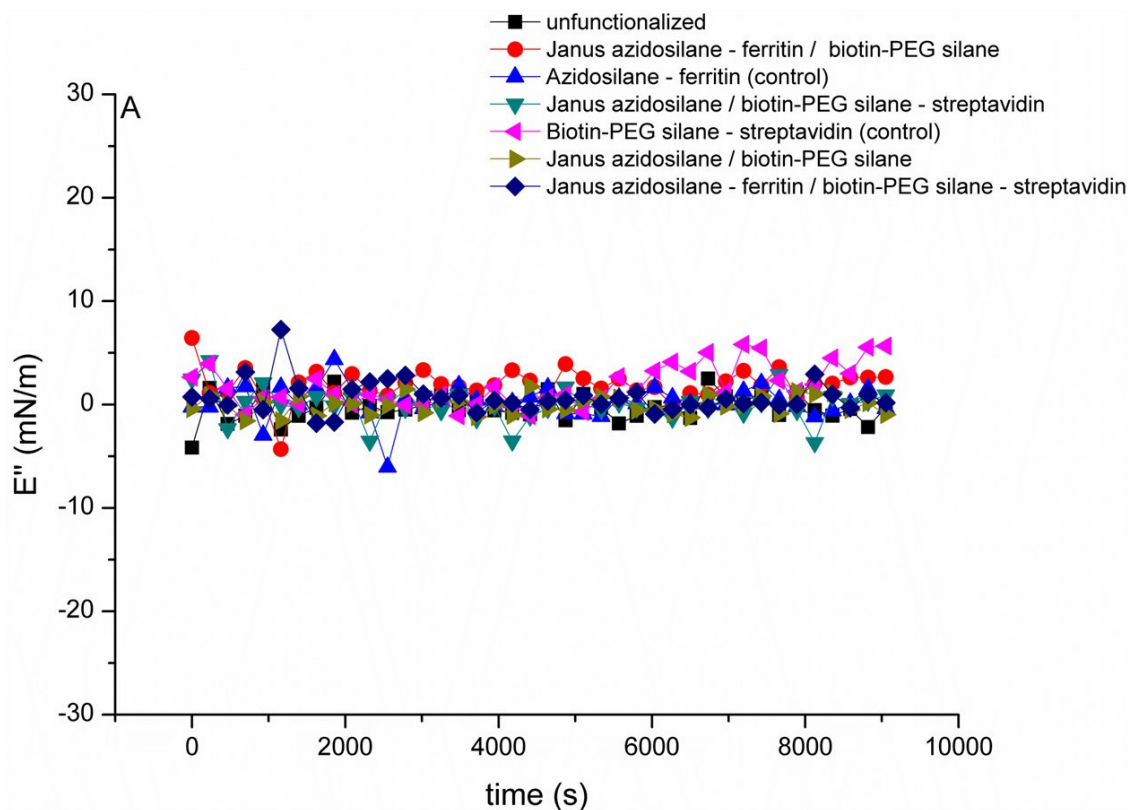
Figure 4-10: Viscous modulus vs time using a pendant drop tensiometer for the above mentioned 80 nm SiNPs. 0.1 M MES buffer was used as the drop phase. A.The two-dimensional viscous modulus E'' of the droplet interface at a constant frequency of 1/s and dA/A of 1%.

All measurements were repeated for 150 nm Janus SiNPs with comparable results besides an even more strongly pronounced surface activity of the dual biofunctionalized particles (Figure 4-11).
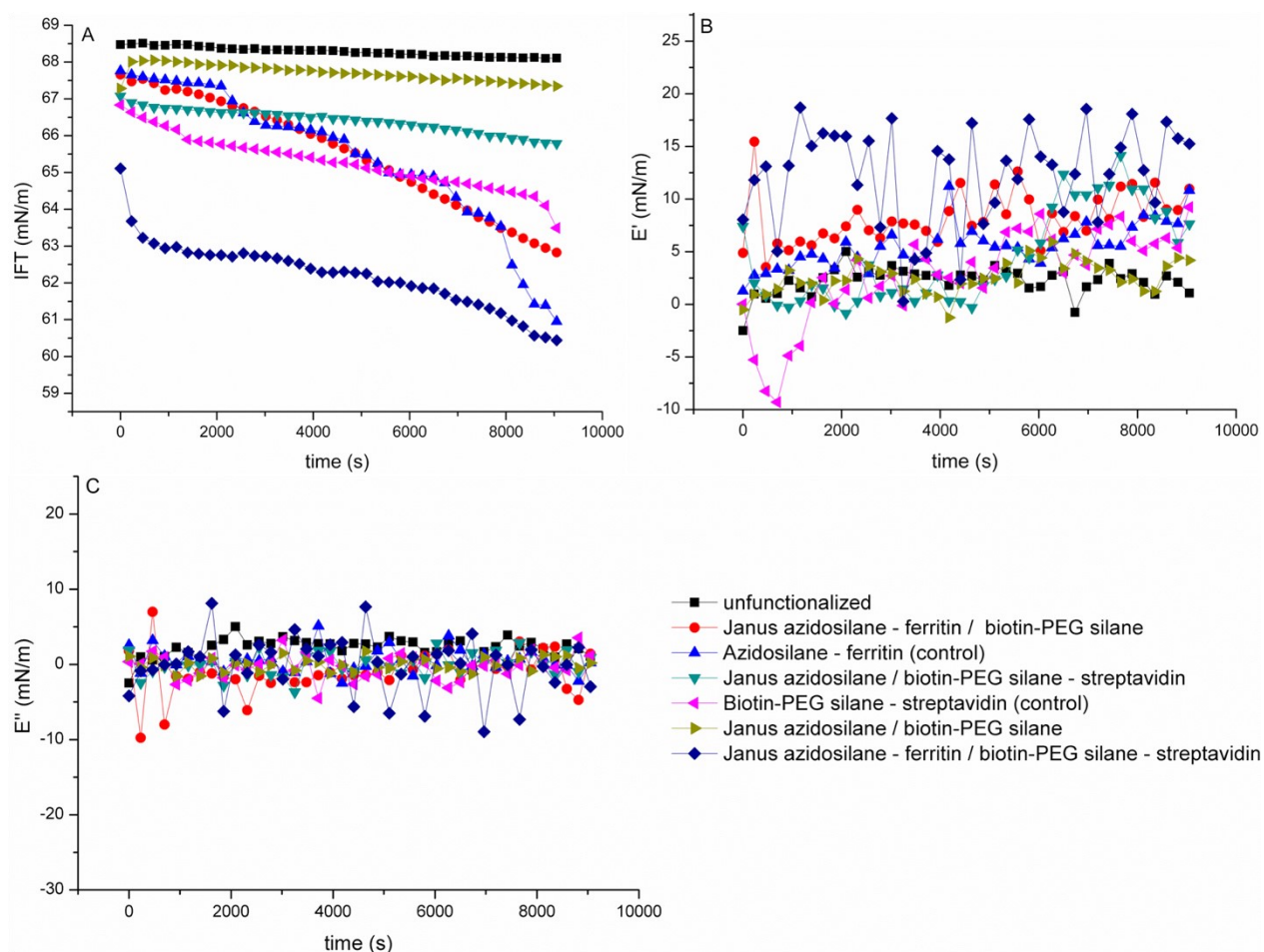
Figure 4-11: Interfacial tension and elastic storage modulus vs time using a pendant drop tensiometer for the 150 nm SiNPs. 10 mM MES buffer was used as the drop phase. A. Average interfacial tensions recorded at the air-water interface. The two-dimensional storage modulus E' (B) and viscous modulus E'' (C) of the droplet interface at a constant frequency of 1/s and an amplitude dA/A of 1 %.

4.2 Conclusion

In summary, our results suggest that the chosen approach is a versatile platform for the face-selective immobilization of two different biomolecules on a single NP surface. This scalable method yields Janus NPs in gram quantities. This method is compatible for applications such as functionalization of biomolecules such as proteins with well-established protein functionalization strategies at mild conditions. However, due to the iterative process with some losses in specificity at every step, only adequate success rates for functionalization with two proteins could be achieved. Still, the Janus particle dispersion showed collective properties that clearly surpassed those of Janus particle

dispersions with only one protein. These features will enable further studies on interactions between Janus NPs and cells or other biological systems and could also be utilized in biomedical applications that benefit from dual functionalities on separate sides of a NP. [15,20]

Chapter 5

Selective, agglomerate-free separation of bacteria using biofunctionalized, magnetic Janus NPs

5. Selective,agglomerate-free separation of bacteria using biofunctionalized magnetic Janus particles

This chapter includes the results of the preparation of Janus particles for magnetic separation of one specific bacterial species from a mixture of bacteria with the added feature of avoiding agglomeration between bacteria. This feature is only possible because of the anisotropic nature of Janus particles. Specifically, we designed nano-sized magnetite@SiO_2 Janus NPs with bifunctional anisotropic properties. Antibodies against one particular bacterial species were immobilized on one side of the NPs via biotin-streptavidin conjugation while the other side was functionalized with PEG chains via silanization, with the aim of passivating this side of the NP against agglomeration. To this end, we functionalized 45 nm SiO_2-coated magnetite NPs with streptavidin-conjugated anti-*E. coli* antibody and with PEG-silane on opposing sides using the wax-in-water Pickering emulsion method. For the bacterial capture and separation experiments we used a mixture of *E. coli* and *Staphylococcus simulans (S.simulans).* The prepared Janus particles were characterized with DLS, TEM and suitable assays to quantify the surface functionalization. The bacterial capture system was analyzed via optical density measurements for measuring capture efficiency, SEM to understand the specificity of the NPs and fluorescence microscopy to study agglomeration of the bacterial suspensions, along with assays for monitoring bacterial viability.

5.1 Results and Discussion

5.1.1   Preparation of azide-functionalized magnetite@SiO_2 NPs

The multistep approach for the preparation of the Janus NPs is illustrated in Figure 5-1. The magnetite@SiO_2 NPs were synthesized using existing protocols. The magnetite NPs were prepared using the thermal decomposition method. [288] The size of the synthesized magnetite particles was about 12 nm $\pm$ 2 nm, as obtained by DLS measurements (Figure 5-1) and further confirmed by using TEM. VSM analysis of magnetite NPs showed

superparamagnetic behavior with a saturation magnetization of 9 emu/g and an absence of magnetization hysteresis (Figure 5-1). Magnetite NPs with a silica cover were prepared according to the protocol described by Ding et. al. [257] The magnetite NPs were then coated with a silica cover using TEOS by way of the reverse microemulsion using cyclohexane (Sigma Aldrich, Germany, product number 227048) in the presence of polyoxyethylene nonylphenylether (IGEPAL®CO-520, Sigma Aldrich, Germany, product number 238643) and the sol-gel method. The prepared NPs are magnetically collected and washed several times with ethanol (Sigma Aldrich, Germany, product number 32205-M).
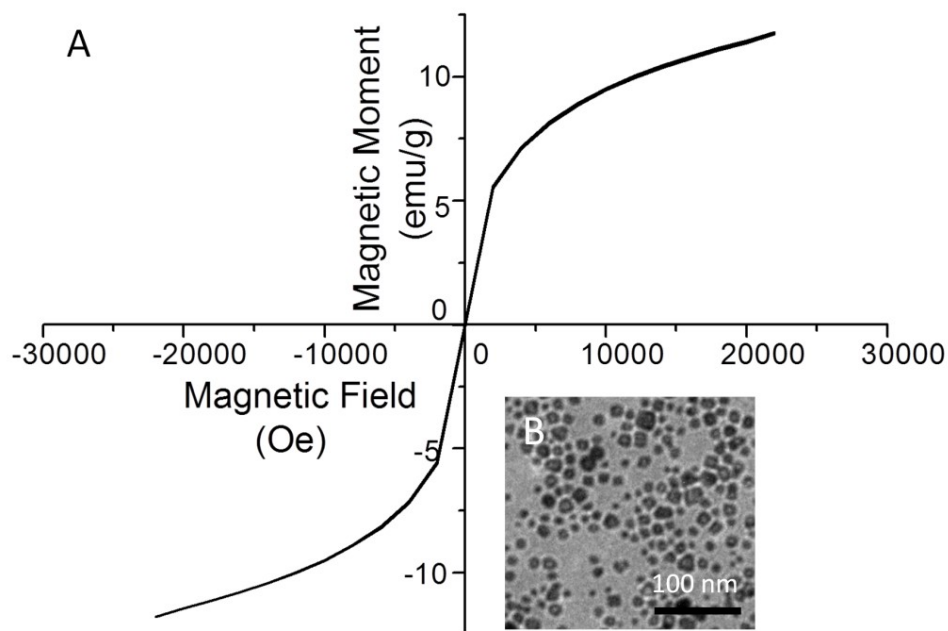
Figure 5-1: (A) Magnetization of magnetite particles showed typical superparamagnetic behavior. (B) TEM micrograph of the prepared magnetite particles. Magnetite NPs were prepared using the thermal decomposition method. The as-prepared magnetite particles had a size of 12 ± 2 nm which was obtained using DLS measurements.

The size of the magnetite@SiO_2 particles was 45.6 ± 2 nm which was again measured using DLS (Figure 5-2 A and B and Figure 5-3) and confirmed by TEM. The PDI of the DLS measurements was 0.15 ± 0.05, which points to a fairly narrow size distribution of the coated particles. The available SSA of the magnetite@SiO_2 particles determined using BET was 4.96×10^{16} nm^2/mg particles. VSM analysis of the coated particles showed that silica-coated particles are superparamagnetic with a moderate saturation magnetization of around 9 emu/g (Figure 5-2 C). The saturation magnetization of the uncoated iron oxide particles was in the same range (Figure 5-1).
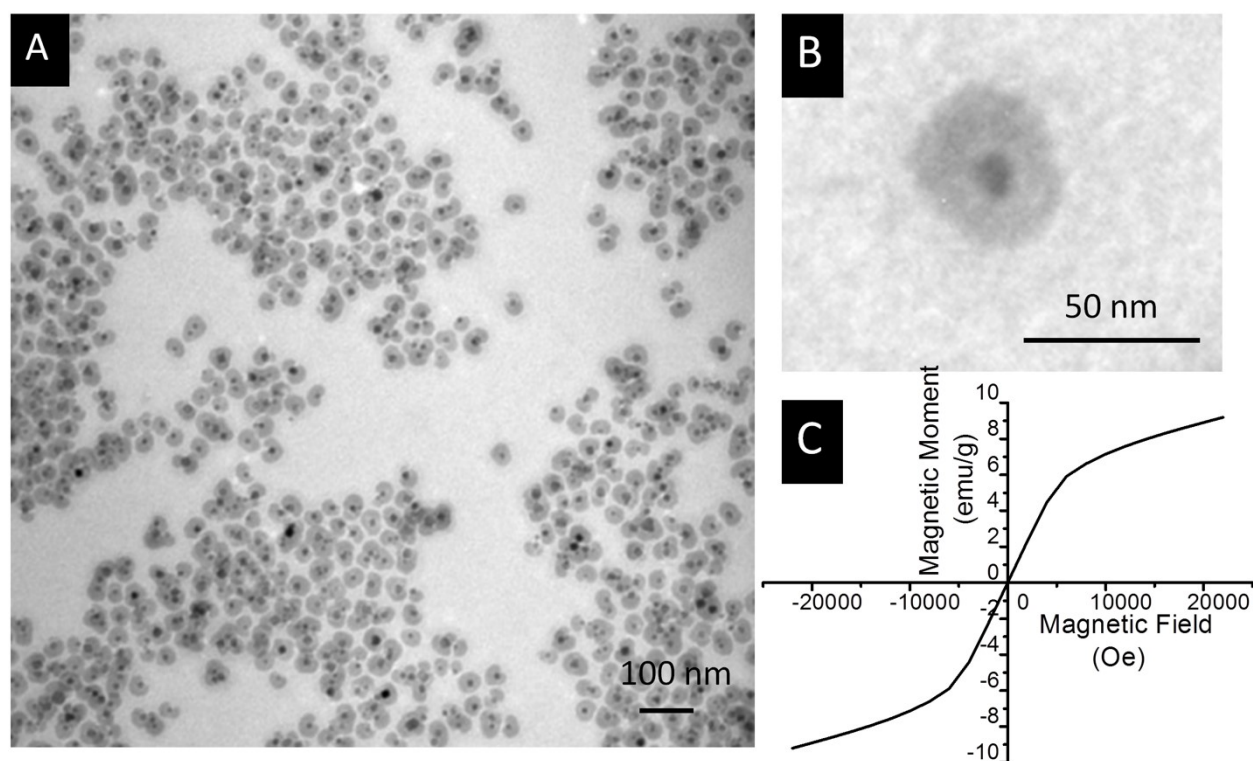
Figure 5-2: TEM micrograph of the prepared magnetite@SiO_2 particles. Magnetite NPs were prepared using the thermal decomposition method and were further coated with silica using the reverse microemulsion method. (A) The as-prepared magnetite@SiO_2 particles had a hydrodynamic diameter of 45.6 ± 2 nm. (B) Close-up of the TEM micrograph of magnetite@SiO_2. (C) Magnetization of magnetite@SiO_2 showed typical superparamagnetic behavior.

The magnetite@SiO_2 particles were functionalized with azide groups using an azidosilane [90,136]. Azide functionalization caused an increase in the hydrodynamic size of the particles from 45.5 ± 2 nm to 50.4 nm ± 4.6 nm. A barely significant decrease in the

negativity of the surface charge from -32 $\pm$ 2.1 mV to -29.3 $\pm$ 2.4 mV was recorded (Figure 5-3), indicating that only a very small amount of active zwitterionic azide groups are present on the particle surface, which was comparable to the results summarized in Chapter 4 [89] and was confirmed using the azide quantification assay.

Functionalization with azide was analyzed using the DBCO-Cy3 assay, which quantifies the fluorescent dye Cy3, which selectively binds to azide groups. The number of azide groups was further normalized to the particle surface area in nm^2, which is shown in Figure 5-3 C [89,136]. DBCO-Cy3 attachment to the unfunctionalized magnetite@SiO$_2$ (0.18 $\pm$ 0.06 groups/particle) was negligible compared to the fully azide-functionalized NPs (8.2 $\pm$ 0.4 groups/particle). The rather low number of active azide groups/particle quantified in this work was comparable to the values obtained in Chapter 4, to one of our published works as well as to the work of LoGuidice et al.[89,136].
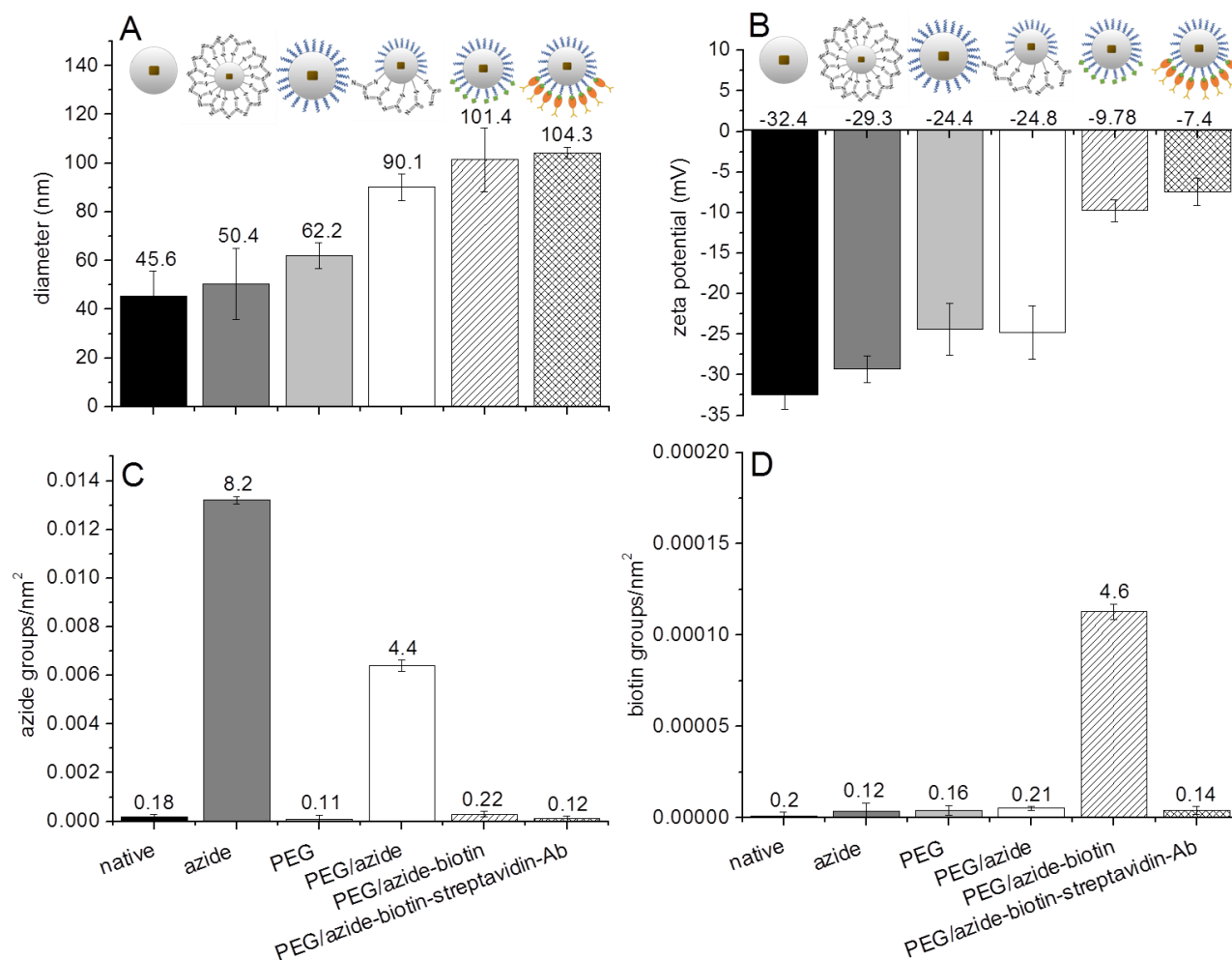
Figure 5-3: Size and surface properties of magnetite@SiO$_2$ before and after different functionalization in PBS (A-B) Size and ZP overviews of the NPs with different surface functionalization was measured via DLS. (C-D) Quantification of azide and biotin functional groups was done to confirm the success of the modification steps. The number of functional groups per particle is specified above each bar. Labels on (C-D) apply to (A-B) as well. The number of available azide and biotin groups on the particles was determined using the fluorescence of DBCO-Cy3 and the Fluoreporter® Biotin quantification kit, respectively. The label "native" represents unfunctionalized magnetite@SiO$_2$ NPs.

5.1.2   Preparation of wax-in-water Pickering emulsions

Since particles at liquid-liquid [27,96] or air-water interface [96] tend to undergo free rotation, a solidifying oil phase, for example paraffin wax, is required for entrapping particles at emulsion droplet interfaces, which enables Janus functionalization of the exposed particle side [16]. In our case, the azide-functionalized NPs were deposited on

the surface of molten wax droplets, followed by cooling and solidifying the droplets, using the method established in our previous publication [89], which was adapted from the approach by Granick et al.[16]. The azide-functionalized magnetite@SiO$_2$ particles (ZP is -29.3 mV) were hydrophobized with the water-soluble surfactant CTAB to facilitate adsorption at the wax droplet surface. Compared to the original protocol, the surfactant concentration was roughly proportional to the increased surface area exhibited by the nanoscale particles [89]. In order to remove the excess of surfactant, which might interfere with the upcoming functionalization steps, the particle-bearing solidified wax droplets were washed several times with water.
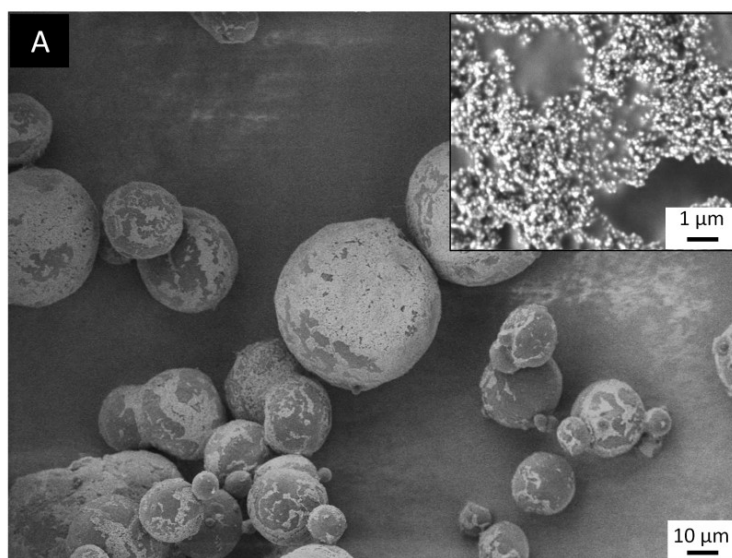
Figure 5-4: (A) SEM micrographs of wax Pickering emulsion droplets after several washing steps. These wax Pickering emulsion droplets were covered with azide-functionalized magnetite@SiO$_2$ particles. Inset: close-up of the NPs on the solid wax droplets.

These solid wax emulsions sustained the washing steps and the upcoming functionalization steps, which was also analyzed by SEM (Figure 5-4). SEM micrographs of particle bearing wax spheres show a size distribution of 500 nm to 50 μm (Figure 5-5 A). An irregular distribution of monolayers of NPs was observed on the wax droplets (Figure 5-5 A, inset) and the azide-functionalized magnetite@SiO$_2$ remained partially embedded in the wax surface [89]. Gram quantities of wax Pickering emulsion droplets are produced using this method and hence can be used for large-scale preparation of Janus NPs.
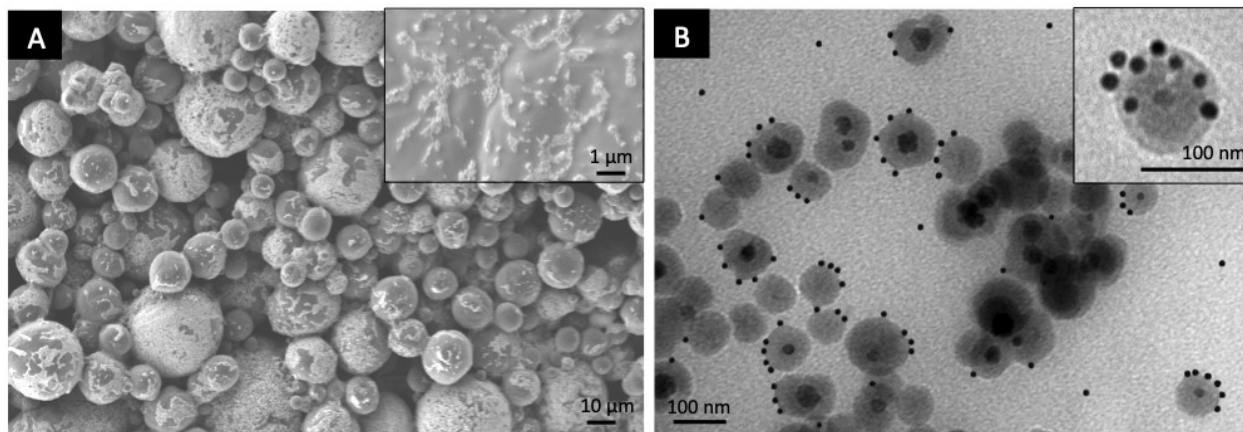
Figure 5-5: (A) SEM micrographs of wax Pickering emulsion droplets prepared using azide-functionalized magnetite@ SiO$_2$ particles. Inset: close-up of the NPs on the solid wax droplets. (B) TEM micrographs of the prepared Janus particles functionalized with PEG chains on one side and biotin groups on the other. Inset: close up of the as-prepared Janus NPs. The presence of biotin is confirmed using 10 nm gold-labeled streptavidin on one side (see Figure 5-6 for additional images).
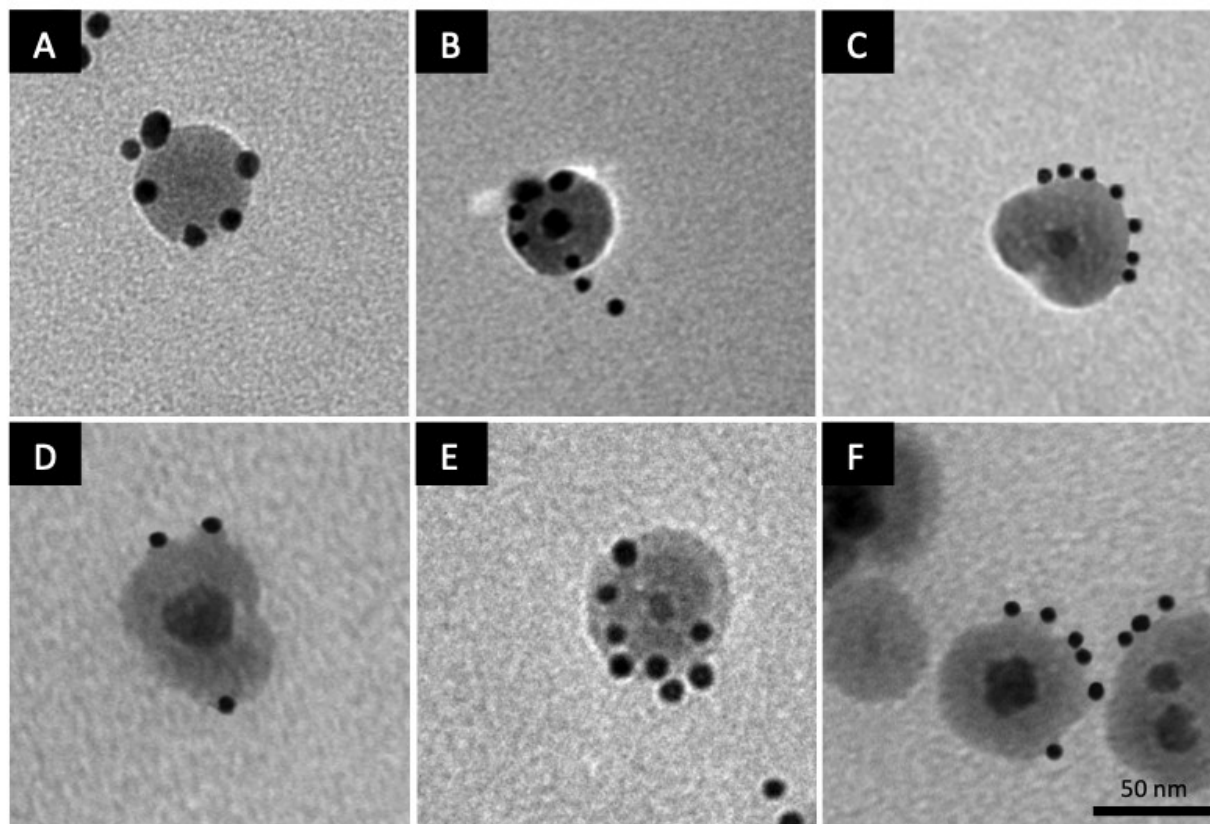
Figure 5-6: (A-G) TEM micrographs of the prepared Janus particles functionalized with PEG chains on one side and biotin groups on the other. The presence of biotin is confirmed using 10 nm gold-labeled streptavidin on one side. The scale bar shown in G applies to panels A-G.

5.1.3   Janus functionalization with PEG-silane

To prepare bifunctional Janus particles, solid wax emulsions were dispersed in ethanol (10 mg/ml) and PEG-silane was added dropwise to the solution under continuous stirring. After 2 h of incubation with the silane, minor loss of NPs was observed from the wax particles (see Figure 5-4). A threefold excess of the silane concentration was used in order to ensure the attachment of the PEG groups in a dense surface coating. After functionalization with PEG groups, cyclohexane was used to dissolve the wax cores and release the PEG/azide magnetite@ SiO_2 NPs. DLS analysis of PEG/azide functionalized NPs in PBS revealed a size of 90.1 ± 3 nm (PDI = 0.15) and a surface charge of -24.8 ± 2.3 mV (Figure 5-3).

After the preparation of the PEG/azide Janus NPs, the amount of azide groups quantified was 4.6 ± 0.15 groups/particle, which is approximately half of the quantified groups on the fully azide-functionalized NPs (Figure 5-3). This also confirms the Janus feature imparted using the partial masking by embedding in the surface of solid wax droplets.

PEG functionalization on NPs has been widely studied to improve targeting efficiencies of NPs by reducing protein corona formation [58,111]. Polymer chains arising from PEGylation on NPs precludes them from interacting with other NPs and components of biological systems, particularly surface-active proteins. This renders such NPs less vulnerable to agglomeration and strongly reduces their interactions with cell surfaces. Therefore, PEG modification was analyzed by adsorption of the protein's fluorescein-isothiocyanate-modified BSA (FITC-BSA) and lysozyme. 10 mg/ml NPs of unfunctionalized, non-Janus (PEG functionalized) and Janus (azide/PEG) were incubated with 2 mg ml^{-1} FITC-BSA for 1 h. After incubation of the NPs, the particles were washed twice, and the amount of protein bound to the NPs (Figure 5-7 A, black bars) and of the unbound protein (Figure 5-7 A, grey bars) were quantified photometrically. The amount of BSA adsorbed on 10 mg of anionic, unfunctionalized magnetite@SiO$_2$ particles was 900 $\pm$ 100 nmol g^{-1} of the respective NPs. Adsorption of FITC-BSA (isoelectric point = 4.5, [289] slightly negatively charged at pH 6.2) was observed on negatively charged NPs, which can be attributed to van-der Waals interactions, hydrophilic, hydrophobic, steric and structural interactions along with electrostatic interactions [132,241]. Lowest protein adsorption was recorded in case of non-Janus (full PEG) magnetite@SiO$_2$, as expected. In the case of the Az/PEG Janus NPs, the amount of adsorbed FITC-BSA was 600 $\pm$ 50 nmol g^{-1}, which was reduced compared to that of the unfunctionalized (900 $\pm$ 100 nmol g^{-1}) but was higher than that of the non-Janus (200 $\pm$ 50 nmol g^{-1}) PEGylated NPs. Summation of adsorbed and supernatant concentrations of FITC-BSA amounts to the initial concentration of FITC-BSA in all experiments (2000 nmol g^{-1}). Additionally, we confirmed PEGylation by adsorbing the protein lysozyme (Figure 5-7 B). Lysozyme exhibits an isoelectric point of 11 [232] and therefore is positively charged in PBS at pH 6.2. Consequently, it adsorbs on negatively charged magnetite@SiO$_2$ due to electrostatic interactions, which would be evidenced by the change in surface charge of the NPs. The ZP of negatively charged unfunctionalized (-32 mV) and azide-functionalized (-29.3 mV) magnetite@SiO$_2$ changed to +10 $\pm$ 8 mV and to +8 $\pm$ 6.2 mV respectively. Hardly any

alteration in the surface charge was observed in the case of non-Janus PEG functionalized NPs, wherein the ZP values underwent a change from -24.4 $\pm$ 4.7 to -22.5 $\pm$ 2.6 mV. Lysozyme adsorption resulted in a moderate change in the ZP of the Janus NPs (Az/PEG) from -24.8 $\pm$ 5 mV to -10 $\pm$ 2 mV.
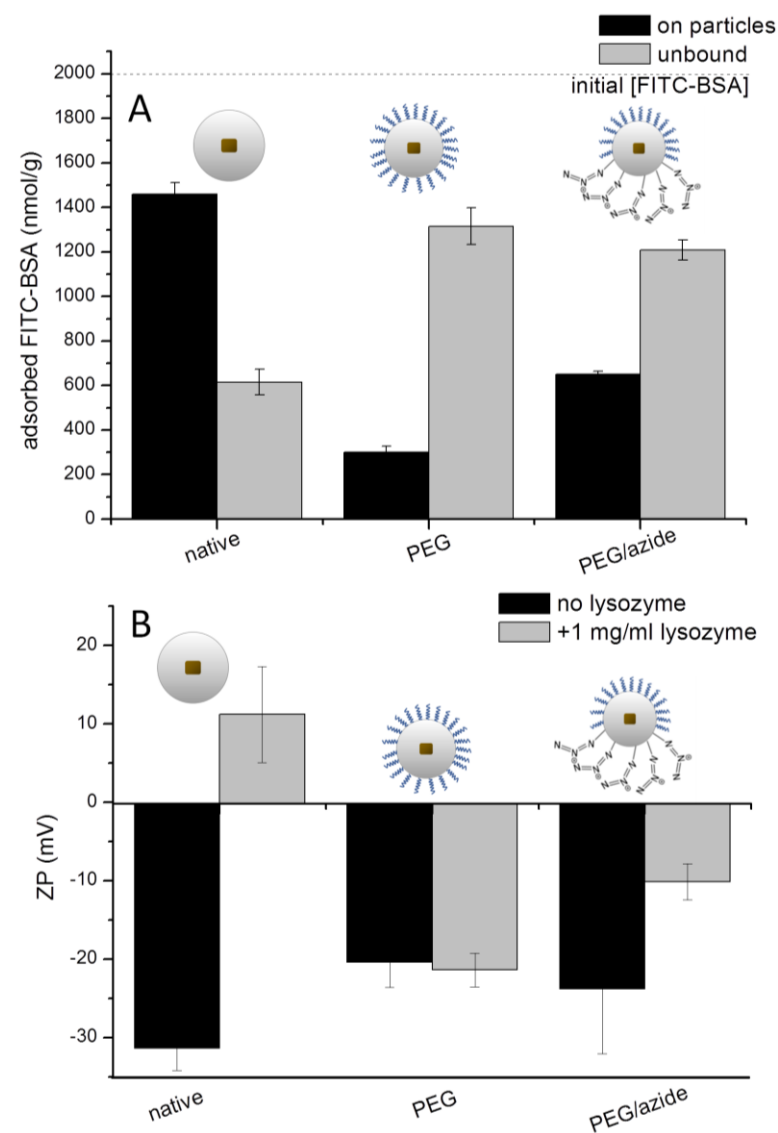
Figure 5-7: Characterization of PEG modification on magnetite@SiO$_2$ NPs before and after functionalization with PEG. (A) Quantification of the amount of FITC-BSA adsorbed on the NPs after PEGylation. (B) ZP changes were analyzed before and after adsorption of lysozyme to qualitatively analyze the success of PEGylation on the respective NPs mentioned under the respective bars.

5.1.4   Biotin functionalization

In order to attach the streptavidin-functionalized antibody for attaining selective *E. coli* capture, the PEG/azide functionalized Janus particles were coupled with the linker acetylene-(PEG)$_4$-biotin via copper mediated click chemistry. After this functionalization step, only a negligible amount of DBCO-Cy3 attached to PEG/azide-biotin NPs (0.22 groups/nm^2), indicating that no unreacted azide groups remain on the surface of the NPs (Figure 5-3 C).

The number of biotin groups obtained via the Fluoreporter assay showed a negligible amount of biotin for all negative control measurements (native, full azide, full PEG and PEG/azide functionalized NPs, Figure 5-3 D). An increase in the number of biotin groups was observed after the linker was attached to yield PEG/azide-biotin Janus NPs 4.6 ± 0.16 groups/particle), which closely corresponds to the number of azide groups on the PEG/azide Janus particle surface, confirming the success of biotin functionalization. As an additional control, we synthesized fully biotin-functionalized magnetite@SiO$_2$ NPs, which showed 8.2 ± 0.18 groups/particle (Figure 5-8 D).

Attachment of biotin groups on PEG/azide-biotin magnetite@SiO$_2$ caused a change in the surface charge of PEG/azide NPs from -24.8 ± 3.2 mV to -9.78 ± 4.1 mV alongside an increase of size from 90.1 ± 4.3 nm to 101 ± 10 nm (Figure 5-3 A, B) [89].

To visually confirm the functionality of the biotin groups towards streptavidin conjugation on one hemisphere of the Janus particles, we incubated PEG/azide-biotin with gold-conjugated streptavidin [290]. As shown in Figure 5-5 B (overview) and 5-5 C (close-up), attachment of the streptavidin-gold on only one half of the NPs was observed (see Figure 5-6 for additional images).

5.1.5   Antibody conjugation for PEG/azide-biotin-streptavidin-Ab Janus particles

The anti-*E. coli* antibody selected for this project specifically binds to the K antigen expressed by serotype *E. coli* K12 [291]. After conjugating the anti-*E. coli* antibody with streptavidin following the protocol provided by the suppliers, PEG/azide-biotin functionalized NPs are functionalized with the antibody on the azide-biotin hemisphere of

the NP, leaving the PEG chains on the other side of the particle. Size and ZP analysis of the PEG/azide-biotin-Ab-functionalized magnetite@SiO$_2$ yielded particles with a size of 104.3 $\pm$ 6.8 nm (Figure 5-3 A) and ZP of -7.4 $\pm$ 4.2 mV (Figure 5-3 B). The particles are colloidally stable despite the complex functionalities and multiple synthesis steps as evidenced by a fairly low PDI of 0.15. As an additional control, we also synthesized non-Janus anti-*E. coli* antibody-coated magnetite@SiO$_2$ NPs with a size of 110.4 $\pm$ 5.7 nm (Figure 5-8 A) and a ZP of +7.45 $\pm$ 2.54 (Figure 5-8 B).
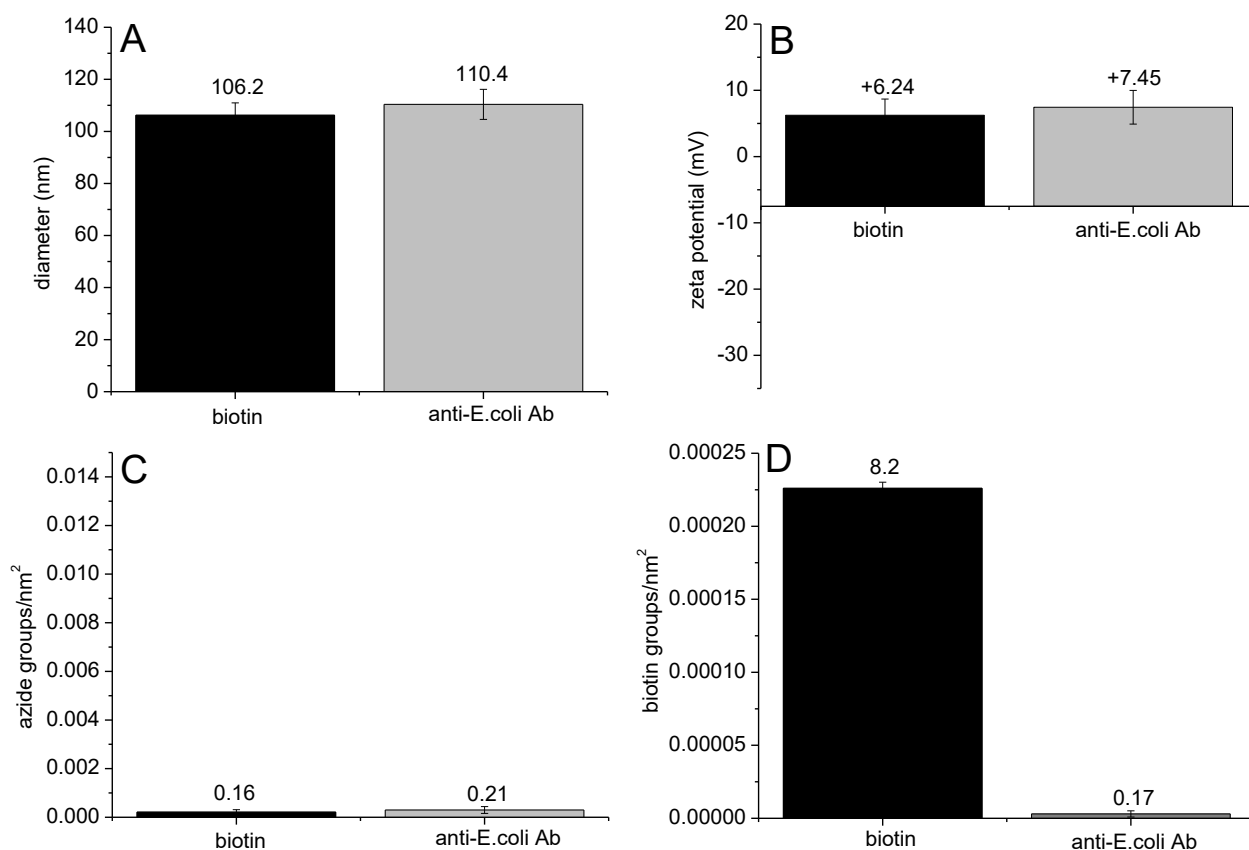
Figure 5-8: Size and surface properties of magnetite@SiO$_2$ after biotin and anti- *E.coli* antibody functionalization. (A-B) Size and ZP overviews of the NPs with the different surface functionalization was measured via DLS. (C-D) Quantification of azide and biotin functional groups was done to confirm the success of the modification steps. The number of functional groups per particle is specified above each bar. Labels on (C-D) apply to (A-B) as well. The number of available azide and biotin groups on the particles was determined using the fluorescence of DBCO-Cy3 and the Fluoreporter® Biotin quantification kit, respectively.

5.1.6 Aggregation of bacteria

The above-described PEG/azide-biotin-streptavidin-Ab Janus particles were designed to capture one specific type of bacterium (*E. coli* K12 in this case) from a mixture of bacterial strains. To this end, the as-prepared particles were incubated with a 1:1 mixture of *E. coli* and *S. simulans* as well as with both strains individually. In order to visualize the bacteria with fluorescence microscopy, the cells were stained via the live/dead method. Green fluorescence shows viable bacterial cells with intact membranes (Figure 5-9). Dead cells (red fluorescence) were not observed in these experiments. The NPs were exposed to *E. coli*, *S. simulans* or both for 1 h after which the live/dead staining procedure was carried out during the period of another 15 min. Figure 5-9 A-C show *E. coli*, *S. simulans* and the combination of both bacterial strains in the absence of NPs. In the presence of the anionic unfunctionalized magnetite@SiO_2 NPs, no bacterial agglomeration was observed in case of either the individual bacteria or a combination of both (Figure 5-9 D-F). After incubation of *E. coli* (Figure 5-9 G) and a mixture of *E. coli* and *S. simulans* (Figure 5-9 I) with NPs fully functionalized with anti-*E. coli* antibody (non-Janus), clusters of bacteria were observed. *S. simulans* alone in the presence of anti-*E. coli* antibody-coated magnetite@SiO_2 remained unaffected from the clustering effect, which shows the specificity of the antibody functionalized NPs. The non-Janus antibody-functionalized particles most likely form cell-NP-cell bridges leading to the formation of bacterial flocs. As expected from our particle design, Janus functionalized PEG/azide-biotin-streptavidin-Ab magnetite@SiO_2 particles prevented agglomeration of *E. coli* cells in the presence (Figure 5-9 L) or absence of *S. simulans* (Figure 5-9 J). *S. simulans* alone remained unaffected by all types of NPs (Figure 5-9 B, E, H, K).
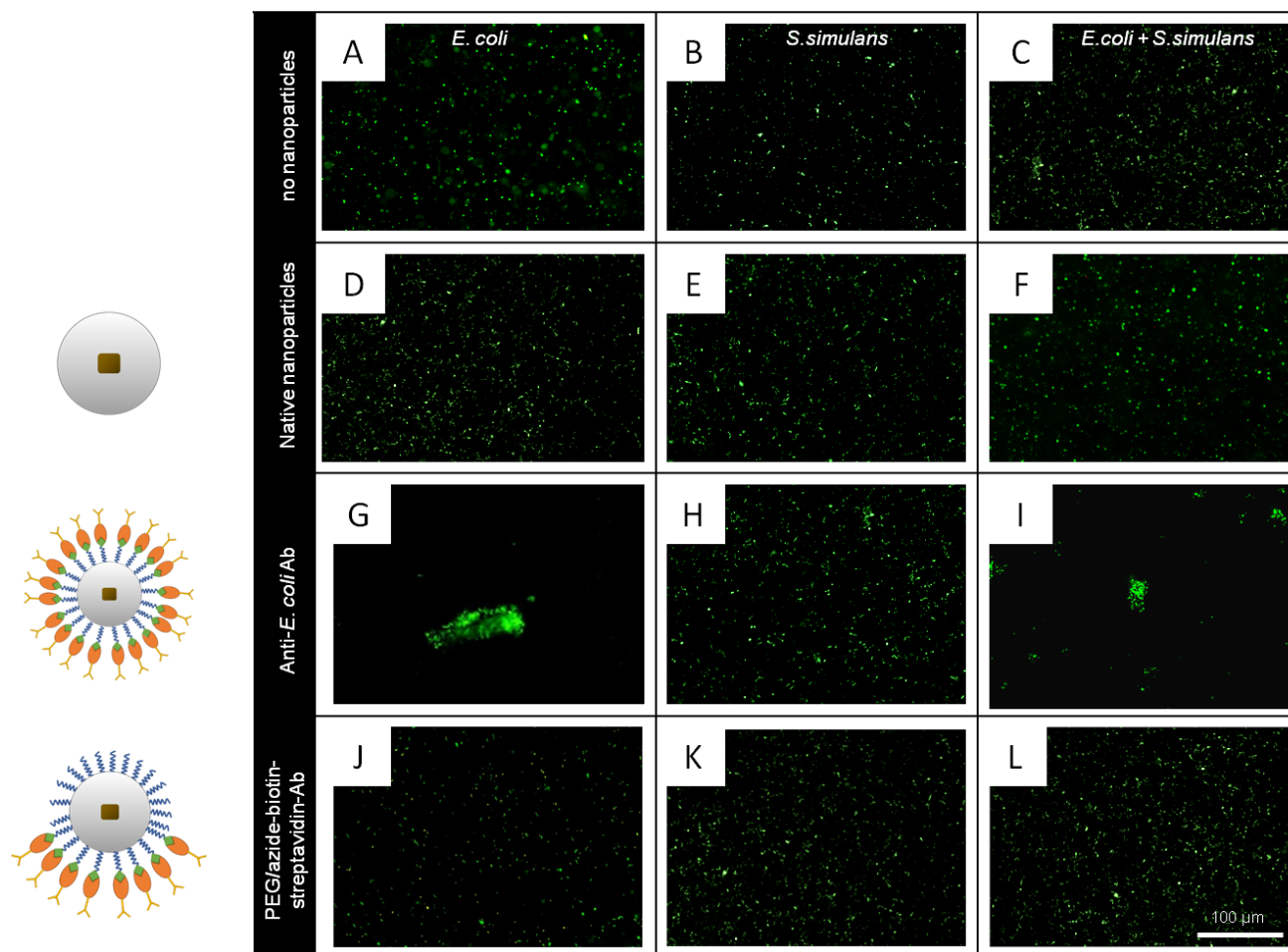
Figure 5-9: Fluorescence microscopy graphs of *E. coli* and *S. simulans* cells without (A-C) or with (D-L) the indicated NPs for 1 h. Live/dead fluorescence staining was used to distinguish between viable (green) and dead (red) cells. The scale bar in L represents 100 µm and applies to all images. The label "native" represents magnetite@SiO$_2$ without any surface modification. Anti-*E. coli* Ab NPs indicate magnetite@SiO$_2$ NPs that are fully functionalized with anti E. coli antibody (non-Janus), whereas PEG/azide-biotin-streptavidin-Ab NPs indicate Janus NPs with the respective functionalities each side.

5.1.7   Bacteria capture efficiency

By placing a neodymium magnet (50.8x50.8x25.4mm, 10.5-12.0 kOe) below the well plates with the bacteria/NP suspensions, the magnetic particles could be extracted with varying amounts of bacteria captured by the particles (Figure 5-10 A, B). After magnetic separation, residual and pellet concentrations of the bacteria were determined, and capture efficiencies were calculated from this data (Figure 5-10 C). In order to determine the amount of PEG/azide-biotin-streptavidin Ab-functionalized Janus NPs required to

magnetically separate *E. coli* cells (OD_{595}), we exposed 10^7 *E. coli* cells to increasing concentrations of particles (1-500 µg/ml) (Figure 5-11) over a period of 24 h. An increase in the capture efficiency was observed with increasing concentration of particles, until a maximum of capture efficiency of 82 ± 3 was recorded at 100 µg/ml which did not further increase with higher particle concentrations. At the same time, 100 µg/ml of PEG/azide-biotin-streptavidin-Ab functionalized Janus NPs were incubated with 10^7 *E. coli* cells/ml at increasing time points ranging from 0-24h (Figure 5-12). Maximum bacterial capture efficiency of 85 ± 6 % was reached at 60 min. We measured the unspecific capture of 5 ± 3 % bacterial cells using negatively charged unfunctionalized magnetite@SiO_2. Capture efficiency from the *E. coli* suspension increased to 80 ± 5 % in the presence of PEG/azide-biotin-streptavidin-Ab functionalized particles. Similarly, the non-Janus NPs showed capture efficiencies 82 ± 9 % from pure *E. coli*. Capture efficiency as recorded by similar publications with isotropic NPs have values ranging from 90-100 %, [116,125,194,196,204,292] the slightly lower capture efficiency we measured is probably caused by the lower saturation magnetization of the magnetic cores of the Janus NPs. In the presence of *S. simulans* alone, all particles showed unspecific capture efficiencies below 10 %.

The Janus NPs demonstrated a capture efficiency of 59 ± 6 % from mixtures of *E. coli* and *S. simulans*. Since only the optical density is measured, the test does not distinguish between the different types of bacteria. With this bacterial mixture, the efficiency of the fully anti-*E. coli* antibody-functionalized (non-Janus) NP was hardly different compared to that of the Janus NPs with 58 ± 3 % (Figure 5-10 C, light grey bars). Here, the overall capture efficiency is reduced because only 50% of the population of cells in the mixture is *E. coli* which binds to the antibody-functionalized particles with high selectivity, as established in the controls and in the agglomeration tests above.
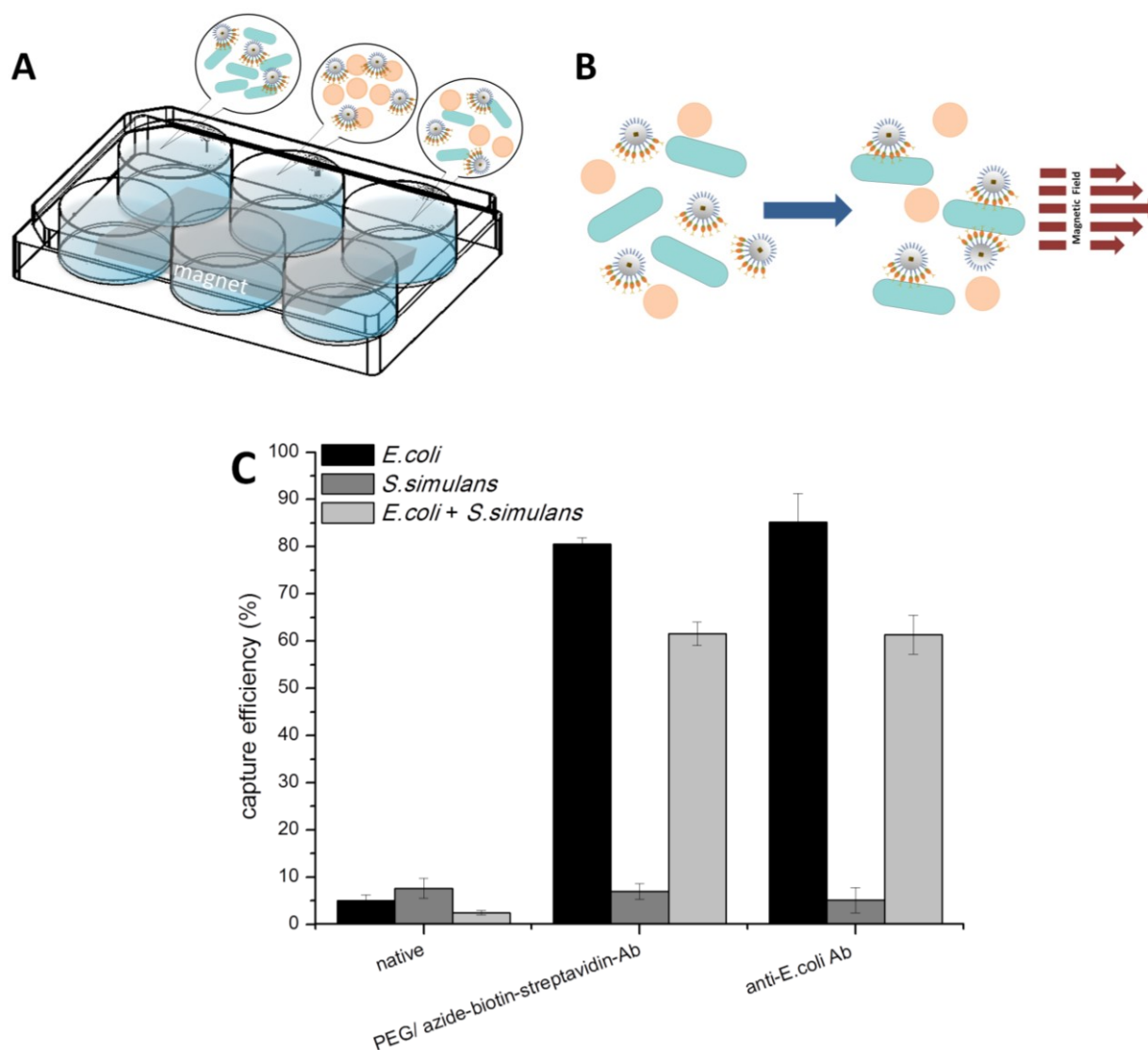
Figure 5-10: (A) Sketch of the experimental setup for the separation process using pure bacterial cultures as well as mixtures of bacteria. (B) Sketch of the capturing and separation principle of the prepared Janus NPs. (C) Capture efficiency was measured using optical density measurements (OD_{595}). The label "native" represents magnetite@SiO_2 particles without any functionalization. Anti-*E. coli* Ab indicates particles that are fully functionalized with anti-*E. coli* antibody (non-Janus), whereas PEG/azide-biotin-streptavidin-Ab NPs indicate the Janus NPs.
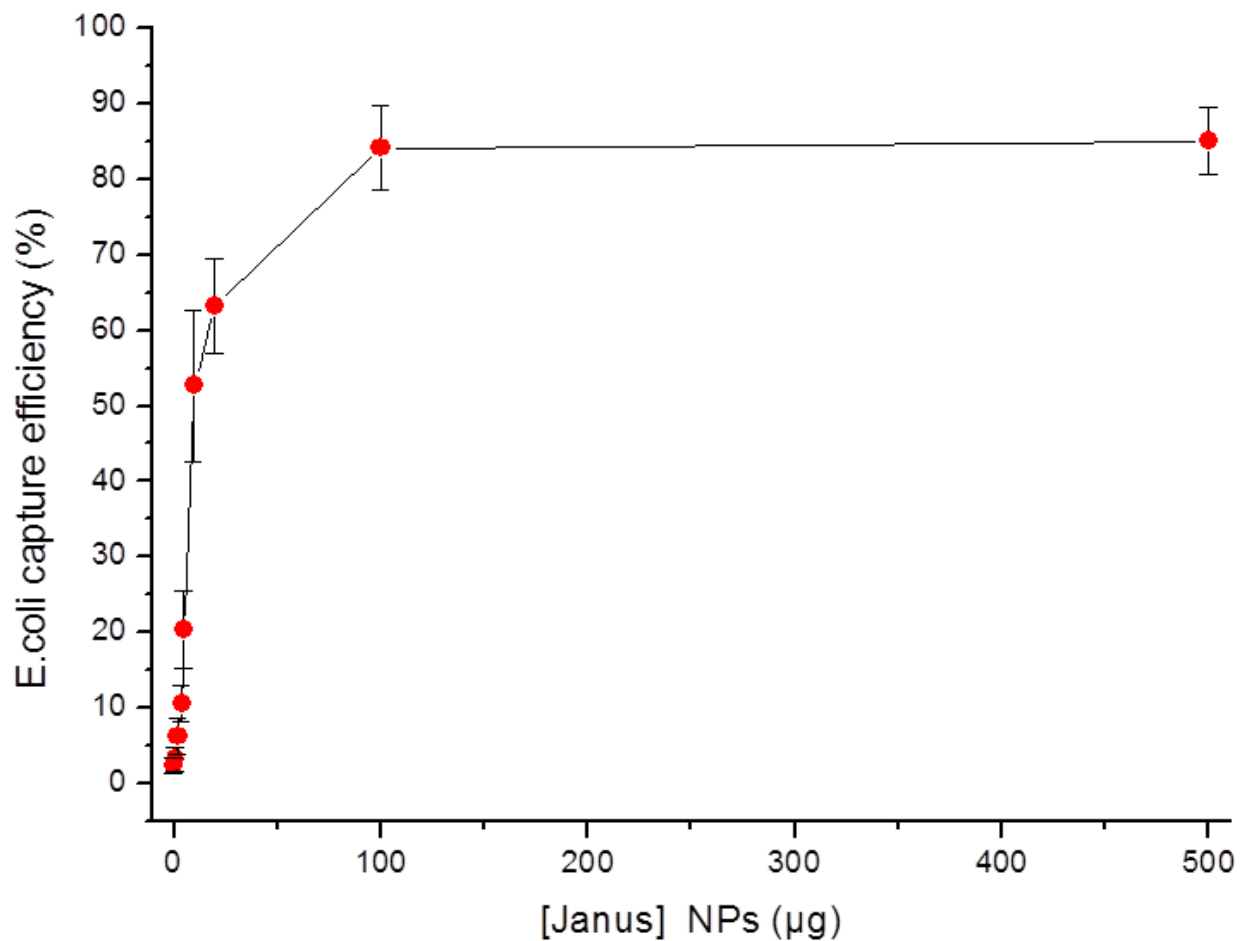
Figure 5-11: *E. coli* capture efficiency (%) measured after 1 h incubation of the 10^7 CFU/ml *E. coli* cells (OD$_{595}$ 0.1) with increasing concentrations of PEG/azide-biotin-streptavidin-Ab functionalized (Janus) NPs(μg) in 1 ml of PBS buffer. Capture efficiency was measured using optical density measurements (OD$_{595}$). The data is expressed as % of the control (cells incubated without NPs). All data are expressed as mean ± SD of values obtained from three independent experiments.
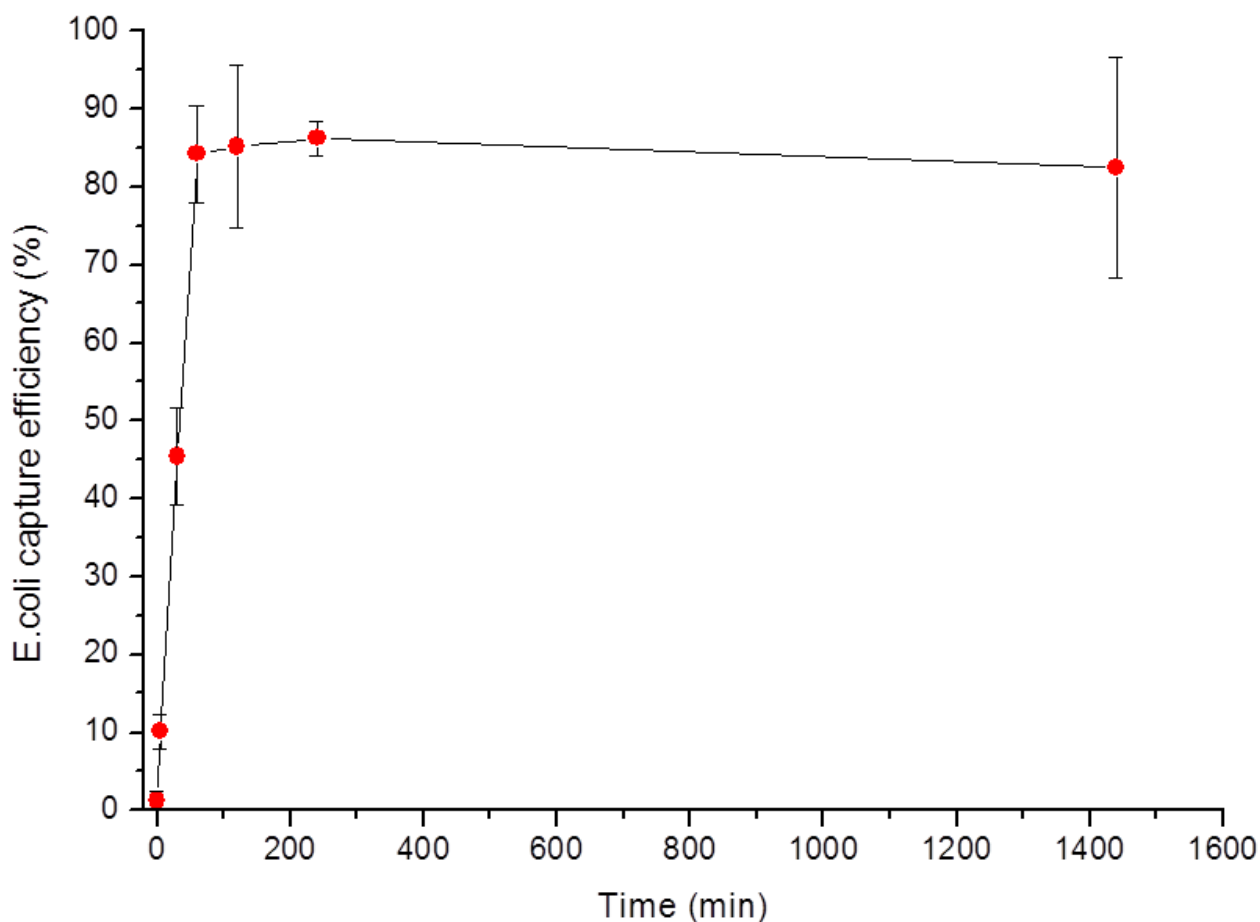
Figure 5-12: Magnetic capture efficiency of 10^7 CFU/ml *E. coli* cells (OD_{595} 0.1) using 100 µg/ml magnetite@SiO_2 PEG/azide-biotin-streptavidin-Ab functionalized Janus NPs in PBS buffer exposed to increasing times, ranging from 0-24h. These data represent three independent data sets using three different batches of NPs and are presented as mean ± SD.

Using SEM analysis, we further confirmed the specificity of the Janus particles towards *E. coli* cells. A 1:1 mixture of *E. coli* and *S. simulans* was incubated without (Figure 5-13 A-B) and with Janus particles (Figure 5-13 C-D) in PBS buffer and the cells were later deposited on a previously functionalized positively charged silica substrate to facilitate bacteria attachment to the substrate surface. Bacteria specific adsorption of the Janus particles, as depicted in Figure 5-13 D, showed the affinity of the Janus particles towards *E .coli* cells only, as indicated by particles adhering in a rough layer at the surfaces of *E. coli* (Figure 5-13 D). *S. simulans* remained free from NPs which is evident in the smooth

surface of the bacteria in the SEM micrographs which remains unchanged after exposure to the particles.
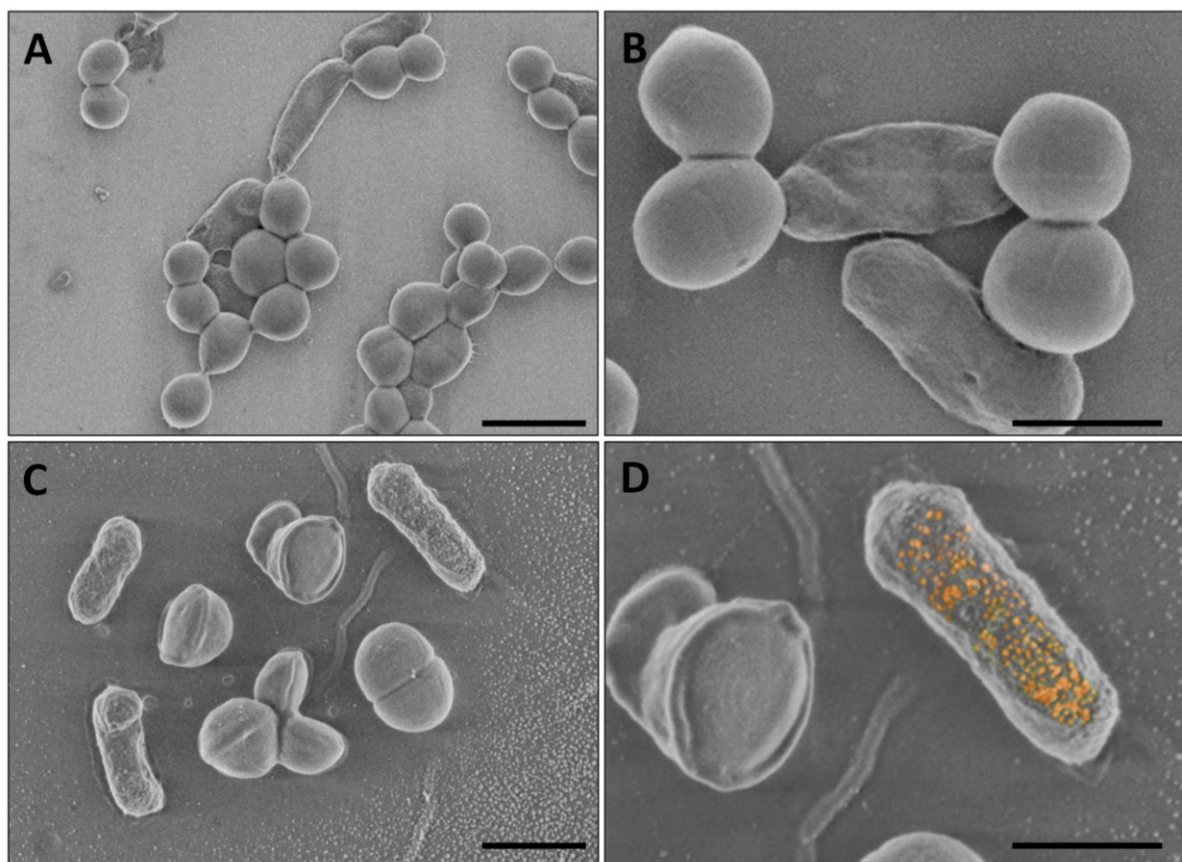
Figure 5-13: (A, B) SEM micrographs of a mixture of *E. coli* and *S. simulans* incubated in the absence (A) or presence of (B) PEG/azide-biotin-streptavidin-Ab-functionalized magnetite@SiO$_2$ NPs (Janus) to visualize selective attachment of NPs on the bacteria. (C,D) Close-up view of the *E. coli* and *S. simulans*. (D) shows pseudo colored (orange) NPs selectively attached to the rod-shaped *E. coli*. The scale bars shown represent 1 µm.

5.1.8   Viability assessment

Viability analysis of *E. coli* and *S. simulans* after exposure to the unfunctionalized, Janus and non-Janus NPs was performed using CFU counts and ATP quantification. To analyze the viability of the bacteria during the capturing procedure, CFU were separately determined from the supernatant and the pellet as obtained by magnetic separation as above. The pellet separated by the magnet was resuspended in fresh PBS and further spread on agar plates. CFU counts are made after 24 h of incubation at 37°C, based on

the principle that each viable cell forms a colony, which is then termed as a CFU (Figure 5-14 A). After the analysis of the respective supernatants after magnetic separation, we detected the remainder of the bacterial populations in the supernatant when normalized to the starting concentration of bacterial cells, therefore indicating that bacterial viability was not compromised after exposure to any of the tested NPs (Figure 5-14 B). The capture efficiency quantified using CFU counts was generally comparable to the OD$_{595}$ measurements (Figure 5-10 C), which indicates that all cells separated using such NPs are viable. The clear exception were the non-Janus antibody-coated particles for which CFU counts from the *E. coli* suspension of only 40 ± 4% were observed which is significantly lower than the OD$_{595}$ value for the bacterial capture of 85 ± 6 % shown in Figure 10. In the presence of the mixed suspension of *S. simulans* and *E. coli*, the non-Janus NPs (fully anti-*E. coli*-Ab functionalized) show similarly decreased CFU counts of 42 ± 10 % compared to 58 ± 3 % in the OD analysis. However, this apparent reduction in viability was not observed in additional ATP tests with the luminescence assay BacTiterGlo (Figure 5-15 A). Here, exposure of *E. coli* to the non-Janus antibody-coated particles resulted in ATP levels of 82 ± 6 % and 12 ± 4 % at the pellet and supernatant, respectively. Similarly, exposure of *E .coli* and *S. simulans* to non-Janus antibody-coated particles yielded ATP levels of 60 ± 5 % and 40 ± 3% at the pellet and supernatant. Otherwise, results of the ATP-based metabolic activity assay were consistent with the CFU counts (Figure 5-14 A and B) as well as with the bacterial separation analysis via OD (Figure 5-10 C).
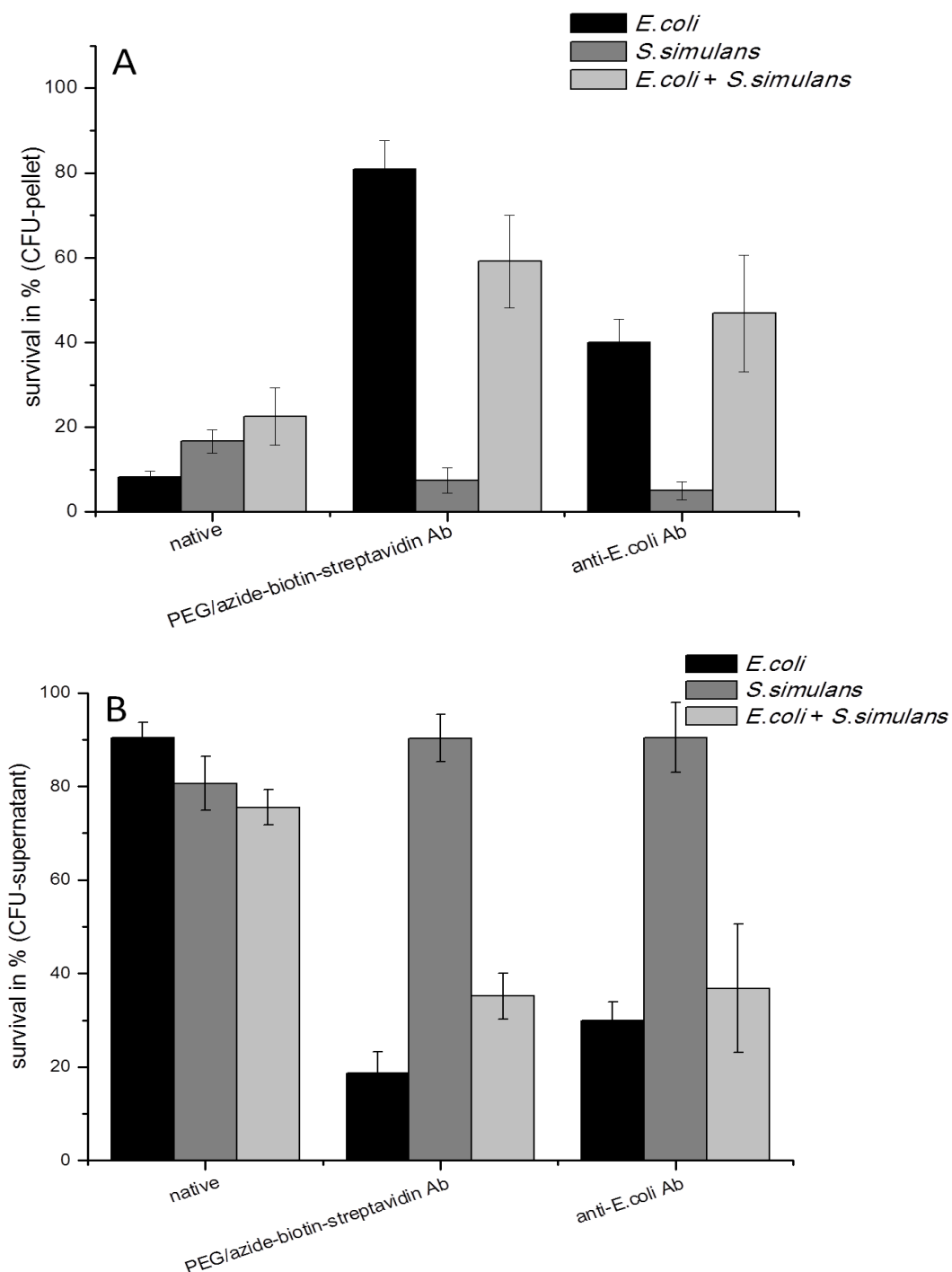
Figure 5-14: Viability of bacterial cells after exposure of 10^7 *E. coli* cells (OD$_{595}$ 0.1) to 100 µg/ml of native, PEG/azide-biotin-streptavidin-Ab (Janus) and fully anti-E. coli Ab (non-Janus) functionalized NPs in PBS buffer. After 1 h of magnetic capture, the cells captured as a pellet (A) and the remaining cells in the supernatant (B) were plated on agar plates to count the CFU. The data is expressed as % of the control (cells incubated without NPs). All data are expressed as mean ± SD of values obtained from three independent experiments.
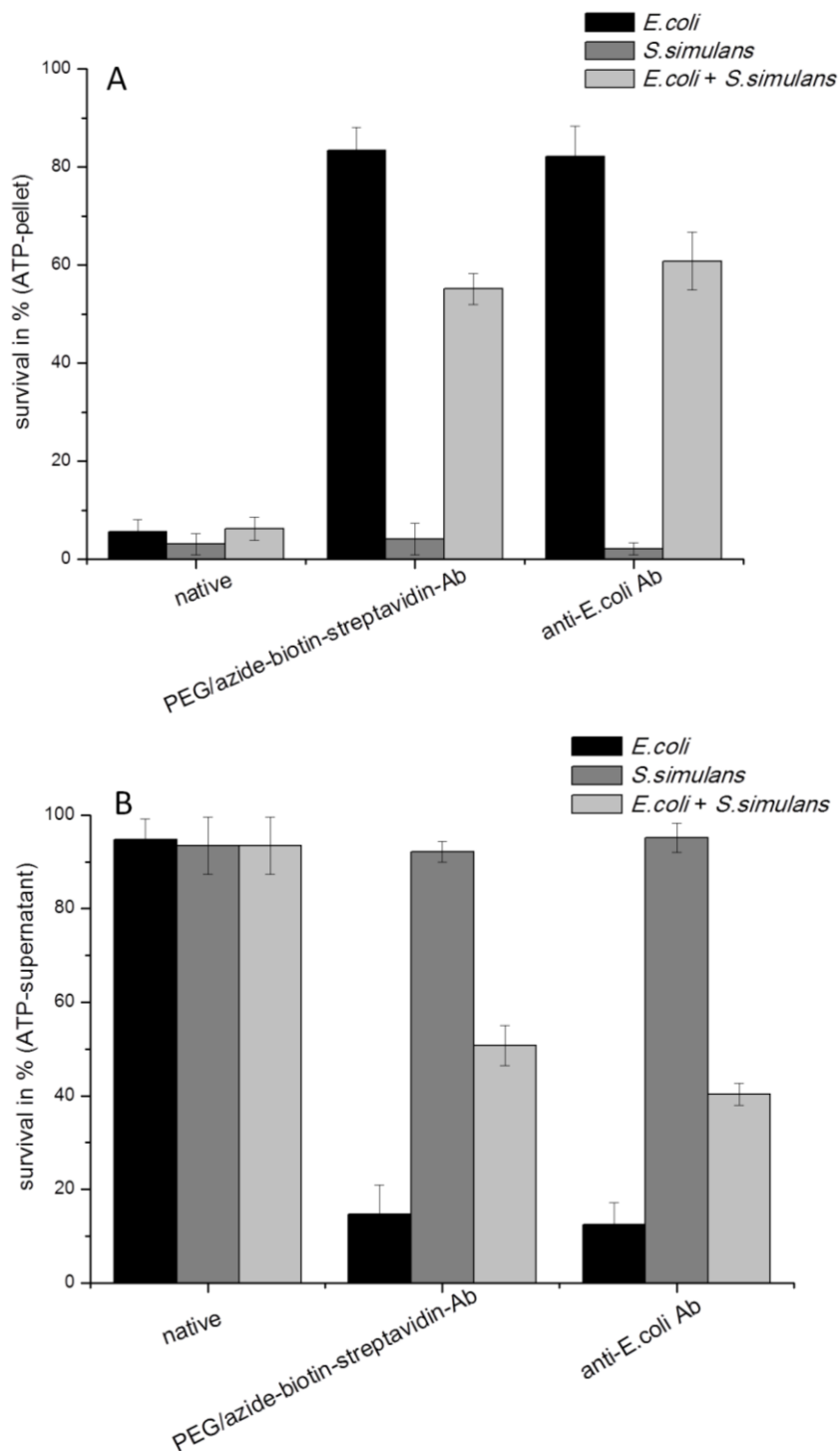
Figure 5-15: Viability of bacterial cells after exposure of 10^7 *E. coli* cells (OD_{595} 0.1) to 10 µg of unfunctionalized, PEG/Az-biotin-streptavidin-Ab (Janus) and fully anti-*E.coli* Ab (non-Janus) functionalized NPs in PBS buffer. After 1 h of magnetic capture, the amount of ATP from the pellet (A) and the supernatant (B) was quantified using the luminescence assay BacTiterGlo. The data is expressed as % of the control (cells incubated without NPs). All data are expressed as mean ± SD of values obtained from three independent experiments.

Most likely, the decrease in bacterial cell counts in the CFU tests can be correlated to clustering of bacteria in the presence of the non-Janus antibody-coated particles, which was also qualitatively observed using fluorescence microscopy (Figure 5-9) and which leads to underestimation of cell counts with the CFU method [191,209,211]. CFU and ATP quantifications performed using other particles such as azide, PEG/azide and PEG/azide-biotin particles as controls showed that cell viability was not compromised. (Figure 5-16).
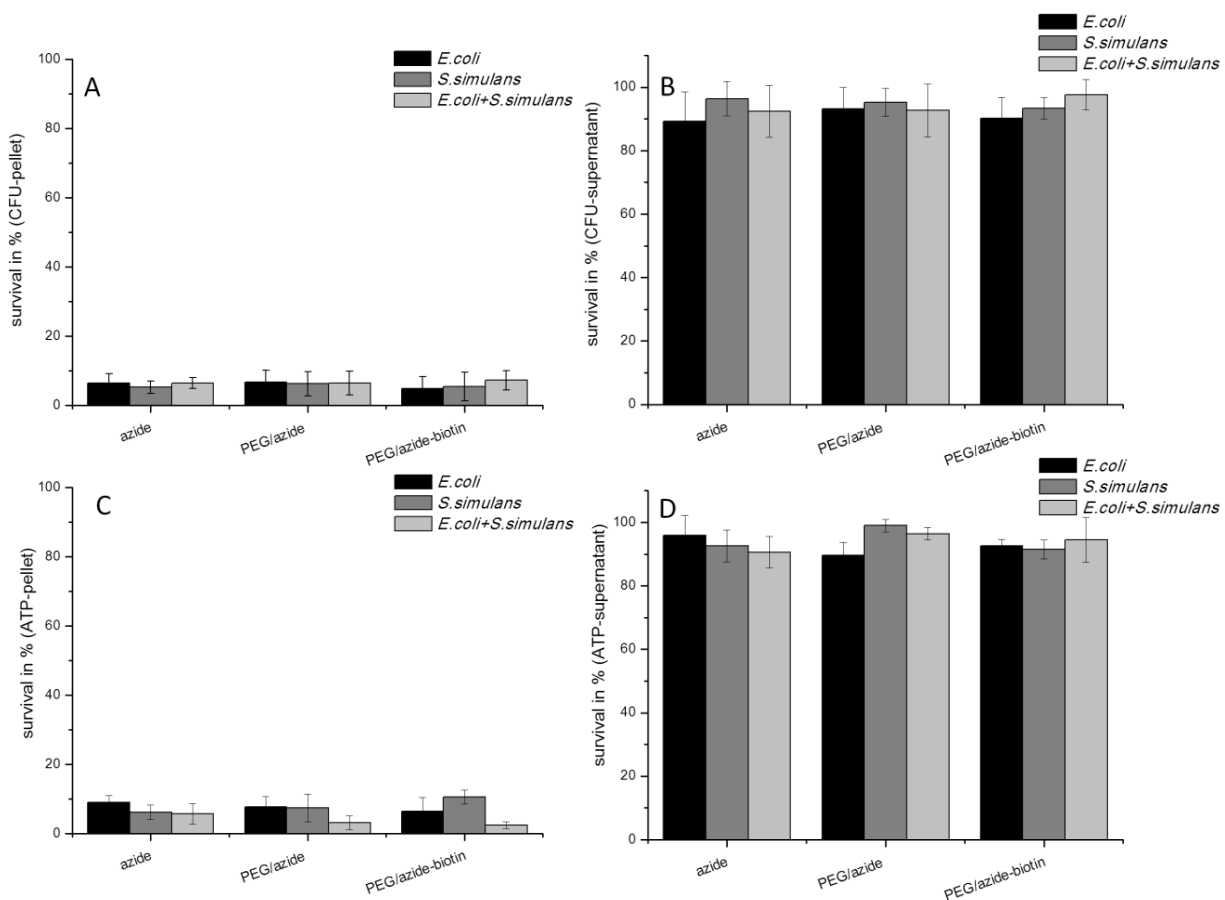
Figure 5-16: Viability of bacterial cells after exposure of 10^7 *E. coli* cells (OD$_{595}$ 0.1) to 10 µg of azide, PEG/azide and PEG/azide-biotin functionalized NPs in PBS buffer. After 1 h of magnetic capture, the amount of CFU from the pellet (A) as well as the supernatant (B) was measured using agar plate based CFU counting method. ATP from the pellet (C) and the supernatant (D) was also quantified using the luminescence assay BacTiterGlo. The data is expressed as % of the control (cells incubated without NPs). All data are expressed as mean ± SD of values obtained from three independent experiments.

5.2 Conclusion

This thesis also presents the use of the wax-in-water Pickering emulsion method for the preparation of Janus particles for highly selective, agglomerate-free bacterial separation. The nanoscale magnetic Janus particles were half-coated with an antibody specifically against *E. coli* and accordingly showed over 80 % capture efficiency with this bacterium, which was comparable to that of NPs fully functionalized with the antibody. Moreover, the prepared NPs did not compromise the viability of the captured bacteria. By design, the Janus NPs possessed the capacity of carrying out bacterial capture without agglomeration between the bacteria, thereby significantly improving bacterial separation procedures for applications that require exact cell counts and precise separation of bacterial species. Despite the seemingly complicated multi-step process, the functionalization strategy based on simple and established methods can be easily scaled and adjusted according to the application of choice. For example, by attaching other antibodies to the Janus NPs, this method can be tailored for the separation of any bacteria of interest from biological samples of varying complexity.

Chapter 6

Janus NPs designed

for extended cell

surface attachment

6. Janus NPs for extended cell surface attachment

In this thesis, we used the findings for microscale Janus particles and introduced a nanoscale Janus particle design, which features membrane anchoring phospholipids on one hemisphere and a PEG stealth coating on the other. By creating such dual-functionalized particles, we aimed to anchor the NPs onto eukaryotic cell membranes and at the same time to inhibit the endocytosis process that leads to uptake of these particles into cells via the passivation layer on the other half of the particle surface. To this end, we synthesized dye-doped SiNPs (50 nm diameter) functionalized with DSPE on one side and PEG on the other side of the particle surface. To facilitate insertion of the phospholipid DSPE into the cell membrane, it was connected to the particle surface via a flexible PEG-linker. The particles were first characterized in terms of their material properties and colloidal behavior. In *in vitro* cell culture studies, the Janus NPs were analyzed jointly with their isotropic (non-Janus) pendants as controls in a mouse fibroblasts cell culture model using 3-day transfer inoculum of 3×10^5 of NIH mouse embryo cells (NIH 3T3) regarding their association to the plasma membrane and their endocytosis properties. Cellular location and distribution patterns of the particles were determined by confocal laser scanning microscopy (CLSM) and TEM. Furthermore, we incubated the NPs together with NIH 3T3 cells in the presence or absence of various endocytose inhibitors to reveal associated internalization pathways.

6.1 Results and Discussion

6.1.1 Exposure of NIH 3T3 fibroblasts to Janus NPs and staining

In vitro cell culture experiments were carried out using the mouse fibroblast cell line NIH 3T3 (passage number 8-25, CLS Cell Line Services GmbH, Germany, product number 400101), and cultured in Dulbecco's Vogt modified Eagle's minimum essential medium

145

(DMEM, high glucose, Invitrogen, Germany, lot number 1206393) supplemented with FCS (Invitrogen, Germany, product number 010M3395) and antibiotic-antimycotic solution (AB/AM, Invitrogen, Germany, product number 1209917). The cells were cultured according to the procedure described by Shakiba et al. and Holthaus et al.[294] DMEM supplemented with 10% FCS and 1% AB/AM were used as the medium for culturing NIH 3T3 cells in an incubator (Labortechnik Göttingen, Germany, product number C200) at 37°C, 10% CO_2 and 95% relative humidity (RH). The cells were cultured in 75 cm^2 flasks for one week and the culture medium was changed every second day. Cells were then trypsinized using trypsin-EDTA solution (0.25% trypsin, 0.02% EDTA, Sigma Aldrich, product number SLBG4376), counted using the Scepter™ 2.0 handheld cell counter (Millipore, Germany) and diluted to attain a final cell density of 1×10^4 cells per ml of culture medium. 1 ml of cell suspension was deposited onto 15 mm glass coverslips (VWR, Germany, lot number 0983) placed in each well of a 6-well PS cell culture plate (NUNC, Fischer Scientific, Germany) and incubated at 37°C, 10% CO_2 and 95% RH. After 30 min, 100 µl of incubation of the cells on the coverslips 100 µl of the respective NP dispersion (1 mg of NPs/ml of DMEM+FCS (10%) +AB/AM (1%) were added onto the cells and incubated for 1 h, 6 h and 24 h at 37 °C covered with aluminium foil and under shaking conditions. NIH 3T3 cells were also incubated in the absence of NPs as a control. Cells were further stained using 1 ml of staining solution which contained 4',6-diamidino-2-phenylindole (DAPI, 0.5µg ml^{-1} of 1 mM PBS, Sigma Aldrich, Germany, product number 1242642) and Alexa fluor 488 phalloidin (AF488, 2U/ml i.e. 10 µg ml^{-1} of 1 mM PBS, Sigma Aldrich, Germany, product number 1151587) as nuclei and cytoplasm- specific dyes. Three channels such as FS02 for DAPI (λ_{ex}:300-400 nm and λ_{em}>420 nm), FS09 for AF 488 (λ_{ex}: 450-490 nm and λ_{em}>515 nm) and FS15 (λ_{ex}: 535-558 nm and λ_{em}>590 nm) for RBITC doped SiNPs were used for imaging. Analysis was done using the AX-10 fluorescence microscope (Zeiss, Germany).

6.1.2　Particle characterization

We used RBITC (RBITC mixed isomers, Sigma Aldrich, Germany, product number MKBJ9031 V) doped SiNPs, which were prepared following the protocol described by Bollhorst et al.[295] which was adapted from the method previously established by

Watanabe et al.[296]. After performing the BET measurements for calculating the SSA of unfunctionalized RBITC doped SiNP cores, prepared using the protocols by [295,296], showed a value of 4.48×10^{16} nm^2/mg particles. Synthesis and functionalization of DSPE/PEG Janus NPs with RBITC-doped SiNP cores is based on our prior established protocol (Chapter 4 and 5) with only minor adaptations.[89,90] Briefly, RBITC-doped SiNP NPs are functionalized with APTES to provide NH$_2$-groups on the particle surface. These particles are added to a heated wax-in-water emulsion to generate wax Pickering emulsion droplets decorated with the NH$_2$- functionalized SiNPs. Here, the surfactant SDS is used to hydrophobize the particle surfaces. SEM images of the wax Pickering emulsion droplets prepared using APTES functionalized NPs are shown in Figure 6-1. The size of the solidified wax Pickering emulsion droplets decorated with amino-functionalized NPs ranged from 30 µm to 80 µm in diameter (Figure 6-1 A), with partially embedded NPs on the surfaces of the wax spheres (Figure 6-1 B). The particles mostly remained on the surface of wax even after several washing steps as observed previously [89,90] thus providing large-scale preparation of Janus NPs
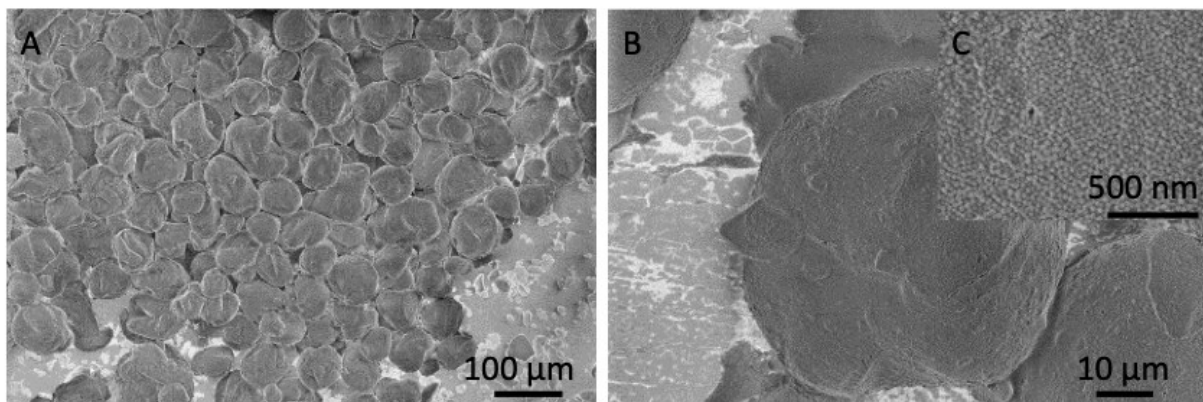
Figure 6-1: SEM analysis of the wax Pickering emulsion droplets prepared using APTES functionalized RBITC-SiO$_2$ Janus NPs. (A) overview of the wax droplets, (B) closeup of a single wax droplet and (C) NPs on the droplet surface from (B).

After the cooling and washing steps, the solvent-exposed particle hemispheres on the solidified wax droplets are functionalized with PEG-silane. Afterwards, the wax is dissolved, and the particles are thereby released from the wax spheres. The originally masked NH$_2$ groups are then functionalized with COOH-PEG-DSPE via EDC-NHS carbodiimide chemistry. Additionally, further isotropic and Janus NPs were prepared as listed in Table 6-1 as controls for the *in vitro* cell culture studies. The prepared particles were characterized regarding their size and ZP by dynamic light scattering before they were used for cell experiments. In order to assess the behavior of the particle dispersion during the cell culture experiments, the particles were analyzed both as a dispersion in a 4 vol% ethanol/water mixture and dispersed in the cell culture medium (DMEM+FCS (10%) + AB/AM (1%)) which was later used in the cell culture studies. DLS analysis of the unfunctionalized RBITC SiO$_2$ NPs dispersed in the ethanol/water mixture revealed a size of 50.5 ± 6 nm (Table 6-1).

Characteristics	liquid medium	unfunctionalized	APTES	APTES/PEG	PEG	DSPE	DSPE/PEG
Particle size (nm)	in 4% ethanol/ water	50.5 ± 6.2	54.1 ± 6.4	65.5 ± 7.8	60.4 ± 10.8	85.6 ± 16.4	86.16 ± 10.4
	DMEM+FCS+A B/AM	52.4 ± 7.25	62.4 ± 4.3	67.2 ± 2.3	58.7 ± 2.6	86.9 ± 7.8	89.7 ± 3.2
PDI	in 4% ethanol/ water	0.13 ± 0.03	0.15 ± 0.04	0.18 ± 0.01	0.14 ± 0.09	0.25 ± 0.05	0.21 ± 0.03
	DMEM+FCS+A B/AM	0.21 ± 0.12	0.22 ± 0.08	0.17 ± 0.06	0.21 ± 0.05	0.24 ± 0.13	0.24 ± 0.07
Zeta potential (mV)	in 4% ethanol/ water	-31.4 ± 4.4	+7.4 ± 8.7	-26.3 ± 1.6	-32.5 ± 7.4	-35.2 ± 6.7	- 40.4 ± 6.4
	DMEM+FCS+A B/AM	-16.7 ± 2.6	-8.3± 2.1	-7.6 ± 4.2	-30.4± 6.2	-20.4± 5.6	-24.4± 3.7
$[NH_2]/nm^2$	in water	1.8 ± 0.3	20.7 ± 6.8	15.3 ± 7.4	4.3 ± 1.8	4.5 ± 3.4	2.5 ± 1.6

Table 6-1: Size and surface properties of the various functionalized RBITC doped SiO_2 NPs. Particle size, PDI and ZP analysis was measured in a 4% ethanol in water mixture and in full cell culture medium consisting of DMEM, FCS and AB/AM. Quantification of the NH_2 groups was performed using the ninhydrin assay in water. The standard deviation is derived from three independent measurements.

A similar hydrodynamic diameter of 52.4 ± 7 nm (Table 6-1) was recorded when these NPs were dispersed in the cell culture medium, showing that colloidal stability was maintained under these conditions. However, APTES-functionalization of the RBITC SiO_2 NPs resulted in a moderate increase of the particle sizes in cell culture medium (62.4 ± 4 nm) indicating slightly decreased colloidal stability, possibly as a result of protein adsorption (mainly BSA as the main constituent of FCS) on the positively charged NP surface [133]. Isotropic PEG functionalization resulted in NPs with a hydrodynamic diameter of 60.4 ± 10.8 nm measured in ethanol/water (Table 6-1). In addition, DLS analysis of PEG-functionalized NPs in cell culture medium lead to a similar hydrodynamic diameter of 58.7 ± 2.6 nm, most likely due to the suppressed protein adsorption of the PEGylated particle surface [129]. The slight increase in hydrodynamic diameter of PEGylated NPs relative to that of unfunctionalized NPs can in this case be attributed to the long-chain PEG groups functionalized on the SiO_2 NPs. The APTES/PEG Janus NPs show somewhat decreased colloidal stability with higher hydrodynamic radius as a result of the anisotropic functionalization. Because of their increased hydrophobicity compared to the hydrophilic unfunctionalized and APTES functionalized particles, fully DSPE-coated

particles show again higher particle sizes and wider size distribution indicated by an increased PDI of 0.25 possibly due to agglomeration of the hydrophobic NPs in the aqueous medium. Finally, the DSPE/PEG Janus NPs displayed a hydrodynamic diameter of 86.2 ± 10.4 nm and 89.7 ± 3 nm in ethanol/water and cell culture medium, respectively (Table 6-1). Along this line, we most likely see some aggregation of DSPE/PEG Janus NPs in the form of a mixture of dimeric agglomerates and individually dispersed particles possibly as a consequence of both the increased hydrophobicity of the DSPE and the Janus character of the particles. The size of the DSPE/PEG NPs seems to be unaffected by the presence of the otherwise surface-active molecules in the cell culture medium. These findings are further substantiated by ZP measurements of all NP types in ethanol/water and cell culture medium, respectively (Table 6-1). Of special note is the positive surface charge of APTES-coated NPs in ethanol/water which reverts to a negative charge in cell culture medium as a result of protein adsorption [112,133]. Correspondingly, a decrease in ZP was observed for the APTES/PEG Janus NPs resuspended in cell culture medium. In all other cases, regardless of the dispersion medium, the NPs remained negatively charged.

Quantification of primary amino groups on the as-prepared NPs was performed using the ninhydrin assay. Here, 20.7 ± 6.8 NH_2 groups per nm^2 of the surface of NH_2 functionalized SiO_2 NP were determined and Janus functionalization of the APTES/PEG NPs reduced the number of quantifiable NH_2 groups to 15.3 ± 7.4 amino groups per nm^2 of the particle surface (Table 6-1).
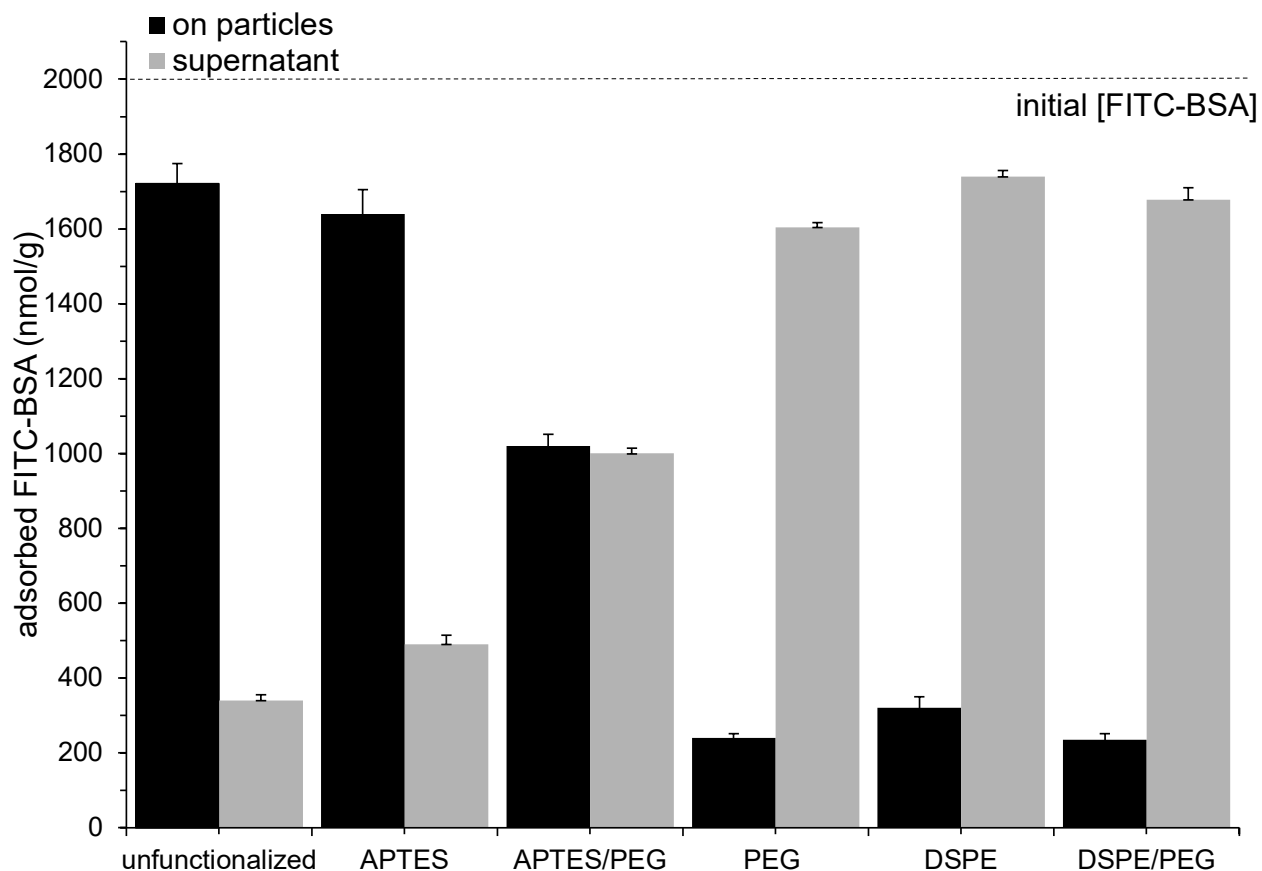
Figure 6-2: Confirmation of the presence of PEG groups by quantification of adsorbed FITC-BSA. The amount of adsorbed FITC-BSA on the NPs was quantified using fluorescence spectroscopy. The total amount of FITC-BSA in each case was 2000 nmol/g of NP.

The success of the PEG-functionalization was further assessed by incubating the particles with FITC-BSA and analyzing the ratio of FITC-BSA adsorbed to the surface of NPs to dissolved FITC-BSA in the supernatant (Figure 6-2). After 1 h of incubation, unfunctionalized and APTES-functionalized NPs showed high amounts of FITC-BSA adsorption (Figure 6-2 A, black bars), whereas negligible amounts of BSA were detected in the respective supernatant (Figure 6-2 B, grey bars). On the other hand, APTES/PEG functionalized NPs showed lower amounts of adsorbed FITC-BSA in comparison to the unfunctionalized and the positively charged APTES functionalized NPs. As control, adsorption of FITC-BSA to PEG functionalized RBITC SiO$_2$ NPs was measured. Low amounts of FITC-BSA on the NPs were detected confirming the success of PEG functionalization.

For FITC-BSA adsorption studies on both DSPE- and DSPE/PEG functionalized particles,

negligible amounts of FITC-BSA adsorption were observed on both particle types. The amounts of BSA adsorption are comparable to those obtained with fully PEG functionalized particles showing that the DSPE-coating also prevents BSA adsorption.

Lastly, direct visualization of the immobilized organic molecules on the surface of the NPs is extremely difficult using TEM due to their poor contrast. In the previous study we grafted proteins bearing ultra-small gold or iron oxide NPs on Janus particles to provide contrast in the TEM, which more directly demonstrated the success of our approach.[90] While, the wax Pickering emulsion technique achieves the preparation of bulk quantities of Janus particles, we also observed that, with NPs, the method does not provide a well-defined Janus balance [89,90].

6.1.3　CLSM analysis of NP interaction and uptake by cultured NIH 3T3 cells
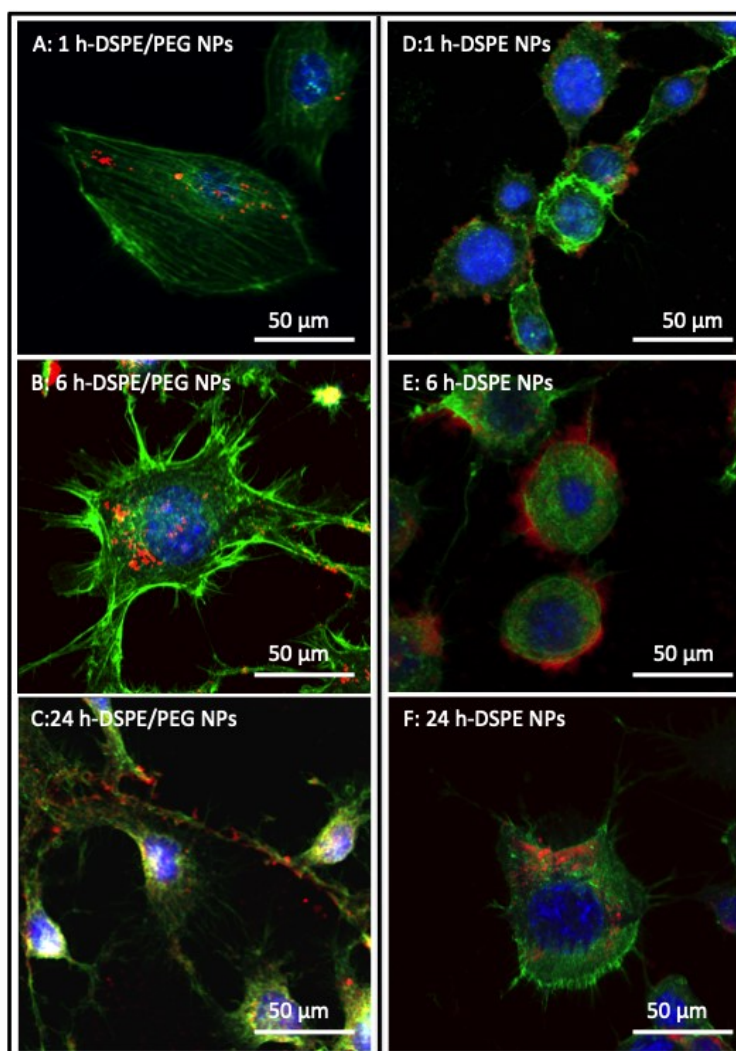
Figure 6-3: CLSM images of NIH 3T3 cells after exposure to Janus DSPE/PEG and fully DSPE functionalized NPs. The cells were incubated with the NPs for 1 h (A, D), 6 h (B, E) and 24 h (C, F) followed by fluorescence staining with specific fluorescent dyes. The nuclei and cytoskeletons are stained using the membrane impermeable dyes DAPI (blue) and AF-488 (green) respectively, whereas the NPs are labelled with RBITC (red).

CLSM was used to investigate the potential attachment and cellular uptake of NPs by cultured NIH 3T3 cells. Figure 6-3 shows representative CLSM images of cultured NIH 3T3 cells incubated with DSPE- and DSPE/PEG-functionalized NPs for 1 h, 6 h and 24 h. The micrographs revealed the association of the NPs to the cells at all time points (Figure 6-3, A-F). Since the cells are very flat, it was not possible to unequivocally discern with Z-

stack images whether the particles were localized inside the cytosol or whether they stayed attached to the surfaces of the cells. (see figure 6-4 for a series of z-stack images).
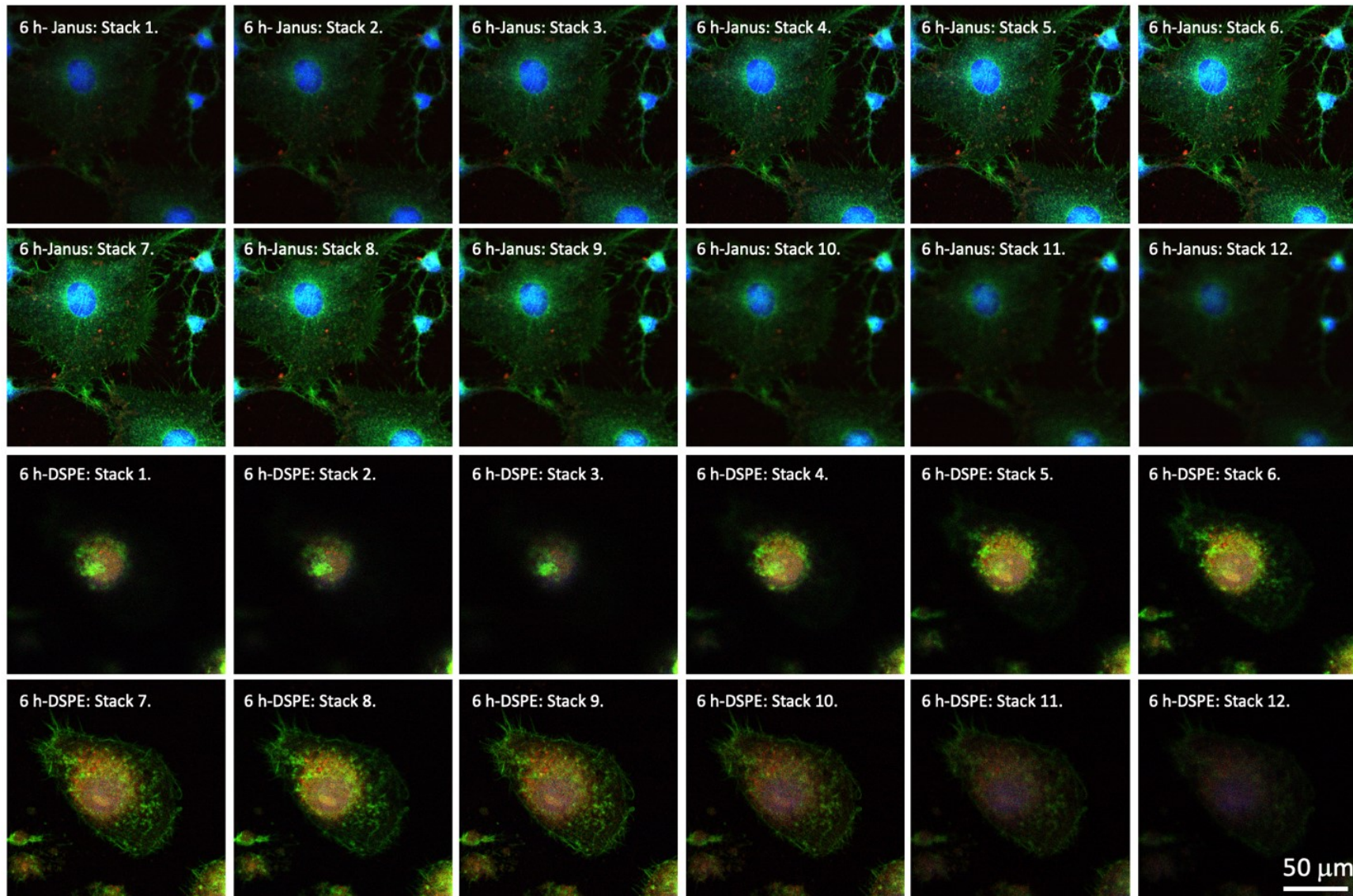
Figure 6-4: Representative Z-stack CLSM images of NIH 3T3 cells after incubation with DSPE/PEG Janus and DSPE particles for 6 h. The images were taken starting at the center and obtained at regular intervals of were 200 nm towards the end of the cell. The nuclei were stained using DAPI (blue), the cytoskeleton was dyed with AF-488 (green) and the NPs were labelled with RBITC (red).

As expected, control experiments without NPs and PEG-functionalized NPs showed no particle association with the cells (Figure 6-5). In contrast, unfunctionalized and APTES-functionalized NPs showed similar or, in the case of APTES, more frequent association relative to DSPE and DESPE/PEG functionalized NPs (Figure 6-6). As mentioned above, APTES-functionalized particles undergo protein adsorption in cell culture medium causing a change in the surface charge. However, the serum proteins adsorbing onto the APTES-functionalized particles did not prevent uptake into the cells, which is in accordance with the results published by Shahabi et al. [129].
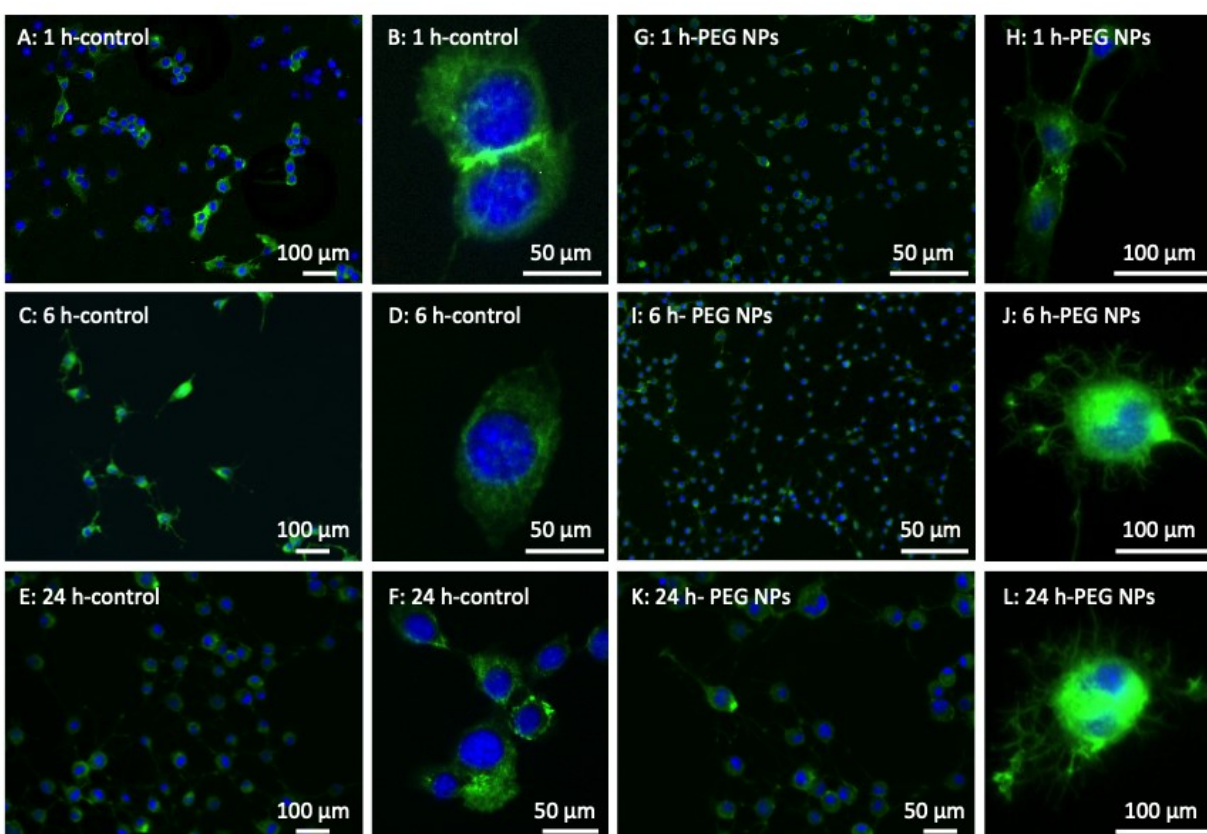
Figure 6-5: Fluorescence microscopy and laser scanning confocal microscopy (X, Y) of NIH 3T3 cells before and after exposure of the fully PEG functionalized NPs. The cells were incubated with PEG functionalized NPs for 1 h, 6 h and 24 h followed by fluorescence staining with specific fluorescent dyes. The merged images were recorded using the DAPI-, FITC- and RBITC- channels. The nuclei and cytoskeletons were stained using the dyes DAPI and AF-488 respectively, whereas the NPs have been labelled with RBITC.
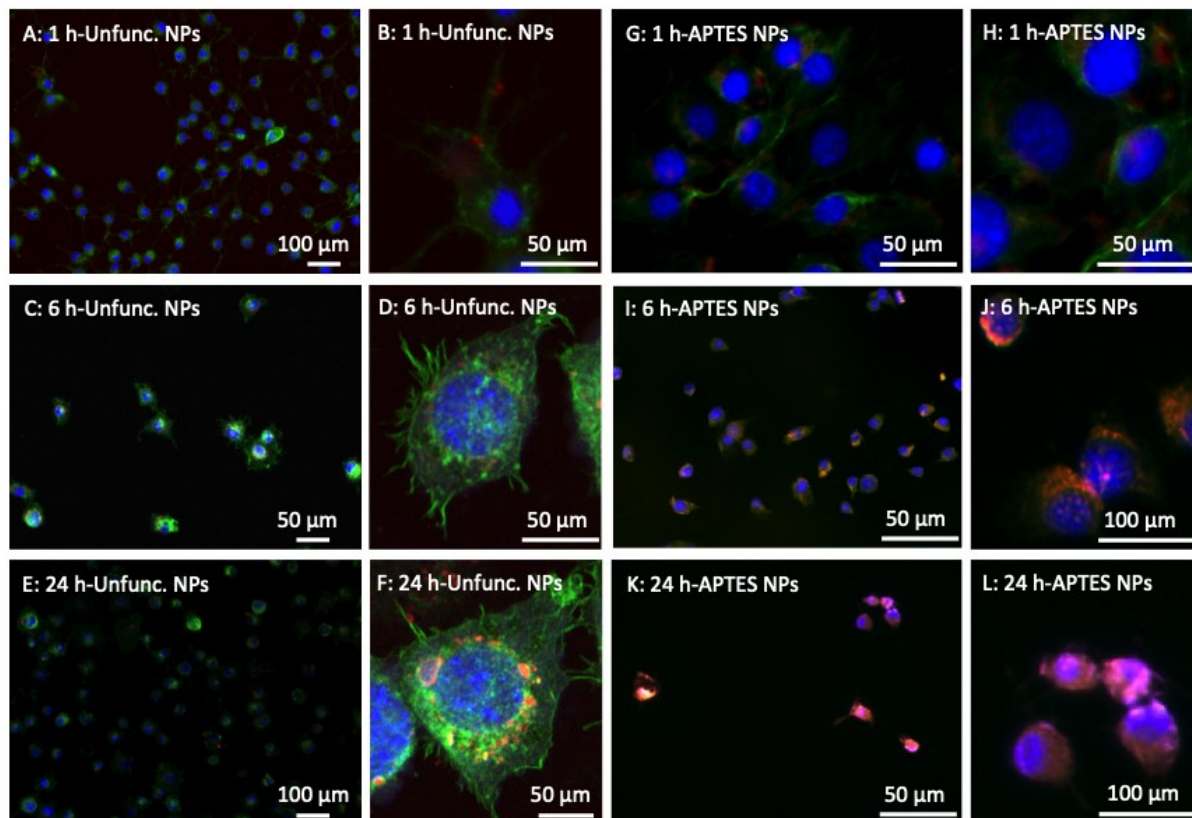
Figure 6-6: Fluorescence microscopy and laser scanning confocal microscopy (X, Y) of NIH 3T3 cells after exposure of the unfunctionalized and APTES functionalized NPs. The cells were incubated with the respective NPs for 1 h, 6 h and 24 h followed by fluorescence staining with specific fluorescent dyes. The merged images were recorded using the DAPI-, FITC- and RBITC- channels. The nuclei and cytoskeleton were stained using the dyes DAPI and AF-488 respectively, whereas the NPs have been labelled with RBITC.

6.1.4 TEM analysis of particle uptake by cultured NIH 3T3 cells

To further observe the cellular uptake of NPs by cultured NIH 3T3 cells, TEM analysis was performed using 50 nm microtome sections of resin-embedded trypsinized cells after their exposure to NPs at different time points (Figure 6-7, 6-8, 6-9). Trypsin treatment detaches adherend cells from tissue culture plates and transfers them into suspension. In TEM analysis, such suspended spherically shaped cells allow efficient cellular localization of NPs at the plasma membrane and in the cytosol. In the micrographs, the cytosol of the cells can be observed as darker gray areas (Figure 6-7). Control experiments using

157

untreated NIH 3T3 cells showed spherical features as lighter gray spots inside the cells that are most likely gas vacuoles (Figure 6-9 A-F). These gas vacuoles were also observed when cells were incubated with NPs. The NPs themselves can be observed as dark gray dots which fit to the DLS-diameter of the particles listed in Table 1.

When incubated with DSPE/PEG Janus NPs, the NPs remained constrained to the outer regions of the cells at all studied time points (Figure 6-7 A-F). Conversely, when cells were incubated with fully DSPE-functionalized NPs, at 1 h (Figure 6-7 A, B), NP accumulation was observed on the cell surfaces. After 6 h of incubation time (Figure 6-7 C, D), the NPs were taken up into cellular microvesicles which was even more pronounced after 24 h of incubation (Figure 6-7 E, F). Most strikingly, a clear distinction between DSPE/PEG- and DSPE-functionalized NPs was observed after 24 h of incubation. The majority of DSPE functionalized NPs were localized inside the cells and, in contrast, when cells were incubated with DSPE/PEG Janus particles, almost no internalization was observed (see Figure 6-9 for further images with these particles). Additionally, the DSPE/PEG Janus NPs seem to be mainly located at extracellular ruffled protrusions of the cell membrane which could possibly be associated to filipodia of the plasma membrane. Figure 6-9 and 6-10 illustrates the internalization of all other types (see Table 6-1) of synthesized NPs which is clearly visible already after 1 h of incubation, as expected.
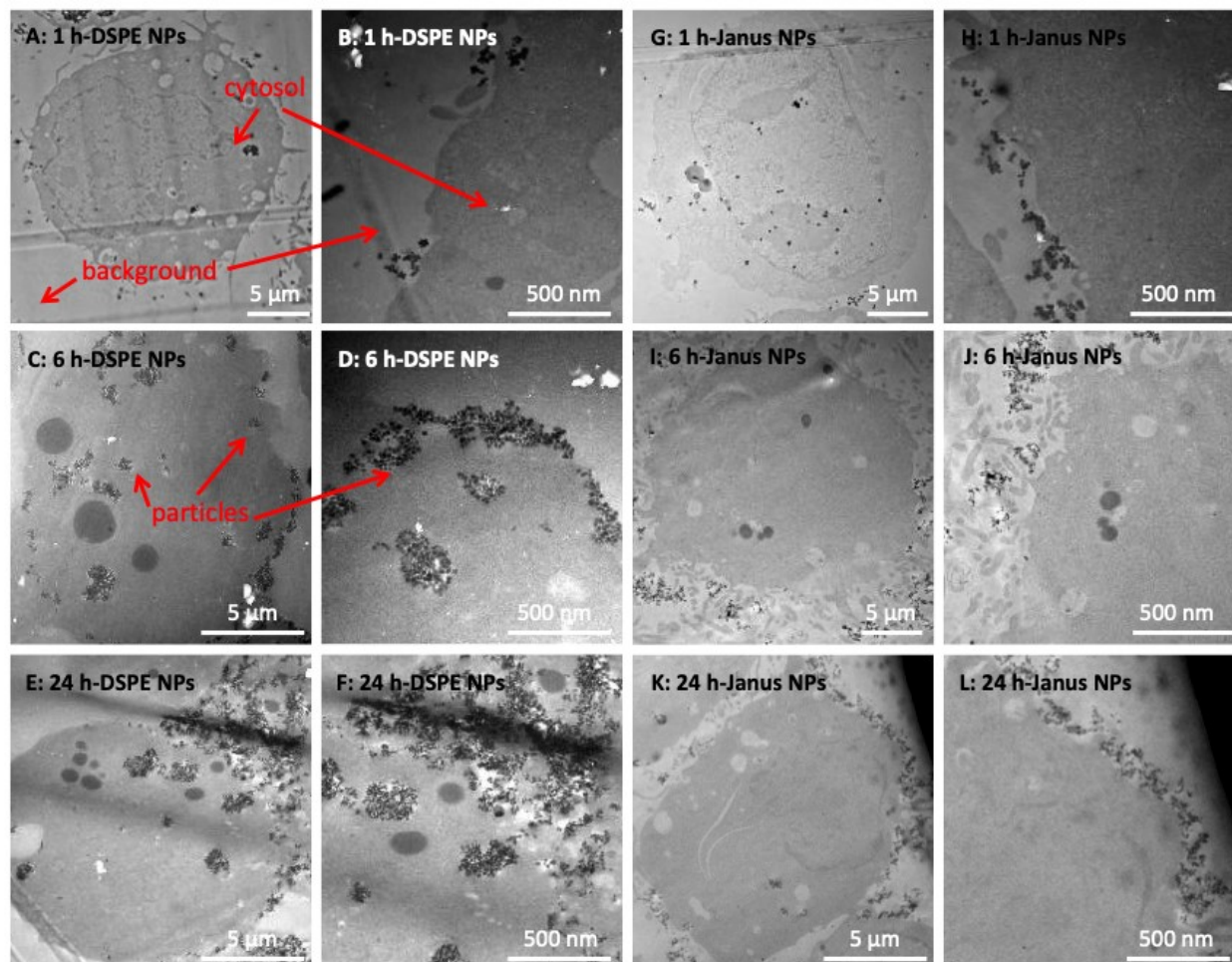
Figure 6-7: TEM of the NIH 3T3 cells after incubation with Janus DSPE/PEG- and isotropic DSPE functionalized NPs for 1 h, 6 h and 24 h. The images of the second and forth column were taken at higher magnification as the images of the first and third column. Each sample was first embedded in epoxy resin followed by performing ultrathin microtome cutting of up to 50 nm followed by TEM analysis. The red arrows indicate the main sources of contrast of the images from which all deductions are inferred.
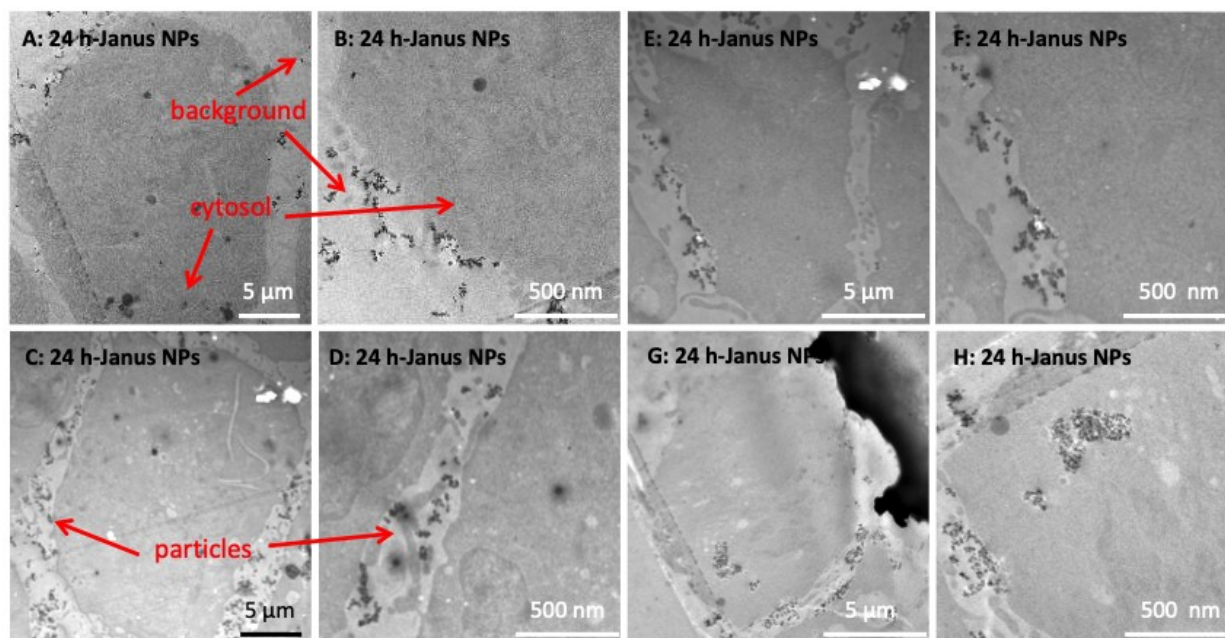
Figure 6-8: TEM of the NIH 3T3 cells after incubation with DSPE/PEG (Janus) RBITC SiO$_2$ NPs for 24 h. The images of the second and forth column are higher magnifications of the images of the first and third row, respectively. Each sample was first embedded in epoxy resin followed by performing ultrathin microtome cutting of up to 50 nm followed by TEM analysis.
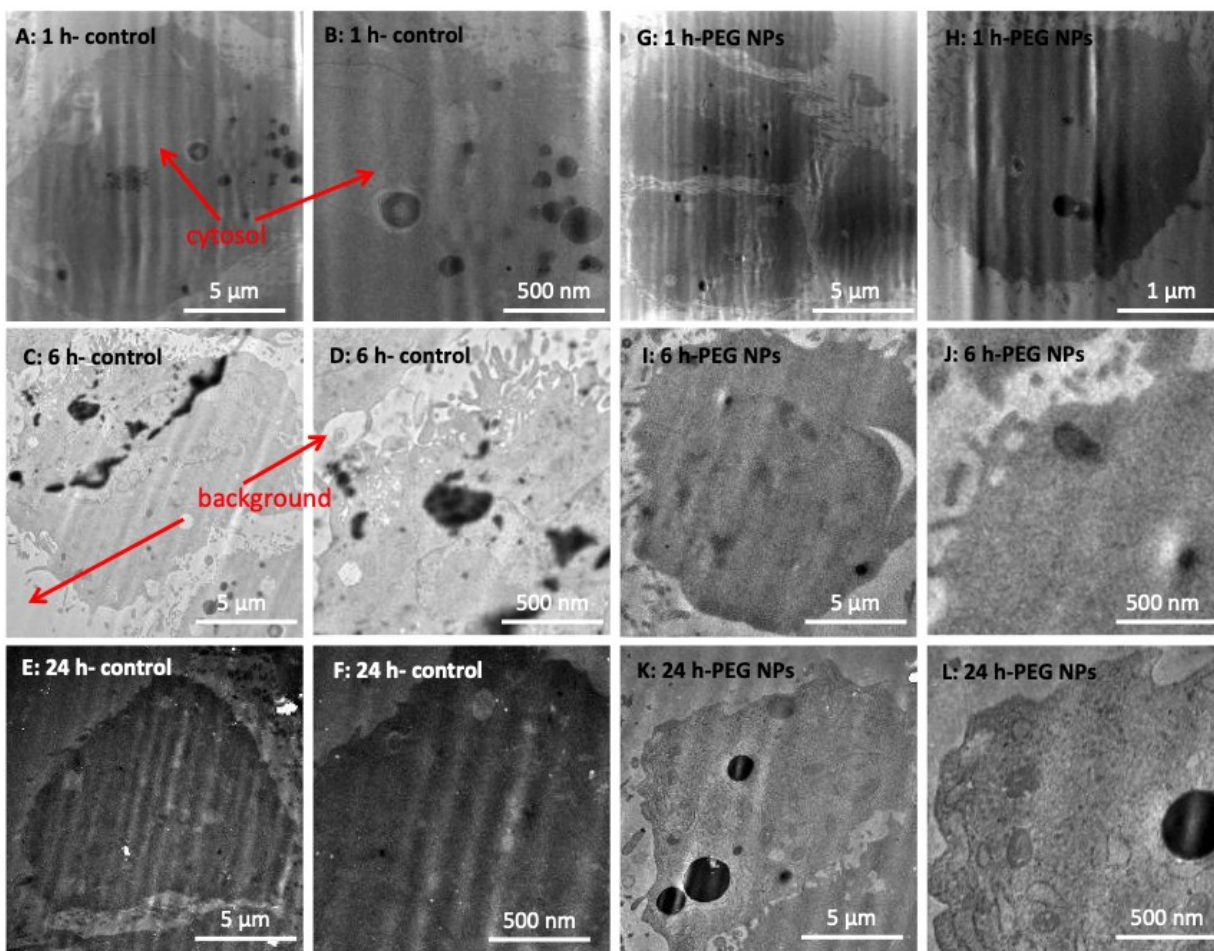
Figure 6-9: TEM of the NIH 3T3 cells after incubation without (control) and with PEG NPs for 1 h, 6 h and 24 h. The images of the second and forth column are higher magnifications of the images of the first and third row, respectively. Each sample was first embedded in epoxy resin followed by performing ultrathin microtome cutting of up to 50 nm followed by TEM analysis.
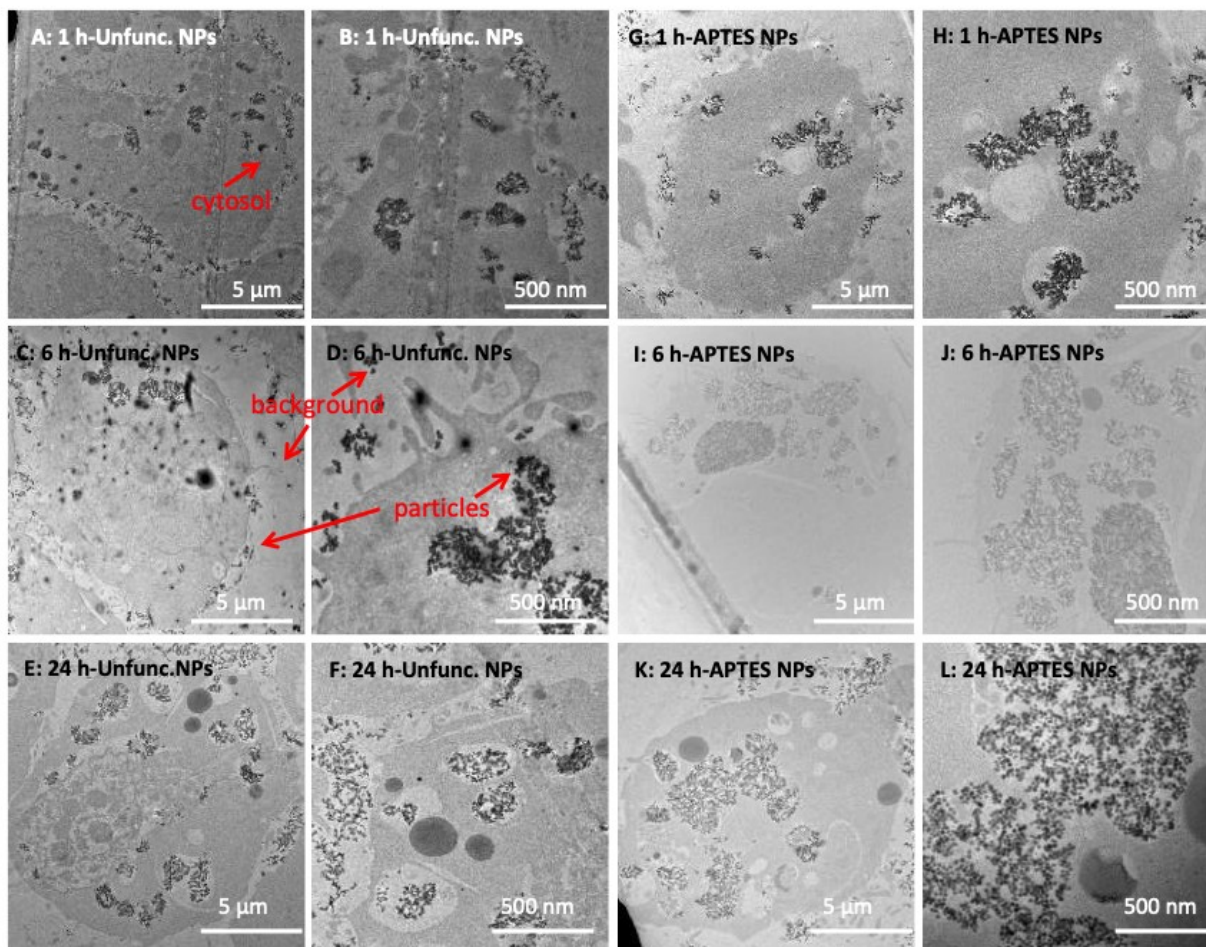
Figure 6-10: TEM of the NIH 3T3 cells after incubation with unfunctionalized and APTES NPs for 1 h, 6 h and 24 h. The images of the second and forth column are higher magnifications of the images of the first and third row, respectively. Each sample was first embedded in epoxy resin followed by performing ultrathin microtome cutting of up to 50 nm followed by TEM analysis.

6.1.5 Particle uptake in the presence of endocytose inhibitors

To further elucidate the endocytosis pathways that are potentially involved in the internalization of functionalized and unfunctionalized NPs, cultured NIH 3T3 cells were incubated with our synthesized NPs in the presence or absence of the common endocytosis inhibitors nystatin and wortmannin as well as with high-sucrose medium and at 4 °C. Figure 6-11 shows representative fluorescence microscopy images of NIH 3T3 cells incubated for 6 h with the respective NPs under the mentioned conditions. Additionally, the results for 1 h and 24 h of incubation are shown in Figures 6-12 and 6-

13. Cell nuclei are stained with DAPI and are illustrated in blue, the RBITC SiO$_2$ NPs are shown in red. Green actin staining has not been included in these images for clarity but is depicted in Figures 6-14 – 6-16 as reference. As expected, without NPs and with fully PEG-coated particles, no particles are visible in any experiments (Figure 6-11, first two rows). As discussed above, unfunctionalized and APTES-coated NPs were strongly internalized in the absence of endocytosis inhibitors (Figure 6-11 – 6-13, third and fourth row). In direct comparison, DSPE- and DSPE/PEG functionalized NPs seem to be taken up to a lesser degree than APTES-coated and unfunctionalized NPs (Figure 6-11 – 6-13, fifth and sixth row). However, on the basis of the fluorescent microscopy images it is difficult to make a distinction between surface attached and internalized NPs.

We assume that all visible extracellular NPs are somehow associated to the cell surface since these still remained after the washing steps. Temperature dependent suppression of endocytosis by incubating NIH 3T3 cells at 4°C (Figure 6-11, second column) caused a strong decrease or slowdown in the uptake of the unfunctionalized and APTES functionalized particles. This mitigation of uptake was also detected for DSPE- and DSPE/PEG-functionalized NPs after 1 h of incubation (Figure 6-12) but is no longer visible after 6 h and 24 h (Figure 6-11 and Figure 6-13). Incubation of NIH 3T3 cells in hypertonic media containing 0.45 M sucrose should overload cell surface receptors involved in receptor-mediated endocytosis (Figure 6-11, third column) [297]. This treatment also resulted in lower uptake rates of unfunctionalized and APTES functionalized NPs relative to those observed for untreated samples incubated under standard culturing conditions (Figure 6-11, first column). However, cellular uptake of DSPE- and DSPE/PEG-functionalized NPs remained unaffected by the high-sucrose medium treatment. The same trend can be observed when the endocytosis inhibitor nystatin is added to the cell culture medium (Figure 6-11, fourth column). Nystatin is known to inhibit caveola-dependent endocytosis [298] and seems to be exclusively effective to prevent cellular uptake of the hydrophilic unfunctionalized and APTES-functionalized NPs. Along this line, in the presence of wortmannin (Figure 6-11, fifth column), a well-characterized macropinocytosis inhibitor,[299] no intracellular accumulation was observed for any NP type.
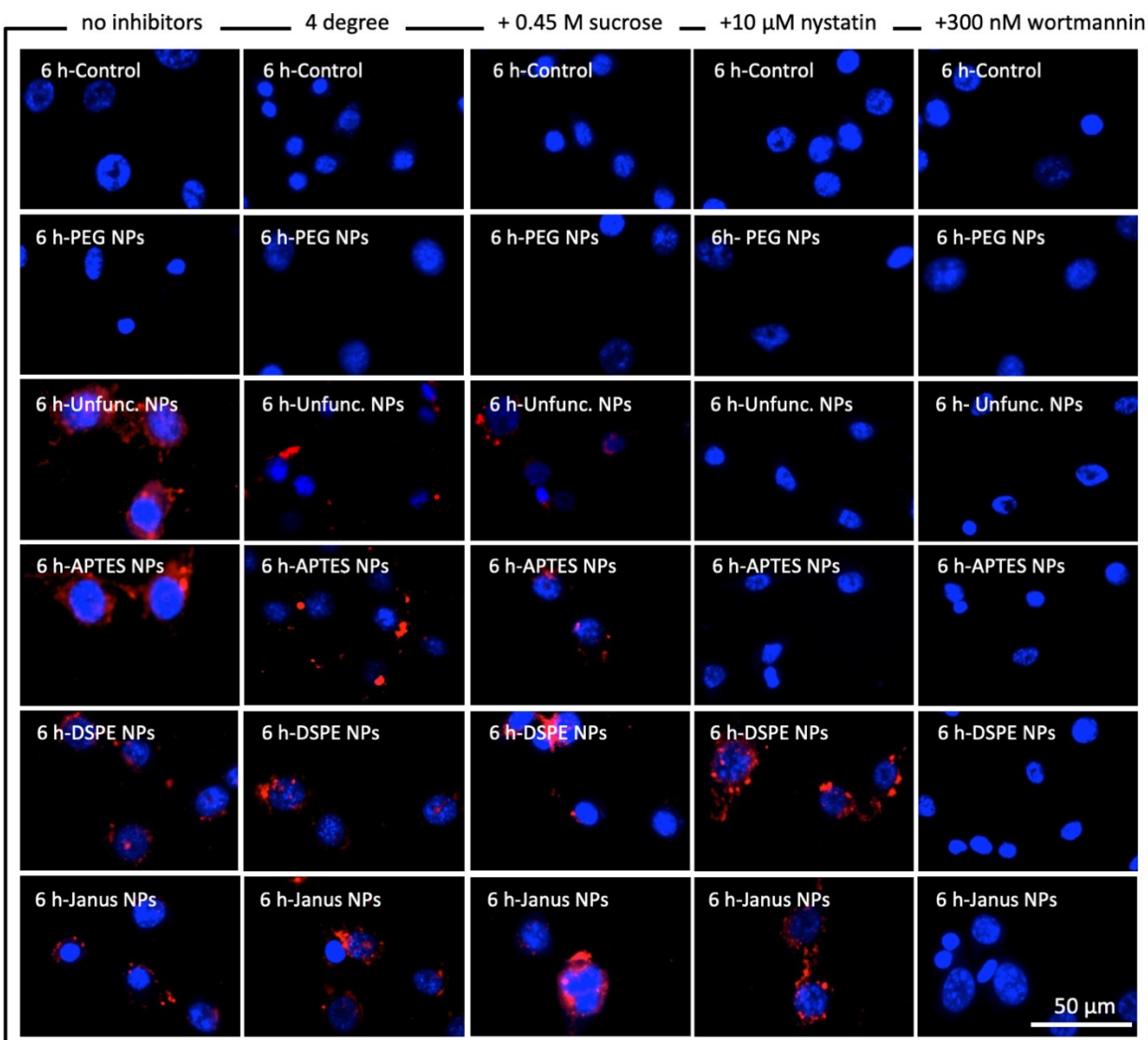
Figure 6-11: Fluorescence microscopy of NIH 3T3 cells before (control) and after exposure of the different NPs for 6 h in the presence and absence of endocytosis inhibitors. 4°C incubation was performed to suppress temperature-dependent endocytosis, hypertonic sucrose concentrations suppressed receptor-mediated endocytosis, nystatin inhibits caveolae-mediated endocytosis and wortmannin inhibits macropinocytosis. The nuclei were stained using DAPI (blue), whereas the NPs were labelled with RBITC (red).
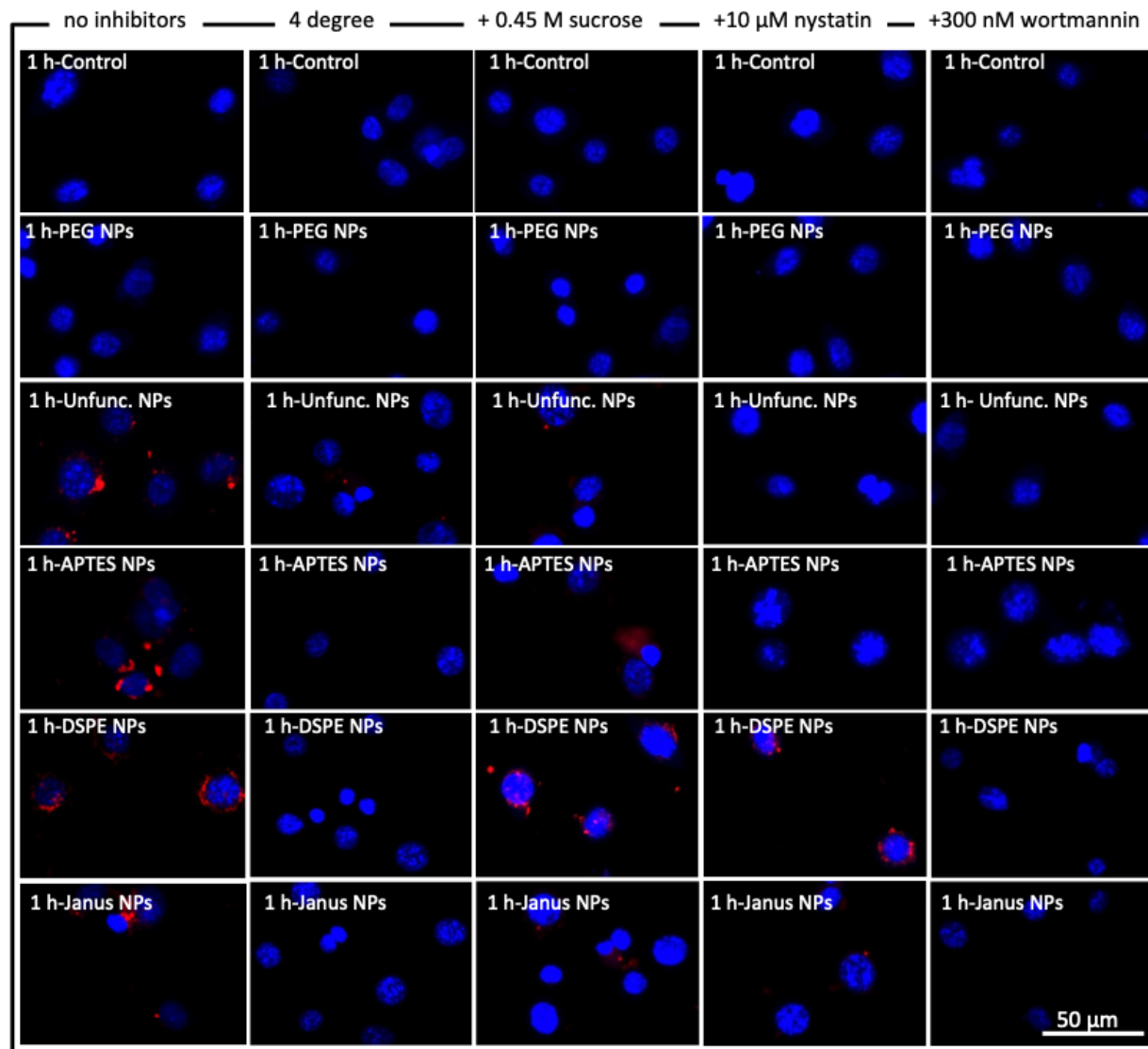
Figure 6-12: Fluorescence microscopy of NIH 3T3 cells before (control) and after exposure of the different NPs for 1 h in the presence and absence of endocytosis inhibitors. 4°C incubation was performed to suppress temperature-dependent endocytosis, hypertonic sucrose suppressed receptor-mediated endocytosis, nystatin inhibits caveolae-mediated endocytosis and wortmannin inhibits macropinocytosis. The nuclei were stained using DAPI (blue), whereas the NPs were labelled with RBITC (red).
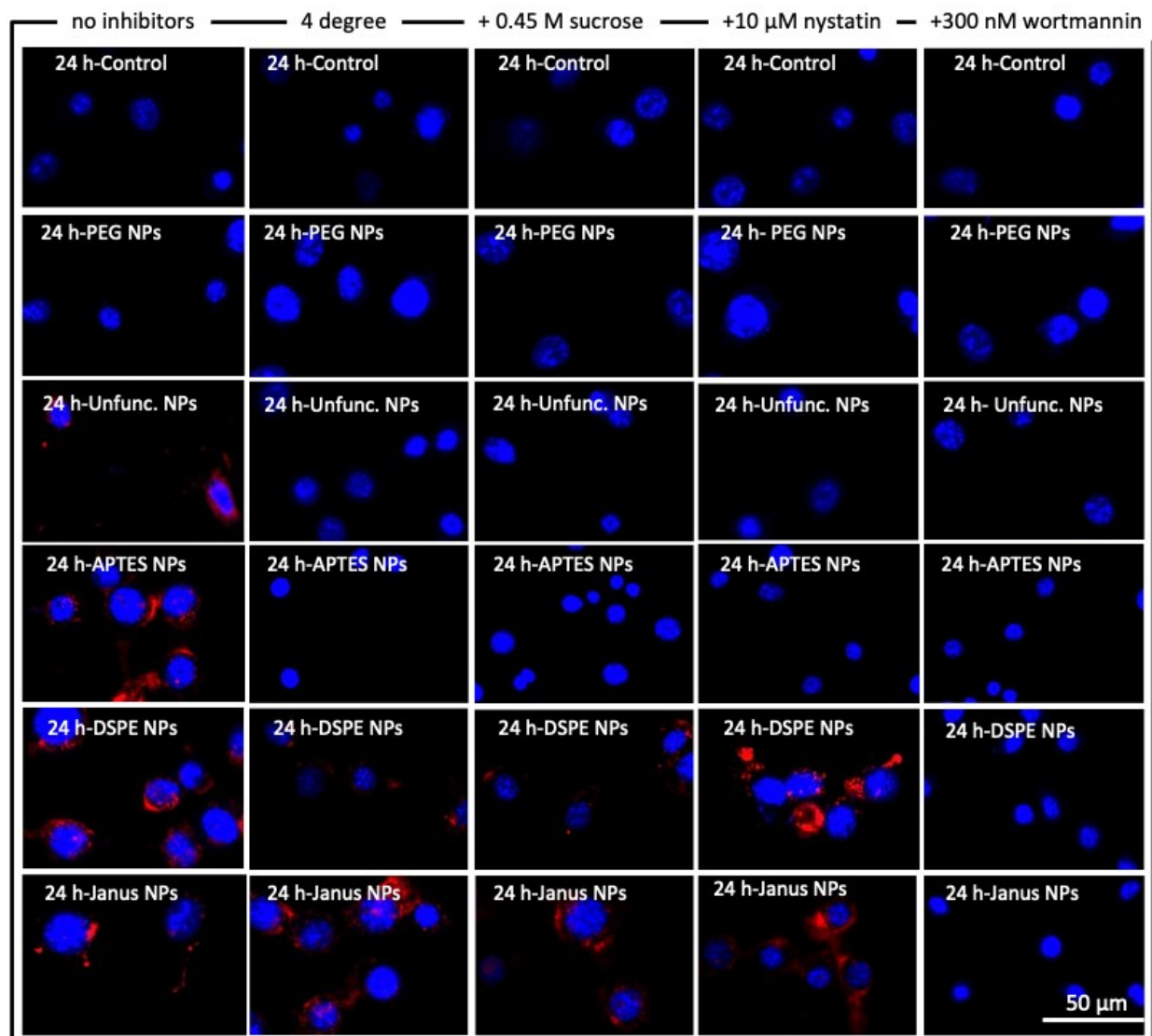
Figure 6-13: Fluorescence microscopy of NIH 3T3 cells before (control) and after exposure of the different NPs for 24 h in the presence and absence of endocytosis inhibitors. 4 °C incubation was performed to suppress temperature-dependent endocytosis, hypertonic sucrose suppressed receptor-mediated endocytosis, nystatin inhibits caveolae-mediated endocytosis and wortmannin inhibits macropinocytosis. The nuclei were stained using DAPI (blue), whereas the NPs were labelled with RBITC (red).
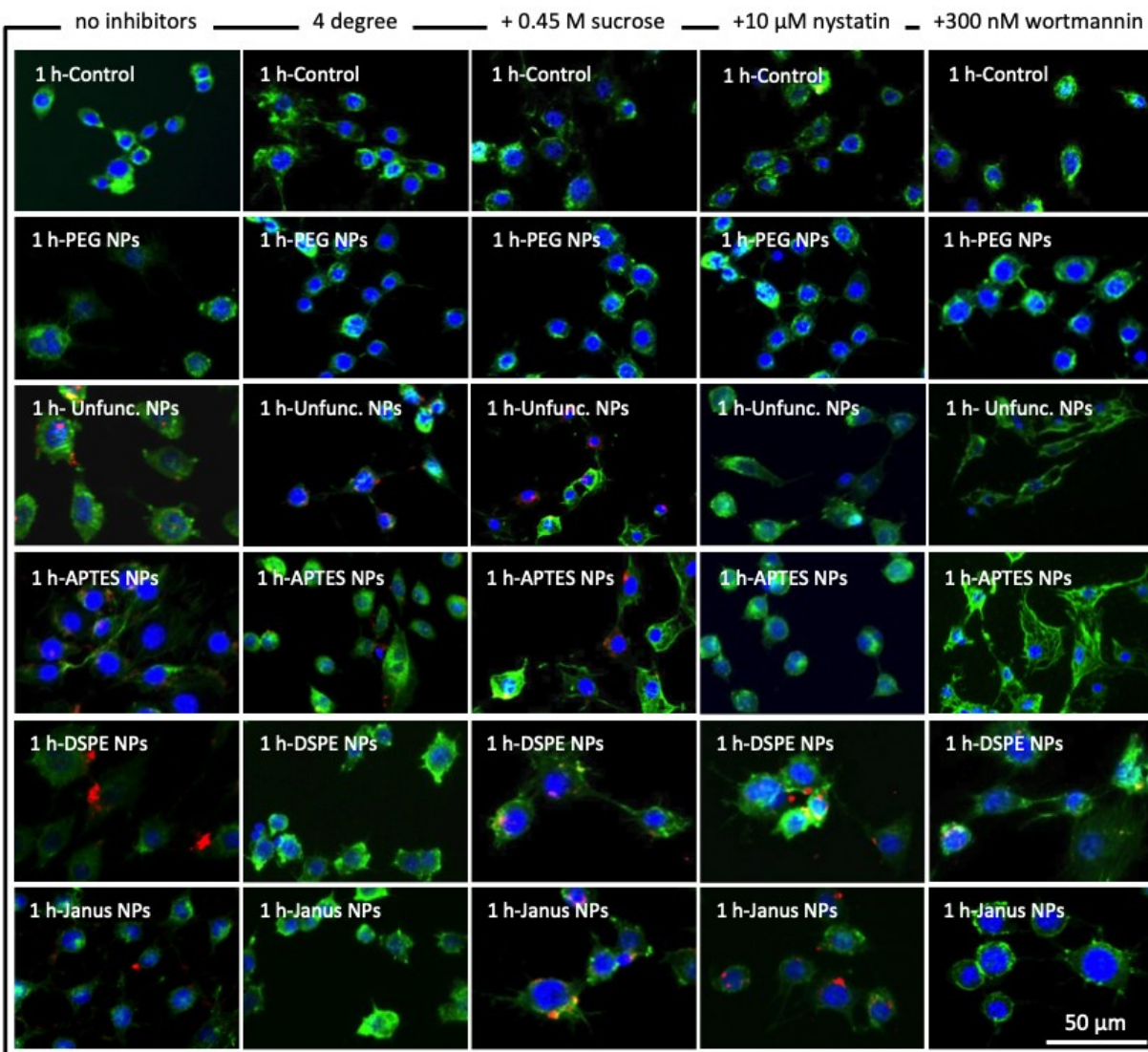
Figure 6-14: Fluorescence microscopy of NIH 3T3 cells before (control) and after exposure of the different NPs for 1 h in the presence and absence of endocytosis inhibitors. 4 °C incubation was performed to suppress temperature-dependent endocytosis, hypertonic sucrose suppressed receptor-mediated endocytosis, nystatin inhibits caveolae-mediated endocytosis and wortmannin inhibits macropinocytosis. The nuclei were stained using DAPI (blue), the cytoskeleton was dyed with AF-488 (green) and the NPs were labelled with RBITC (red).
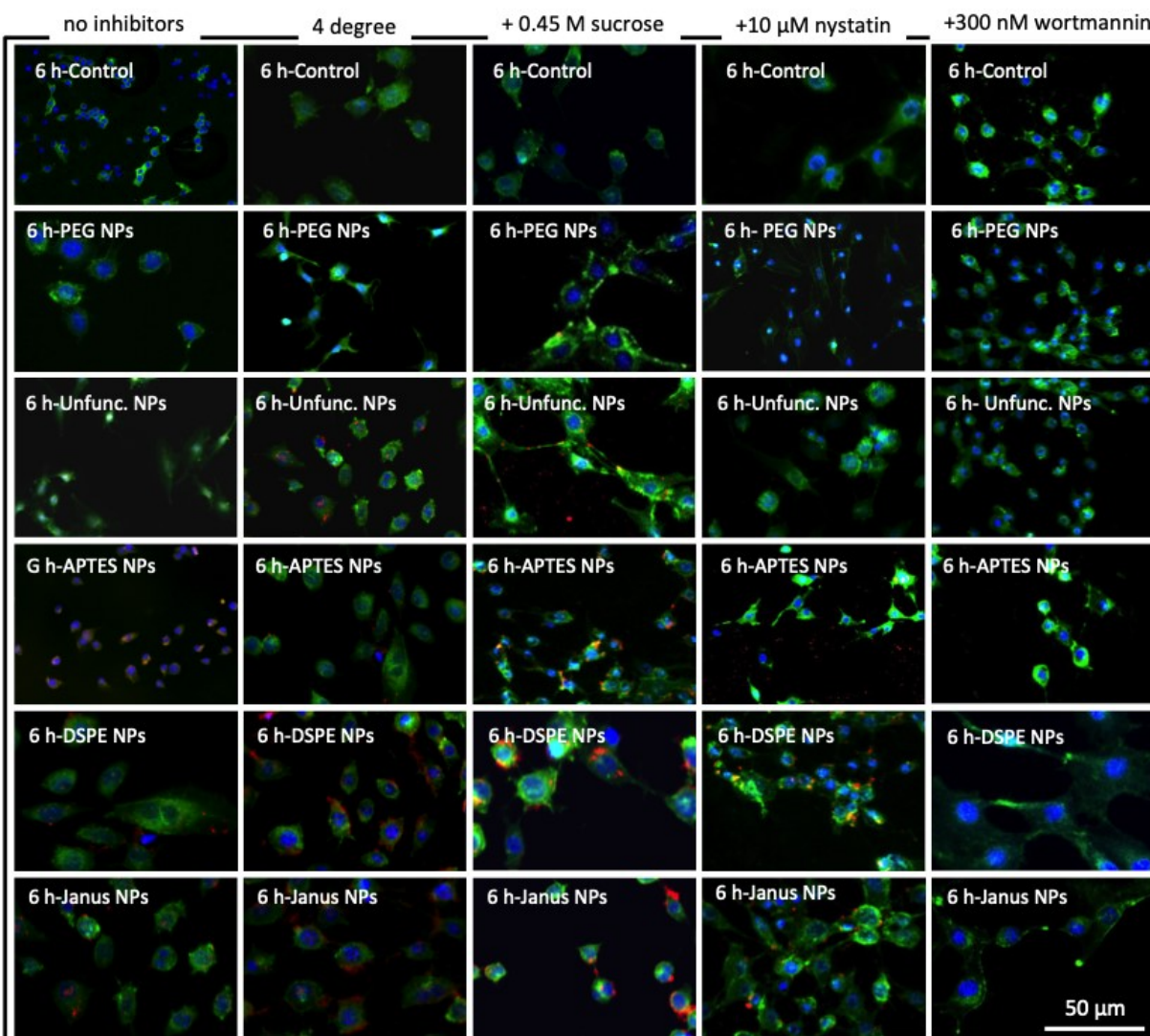
Figure 6-15: Fluorescence microscopy of NIH 3T3 cells before (control) and after exposure of the different NPs for 6 h in the presence and absence of endocytosis inhibitors. 4 °C incubation was performed to suppress temperature-dependent endocytosis, hypertonic sucrose suppressed receptor-mediated endocytosis, nystatin inhibits caveolae-mediated endocytosis and wortmannin inhibits macropinocytosis. The nuclei were stained using DAPI (blue), the cytoskeleton was dyed with AF-488 (green) and the NPs were labelled with RBITC (red).
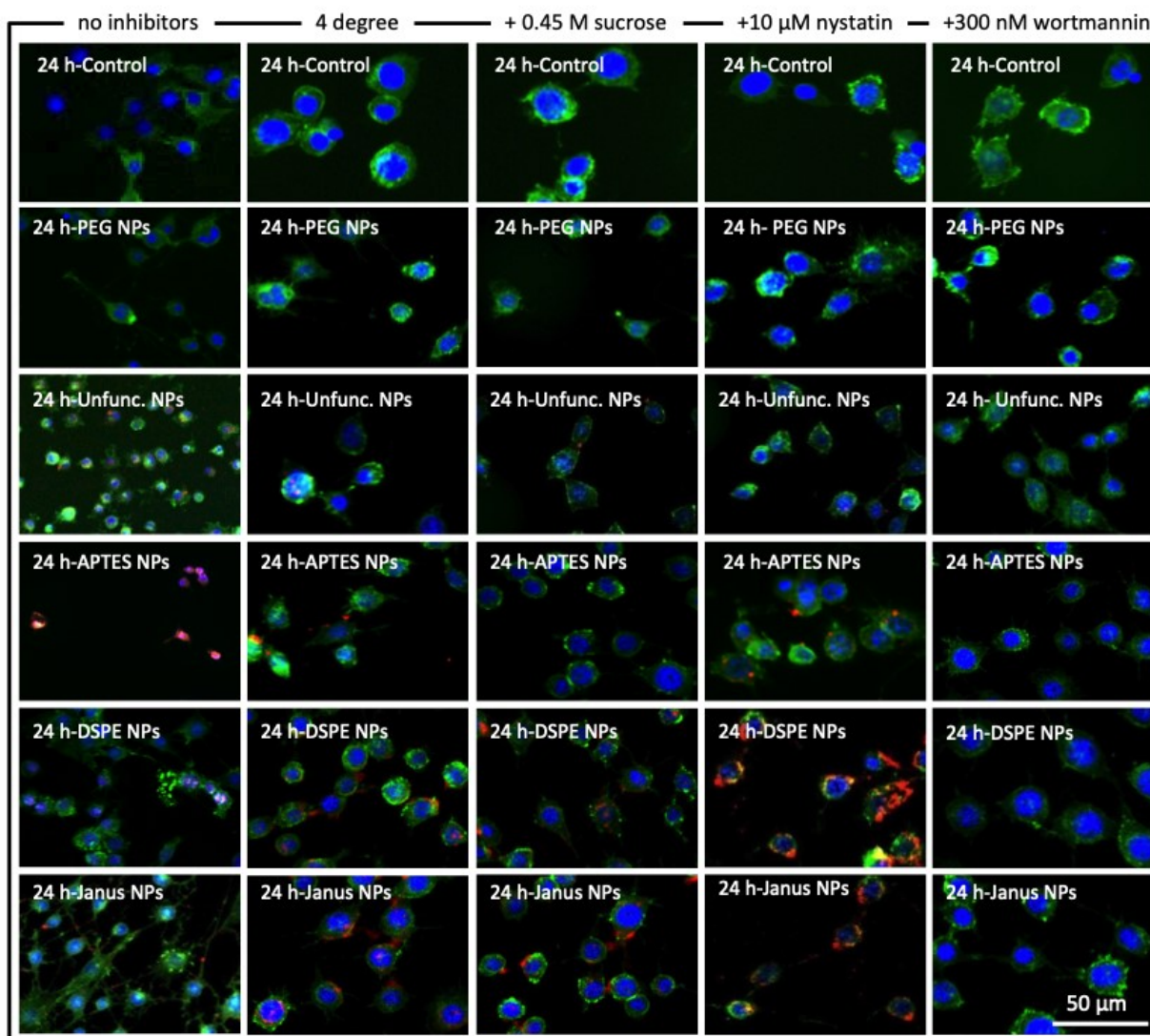
Figure 6-16: Fluorescence microscopy of NIH 3T3 cells before (control) and after exposure of the different NPs for 24 h in the presence and absence of endocytosis inhibitors. 4 °C incubation was performed to suppress temperature-dependent endocytosis, hypertonic sucrose suppressed receptor-mediated endocytosis, nystatin inhibits caveolae-mediated endocytosis and wortmannin inhibits macropinocytosis. The nuclei were stained using DAPI (blue), the cytoskeleton was dyed with AF-488 (green) and the NPs were labelled with RBITC (red).

While a straightforward interpretation of these results is difficult since several endocytosis pathways might be active for one particle type, they indicate that both caveolae-dependent endocytosis and macropinocytosis are involved in the uptake of isotropic APTES-coated and unfunctionalized NPs. The interaction of NIH 3T3 cells with isotropic DSPE- and DSPE/PEG-functionalized Janus NPs is not strongly affected by the presence of nystatin or the high sucrose concentration. Conversely, suppression of macropinocytosis via wortmannin inhibited the association of both DSPE- and DSPE/PEG-functionalized NPs. These results indicate that macropinocytosis seems to be the main endocytosis pathway for the uptake of the fully DSPE-coated NPs. Although the TEM analysis (Figure 6-8) suggests that the DSPE/PEG functionalized Janus NPs are mainly attached to the cell surface and are only barely taken up to some extent, some effects of macropinocytosis seem to be involved in firmly attaching the NPs to the cell surface. This is to some degree substantiated by the observation of the roughened cell surface in the presence of the Janus NPs in the TEM micrographs (Figure 6-7 G-L). These results could be an evidence for an interrupted macropinocytosis process that accumulates the NPs at the cell surface without forming closed macropinosomes and subsequent transfer into the cytosol.

6.1.6　Cell viability

As discussed above, in the presence of endocytosis inhibitors, NP uptake and/or interaction with cell surface molecules is affected. Hence, the viability of the cells in the presence of the inhibitors in combination with the different NP types was analyzed. To this end, we used the WST-1 cell proliferation assay and quantified the release of cytosolic LDH, which indicates membrane and consequently cell damage, and thus can be used to determine cell viability. In the absence of endocytosis inhibitors, overall, LDH release of around 20% and a slight reduction of cellular WST-1 was observed (Figure 6-17 A, B). The LDH release was generally unaffected by the type of NP used, regardless of the addition of inhibitors. Without wortmannin at 24 h, a slight decrease of the WST-1 reduction capacity (85%) was recorded in the presence of DSPE/PEG-functionalized Janus NPs (Figure 6-17 A, B). This might be a result of the observed deformations of the cell surface and the associated stresses to the cells. The presence of wortmannin slightly affects mitochondrial activity, as observed by a WST-1 reduction capacity to 75-80% at

24 h of incubation (Figure 6-17 C,D).
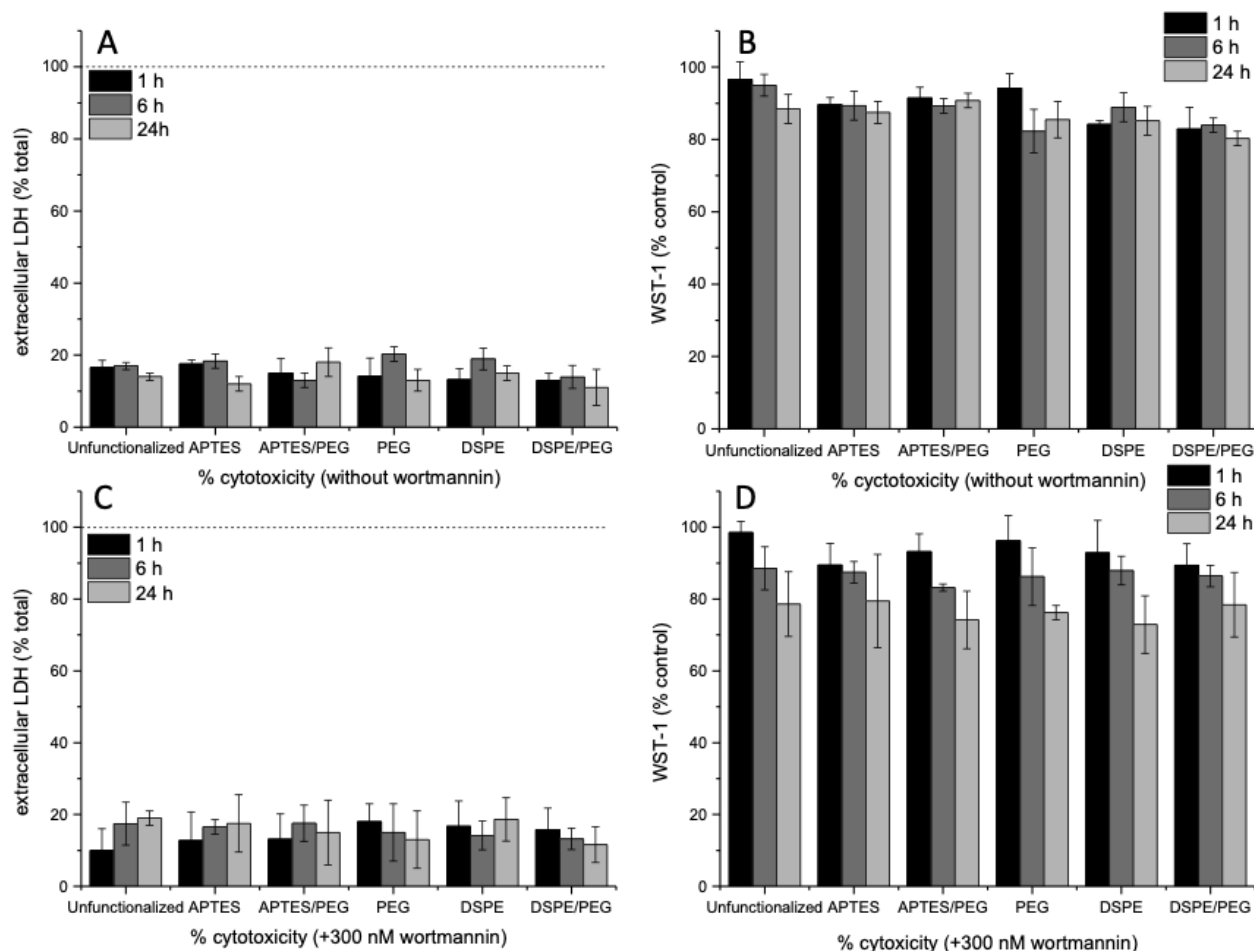
Figure 6-17: Cell viability analysis of NIH 3T3 cells after incubation with the different NP types in the presence and absence of the macropinocytosis inhibitor wortmannin for 1, 6 and 24 h of incubation. Membrane integrity was measured via the LDH assay (A, C) whereas mitochondrial viability was assessed with the WST-1 assay (B, D).

Similar observations were made in the presence of the other endocytosis inhibitors sucrose (Figure 6-18 A,C) and nystatin (Figure 6-18 B,D). Here, WST-1 reduction capacity was decreased in the presence of nystatin (80%) and high-sucrose media (70%) with all NP types at the 24 h time point. Since further degradation in cell viability would make interpretation of the experiments difficult, we did not perform longer incubation experiments.

171
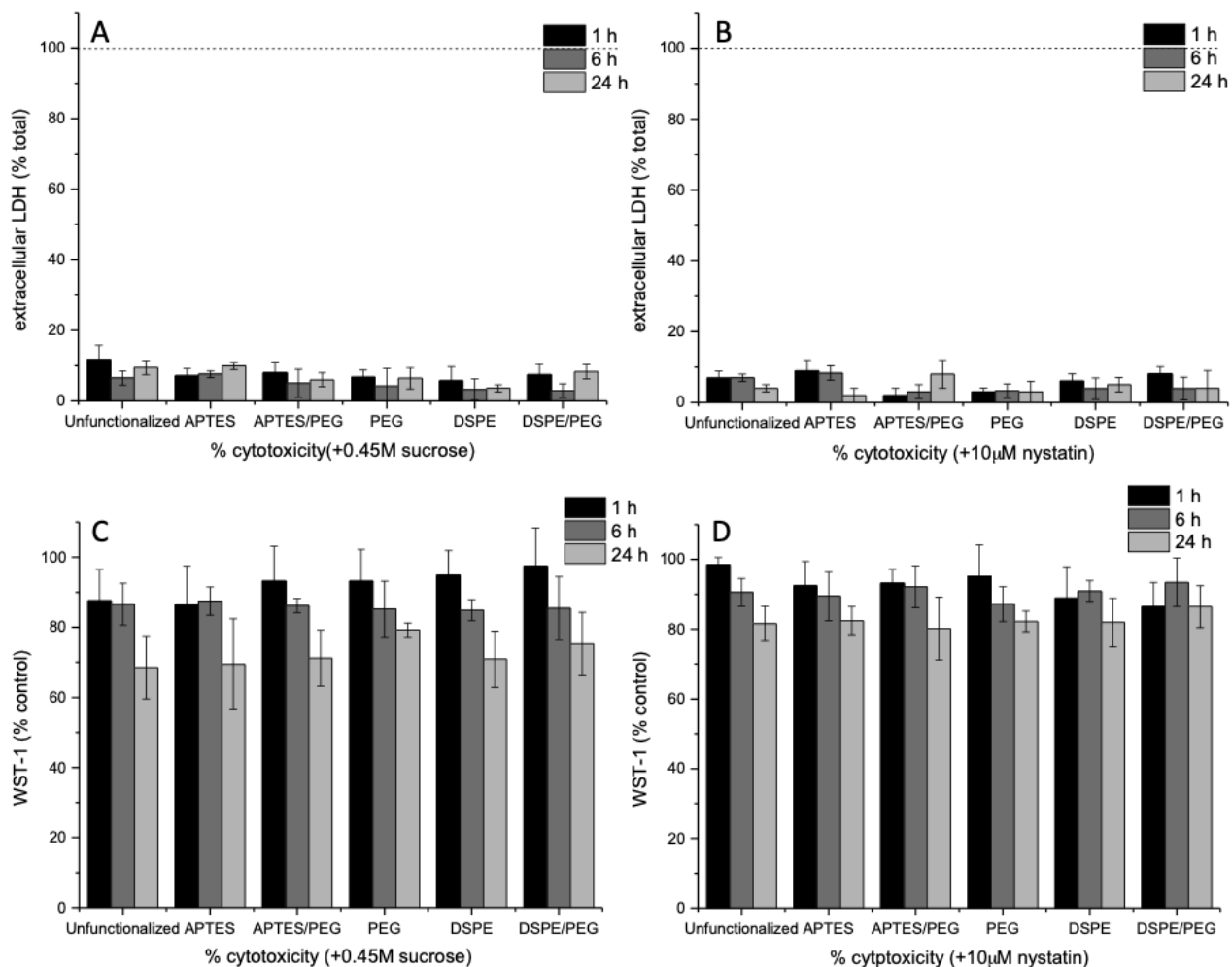
Figure 6-18: Cell viability after incubation with different NP types in the presence hypertonic sucrose and nystatin for 1h, 6 h and 24 h. Membrane integrity was measured via the LDH assay (A, B) and mitochondrial viability was assessed using the WST-1 assay (C, D).
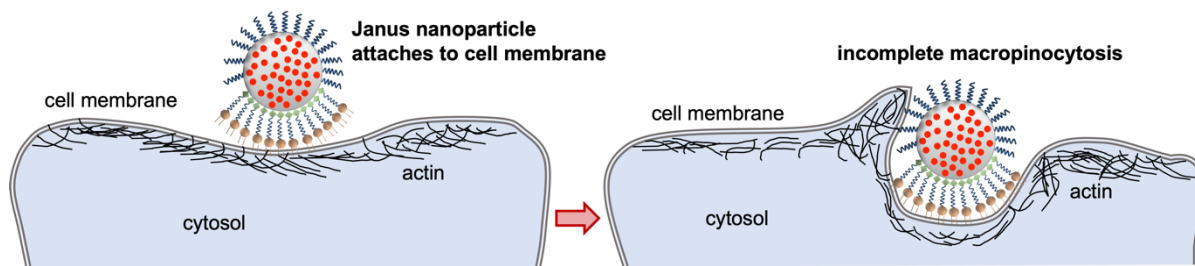
Figure 6-19: Scheme of the assumed interactions of the Janus NPs with the cell membrane. The particles attach to the membrane via insertion of the hydrophobic tails of the DSPE functionalization in the phospholipid bilayer of the cell membrane. This triggers macropinocytosis which is obstructed by the PEG functionalization leading to firm attachment of the particle to the cell surface without full endocytosis.

6.2 Conclusion

This thesis also includes the synthesis of DSPE/PEG-functionalized Janus NPs, along with a series of non-Janus NPs, via the wax-in-water Pickering emulsion strategy. All types of NPs showed reasonable colloidal stability, particularly in the cell medium in which the endocytosis experiments were carried out. The isotropic NPs were taken up into the cells with the exception of the fully PEG-coated NPs. This uptake behavior was expected and is also well-documented in the literature. [217,218] Conversely, the DSPE/PEG-functionalized Janus NPs behaved similarly to the Janus microparticles investigated by Gao and Yu [221] which generate relatively large membrane protrusions that eventually engulf the microparticles via the macropinocytosis pathway. Surprisingly, the nano-sized Janus particles investigated in this thesis were not taken up at all and only seem to be grabbed by the cell membrane in a process that can be inhibited by the presence of wortmannin during incubation (schematically shown in Figure 6-19). Accordingly, we assumed that an incomplete macropinocytosis process might be responsible for accumulating the Janus NPs at the cell surface. Further studies are necessary to transfer these findings to other cell types. It will also be interesting to analyze in a further study whether the hydrophobic membrane anchor might in part be responsible for the observations, compared, e.g., to particles binding to a CD3 receptor. Anisotropic particles that are designed to stay permanently attached to membrane surfaces might prove eminently useful in biomedical applications. Particularly magnetized Janus NPs could be able to move or otherwise manipulate individual cells non-invasively by serving as a magnetic handle at the cell membrane leading to novel tools for the field of magnetic tissue engineering. Furthermore, nature has already brought forth anisotropic NPs that are able to inject their DNA or RNA into cells after latching onto cell surfaces. Accordingly, myovirus bacteriophages and similar viruses could act as templates for even more sophisticated anisotropic NP drug or gene delivery systems in the future.

7. Conclusion

Janus particles are a popular particle type with potential as biological probing agents, as surfactants, catalysts, nanoprobes, bio tagging and drug delivery agents. A wide variety of properties have been functionalized on particle surfaces to impart multifunctionality and thus Janus character. The combination of magnetic, inorganic, polymeric or biological properties have been demonstrated for the synthesis of excellent examples of Janus particles applicable in several fields. A large body of the Janus particle research till date has been focused on the preparation of micro-sized particles, their characterization and furthermore their promising applications. However, there is a limited amount on the synthesis techniques and applications of nanoscale particles. One such synthesis technique proposed by Granick et al., the wax Pickering emulsion technique has been proved to be successful for the synthesis of nanosized Janus particles. Noteworthy features of the wax Pickering emulsion technique include the low cost of preparation, the possibility of large-scale preparation and the opportunity to immobilize a wide array of functionalities of choice on NPs. Along with this, some disadvantages include less control over the Janus balance on the specific hemispheres of the particles and the multi-step preparation to achieve the Janus aspect.

Keeping the merits and challenges of this method in mind, we successfully demonstrated the preparation of bio functional nanoscale Janus particles in large gram quantities using the wax Pickering emulsion technique and further applied them for specific tailored cell interactions

8. Outlook

Janus particles have been synthesized using an array of techniques and a wide variety of materials. A combination of these material types on a single particle type have been used to create versatile Janus particles of different size ranges. Such highly applicable tools have further been used in the field of theranostics, biomedical, imaging, therapeutic, drug delivery and biotechnological applications.

Challenges as a part of the preparation of Janus particles at the nanoscale include scalability as well as controlling the Janus balance on the engineered particles. In this thesis, we have studied the aspect of Janus particle preparation with tunable surface functionalities and applied them onto prokaryotic and eukaryotic biological systems. Janus particles with their multifunctional properties exhibiting surface and structural anisotropy have been put forth as potential tools for biomedical applications. However, a limited amount of research is focused on understanding the behavior of the particles when they encounter biological systems, which needs to be further explored. Understanding the response of cellular systems when they meet Janus particles could be used to alter the response of such systems. As summarized by Gao et al., cellular entry of the particles into the immune cells such as macrophages was studied, and more efforts need to be dedicated to this aspect to achieve a better understanding of Janus particle interactions both *in vitro* and *in vivo*.

Elucidating cell-based NP interactions when used as potential bio application agents can be done using Janus particles. NPs can be designed following the T2-phage structures. Such virus-like particles are aimed to have a targeting head and a tail comparable to the structures of T2-phages. They can be engineered to project cell docking and pH/heat sensitive molecule on the other half of the particle surface. When such nanostructures are then additionally loaded with drugs that are released due to heat/pH stimuli, targeted therapy using multifunctional NPs can be achieved [300]. For NPs to be applicable as drug delivery agents or for other such biomedical applications, they need to bypass the blood-brain barrier. Functionalization of transferrin on NPs has been observed to cause particles to enter the blood-brain barrier and thereafter increase the chances of targeted therapy. Janus particles could be designed with immobilized transferrin to cross the blood-

brain barrier and ensuring the delivery of NPs aimed for brain-related or other such diseases of the central nervous system.[301]

In general, efforts can be made to harness the potential of nanosized Janus particles using established techniques and detailed characterization in this thesis to ensure interesting future applications and endeavors.

9. References

1. Du, J., and O'Reilly, R.K. (2011) Anisotropic particles with patchy, multicompartment and Janus architectures: preparation and application. *Chem. Soc. Rev.*, **40** (5), 2402.
2. Lattuada, M., and Hatton, T.A. (2011) Synthesis, properties and applications of Janus nanoparticles. *Nano Today*, **6** (3), 286–308.
3. Walther, A., and Müller, A.H.E. (2008) Janus particles. *Soft Matter*, **4** (4), 663.
4. Lee, K.J., Yoon, J., and Lahann, J. (2011) Recent advances with anisotropic particles. *Current Opinion in Colloid & Interface Science*, **16** (3), 195–202.
5. Thorkelsson, K., Bai, P., and Xu, T. (2015) Self-assembly and applications of anisotropic nanomaterials: A review. *Nano Today*, **10** (1), 48–66.
6. Yi, Y., Sanchez, L., Gao, Y., and Yu, Y. (2016) Janus particles for biological imaging and sensing. *Analyst*, **141** (12), 3526–3539.
7. Walther, A., and Müller, A.H.E. (2013) Janus Particles: Synthesis, Self-Assembly, Physical Properties, and Applications. *Chem. Rev.*, **113** (7), 5194–5261.
8. Suh, J., Wirtz, D., and Hanes, J. (2003) Efficient active transport of gene nanocarriers to the cell nucleus. *Proceedings of the National Academy of Sciences*, **100** (7), 3878–3882.
9. Treccani, L., Yvonne Klein, T., Meder, F., Pardun, K., and Rezwan, K. (2013) Functionalized ceramics for biomedical, biotechnological and environmental applications. *Acta Biomaterialia*, **9** (7), 7115–7150.
10. Pang, X., Wan, C., Wang, M., and Lin, Z. (2014) Strictly Biphasic Soft and Hard Janus Structures: Synthesis, Properties, and Applications. *Angew. Chem. Int. Ed.*, **53** (22), 5524–5538.
11. Lin, W., Swartz, L.A., Li, J.-R., Liu, Y., and Liu, G. (2013) Particle Lithography Enables Fabrication of Multicomponent Nanostructures. *J. Phys. Chem. C*, **117** (44), 23279–23285.
12. Erb, R.M., Jenness, N.J., Clark, R.L., and Yellen, B.B. (2009) Towards Holonomic Control of Janus Particles in Optomagnetic Traps. *Adv. Mater.*, **21** (47), 4825–4829.
13. Yang, S., Xu, J., Wang, Z., Zeng, H., and Lei, Y. (2011) Janus particle arrays with multiple structural controlling abilities synthesized by seed-directed deposition. *J. Mater. Chem.*, **21** (32), 11930.
14. Zhang, J., Grzybowski, B.A., and Granick, S. (2017) Janus Particle Synthesis, Assembly, and Application. *Langmuir*, **33** (28), 6964–6977.
15. Villalonga, R., Díez, P., Sánchez, A., Aznar, E., Martínez-Máñez, R., and Pingarrón, J.M. (2013) Enzyme-Controlled Sensing-Actuating Nanomachine Based on Janus Au-Mesoporous Silica Nanoparticles. *Chem. Eur. J.*, **19** (24), 7889–7894.
16. Hong, L., Jiang, S., and Granick, S. (2006) Simple Method to Produce Janus Colloidal Particles in Large Quantity. *Langmuir*, **22** (23), 9495–9499.
17. Perro, A., Meunier, F., Schmitt, V., and Ravaine, S. (2009) Production of large quantities of "Janus" nanoparticles using wax-in-water emulsions. *Colloids and Surfaces A: Physicochemical and Engineering Aspects*, **332** (1), 57–62.
18. Zenerino, A., Peyratout, C., and Aimable, A. (2015) Synthesis of fluorinated ceramic Janus particles via a Pickering emulsion method. *Journal of Colloid and Interface Science*, **450**, 174–181.

19. Kaewsaneha, C., Tangboriboonrat, P., Polpanich, D., Eissa, M., and Elaissari, A. (2013) Janus Colloidal Particles: Preparation, Properties, and Biomedical Applications. *ACS Appl. Mater. Interfaces*, **5** (6), 1857–1869.
20. Sánchez, A., Díez, P., Martínez-Ruíz, P., Villalonga, R., and Pingarrón, J.M. (2013) Janus Au-mesoporous silica nanoparticles as electrochemical biorecognition-signaling system. *Electrochemistry Communications*, **30**, 51–54.
21. Wu, L.Y., Ross, B.M., Hong, S., and Lee, L.P. (2010) Bioinspired Nanocorals with Decoupled Cellular Targeting and Sensing Functionality. *Small*, **6** (4), 503–507.
22. Hsieh, H.-Y., Huang, T.-W., Xiao, J.-L., Yang, C.-S., Chang, C.-C., Chu, C.-C., Lo, L.-W., Wang, S.-H., Wang, P.-C., Chieng, C.-C., Lee, C.-H., and Tseng, F.-G. (2012) Fabrication and modification of dual-faced nano-mushrooms for tri-functional cell theranostics: SERS/fluorescence signaling, protein targeting, and drug delivery. *J. Mater. Chem.*, **22** (39), 20918.
23. Brandenburg, B., Lee, L.Y., Lakadamyali, M., Rust, M.J., Zhuang, X., and Hogle, J.M. (2007) Imaging Poliovirus Entry in Live Cells. *PLoS Biol*, **5** (7), e183.
24. Lee, K., and Yu, Y. (2017) Janus nanoparticles for T cell activation: clustering ligands to enhance stimulation. *J. Mater. Chem. B*, **5** (23), 4410–4415.
25. Fernandez-Rodriguez, M.A., Song, Y., Rodríguez-Valverde, M.Á., Chen, S., Cabrerizo-Vilchez, M.A., and Hidalgo-Alvarez, R. (2014) Comparison of the Interfacial Activity between Homogeneous and Janus Gold Nanoparticles by Pendant Drop Tensiometry. *Langmuir*, **30** (7), 1799–1804.
26. Fernandez-Rodriguez, M.A., Chen, L., Deming, C.P., Rodriguez-Valverde, M.A., Chen, S., Cabrerizo-Vilchez, M.A., and Hidalgo-Alvarez, R. (2016) A simple strategy to improve the interfacial activity of true Janus gold nanoparticles: a shorter hydrophilic capping ligand. *Soft Matter*, **12** (1), 31–34.
27. Glaser, N., Adams, D.J., Böker, A., and Krausch, G. (2006) Janus Particles at Liquid−Liquid Interfaces. *Langmuir*, **22** (12), 5227–5229.
28. Schick, I., Lorenz, S., Gehrig, D., Schilmann, A.-M., Bauer, H., Panthöfer, M., Fischer, K., Strand, D., Laquai, F., and Tremel, W. (2014) Multifunctional Two-Photon Active Silica-Coated Au@MnO Janus Particles for Selective Dual Functionalization and Imaging. *J. Am. Chem. Soc.*, **136** (6), 2473–2483.
29. Ding, H., and Ma, Y. (2012) Interactions between Janus particles and membranes. *Nanoscale*, **4** (4), 1116–1122.
30. Janib, S.M., Moses, A.S., and MacKay, J.A. (2010) Imaging and drug delivery using theranostic nanoparticles. *Advanced Drug Delivery Reviews*, **62** (11), 1052–1063.
31. Chen, B., Jia, Y., Gao, Y., Sanchez, L., Anthony, S.M., and Yu, Y. (2014) Janus Particles as Artificial Antigen-Presenting Cells for T Cell Activation. *ACS Appl. Mater. Interfaces*, **6** (21), 18435–18439.
32. López, V., Villegas, M.R., Rodríguez, V., Villaverde, G., Lozano, D., Baeza, A., and Vallet-Regí, M. (2017) Janus Mesoporous Silica Nanoparticles for Dual Targeting of Tumor Cells and Mitochondria. *ACS Appl. Mater. Interfaces*, **9** (32), 26697–26706.
33. Yi, Y., Sanchez, L., Gao, Y., Lee, K., and Yu, Y. (2017) Interrogating Cellular Functions with Designer Janus Particles. *Chem. Mater.*, **29** (4), 1448–1460.
34. Tang, J.L., Schoenwald, K., Potter, D., White, D., and Sulchek, T. (2012) Bifunctional Janus Microparticles with Spatially Segregated Proteins. *Langmuir*, **28** (26), 10033–10039.
35. Li, B., Wang, M., Chen, K., Cheng, Z., Chen, G., and Zhang, Z. (2015) Synthesis of Biofunctional Janus Particles. *Macromol. Rapid Commun.*, **36** (12), 1200–1204.

36. Hatto, P. ISO concensus definitions relevant to nanomaterials and nanotechnologies.

37. ISO/TS 80004-1 (2015) Nanotechnologies–Vocabulary–Part 1: Core Terms.

38. Boverhof, D.R., Bramante, C.M., Butala, J.H., Clancy, S.F., Lafranconi, M., West, J., and Gordon, S.C. (2015) Comparative assessment of nanomaterial definitions and safety evaluation considerations. *Regulatory Toxicology and Pharmacology*, **73** (1), 137–150.

39. Lu (陸述義), P.J., and Weitz, D.A. (2013) Colloidal Particles: Crystals, Glasses, and Gels. *Annu. Rev. Condens. Matter Phys.*, **4** (1), 217–233.

40. Lächelt, U., Wuttke, S., and Engelke, H. (2020) Colloidal nanoparticles as pharmaceutical agents, in *Frontiers of Nanoscience*, vol. 16, Elsevier, pp. 89–115.

41. Ashok, A., Kumar, A., and Tarlochan, F. (2020) Colloidal metal oxide nanocrystals in catalysis, in *Colloidal Metal Oxide Nanoparticles*, Elsevier, pp. 247–288.

42. Otto, D.P., Otto, A., and De Villiers, M.M. (2015) Differences in physicochemical properties to consider in the design, evaluation and choice between microparticles and nanoparticles for drug delivery. *Expert opinion on drug delivery*, **12** (5), 763–777.

43. Navya, P.N., and Daima, H.K. (2016) Rational engineering of physicochemical properties of nanomaterials for biomedical applications with nanotoxicological perspectives. *Nano Convergence*, **3** (1), 1.

44. Bernard, P., Stelmachowski, P., Broś, P., Makowski, W., and Kotarba, A. (2021) Demonstration of the Influence of Specific Surface Area on Reaction Rate in Heterogeneous Catalysis. *J. Chem. Educ.*, acs.jchemed.0c01101.

45. Bhardwaj, V., Kaushik, A., Khatib, Z.M., Nair, M., and McGoron, A.J. (2019) Recalcitrant Issues and New Frontiers in Nano-Pharmacology. *Front. Pharmacol.*, **10**, 1369.

46. Jain, K. (2010) Advances in the field of nanooncology. *BMC medicine*, **8** (1), 1–11.

47. Mg, K., V, K., and F, H. (2015) History and Possible Uses of Nanomedicine Based on Nanoparticles and Nanotechnological Progress. *J Nanomed Nanotechnol*, **06** (06).

48. Noble, G.T., Stefanick, J.F., Ashley, J.D., Kiziltepe, T., and Bilgicer, B. (2014) Ligand-targeted liposome design: challenges and fundamental considerations. *Trends in Biotechnology*, **32** (1), 32–45.

49. Çağdaş, M., Sezer, A.D., and Bucak, S. (2014) Liposomes as potential drug carrier systems for drug delivery. *Application of nanotechnology in drug delivery*, 1–100.

50. Pedziwiatr-Werbicka, E., Horodecka, K., Shcharbin, D., and Bryszewska, M. (2020) Nanoparticles in Combating Cancer: Opportunities and Limitations. A Brief Review. *CMC*, **28** (2), 346–359.

51. Wang, M., and Thanou, M. (2010) Targeting nanoparticles to cancer. *Pharmacological research*, **62** (2), 90–99.

52. Brigger, I., Dubernet, C., and Couvreur, P. (2012) Nanoparticles in cancer therapy and diagnosis. *Advanced drug delivery reviews*, **64**, 24–36.

53. Cho, K., Wang, X., Nie, S., and Shin, D.M. (2008) Therapeutic nanoparticles for drug delivery in cancer. *Clinical cancer research*, **14** (5), 1310–1316.

54. Mohanraj, V., and Chen, Y. (2006) Nanoparticles-a review. *Tropical journal of pharmaceutical research*, **5** (1), 561–573.

55. Zhang, L., Gu, F., Chan, J., Wang, A., Langer, R., and Farokhzad, O. (2008) Nanoparticles in medicine: therapeutic applications and developments. *Clinical pharmacology & therapeutics*, **83** (5), 761–769.

56. Yallapu, M.M., Gupta, B.K., Jaggi, M., and Chauhan, S.C. (2010) Fabrication of curcumin encapsulated PLGA nanoparticles for improved therapeutic effects in metastatic cancer cells. *Journal of colloid and interface science*, **351** (1), 19–29.

57. Conde, J., Dias, J.T., GrazÃº, V., Moros, M., Baptista, P.V., and de la Fuente, J.M. (2014) Revisiting 30 years of biofunctionalization and surface chemistry of inorganic nanoparticles for nanomedicine. *Front. Chem.*, **2**.

58. Monopoli, M.P., Åberg, C., Salvati, A., and Dawson, K.A. (2012) Biomolecular coronas provide the biological identity of nanosized materials. *Nature Nanotech*, **7** (12), 779–786.

59. Navya, P.N., Kaphle, A., Srinivas, S.P., Bhargava, S.K., Rotello, V.M., and Daima, H.K. (2019) Current trends and challenges in cancer management and therapy using designer nanomaterials. *Nano Convergence*, **6** (1), 23.

60. Wang, Y., Santos, A., Evdokiou, A., and Losic, D. (2015) An overview of nanotoxicity and nanomedicine research: principles, progress and implications for cancer therapy. *J. Mater. Chem. B*, **3** (36), 7153–7172.

61. De, M., Ghosh, P.S., and Rotello, V.M. (2008) Applications of Nanoparticles in Biology. *Adv. Mater.*, **20** (22), 4225–4241.

62. McIntosh, C.M., Esposito, E.A., Boal, A.K., Simard, J.M., Martin, C.T., and Rotello, V.M. (2001) Inhibition of DNA Transcription Using Cationic Mixed Monolayer Protected Gold Clusters. *J. Am. Chem. Soc.*, **123** (31), 7626–7629.

63. Lakowicz, J.R., Gryczynski, I., Gryczynski, Z., Nowaczyk, K., and Murphy, C.J. (2000) Time-Resolved Spectral Observations of Cadmium-Enriched Cadmium Sulfide Nanoparticles and the Effects of DNA Oligomer Binding. *Analytical Biochemistry*, **280** (1), 128–136.

64. Guo, H., Idris, N.M., and Zhang, Y. (2011) LRET-Based Biodetection of DNA Release in Live Cells Using Surface-Modified Upconverting Fluorescent Nanoparticles. *Langmuir*, **27** (6), 2854–2860.

65. Xiao, Y. (2003) "Plugging into Enzymes": Nanowiring of Redox Enzymes by a Gold Nanoparticle. *Science*, **299** (5614), 1877–1881.

66. Astuti, Y., Palomares, E., Haque, S.A., and Durrant, J.R. (2005) Triplet State Photosensitization of Nanocrystalline Metal Oxide Electrodes by Zinc-Substituted Cytochrome *c* : Application to Hydrogen Evolution. *J. Am. Chem. Soc.*, **127** (43), 15120–15126.

67. de Gennes, P.G. (1992) Soft matter. *Rev. Mod. Phys.*, **64** (3), 645–648.

68. Casagrande, C., Fabre, P., Raphaël, E., and Veyssié, M. (1989) "Janus Beads": Realization and Behaviour at Water/Oil Interfaces. *Europhys. Lett.*, **9** (3), 251–255.

69. Wang, F., Pauletti, G.M., Wang, J., Zhang, J., Ewing, R.C., Wang, Y., and Shi, D. (2013) Dual surface-functionalized janus nanocomposites of polystyrene/Fe3O4@ SiO2 for simultaneous tumor cell targeting and stimulus-induced drug release. *Advanced materials*, **25** (25), 3485–3489.

70. Li, X., Zhou, L., Wei, Y., El-Toni, A.M., Zhang, F., and Zhao, D. (2014) Anisotropic Growth-Induced Synthesis of Dual-Compartment Janus Mesoporous Silica Nanoparticles for Bimodal Triggered Drugs Delivery. *J. Am. Chem. Soc.*, **136** (42), 15086–15092.

71. Poon W.C.K. (2013) From Clarkia to Escherichia and Janus: The physics of natural and synthetic active colloids. *ENFI*, **184** (Physics of Complex Colloids), 317–386.

72. Chirra, H.D., Sexton, T., Biswal, D., Hersh, L.B., and Hilt, J.Z. (2011) Catalase-coupled gold nanoparticles: Comparison between the carbodiimide and biotin–streptavidin methods. *Acta Biomaterialia*, **7** (7), 2865–2872.

73. Tanaka, T., Okayama, M., Minami, H., and Okubo, M. (2010) Dual stimuli-responsive "mushroom-like" Janus polymer particles as particulate surfactants. *Langmuir*, **26** (14), 11732–11736.

74. Ku, K.H., Lee, Y.J., Yi, G.-R., Jang, S.G., Schmidt, B.V., Liao, K., Klinger, D., Hawker, C.J., and Kim, B.J. (2017) Shape-tunable biphasic janus particles as pH-responsive switchable surfactants. *Macromolecules*, **50** (23), 9276–9285.

75. Fu, J., An, D., Song, Y., Wang, C., Qiu, M., and Zhang, H. (2020) Janus nanoparticles for cellular delivery chemotherapy: Recent advances and challenges. *Coordination Chemistry Reviews*, **422**, 213467.

76. Nisisako, T., Torii, T., Takahashi, T., and Takizawa, Y. (2006) Synthesis of Monodisperse Bicolored Janus Particles with Electrical Anisotropy Using a Microfluidic Co-Flow System. *Adv. Mater.*, **18** (9), 1152–1156.

77. Rahmani, S., Park, T.-H., Dishman, A.F., and Lahann, J. (2013) Multimodal delivery of irinotecan from microparticles with two distinct compartments. *Journal of Controlled Release*, **172** (1), 239–245.

78. Misra, A.C., Bhaskar, S., Clay, N., and Lahann, J. (2012) Multicompartmental Particles for Combined Imaging and siRNA Delivery. *Adv. Mater.*, **24** (28), 3850–3856.

79. Hu, S.-H., Chen, S.-Y., and Gao, X. (2012) Multifunctional Nanocapsules for Simultaneous Encapsulation of Hydrophilic and Hydrophobic Compounds and On-Demand Release. *ACS Nano*, **6** (3), 2558–2565.

80. Ruhland, T.M., McKenzie, H.S., Skelhon, T.S., Bon, S.A., Walther, A., and Müller, A.H. (2015) Nanoscale hybrid silica/polymer Janus particles with a double-responsive hemicorona. *Polymer*, **79**, 299–308.

81. Dendukuri, D., Pregibon, D.C., Collins, J., Hatton, T.A., and Doyle, P.S. (2006) Continuous-flow lithography for high-throughput microparticle synthesis. *Nature Mater*, **5** (5), 365–369.

82. Bong, K.W., Bong, K.T., Pregibon, D.C., and Doyle, P.S. (2010) Hydrodynamic Focusing Lithography. *Angewandte Chemie*, **122** (1), 91–94.

83. Zhang, S., Li, Z., Samarajeewa, S., Sun, G., Yang, C., and Wooley, K.L. (2011) Orthogonally Dual-Clickable Janus Nanoparticles via a Cyclic Templating Strategy. *J. Am. Chem. Soc.*, **133** (29), 11046–11049.

84. Wei, D., Ge, L., Lu, S., Li, J., and Guo, R. (2017) Janus Particles Templated by Janus Emulsions and Application as a Pickering Emulsifier. *Langmuir*, **33** (23), 5819–5828.

85. Gong, J., Zu, X., Li, Y., Mu, W., and Deng, Y. (2011) Janus particles with tunable coverage of zinc oxide nanowires. *J. Mater. Chem.*, **21** (7), 2067.

86. Yang, S., Guo, F., Kiraly, B., Mao, X., Lu, M., Leong, K.W., and Huang, T.J. (2012) Microfluidic synthesis of multifunctional Janus particles for biomedical applications. *Lab Chip*, **12** (12), 2097.

87. Pawar, A.B., and Kretzschmar, I. (2010) Fabrication, Assembly, and Application of Patchy Particles: Fabrication, Assembly, and Application …. *Macromol. Rapid Commun.*, **31** (2), 150–168.

88. Yánez-Sedeño, P., Campuzano, S., and Pingarrón, J.M. (2017) Janus particles for (bio)sensing. *Applied Materials Today*, **9**, 276–288.

89. Kadam, R., Zilli, M., Maas, M., and Rezwan, K. (2018) Nanoscale Janus Particles with Dual Protein Functionalization. *Part. Part. Syst. Charact.*, **35** (3), 1700332.

90. Kadam, R., Maas, M., and Rezwan, K. (2019) Selective, Agglomerate-Free Separation of Bacteria Using Biofunctionalized, Magnetic Janus Nanoparticles. *ACS Appl. Bio Mater.*, **2** (8), 3520–3531.

91. Kadam, R., Ghawali, J., Waespy, M., Maas, M., and Rezwan, K. (2020) Janus nanoparticles designed for extended cell surface attachment. *Nanoscale*, **12** (36), 18938–18949.

92. Pickering, S. (1907) Cxcvi. *J. Chem. Soc., Trans*, **91** (0), 2001–2021.

93. Wittmeier, A., Leeth Holterhoff, A., Johnson, J., and Gibbs, J.G. (2015) Rotational Analysis of Spherical, Optically Anisotropic Janus Particles by Dynamic Microscopy. *Langmuir*, **31** (38), 10402–10410.

94. Hong, L., Jiang, S., and Granick, S. (2006) Simple Method to Produce Janus Colloidal Particles in Large Quantity. *Langmuir*, **22** (23), 9495–9499.

95. Wang, K., Li, F., Tian, D., Xu, J., Liu, Y., Hou, Z., Zhou, H., Chen, S., Zhu, J., and Yang, Z. (2019) Segmental Janus nanoparticles of polymer composites. *Chem. Commun.*, **55** (56), 8114–8117.

96. Fujimoto, K., Nakahama, K., Shidara, M., and Kawaguchi, H. (1999) Preparation of Unsymmetrical Microspheres at the Interfaces. *Langmuir*, **15** (13), 4630–4635.

97. Jiang, S., Schultz, M.J., Chen, Q., Moore, J.S., and Granick, S. (2008) Solvent-Free Synthesis of Janus Colloidal Particles. *Langmuir*, **24** (18), 10073–10077.

98. Xiao, Z., Cao, H., Jiang, X., and Kong, X.Z. (2018) Pickering Emulsion Formation of Paraffin Wax in an Ethanol–Water Mixture Stabilized by Primary Polymer Particles and Wax Microspheres Thereof. *Langmuir*, **34** (6), 2282–2289.

99. Kaewsaneha, C., Tangboriboonrat, P., Polpanich, D., Eissa, M., and Elaissari, A. (2013) Preparation of Janus colloidal particles via Pickering emulsion: An overview. *Colloids and Surfaces A: Physicochemical and Engineering Aspects*, **439**, 35–42.

100. Archer, R.J., Parnell, A.J., Campbell, A.I., Howse, J.R., and Ebbens, S.J. (2018) A Pickering Emulsion Route to Swimming Active Janus Colloids. *Adv. Sci.*, **5** (2), 1700528.

101. Pardhy, N.P., and Budhlall, B.M. (2010) Pickering Emulsion as a Template to Synthesize Janus Colloids with Anisotropy in the Surface Potential. *Langmuir*, **26** (16), 13130–13141.

102. Perro, A., Meunier, F., Schmitt, V., and Ravaine, S. (2009) Production of large quantities of "Janus" nanoparticles using wax-in-water emulsions. *Colloids and Surfaces A: Physicochemical and Engineering Aspects*, **332** (1), 57–62.

103. Berger, S., Synytska, A., Ionov, L., Eichhorn, K.-J., and Stamm, M. (2008) Stimuli-Responsive Bicomponent Polymer Janus Particles by "Grafting from"/"Grafting to" Approaches. *Macromolecules*, **41** (24), 9669–9676.

104. Jiang, S., and Granick, S. (2008) Controlling the Geometry (Janus Balance) of Amphiphilic Colloidal Particles. *Langmuir*, **24** (6), 2438–2445.

105. Jiang, S., and Granick, S. (2007) Janus balance of amphiphilic colloidal particles. *The Journal of Chemical Physics*, **127** (16), 161102.

106. Pompe, T., and Herminghaus, S. (2000) Three-Phase Contact Line Energetics from Nanoscale Liquid Surface Topographies. *Phys. Rev. Lett.*, **85** (9), 1930–1933.

107. Aveyard, R., Binks, B.P., and Clint, J.H. (2003) Emulsions stabilised solely by colloidal particles. *Advances in Colloid and Interface Science*, **100**, 503–546.

108.   Lebdioua, K., Aimable, A., Cerbelaud, M., Videcoq, A., and Peyratout, C. (2018) Influence of different surfactants on Pickering emulsions stabilized by submicronic silica particles. *Journal of Colloid and Interface Science*, **520**, 127–133.

109.   Graf, C., Gao, Q., Schütz, I., Noufele, C.N., Ruan, W., Posselt, U., Korotianskiy, E., Nordmeyer, D., Rancan, F., Hadam, S., Vogt, A., Lademann, J., Haucke, V., and Rühl, E. (2012) Surface Functionalization of Silica Nanoparticles Supports Colloidal Stability in Physiological Media and Facilitates Internalization in Cells. *Langmuir*, **28** (20), 7598–7613.

110.   Liberman, A., Mendez, N., Trogler, W.C., and Kummel, A.C. (2014) Synthesis and surface functionalization of silica nanoparticles for nanomedicine. *Surface Science Reports*, **69** (2–3), 132–158.

111.   Bantz, C., Koshkina, O., Lang, T., Galla, H.-J., Kirkpatrick, C.J., Stauber, R.H., and Maskos, M. (2014) The surface properties of nanoparticles determine the agglomeration state and the size of the particles under physiological conditions. *Beilstein J. Nanotechnol.*, **5**, 1774–1786.

112.   Shahabi, S., Döscher, S., Bollhorst, T., Treccani, L., Maas, M., Dringen, R., and Rezwan, K. (2015) Enhancing Cellular Uptake and Doxorubicin Delivery of Mesoporous Silica Nanoparticles via Surface Functionalization: Effects of Serum. *ACS Appl. Mater. Interfaces*, **7** (48), 26880–26891.

113.   Huh, S., Wiench, J.W., Yoo, J.-C., Pruski, M., and Lin, V.S.-Y. (2003) Organic Functionalization and Morphology Control of Mesoporous Silicas via a Co-Condensation Synthesis Method. *Chem. Mater.*, **15** (22), 4247–4256.

114.   Honegger, T., Sarla, S., Lecarme, O., Berton, K., Nicolas, A., and Peyrade, D. (2011) Selective grafting of proteins on Janus particles: Adsorption and covalent coupling strategies. *Microelectronic Engineering*, **88** (8), 1852–1855.

115.   Gu, H., Xu, K., Xu, C., and Xu, B. (2006) Biofunctional magnetic nanoparticles for protein separation and pathogen detection. *Chem. Commun.*, (9), 941.

116.   Chang, Z., Wang, Z., Shao, D., Yue, J., Lu, M., Li, L., Ge, M., Yang, D., Li, M., Yan, H., Xu, Q., and Dong, W. (2018) Fluorescent-magnetic Janus nanorods for selective capture and rapid identification of foodborne bacteria. *Sensors and Actuators B: Chemical*, **260**, 1004–1011.

117.   Mugica, L.C., Rodríguez-Molina, B., Ramos, S., and Kozina, A. (2016) Surface functionalization of silica particles for their efficient fluorescence and stereo selective modification. *Colloids and Surfaces A: Physicochemical and Engineering Aspects*, **500**, 79–87.

118.   Thornton, P.D., and Heise, A. (2010) Highly Specific Dual Enzyme-Mediated Payload Release from Peptide-Coated Silica Particles. *J. Am. Chem. Soc.*, **132** (6), 2024–2028.

119.   Ruan, L., Chen, W., Wang, R., Lu, J., and Zink, J.I. (2019) Magnetically Stimulated Drug Release Using Nanoparticles Capped by Self-Assembling Peptides. *ACS Appl. Mater. Interfaces*, **11** (47), 43835–43842.

120.   He, X., Zhao, Y., He, D., Wang, K., Xu, F., and Tang, J. (2012) ATP-Responsive Controlled Release System Using Aptamer-Functionalized Mesoporous Silica Nanoparticles. *Langmuir*, **28** (35), 12909–12915.

121.   Varshney, M., Yang, L., Su, X.-L., and Li, Y. (2005) Magnetic Nanoparticle-Antibody Conjugates for the Separation of Escherichia coli O157:H7 in Ground Beef. *Journal of Food Protection*, **68** (9), 1804–1811.

122.	Nakamura, Noriyuki., Burgess, J.Grant., Yagiuda, Kaoru., Kudo, Satoko., Sakaguchi, Toshifumi., and Matsunaga, Tadashi. (1993) Detection and removal of Escherichia coli using fluorescein isothiocyanate conjugated monoclonal antibody immobilized on bacterial magnetic particles. *Anal. Chem.*, **65** (15), 2036–2039.

123.	Bhaisare, M.L., Abdelhamid, H.N., Wu, B.-S., and Wu, H.-F. (2014) Rapid and direct MALDI-MS identification of pathogenic bacteria from blood using ionic liquid-modified magnetic nanoparticles (Fe 3 O 4@ SiO 2). *Journal of Materials Chemistry B*, **2** (29), 4671–4683.

124.	Chang, Z., Wang, Z., Lu, M., Li, M., Li, L., Zhang, Y., Shao, D., and Dong, W. (2017) Magnetic Janus nanorods for efficient capture, separation and elimination of bacteria. *RSC Adv.*, **7** (6), 3550–3553.

125.	Chen, L. (2012) Bioconjugated Magnetic Nanoparticles for Rapid Capture of Gram-positive Bacteria. *J Biosens Bioelectron*, **01** (S11).

126.	Fang, W., Han, C., Zhang, H., Wei, W., Liu, R., and Shen, Y. (2016) Preparation of amino-functionalized magnetic nanoparticles for enhancement of bacterial capture efficiency. *RSC Adv.*, **6** (72), 67875–67882.

127.	Chen, Z., Hsu, F.-C., Battigelli, D., and Chang, H.-C. (2006) Capture and release of viruses using amino-functionalized silica particles. *Analytica Chimica Acta*, **569** (1–2), 76–82.

128.	Zerda, K.S., Gerba, C.P., Hou, K.C., and Goyal, S.M. (1985) Adsorption of viruses to charge-modified silica. *Appl. Environ. Microbiol.*, **49** (1), 91.

129.	Shahabi, S., Treccani, L., Dringen, R., and Rezwan, K. (2015) Modulation of Silica Nanoparticle Uptake into Human Osteoblast Cells by Variation of the Ratio of Amino and Sulfonate Surface Groups: Effects of Serum. *ACS Appl. Mater. Interfaces*, **7** (25), 13821–13833.

130.	Huang, Y.-F., Wang, Y.-F., and Yan, X.-P. (2010) Amine-Functionalized Magnetic Nanoparticles for Rapid Capture and Removal of Bacterial Pathogens. *Environ. Sci. Technol.*, **44** (20), 7908–7913.

131.	Soto-Cantu, E., Cueto, R., Koch, J., and Russo, P.S. (2012) Synthesis and Rapid Characterization of Amine-Functionalized Silica. *Langmuir*, **28** (13), 5562–5569.

132.	Meder, F., Kaur, S., Treccani, L., and Rezwan, K. (2013) Controlling Mixed-Protein Adsorption Layers on Colloidal Alumina Particles by Tailoring Carboxyl and Hydroxyl Surface Group Densities. *Langmuir*, **29** (40), 12502–12510.

133.	Meder, F., Daberkow, T., Treccani, L., Wilhelm, M., Schowalter, M., Rosenauer, A., Mädler, L., and Rezwan, K. (2012) Protein adsorption on colloidal alumina particles functionalized with amino, carboxyl, sulfonate and phosphate groups. *Acta Biomaterialia*, **8** (3), 1221–1229.

134.	Ruizendaal, L., Pujari, S.P., Gevaerts, V., Paulusse, J.M.J., and Zuilhof, H. (2011) Biofunctional Silicon Nanoparticles by Means of Thiol-Ene Click Chemistry. *Chem. Asian J.*, **6** (10), 2776–2786.

135.	Nobs, L., Buchegger, F., Gurny, R., and Allémann, E. (2003) Surface modification of poly(lactic acid) nanoparticles by covalent attachment of thiol groups by means of three methods. *International Journal of Pharmaceutics*, **250** (2), 327–337.

136.	Lo Giudice, M.C., Meder, F., Polo, E., Thomas, S.S., Alnahdi, K., Lara, S., and Dawson, K.A. (2016) Constructing bifunctional nanoparticles for dual targeting: improved grafting and surface recognition assessment of multiple ligand nanoparticles. *Nanoscale*, **8** (38), 16969–16975.

137. Gole, A., and Murphy, C.J. (2008) Azide-Derivatized Gold Nanorods: Functional Materials for "Click" Chemistry. *Langmuir*, **24** (1), 266–272.

138. Niemeyer, C.M. (2001) Nanoparticles, Proteins, and Nucleic Acids: Biotechnology Meets Materials Science. *Angewandte Chemie International Edition*, **40** (22), 4128–4158.

139. Krasnoslobodtsev, A.V., and Smirnov, S.N. (2002) Effect of Water on Silanization of Silica by Trimethoxysilanes. *Langmuir*, **18** (8), 3181–3184.

140. Yadav, A.R., Sriram, R., Carter, J.A., and Miller, B.L. (2014) Comparative study of solution–phase and vapor–phase deposition of aminosilanes on silicon dioxide surfaces. *Materials Science and Engineering: C*, **35**, 283–290.

141. Cheng, W., and McCown, M. (1985) Effect of alkyl chain length on surface silanization of silica. *Journal of Chromatography A*, **318**, 173–185.

142. Rostamzadeh, P., Mirabedini, S.M., and Esfandeh, M. (2014) APS-silane modification of silica nanoparticles: effect of treatment's variables on the grafting content and colloidal stability of the nanoparticles. *J Coat Technol Res*, **11** (4), 651–660.

143. Khung, Y.L., and Narducci, D. (2015) Surface modification strategies on mesoporous silica nanoparticles for anti-biofouling zwitterionic film grafting. *Advances in colloid and interface science*, **226**, 166–186.

144. Kolb HC, Finn MG, and Sharpless KB (2001) Click Chemistry: Diverse Chemical Function from a Few Good Reactions. *Angew Chem Int Ed Engl*, **40** (11), 2004–2021.

145. Liang, L., and Astruc, D. (2011) The copper(I)-catalyzed alkyne-azide cycloaddition (CuAAC) "click" reaction and its applications. An overview. *Coordination Chemistry Reviews*, **255** (23–24), 2933–2945.

146. Kolb, H.C., and Sharpless, K.B. (2003) The growing impact of click chemistry on drug discovery. *Drug Discovery Today*, **8** (24), 1128–1137.

147. Aslan, K., Luhrs, C.C., and Pérez-Luna, V.H. (2004) Controlled and Reversible Aggregation of Biotinylated Gold Nanoparticles with Streptavidin. *J. Phys. Chem. B*, **108** (40), 15631–15639.

148. Heo, D.N., Yang, D.H., Moon, H.-J., Lee, J.B., Bae, M.S., Lee, S.C., Lee, W.J., Sun, I.-C., and Kwon, I.K. (2012) Gold nanoparticles surface-functionalized with paclitaxel drug and biotin receptor as theranostic agents for cancer therapy. *Biomaterials*, **33** (3), 856–866.

149. Patil, Y.B., Toti, U.S., Khdair, A., Ma, L., and Panyam, J. (2009) Single-step surface functionalization of polymeric nanoparticles for targeted drug delivery. *Biomaterials*, **30** (5), 859–866.

150. Green, N.M. (1975) Avidin, in *Advances in Protein Chemistry*, vol. 29, Elsevier, pp. 85–133.

151. Sperling, R.A., and Parak, W.J. (2010) Surface modification, functionalization and bioconjugation of colloidal inorganic nanoparticles. *Phil. Trans. R. Soc. A.*, **368** (1915), 1333–1383.

152. Chavanpatil, M., Patil, Y., and Panyam, J. (2006) Susceptibility of nanoparticle-encapsulated paclitaxel to P-glycoprotein-mediated drug efflux. *International Journal of Pharmaceutics*, **320** (1–2), 150–156.

153. Xie, J., Xu, C., Kohler, N., Hou, Y., and Sun, S. (2007) Controlled PEGylation of Monodisperse Fe3O4 Nanoparticles for Reduced Non-Specific Uptake by Macrophage Cells. *Adv. Mater.*, **19** (20), 3163–3166.

154.   Sanz, V., Conde, J., Hernández, Y., Baptista, P.V., Ibarra, M.R., and de la Fuente, J.M. (2012) Effect of PEG biofunctional spacers and TAT peptide on dsRNA loading on gold nanoparticles. *J Nanopart Res*, **14** (6), 917.

155.   Sanchez, L., Yi, Y., and Yu, Y. (2017) Effect of partial PEGylation on particle uptake by macrophages. *Nanoscale*, **9** (1), 288–297.

156.   Kanaras, A.G., Kamounah, F.S., Schaumburg, K., Kiely, C.J., and Brust, M. (2002) Thioalkylated tetraethylene glycol: a new ligand for water soluble monolayer protected gold clusters. *Chem. Commun.*, (20), 2294–2295.

157.   Simpson, C.A., Agrawal, A.C., Balinski, A., Harkness, K.M., and Cliffel, D.E. (2011) Short-Chain PEG Mixed Monolayer Protected Gold Clusters Increase Clearance and Red Blood Cell Counts. *ACS Nano*, **5** (5), 3577–3584.

158.   Sawant, R.R., and Torchilin, V.P. (2012) Multifunctional nanocarriers and intracellular drug delivery. *Current Opinion in Solid State and Materials Science*, **16** (6), 269–275.

159.   Liu, Y., Han, X., He, L., and Yin, Y. (2012) Thermoresponsive Assembly of Charged Gold Nanoparticles and Their Reversible Tuning of Plasmon Coupling. *Angew. Chem. Int. Ed.*, **51** (26), 6373–6377.

160.   Grzelczak, M., Vermant, J., Furst, E.M., and Liz-Marzán, L.M. (2010) Directed Self-Assembly of Nanoparticles. *ACS Nano*, **4** (7), 3591–3605.

161.   McGorty, R., Fung, J., Kaz, D., and Manoharan, V.N. (2010) Colloidal self-assembly at an interface. *Materials Today*, **13** (6), 34–42.

162.   Brewer, S.H., Glomm, W.R., Johnson, M.C., Knag, M.K., and Franzen, S. (2005) Probing BSA Binding to Citrate-Coated Gold Nanoparticles and Surfaces. *Langmuir*, **21** (20), 9303–9307.

163.   Brancolini, G., Kokh, D.B., Calzolai, L., Wade, R.C., and Corni, S. (2012) Docking of Ubiquitin to Gold Nanoparticles. *ACS Nano*, **6** (11), 9863–9878.

164.   Strozyk, M.S., Chanana, M., Pastoriza-Santos, I., Pérez-Juste, J., and Liz-Marzán, L.M. (2012) Protein/Polymer-Based Dual-Responsive Gold Nanoparticles with pH-Dependent Thermal Sensitivity. *Adv. Funct. Mater.*, **22** (7), 1436–1444.

165.   Chang, J., Paillard, A., Passirani, C., Morille, M., Benoit, J.-P., Betbeder, D., and Garcion, E. (2012) Transferrin Adsorption onto PLGA Nanoparticles Governs Their Interaction with Biological Systems from Blood Circulation to Brain Cancer Cells. *Pharm Res*, **29** (6), 1495–1505.

166.   Conde, J., Ambrosone, A., Sanz, V., Hernandez, Y., Marchesano, V., Tian, F., Child, H., Berry, C.C., Ibarra, M.R., Baptista, P.V., Tortiglione, C., and de la Fuente, J.M. (2012) Design of Multifunctional Gold Nanoparticles for *In Vitro* and *In Vivo* Gene Silencing. *ACS Nano*, **6** (9), 8316–8324.

167.   Sheehan, J.C., Preston, J., and Cruickshank, P.A. (1965) A Rapid Synthesis of Oligopeptide Derivatives without Isolation of Intermediates. *J. Am. Chem. Soc.*, **87** (11), 2492–2493.

168.   Susumu, K., Uyeda, H.T., Medintz, I.L., Pons, T., Delehanty, J.B., and Mattoussi, H. (2007) Enhancing the Stability and Biological Functionalities of Quantum Dots via Compact Multifunctional Ligands. *J. Am. Chem. Soc.*, **129** (45), 13987–13996.

169.   Pandey, P., Singh, S.P., Arya, S.K., Gupta, V., Datta, M., Singh, S., and Malhotra, B.D. (2007) Application of Thiolated Gold Nanoparticles for the Enhancement of Glucose Oxidase Activity. *Langmuir*, **23** (6), 3333–3337.

170.   Rostro-Kohanloo, B.C., Bickford, L.R., Payne, C.M., Day, E.S., Anderson, L.J.E., Zhong, M., Lee, S., Mayer, K.M., Zal, T., Adam, L., Dinney, C.P.N., Drezek, R.A.,

West, J.L., and Hafner, J.H. (2009) The stabilization and targeting of surfactant-synthesized gold nanorods. *Nanotechnology*, **20** (43), 434005.

171. Weissleder, R., Kelly, K., Sun, E.Y., Shtatland, T., and Josephson, L. (2005) Cell-specific targeting of nanoparticles by multivalent attachment of small molecules. *Nat Biotechnol*, **23** (11), 1418–1423.

172. Lin, C.-A.J., Sperling, R.A., Li, J.K., Yang, T.-Y., Li, P.-Y., Zanella, M., Chang, W.H., and Parak, W.J. (2008) Design of an Amphiphilic Polymer for Nanoparticle Coating and Functionalization. *Small*, **4** (3), 334–341.

173. Ballou, B., Lagerholm, B.C., Ernst, L.A., Bruchez, M.P., and Waggoner, A.S. (2004) Noninvasive Imaging of Quantum Dots in Mice. *Bioconjugate Chem.*, **15** (1), 79–86.

174. Dhar, S., Daniel, W.L., Giljohann, D.A., Mirkin, C.A., and Lippard, S.J. (2009) Polyvalent Oligonucleotide Gold Nanoparticle Conjugates as Delivery Vehicles for Platinum(IV) Warheads. *J. Am. Chem. Soc.*, **131** (41), 14652–14653.

175. Lattuada, M., and Hatton, T.A. (2007) Preparation and Controlled Self-Assembly of Janus Magnetic Nanoparticles. *J. Am. Chem. Soc.*, **129** (42), 12878–12889.

176. Lattuada, M., and Hatton, T.A. (2011) Synthesis, properties and applications of Janus nanoparticles. *Nano Today*, **6** (3), 286–308.

177. Walther, A., Matussek, K., and Müller, A.H.E. (2008) Engineering Nanostructured Polymer Blends with Controlled Nanoparticle Location using Janus Particles. *ACS Nano*, **2** (6), 1167–1178.

178. Xu, L.-P., Pradhan, S., and Chen, S. (2007) Adhesion Force Studies of Janus Nanoparticles. *Langmuir*, **23** (16), 8544–8548.

179. Worwood, M. (1990) Ferritin. *Blood Reviews*, **4** (4), 259–269.

180. Zhang, J., Wang, X., Wu, D., Liu, L., and Zhao, H. (2009) Bioconjugated Janus Particles Prepared by in Situ Click Chemistry. *Chem. Mater.*, **21** (17), 4012–4018.

181. Guix, M., Meyer, A.K., Koch, B., and Schmidt, O.G. (2016) Carbonate-based Janus micromotors moving in ultra-light acidic environment generated by HeLa cells in situ. *Sci Rep*, **6** (1), 21701.

182. Silvera Batista, C.A., Larson, R.G., and Kotov, N.A. (2015) Nonadditivity of nanoparticle interactions. *Science*, **350** (6257), 1242477–1242477.

183. Bradley, L.C., Stebe, K.J., and Lee, D. (2016) Clickable Janus Particles. *J. Am. Chem. Soc.*, **138** (36), 11437–11440.

184. Kirillova, A., Ionov, L., Roisman, I.V., and Synytska, A. (2016) Hybrid Hairy Janus Particles for Anti-Icing and De-Icing Surfaces: Synergism of Properties and Effects. *Chem. Mater.*, **28** (19), 6995–7005.

185. Rucinskaite, G., Thompson, S.A., Paterson, S., and de la Rica, R. (2017) Enzyme-coated Janus nanoparticles that selectively bind cell receptors as a function of the concentration of glucose. *Nanoscale*, **9** (17), 5404–5407.

186. Chernousova, S., and Epple, M. (2013) Silver as Antibacterial Agent: Ion, Nanoparticle, and Metal. *Angew. Chem. Int. Ed.*, **52** (6), 1636–1653.

187. Kim, J.-W., Hyung-Mo Moon, Tung, S., and Hyun-Ho Lee (2009) Highly effective bacterial removal system using carbon nanotube clusters. *2009 4th IEEE International Conference on Nano/Micro Engineered and Molecular Systems*, 1062–1064.

188. Wehling, J., Dringen, R., Zare, R.N., Maas, M., and Rezwan, K. (2014) Bactericidal Activity of Partially Oxidized Nanodiamonds. *ACS Nano*, **8** (6), 6475–6483.

189. Maas, M. (2016) Carbon Nanomaterials as Antibacterial Colloids. *Materials*, **9** (8), 617.

190. Chu, Y.W., Engebretson, D.A., and Carey, J.R. (2013) Bioconjugated Magnetic Nanoparticles for the Detection of Bacteria. *Journal of Biomedical Nanotechnology*, **9** (12), 1951–1961.

191. Wehling, J., Volkmann, E., Grieb, T., Rosenauer, A., Maas, M., Treccani, L., and Rezwan, K. (2013) A critical study: Assessment of the effect of silica particles from 15 to 500 nm on bacterial viability. *Environmental Pollution*, **176**, 292–299.

192. Arruebo, M., Fernández-Pacheco, R., Ibarra, M.R., and Santamaría, J. (2007) Magnetic nanoparticles for drug delivery. *Nano Today*, **2** (3), 22–32.

193. Mahmoudi, M., Sahraian, M.A., Shokrgozar, M.A., and Laurent, S. (2011) Superparamagnetic Iron Oxide Nanoparticles: Promises for Diagnosis and Treatment of Multiple Sclerosis. *ACS Chem. Neurosci.*, **2** (3), 118–140.

194. Jin, Y., Liu, F., Shan, C., Tong, M., and Hou, Y. (2014) Efficient bacterial capture with amino acid modified magnetic nanoparticles. *Water Research*, **50**, 124–134.

195. Teja, A.S., and Koh, P.-Y. (2009) Synthesis, properties, and applications of magnetic iron oxide nanoparticles. *Progress in Crystal Growth and Characterization of Materials*, **55** (1–2), 22–45.

196. Zhang, D., Berry, J.P., Zhu, D., Wang, Y., Chen, Y., Jiang, B., Huang, S., Langford, H., Li, G., Davison, P.A., Xu, J., Aries, E., and Huang, W.E. (2015) Magnetic nanoparticle-mediated isolation of functional bacteria in a complex microbial community. *ISME J*, **9** (3), 603–614.

197. Shan, Z., Wu, Q., Wang, X., Zhou, Z., Oakes, K.D., Zhang, X., Huang, Q., and Yang, W. (2010) Bacteria capture, lysate clearance, and plasmid DNA extraction using pH-sensitive multifunctional magnetic nanoparticles. *Analytical Biochemistry*, **398** (1), 120–122.

198. Widjojoatmodjo, M.N., Fluit, A.C., Torensma, R., Keller, B.H.I., and Verhoef, J. (1991) Evaluation of the Magnetic Immuno PCR assay for rapid detection ofSalmonella. *Eur. J. Clin. Microbiol. Infect. Dis.*, **10** (11), 935–938.

199. Matsunaga, T., Nakayama, H., Okochi, M., and Takeyama, H. (2001) Fluorescent detection of cyanobacterial DNA using bacterial magnetic particles on a MAG-microarray. *Biotechnol. Bioeng.*, **73** (5), 400–405.

200. Dinali, R., Ebrahiminezhad, A., Manley-Harris, M., Ghasemi, Y., and Berenjian, A. (2017) Iron oxide nanoparticles in modern microbiology and biotechnology. *Critical Reviews in Microbiology*, **43** (4), 493–507.

201. Wen, C.-Y., Jiang, Y.-Z., Li, X.-Y., Tang, M., Wu, L.-L., Hu, J., Pang, D.-W., and Zeng, J.-B. (2017) Efficient Enrichment and Analyses of Bacteria at Ultralow Concentration with Quick-Response Magnetic Nanospheres. *ACS Appl. Mater. Interfaces*, **9** (11), 9416–9425.

202. Cheng, Y., Liu, Y., Huang, J., Li, K., Zhang, W., Xian, Y., and Jin, L. (2009) Combining biofunctional magnetic nanoparticles and ATP bioluminescence for rapid detection of Escherichia coli. *Talanta*, **77** (4), 1332–1336.

203. Gao, X.-L., Shao, M.-F., Xu, Y.-S., Luo, Y., Zhang, K., Ouyang, F., and Li, J. (2016) Non-selective Separation of Bacterial Cells with Magnetic Nanoparticles Facilitated by Varying Surface Charge. *Front. Microbiol.*, **7**.

204. Wang, C., and Irudayaraj, J. (2010) Multifunctional Magnetic-Optical Nanoparticle Probes for Simultaneous Detection, Separation, and Thermal Ablation of Multiple Pathogens. *Small*, **6** (2), 283–289.

205. Chan, F.T.H., and Mackenzie, A.M.R. (1984) Advantage of Using Enrichment-Culture Techniques to Isolate Campylobacter jejuni from Stools. *Journal of Infectious Diseases*, **149** (3), 481–482.
206. Lee, J.-J., Jeong, K.J., Hashimoto, M., Kwon, A.H., Rwei, A., Shankarappa, S.A., Tsui, J.H., and Kohane, D.S. (2014) Synthetic Ligand-Coated Magnetic Nanoparticles for Microfluidic Bacterial Separation from Blood. *Nano Lett.*, **14** (1), 1–5.
207. Larsen, M.U., Seward, M., Tripathi, A., and Shapley, N.C. (2009) Biocompatible nanoparticles trigger rapid bacteria clustering. *Biotechnol Progress*, **25** (4), 1094–1102.
208. Jiang, W., Mashayekhi, H., and Xing, B. (2009) Bacterial toxicity comparison between nano- and micro-scaled oxide particles. *Environmental Pollution*, **157** (5), 1619–1625.
209. Campanhã, M.T.N., Mamizuka, E.M., and Carmona-Ribeiro, A.M. (1999) Interactions between cationic liposomes and bacteria: the physical-chemistry of the bactericidal action. *Journal of Lipid Research*, **40** (8), 1495–1500.
210. Truelstrup Hansen, L., Austin, J.W., and Gill, T.A. (2001) Antibacterial effect of protamine in combination with EDTA and refrigeration. *International Journal of Food Microbiology*, **66** (3), 149–161.
211. Luo, P.G., Tzeng, T.-R., Qu, L., Lin, Y., Caldwell, E., Latour, R.A., Stutzenberger, F., and Sun, Y.-P. (2005) Quantitative Analysis of Bacterial Aggregation Mediated by Bioactive Nanoparticles. *Journal of Biomedical Nanotechnology*, **1** (3), 291–296.
212. Wilhelm, S., Tavares, A.J., Dai, Q., Ohta, S., Audet, J., Dvorak, H.F., and Chan, W.C.W. (2016) Analysis of nanoparticle delivery to tumours. *Nat Rev Mater*, **1** (5), 16014.
213. Torrice, M. (2016) Does nanomedicine have a delivery problem?
214. Shao, D., Li, J., Zheng, X., Pan, Y., Wang, Z., Zhang, M., Chen, Q.-X., Dong, W.-F., and Chen, L. (2016) Janus "nano-bullets" for magnetic targeting liver cancer chemotherapy. *Biomaterials*, **100**, 118–133.
215. Wang, Z., Chang, Z., Lu, M., Shao, D., Yue, J., Yang, D., Zheng, X., Li, M., He, K., Zhang, M., Chen, L., and Dong, W. (2018) Shape-controlled magnetic mesoporous silica nanoparticles for magnetically-mediated suicide gene therapy of hepatocellular carcinoma. *Biomaterials*, **154**, 147–157.
216. Vilela, D., Stanton, M.M., Parmar, J., and Sánchez, S. (2017) Microbots Decorated with Silver Nanoparticles Kill Bacteria in Aqueous Media. *ACS Appl. Mater. Interfaces*, **9** (27), 22093–22100.
217. Park, J.H., and Oh, N. (2014) Endocytosis and exocytosis of nanoparticles in mammalian cells. *IJN*, 51.
218. Zhang, S., Gao, H., and Bao, G. (2015) Physical Principles of Nanoparticle Cellular Endocytosis. *ACS Nano*, **9** (9), 8655–8671.
219. Vácha, R., Martinez-Veracoechea, F.J., and Frenkel, D. (2011) Receptor-Mediated Endocytosis of Nanoparticles of Various Shapes. *Nano Lett.*, **11** (12), 5391–5395.
220. Schöttler, S., Becker, G., Winzen, S., Steinbach, T., Mohr, K., Landfester, K., Mailänder, V., and Wurm, F.R. (2016) Protein adsorption is required for stealth effect of poly(ethylene glycol)- and poly(phosphoester)-coated nanocarriers. *Nature Nanotech*, **11** (4), 372–377.

221.   Gao, Y., and Yu, Y. (2013) How Half-Coated Janus Particles Enter Cells. *J. Am. Chem. Soc.*, **135** (51), 19091–19094.

222.   He, W., Frueh, J., Wu, Z., and He, Q. (2016) Leucocyte Membrane-Coated Janus Microcapsules for Enhanced Photothermal Cancer Treatment. *Langmuir*, **32** (15), 3637–3644.

223.   He, W., Frueh, J., Wu, Z., and He, Q. (2016) How Leucocyte Cell Membrane Modified Janus Microcapsules are Phagocytosed by Cancer Cells. *ACS Appl. Mater. Interfaces*, **8** (7), 4407–4415.

224.   Wang, Z., Wang, Y., Chang, Z., Li, L., Zhang, Y., Lu, M., Zheng, X., Li, M., Shao, D., Li, J., Chen, L., and Dong, W. (2017) Berberine-loaded Janus nanocarriers for magnetic field-enhanced therapy against hepatocellular carcinoma. *Chem Biol Drug Des*, **89** (3), 464–469.

225.   Poggi, E., and Gohy, J.-F. (2017) Janus particles: from synthesis to application. *Colloid Polym Sci*, **295** (11), 2083–2108.

226.   Ling, X.Y., Phang, I.Y., Acikgoz, C., Yilmaz, M.D., Hempenius, M.A., Vancso, G.J., and Huskens, J. (2009) Janus Particles with Controllable Patchiness and Their Chemical Functionalization and Supramolecular Assembly. *Angew. Chem. Int. Ed.*, **48** (41), 7677–7682.

227.   Gao, Y., and Yu, Y. (2015) Macrophage Uptake of Janus Particles Depends upon Janus Balance. *Langmuir*, **31** (9), 2833–2838.

228.   Ding, H., and Ma, Y. (2015) Theoretical and Computational Investigations of Nanoparticle-Biomembrane Interactions in Cellular Delivery. *Small*, **11** (9–10), 1055–1071.

229.   Yoshida, M., Roh, K.-H., Mandal, S., Bhaskar, S., Lim, D., Nandivada, H., Deng, X., and Lahann, J. (2009) Structurally Controlled Bio-hybrid Materials Based on Unidirectional Association of Anisotropic Microparticles with Human Endothelial Cells. *Adv. Mater.*, **21** (48), 4920–4925.

230.   Kim, J.U., and Matsen, M.W. (2009) Positioning Janus Nanoparticles in Block Copolymer Scaffolds. *Phys. Rev. Lett.*, **102** (7), 078303.

231.   Feng, X., Fryxell, G.E., Wang, L.-Q., Kim, A.Y., Liu, J., and Kemner, K.M. (1997) Functionalized Monolayers on Ordered Mesoporous Supports. *Science*, **276** (5314), 923–926.

232.   Price, W.S., Tsuchiya, F., and Arata, Y. (1999) Lysozyme Aggregation and Solution Properties Studied Using PGSE NMR Diffusion Measurements. *J. Am. Chem. Soc.*, **121** (49), 11503–11512.

233.   Li, D., He, Q., Cui, Y., Duan, L., and Li, J. (2007) Immobilization of glucose oxidase onto gold nanoparticles with enhanced thermostability. *Biochemical and Biophysical Research Communications*, **355** (2), 488–493.

234.   Bhattacharjee, S. (2016) DLS and zeta potential – What they are and what they are not? *Journal of Controlled Release*, **235**, 337–351.

235.   Xu, R. (2008) Progress in nanoparticles characterization: Sizing and zeta potential measurement. *Particuology*, **6** (2), 112–115.

236.   Takahashi, K., Ohuchi, S., Saito, K., Hirasawa, M., and Sakurai, H. (2018) Simultaneous determination of the size and concentration of fine bubbles in water by laser-light scattering. *Appl. Opt.*, **57** (2), 225.

237.   Mulholland, G.W., Bohren, C.F., and Fuller, K.A. (1994) Light Scattering by Agglomerates: Coupled Electric and Magnetic Dipole Method. *Langmuir*, **10** (8), 2533–2546.

238.   Mie, G. (1908) Beiträge zur Optik trüber Medien, speziell kolloidaler Metallösungen. *Ann. Phys.*, **330** (3), 377–445.

239.   Clogston, J.D., and Patri, A.K. (2011) Zeta potential measurement, in *Characterization of nanoparticles intended for drug delivery*, Springer, pp. 63–70.

240.   Sze, A., Erickson, D., Ren, L., and Li, D. (2003) Zeta-potential measurement using the Smoluchowski equation and the slope of the current–time relationship in electroosmotic flow. *Journal of Colloid and Interface Science*, **261** (2), 402–410.

241.   Patil, S., Sandberg, A., Heckert, E., Self, W., and Seal, S. (2007) Protein adsorption and cellular uptake of cerium oxide nanoparticles as a function of zeta potential. *Biomaterials*, **28** (31), 4600–4607.

242.   Graf, C., Gao, Q., Schütz, I., Noufele, C.N., Ruan, W., Posselt, U., Korotianskiy, E., Nordmeyer, D., Rancan, F., Hadam, S., Vogt, A., Lademann, J., Haucke, V., and Rühl, E. (2012) Surface Functionalization of Silica Nanoparticles Supports Colloidal Stability in Physiological Media and Facilitates Internalization in Cells. *Langmuir*, **28** (20), 7598–7613.

243.   Reimer, L. (2000) Scanning Electron Microscopy: Physics of Image Formation and Microanalysis, Second Edition. *Meas. Sci. Technol.*, **11** (12), 1826–1826.

244.   Zhou, W., Apkarian, R., Wang, Z.L., and Joy, D. (2006) Fundamentals of Scanning Electron Microscopy (SEM), in *Scanning Microscopy for Nanotechnology* (eds.Zhou, W., and Wang, Z.L.), Springer New York, New York, NY, pp. 1–40.

245.   Joo, J., Yim, C., Kwon, D., Lee, J., Shin, H.H., Cha, H.J., and Jeon, S. (2012) A facile and sensitive detection of pathogenic bacteria using magnetic nanoparticles and optical nanocrystal probes. *Analyst*, **137** (16), 3609.

246.   Hayat, M.E. (2012) *Basic techniques for transmission electron microscopy*, Elsevier.

247.   Reimer, L. (2013) *Transmission electron microscopy: physics of image formation and microanalysis*, Springer.

248.   Apte, K., Stick, R., and Radmacher, M. (2017) Mechanics in human fibroblasts and progeria: Lamin A mutation E145K results in stiffening of nuclei: Mechanics in human fibroblasts and progeria. *J Mol Recognit*, **30** (2), e2580.

249.   AM Worthington (1881) II. On pendent drops. *Proc. R. Soc. Lond.*, **32** (212–215), 362–377.

250.   (2021) Pendant drop method - Optical determination of the surface/interfacial tension.

251.   Binks, B.P., and Fletcher, P.D.I. (2001) Particles Adsorbed at the Oil−Water Interface: A Theoretical Comparison between Spheres of Uniform Wettability and "Janus" Particles. *Langmuir*, **17** (16), 4708–4710.

252.   Hwang, N., and Barron, A.R. (2011) BET surface area analysis of nanoparticles. *The Connexions project*, 1–11.

253.   Naderi, M. (2015) Surface Area, in *Progress in Filtration and Separation*, Elsevier, pp. 585–608.

254.   Shaji, A., and Zachariah, A.K. (2017) Surface Area Analysis of Nanomaterials, in *Thermal and Rheological Measurement Techniques for Nanomaterials Characterization*, Elsevier, pp. 197–231.

255.   Foner, S. (1956) Vibrating Sample Magnetometer. *Review of Scientific Instruments*, **27** (7), 548–548.

256.   Hu, C., Gao, Z., and Yang, X. (2006) Fabrication and magnetic properties of Fe3O4 octahedra. *Chemical Physics Letters*, **429** (4–6), 513–517.

257. Ding, H.L., Zhang, Y.X., Wang, S., Xu, J.M., Xu, S.C., and Li, G.H. (2012) Fe_3O_4@SiO_2 Core/Shell Nanoparticles: The Silica Coating Regulations with a Single Core for Different Core Sizes and Shell Thicknesses. *Chem. Mater.*, **24** (23), 4572–4580.

258. Lichtman, J.W., and Conchello, J.-A. (2005) Fluorescence microscopy. *Nat Methods*, **2** (12), 910–919.

259. Rost, F.W. (1992) *Fluorescence microscopy*, Cambridge University Press.

260. Herman, B. (1998) Fluorescence Microscopy. *Current Protocols in Cell Biology*, **00** (1).

261. Smibert, R. (1994) Phenotypic characterization. *Methods for general and molecular bacteriology*.

262. Koch, A.L. (1970) Turbidity measurements of bacterial cultures in some available commercial instruments. *Analytical Biochemistry*, **38** (1), 252–259.

263. Koch, A.L., and Ehrenfeld, E. (1968) The size and shape of bacteria by light scattering measurements. *Biochimica et Biophysica Acta (BBA) - General Subjects*, **165** (2), 262–273.

264. (2020) Measuring Biomass in Shake Flasks: Offline OD vs. Online Backscatter Light.

265. Oliver James D. (2005) The Viable but Nonculturable State in Bacteria. *The Viable but Nonculturable State in Bacteria*, **4** (1), 93–100.

266. Berridge, M.V., Herst, P.M., and Tan, A.S. (2005) Tetrazolium dyes as tools in cell biology: New insights into their cellular reduction, in *Biotechnology Annual Review*, vol. 11, Elsevier, pp. 127–152.

267. Riss, Terry L (2013) *Cell viability assays*, Eli Lilly & Company and the National Center for Advancing Translational Sciences, Bethesda (MD).

268. Niles, A.L., Moravec, R.A., Eric Hesselberth, P., Scurria, M.A., Daily, W.J., and Riss, T.L. (2007) A homogeneous assay to measure live and dead cells in the same sample by detecting different protease markers. *Analytical Biochemistry*, **366** (2), 197–206.

269. Riss, T.L., and Moravec, R.A. (2004) Use of Multiple Assay Endpoints to Investigate the Effects of Incubation Time, Dose of Toxin, and Plating Density in Cell-Based Cytotoxicity Assays. *ASSAY and Drug Development Technologies*, **2** (1), 51–62.

270. Riss, Terry L Cell viability assays.

271. Liu, H., Du, Y., Wang, X., and Sun, L. (2004) Chitosan kills bacteria through cell membrane damage. *International Journal of Food Microbiology*, **95** (2), 147–155.

272. Sieuwerts, S., de Bok, F.A.M., Mols, E., de Vos, W.M., and van Hylckama Vlieg, J.E.T. (2008) A simple and fast method for determining colony forming units. *Letters in Applied Microbiology*, **47** (4), 275–278.

273. Bakken, L.R., and Olsen, R.A. (1987) The relationship between cell size and viability of soil bacteria. *Microb Ecol*, **13** (2), 103–114.

274. Cole, H.A., Wimpenny, J.W.T., and Hughes, D.E. (1967) The ATP pool in Escherichia coli. I. Measurement of the pool using a modified luciferase assay. *Biochimica et Biophysica Acta (BBA) - Bioenergetics*, **143** (3), 445–453.

275. Wilson, T. (1980) Imaging properties and applications of scanning optical microscopes. *Appl. Phys.*, **22** (2), 119–128.

276.	Brakenhoff, G.J., Blom, P., and Barends, P. (1979) Confocal scanning light microscopy with high aperture immersion lenses. *Journal of Microscopy*, **117** (2), 219–232.

277.	Bozzola, J.J., and Russell, L.D. (1999) *Electron microscopy: principles and techniques for biologists*, Jones & Bartlett Learning.

278.	Richardson, K., Jarett, L., and Finke, E. (1960) Embedding in epoxy resins for ultrathin sectioning in electron microscopy. *Stain technology*, **35** (6), 313–323.

279.	Goldstein, J.I., Newbury, D.E., Echlin, P., Joy, D.C., Fiori, C., and Lifshin, E. (1981) Preparation of biological samples for scanning electron microscopy, in *Scanning electron microscopy and X-ray microanalysis*, Springer, pp. 495–539.

280.	Legrand, C., Bour, J., Jacob, C., Capiaumont, J., Martial, A., Marc, A., Wudtke, M., Kretzmer, G., Demangel, C., and Duval, D. (1992) Lactate dehydrogenase (LDH) activity of the number of dead cells in the medium of cultured eukaryotic cells as marker. *Journal of biotechnology*, **25** (3), 231–243.

281.	Korzeniewski, C., and Callewaert, D.M. (1983) An enzyme-release assay for natural cytotoxicity. *Journal of immunological methods*, **64** (3), 313–320.

282.	Dominic A.Scudiero, Robert H. Shoemaker, (second), Kenneth D. Paull, (third), Anne Monks, (fourth), Siobhan Tierney (fifth), fifth, Thomas H. Nofziger, sixth, and Michael R. Boyd, last (1988) Evaluation of a Soluble Tetrazolium/Formazan Assay for Cell Growth and Drug Sensitivity in Culture Using Human and Other Tumor Cell Lines. **48** (17), 4827–4833.

283.	Lauth, V., Maas, M., and Rezwan, K. (2017) An evaluation of colloidal and crystalline properties of CaCO 3 nanoparticles for biological applications. *Materials Science and Engineering: C*, **78**, 305–314.

284.	Brennan, J.L., Hatzakis, N.S., Tshikhudo, T.R., Razumas, V., Patkar, S., Vind, J., Svendsen, A., Nolte, R.J.M., Rowan, A.E., and Brust, M. (2006) Bionanoconjugation via Click Chemistry: The Creation of Functional Hybrids of Lipases and Gold Nanoparticles. *Bioconjugate Chem.*, **17** (6), 1373–1375.

285.	McGorty, R., Fung, J., Kaz, D., and Manoharan, V.N. (2010) Colloidal self-assembly at an interface. *Materials Today*, **13** (6), 34–42.

286.	Hänni-Ciunel, K., Schelero, N., and von Klitzing, R. (2009) Negative charges at the air/water interface and their consequences for aqueous wetting films containing surfactants. *Faraday Discuss.*, **141**, 41–53.

287.	Makievski, A.V., Fainerman, V.B., Bree, M., Wüstneck, R., Krägel, J., and Miller, R. (1998) Adsorption of Proteins at the Liquid/Air Interface. *J. Phys. Chem. B*, **102** (2), 417–425.

288.	Park, J., An, K., Hwang, Y., Park, J.-G., Noh, H.-J., Kim, J.-Y., Park, J.-H., Hwang, N.-M., and Hyeon, T. (2004) Ultra-large-scale syntheses of monodisperse nanocrystals. *Nature Mater*, **3** (12), 891–895.

289.	Matsumoto, H., Koyama, Y., and Tanioka, A. (2003) Interaction of proteins with weak amphoteric charged membrane surfaces: effect of pH. *Journal of Colloid and Interface Science*, **264** (1), 82–88.

290.	Yi, Y., Sanchez, L., Gao, Y., and Yu, Y. (2016) Janus particles for biological imaging and sensing. *Analyst*, **141** (12), 3526–3539.

291.	Farka, Z., Kovář, D., and Skládal, P. (2014) Rapid Detection of Microorganisms Based on Active and Passive Modes of QCM. *Sensors*, **15** (1), 79–92.

292.   Jin, Y., Deng, J., Liang, J., Shan, C., and Tong, M. (2015) Efficient bacteria capture and inactivation by cetyltrimethylammonium bromide modified magnetic nanoparticles. *Colloids and Surfaces B: Biointerfaces*, **136**, 659–665.

293.   Shahabi, S., Treccani, L., Dringen, R., and Rezwan, K. (2015) Modulation of Silica Nanoparticle Uptake into Human Osteoblast Cells by Variation of the Ratio of Amino and Sulfonate Surface Groups: Effects of Serum. *ACS Appl. Mater. Interfaces*, **7** (25), 13821–13833.

294.   Holthaus, M.G., Stolle, J., Treccani, L., and Rezwan, K. (2012) Orientation of human osteoblasts on hydroxyapatite-based microchannels. *Acta Biomaterialia*, **8** (1), 394–403.

295.   Bollhorst, T., Shahabi, S., Wörz, K., Petters, C., Dringen, R., Maas, M., and Rezwan, K. (2015) Bifunctional Submicron Colloidosomes Coassembled from Fluorescent and Superparamagnetic Nanoparticles. *Angew. Chem.*, **127** (1), 120–125.

296.   Watanabe, R., Yokoi, T., Kobayashi, E., Otsuka, Y., Shimojima, A., Okubo, T., and Tatsumi, T. (2011) Extension of size of monodisperse silica nanospheres and their well-ordered assembly. *Journal of Colloid and Interface Science*, **360** (1), 1–7.

297.   Heuser, J.E., and Anderson, R.G. (1989) Hypertonic media inhibit receptor-mediated endocytosis by blocking clathrin-coated pit formation. *Journal of Cell Biology*, **108** (2), 389–400.

298.   Payne, C.K., Jones, S.A., Chen, C., and Zhuang, X. (2007) Internalization and Trafficking of Cell Surface Proteoglycans and Proteoglycan-Binding Ligands. *Traffic*, **8** (4), 389–401.

299.   Spiro, D.J., Boll, W., Kirchhausen, T., and Wessling-Resnick, M. (1996) Wortmannin alters the transferrin receptor endocytic pathway in vivo and in vitro. *MBoC*, **7** (3), 355–367.

300.   Gao, P., Sun, S., Wang, Y., Wei, Y., and Jiang, Y. (2022) Biodegradable T2-phage-like Janus nanoparticles for actively-targeted and chemo-photothermal synergistic therapy. *Chemical Engineering Journal*, **428**, 131284.

301.   Zhang, T.-T., Li, W., Meng, G., Wang, P., and Liao, W. (2016) Strategies for transporting nanoparticles across the blood–brain barrier. *Biomater. Sci.*, **4** (2), 219–229.

10. Appendix

10.1   List of publications

Kadam.R, Ghawali.J, Waespy.M, Maas.M and Rezwan.K., „Janus NPs for extended cell surface attachment" *RSC Nanoscale*, **2020**, 12, 18938-18949.

Kadam.R, Maas.M and Rezwan.K. „Selective, agglomerate-free separation of bacteria using biofunctionalized, magnetic Janus NPs, *ACS Applied Bio Materials*, **2019**, 8, 3528-3531.

Kadam.R, Zilli.M, Maas.M and Rezwan.K. „Nanoscale Janus particles with dual protein functionalization" *Particle and Particle systems characterization*, **2018**, 35, 1700332

Blumrich,E., **Kadam,R.** and Dringen,R. "The Protein Tyrosine Kinase Inhibitor Tyrphostin 23 Strongly Accelerates Glycolytic Lactate Production in Cultured Primary Astrocytes" *NeuroChem Res*, **2016**, 41, 2607-2618

10.2 List of oral/poster presentations

1. 13th Zsigmondy colloqium of the German Colloid Society. Saarbrücken, Germany

   Kadam,R., Zilli,M., Maas,M., Rezwan,K. *Nanoscale Janus particles with dual protein functionalization*. (Poster presentation)

2. Centre Européen de Calcul Antomique et Moléculaire (CECAM) workshop. Bremen, Germany

   Kadam,R., Zilli,M., Maas,M., Rezwan,K. *Nanoscale Janus particles with dual protein functionalization*. (Poster presentation)

10.3   List of supervised students

During the work of this thesis, projects from the following students were supervised:

1. **Internship** "Aerogel production using Janus particles" **Cristiano Enke**. Materials Engineering, Federal University of Santa Catarina (UFSC), September. 2017 to December. 2017

2. **Internship** "Bionanoconjugation via Click chemistry: Creating hybrids of silica particles and proteins" **Marina Zilli**. Materials Engineering, Federal University of Santa Catarina (UFSC), September. 2016 to December. 2016.

Curriculum Vitae

Reshma Sampat Kadam

Email   reshma.kadam@hotmail.com
LinkedIn   www.linkedin.com/in/reshma-kadam

EDUCATION

- **06.2015 - present**

  Centre of Advanced Ceramics, University of Bremen. Bremen, Germany.
  Ph.D. in Engineering Sciences.
  Doctoral dissertation: "A novel platform for the synthesis of inorganic Janus NPs with tailored cell interactions- in prokaryotic and eukaryotic systems"

- **10.2012 - 01.2015**

  University of Bremen. Bremen, Germany.
  Master of Science in Biochemistry and Molecular Biology.
  Final score: German GPA 1.7 (excellent)
  Master thesis: "Acute stimulation of glycolytic flux by Tyrphostin 23 and Metformin in cultured brain astrocytes"

- **07.2009 - 06.2012**

  Pune University. Maharashtra, India.
  Bachelor of Science in Microbiology.
  Final score: 85% (excellent)
  Subjects: Organic and inorganic Chemistry, Industrial Microbiology, Genetics, Statistics and Mathematics

- **06.2009**

  Apte Junior College. Maharashtra, India.
  Higher secondary school degree

EXPERIENCE

- **06.2015 - 10.2019**

  Centre of Advanced Ceramics, University of Bremen. Bremen, Germany.
  Scientific researcher
  - developed methodology for isolation of microbes from a mixture of bacteria
  - developed NPs for tagging of fibroblasts with NPs for up to 6 h of endocytosis-free attachment
  - trained students in project planning and management including
  - supervised general functioning of four biological laboratories for maintenance of appropriate biological safety standards

- **07.2013 - 12.2013**

  University of Bremen, Bremen, Germany.
  Student research assistant
  - trained in techniques such as gene cloning in microbes, PCR sequencing, data interpretation and writing publications
  - experimental planning and documentation

- **08.2011 - 12.2011**

  Swasti Agro Bioproducts Pvt. Ltd. Maharashtra, India.
  Research assistant (Internship)
    - trained in techniques such as sterile working, PCR, gene cloning, GMP
    - data analysis

- **06.2011 - 08.2011**

  Serum Institute of India Pvt.Ltd. Maharashtra, India.
  Research assistant (Internship)
    - learnt techniques such as HPLC, PCR, gas chromatography, GMP, vaccine formulations (typhoid, pertussis, measles)
    - data procurement, analysis and hands-on experience as a bench scientist

SKILLS

- **Languages**

  English (native speaker), German (level C1), Hindi (native speaker)

- **Computer skills**

  Microsoft Office, Adobe Photoshop, Adobe Lightroom

- **Lab work skills**

  Good Laboratory practice (GLP), GMP, biotechnology-based skills, microbial analysis, cell culture and imaging, NP synthesis and characterization, cloning, microscopy-based skillls.

- **Other skills**

  critical thinking, scientific writing, problem-solving, intercultural competence

- **Other**

  German Class B driver's license

PUBLICATIONS

- **2020**

  Kadam.R, Ghawali,J, Waespy,M, Maas,M, Rezwan.K, **RSC Nanoscale (2020)**, *Janus NPs for extended cell surface attachment.*
  doi: 10.1039/D0NR04061D

- **2019**

  Kadam,R., Maas,M., Rezwan,K. **ACS Applied Bio Materials (2019)**, *Selective, agglomerate-free separation of bacteria using biofunctionalized, magnetic Janus NPs.*
  doi:10.1002/acsabm.9b00415

- **2018**

  Kadam,R., Zilli,M., Maas,M., Rezwan,K. **Part. Part. Syst. Charact (2018)**, *Nanoscale Janus particles with dual protein functionalization.*
  doi:10.1002/ppsc.201700332

- **2016**

  Blumrich,E., **Kadam,R.** & Dringen,R. **NeuroChem Res** (**2016**) *The Protein Tyrosine Kinase Inhibitor Tyrphostin 23 Strongly Accelerates Glycolytic Lactate Production in Cultured Primary Astrocytes.*
  doi:10.1007/s11064-016-1972-3